# Light-cone effects in the galaxy 2-point function

Tansella, Vittorio

UNIVERSITÉ DE GENÈVE
Section de Physique
Département de Physique Théorique

FACULTÉ DES SCIENCES
Professeure Ruth DURRER

---

# Light-cone effects in the galaxy 2-point function

THÈSE

présentée à la Faculté des sciences de l'Université de Genève
pour obtenir le grade de
Docteur ès sciences, mention physique

par

**Vittorio TANSELLA**

de
Milano (Italie)

Thèse N° 5267

GENÈVE
Atelier de reproduction de la Section de Physique
2018

UNIVERSITÉ DE GENÈVE

FACULTÉ DES SCIENCES

DOCTORAT ÈS SCIENCES, MENTION PHYSIQUE

**Thèse de Monsieur Vittorio TANSELLA**

intitulée :

**«Light-cone Effects in the Galaxy 2-point Function»**

La Faculté des sciences, sur le préavis de Madame R. DURRER, professeure ordinaire et directrice de thèse (Département de physique théorique), Madame C. BONVIN, professeure assistante (Département de physique théorique), Monsieur C. CLARKSON, docteur (School of Physics and Astronomy, Queen Mary University of London, United Kingdom), Monsieur V. DESJACQUES, professeur (Department of Physics, Technion - Israel Institute of Technology, Haifa, Israël), autorise l'impression de la présente thèse, sans exprimer d'opinion sur les propositions qui y sont énoncées.

Genève, le 15 octobre 2018

**Thèse - 5267 -**

**Le Doyen**

N.B. - La thèse doit porter la déclaration précédente et remplir les conditions énumérées dans les "Informations relatives aux thèses de doctorat à l'Université de Genève".

# Abstract

This thesis investigates one of the most important observables in cosmology: the galaxy two-point function. The proper characterisation of this quantity is of the utmost importance if we want to compare theoretical predictions with the experimental results coming from planned redshift surveys. In particular we focus here on the modification that light-cone effects introduce – at large scales – in the correlation function. We start by computing, through first-order cosmological perturbation theory, expressions describing the galaxy distribution in the universe, i.e. galaxy number counts. These results are then used in order to construct the fully relativistic correlation function, which is valid in full-sky, i.e. beyond the so-called flat-sky approximation. A publicly available code is provided for fast and accurate numerical evaluation of the two-point function which allows us to forecast the possibility, with future or planned experiments, of constraining cosmological parameters through the multipoles decomposition of the correlation function. Other relevant topics, related to the two-point function, that we discuss in this work are: the regularisation of an apparent infra-red divergence in the potentials terms such as the Sachs-Wolfe effect, the existence of a second feature in the matter correlation function due to the baryon-baryon correlation in the early universe and, finally, a framework to analyse a possible anisotropic component in the two-point function.

# Contents

# Acknowledgements

First and foremost, I would like to express my gratitude to Ruth Durrer for her support, her passion and her teaching during the three years of my doctorate.

I am also indebted with Camille Bonvin, Martin Kunz, Michele Maggiore and Toni Riotto for their mentorship.

I am very grateful to my collaborators Ruth Durrer, Camille Bonvin, Giulia Cusin, Antonio Riotto, Alex Kehagias, Basundhara Ghosh, Elena Sellentin, Goran Jelic-Cizmek, Ignacy Sawicki, Julian Adamek, Nicola Bartolo, Martin Kunz, Michele Liguori, Ermis Mitsou, Fulvio Scaccabarozzi, Maresuke Shiraishi and Jaiyul Yoo for their helping in occasion of the work we did together.

A special thanks to my colleagues and friends Enis Belgacem, Giulia Cusin, Yves Dirian, Pierre Fleury, Fabien Lacasa, Francesco Montanari, Davide Racco, Fulvio Scaccabarozzi and many others. I would also like to thank again Pierre Fleury for having corrected my French introduction.

## Jury Members

- Prof. Camille Bonvin
  Département de Physique Théorique & Center for Astroparticle Physics, Université de Genève, 24 quai E. Ansermet, CH-1211 Genève 4, Switzerland

- Dr. Chris Clarkson
  School of Physics and Astronomy, Queen Mary, University of London, Mile End, London, UK
  Department of Physics and Astronomy, University of the Western Cape, Cape Town 7535, South Africa
  Department of Mathematics and Applied Mathematics, University of Cape Town, Rondebosch 7701, South Africa

- Prof. Vincent Desjacques
  Physics department and Asher Space Science Institute, Technion, 3200003 Haifa, Israel

- Prof. Ruth Durrer
  Département de Physique Théorique & Center for Astroparticle Physics, Université de Genève, 24 quai E. Ansermet, CH-1211 Genève 4, Switzerland

I would like to thank them all for having accepted to be part of the Jury for my Thesis defense.

# List of Publications

The following works have been considered as part of this thesis:

[134] R. Durrer and V. Tansella, "*Vector perturbations of galaxy number counts*", **JCAP 1607** (2016) 037, [arXiv:1605.05974].

[294] V. Tansella, C. Bonvin, R. Durrer, B. Ghosh and E. Sellentin, "*The full-sky relativistic correlation function and power spectrum of galaxy number counts. Part I: Theoretical aspects*", **JCAP 1803** (2018) 019, [arXiv:1708.00492].

[292] V. Tansella "*On the $2^{nd}$ feature of the matter two-point function*" **Phys.Rev. D97** (2018) 10, [arXiv:1804.05826].

[295] V. Tansella, G. Jelic-Cizmek, C. Bonvin and R. Durrer "*COFFE: a code for the full-sky relativistic galaxy correlation function*" **JCAP 1810** (2018) 032, [arXiv:1806.11090].

[293] V. Tansella, C. Bonvin, G. Cusin, R. Durrer, M. Kunz and I. Sawicki "*Redshift-space distortions from vector perturbations II: Anisotropic signal*" **in publication**, [arXiv:1807.00731].

[230] E. Mitsou, R. Durrer, F. Scaccabarozzi, V. Tansella and J. Yoo "*Observer terms and ensemble averages*" **in preparation**

Additional publications related to this work:

[9] J. Adamek, R. Durrer and V. Tansella "*Lensing signals from Spin-2 perturbations*", **JCAP 1601** (2016) 024, [arXiv:1510.01566].

[113] G. Cusin, V. Tansella and R. Durrer, "*Vorticity generation in the Universe: A perturbative approach*"
**Phys.Rev D95** (2017) 6, [arXiv:1612.00783].

[36] N. Bartolo, A. Kehagias, M. Liguori, A. Riotto, M. Shiraishi and V. Tansella "*Detecting higher spin fields through statistical anisotropy in the CMB and galaxy power spectra*"
**Phys.Rev. D97** (2018) 2, [arXiv:1709.05695].

# Résumé

La cosmologie physique est la branche de la physique et de l'astrophysique qui étudie les origines physiques et l'évolution de l'univers. Il comprend également l'étude de la nature de l'univers à grande échelle. Pour décrire l'univers, il est indispensable de faire appel à la relativité générale, découverte par Albert Einstein en 1915. En considérant qu'il est improbable que la dynamique de l'univers soit dominée par des interactions à courte distance et que, en moyenne, l'univers n'est pas chargé électriquement, il n'est pas surprenant qu'une théorie de la gravité soit nécessaire pour aborder la cosmologie scientifiquement. Ainsi, à partir de 1915, il devint possible d'étudier l'univers à partir de deux piliers de la science moderne: la relativité générale et, plus tard, le modèle standard de la physique des particules (en particulier en ce qui concerne l'univers primordial). En 1922, Alexander Friedmann introduisit l'idée d'un univers en expansion et, en 1929, l'astronome américain Edwin Hubble découvrit que la distance des galaxies était proportionnelle à leur décalage spectral (*redshift* en anglais), confirmant que les galaxies s'éloignent de leur observateur. Cette observation, associée à la métrique et aux équations de Friedman-Lemaître-Robertson-Walker (FLRW), a jeté les bases du modèle standard de la cosmologie. Un important travail théorique sur l'histoire thermique de l'univers a été entrepris par Gamow, Alpher and Herman et, en 1964, la plus vieille image de l'univers qu'il soit possible d'obtenir a été découverte par hasard par Penzias et Wilson: le fond diffus cosmologique (rayonnement fossile ou CMB, issu de l'anglais).

Le fond diffus cosmologique était une observable clé et très important pour l'étude de la cosmologie, car ses propriétés sont liées aux paramètres qui décrivent l'univers. Á partir de 1989 la NASA et l'ESA ont décidé d'envoyer trois satellites en orbite dans le but d'étudier le rayonnement fossile, et les données collectées ont aidé à établir le modèle standard de la cosmologie qu'on appelle ΛCDM (pour Λ *Cold Dark Matter* en anglais). Ce modèle de concordance décrit un univers homogéne et isotrope (à grande échelle), âgé de 13.8 milliards d'années, dont la courbure spatiale est nulle et qui contient 26.5% de matière noire, 68.6% d'énergie sombre alors que la matière ordinaire (baryonique) ne représente que 4.9% de l'univers. La matière noire n'interagit pas avec la lumière mais peut être décelée par son at-

traction gravitationnelle. La composante appelée énergie sombre peut être modélisée par une constante cosmologique $\Lambda$ dans les équations d'Einstein (d'oú le nom $\Lambda$CDM). Cette dernière forme d'énergie est responsable de la récente expansion accélérée de l'univers découverte par le *Supernova Cosmology Project* et le *High-Z Supernova Search Team* en 1998. Le problème est que le 95% de l'univers est inconnu: on peux détecter la matière noire de façon indirecte (car la matière noire, comme la matière ordinaire, exerce une attraction gravitationnelle) mais aucune détection directe n'a été jamais annoncée, et la valeur de $\Lambda$ mesurée est plus petite de plusieurs ordres de grandeur que ce qu'on attendrait de la contribution des fluctuations quantiques du vide. La caractérisation de l'univers sombre est donc un des objectifs les plus importants de la recherche cosmologique d'aujourd'hui et de demain.

Mises à part les observations du fond diffus cosmologique, beaucoup d'expériences pour étudier la structure à grande échelle de l'univers sont actuellement en cours ou prévues. Il s'agit de grands relevés des galaxies, ou relevés du décalage vers le rouge (*redshift survey* en anglais): la mesure d'une section du ciel pour detecter le décalage vers le rouge des galaxies (ou des autres objects) et leur distribution. Un relevé du décalage vers le rouge, comme par example *Euclid*, donne un catalogue de millions des galaxies, leur positions et leur *redshift*. Une interprétation correcte de ces données est fondamentale si nous voulons les relier correctement aux paramètres cosmologiques. Parmi les nombreuses complications et subtilités de cette tâche, le sujet principal de cette thèse est étudier comment les effets relativistes (ou *light-cone effects*) affectent les observables que l'on peut construire a partir de catalogues des galaxies. L'origine des effets relativistes est le changement de coordonnées de la métrique de référence (*background metric*), par rapport aux vraies coordonnées observées (position et décalage vers le rouge d'un objet). En d'autres termes, l'origine physique des effets de projection se situe dans la déviation des rayons lumineux en suivant la courbure de l'espace-temps, en accord avec la théorie d'Einstein. En effet l'univers n'est pas complètement homogène, à cause de la présence de structures: il est cependant possible tenir compte, en utilisant la théorie des perturbations cosmologiques, des effets relativistes qui influencent la distribution de galaxies en fonction du position et du décalage vers le rouge.

Dans le chapitre 1 j'introduis les sujets traités dans cette thèse: une brève histoire de la cosmologie avec ses découvertes principales expérimental comme théorique. Une attention particulière est réservée à l'introduction de la formation des structures et aux effets relativistes.

Dans le chapitre 2, reproduisant la référence [134], je montre comment tenir compte, au première ordre de la théorie des perturbations, des effets relativistes qui concernent l'observable le plus simple qu'on peut faire avec un relevé du décalage vers le rouge: comptage de galaxies (*galaxy number counts* en anglais). Cette analyse, qui se trouve déjà dans la littérature, est enrichie en considérant la contribution des perturbations vectorielles et tensorielles.

Dans le chapitre 3, reproduisant la référence [294], je commence l'étude de la fonction de corrélation à deux points, en développant le cadre théorique qui permet la caractérisation et

l'étude des effets relativistes sur la fonction à deux points.

Dans le chapitre 4, reproduisant la référence [295], je décris comment les résultats du chapitre précédent nous ont permis d'écrire un code qui calcule efficacement la fonction de corrélation. Le code est accessible au public et toutes les corrections relativistes sont inclues au niveau linéaire. On utilise des techniques basées sur les matrices de Fisher pour analyser en détail les capacités des prochaines expériences telles que *SKA* et *Euclid* pour contraindre l'effet de lentille gravitationnelle utilisant la fonction à deux point. Par ailleurs, je discute une subtilité: comment éviter une divergence infra-rouge qui affecte certaines corrections relativistes à la fonction de corrélation. Une discussion plus détaillé sur ce dernier point est présentée dans le chapitre 7.

Dans le chapitre 5, reproduisant la référence [292], je présente une nouvelle observation concernant la fonction à deux points: l'existence d'un deuxième signal (ou "trait") due à la corrélation baryonique dans l'univers primordial.

Dans le chapitre 6, reproduisant la référence [293], je décris comment comment les multipoles de la fonction de corrélation peuvent être analysés dans le cas où ils comprennent un signal vectoriel anisotrope. On développe des nouvelles observables spécifiques au cas anisotrope et l'analyse de Fisher est utilisée une nouvelle fois pour établir des contraintes sur les paramètres caractérisant l'anisotropie.

# Notation

**Fourier transform** We will use asymmetric conventions for the Fourier transform:

$$F(\mathbf{x}) = \int \frac{d^n k}{(2\pi)^n} \tilde{F}(\mathbf{k}) e^{-i\mathbf{k}\cdot\mathbf{x}} ,$$
$$\tilde{F}(\mathbf{k}) = \int d^n x \, F(\mathbf{x}) e^{i\mathbf{k}\cdot\mathbf{x}} ,$$

and we will sometimes omit the tilde if there is no ambiguity $\tilde{F}(\mathbf{k}) = F(\mathbf{k}) = F_{\mathbf{k}}$. The dirac delta satisfies

$$\int d^n x \, e^{i\mathbf{k}\cdot\mathbf{x}} = (2\pi)^n \delta^{(n)}(\mathbf{k}) .$$
$$\int d^n k \, e^{i\mathbf{k}\cdot\mathbf{x}} = \delta^{(n)}(\mathbf{x}) .$$

The power spectrum of a statistically homogeneous and isotropic random variable $F$ is defined

$$\langle F(\mathbf{k}) F^*(\mathbf{k}') \rangle = (2\pi)^3 \delta^{(3)}(\mathbf{k} - \mathbf{k}') P_F(k) ,$$

and the dimensionless (if $F(\mathbf{x})$ is dimensionless) power spectrum is obtained via

$$\mathcal{P}_F(k) = \frac{k^3}{2\pi^2} P_F(k) .$$

**Signature and indices** We use the metric signature $(-,+,+,+)$ throughout the thesis, while for the indices we follow, when possible, the following rules: greek indices $\alpha, \beta, ...$ are space-time indices and run from 0 to 3, latin indices $i, j, k, ...$ are spatial indices and run from 1 to 3. We sometimes use indices $a, b, ...$ running from 1 to 2 for angular coordinates. Uppercase indices $A, B, C, ...$ are not tensor indices but labels or tags.

**Derivatives** We work mainly in conformal time $\eta$ and derivatives w.r.t. $\eta$ are denoted by an over-dot: $\dot{F}$. Covariant derivatives $\nabla_\mu$ and spatial gradients $\nabla_i$ are distinguishable by the type of index. The spatial Laplacian is denoted by $\Delta$ while the angular Laplacian by $\Delta_\Omega$.

**List of symbols** For reference we report here the list of symbols used in this thesis.

| **background** | |
|---|---|
| $a$ | scale factor |
| $H$ | Hubble parameter ($H_0$ Hubble parameter today) |
| $\mathcal{H}$ | comoving Hubble parameter $\mathcal{H} = aH$ ($\mathcal{H}_0 = H_0$ with our normalization of $a$) |
| $h$ | reduced Hubble parameter $h = H_0/100$ |
| $\bar{\rho}_X$ | energy density of the species $X$ |
| $\rho_c$ | critical density $\rho_c = 3H^2/(8\pi G)$ |
| $\Omega_X$ | density parameter $\Omega_X = \bar{\rho}_X/\rho_c$ |
| $\eta$, ($\eta_0$) | conformal time (today) |
| $t$, ($t_0$) | cosmic time (today) |
| $\chi$ | comoving distance $\chi = \eta_0 - \eta$ (denoted $\bar{\chi}$ in chapter 3) |
| $z$ | redshift |
| $\bar{\mathcal{D}}_L$ | luminosity distance |
| **perturbations** | |
| $\mathbf{n}$, $\hat{n}$ | line-of-sight direction of an object at $\mathbf{x} = \chi(z)\mathbf{n}$ ($-\mathbf{n}$ in chapter 3) |
| $\mathbf{r}$ | distance between two tracers $\mathbf{r} = \mathbf{x}_1 - \mathbf{x}_2$ |
| $\Phi(\mathbf{x})$, $\Psi(\mathbf{x})$ | Bardeen potentials |
| $S_i(\mathbf{x})$, $H_{ij}(\mathbf{x})$ | vector and tensor metric perturbations |
| $\delta(\mathbf{x})$ | CDM density constrast in longitudinal gauge |
| $\delta_c(\mathbf{x})$ | CDM density constrast in comoving gauge |
| $\Delta_g(\mathbf{n}, z)$ | observable galaxy density contrast (number counts) |
| $n_g(\mathbf{n}, z)$ | galaxy density per redshift and solid angle bins |
| $\mathbf{v}(\mathbf{x})$ | velocity perturbation in longitudinal gauge |
| $v(\mathbf{x})$ | velocity potential $\mathbf{v} = -\nabla v$ |
| $V(k)$ | defined as $v(k) = k^{-1}V(k)$ ($V(\mathbf{x})$ is dimensionless) |
| $\Sigma_i(\mathbf{x})$, $v_i^{(V)}(\mathbf{x})$ | vector part of $\mathbf{v}$: $\partial^i\Sigma_i = 0$ |
| $\Omega_i(\mathbf{x})$ | relativistic vorticity $\Omega_i = \Sigma_i - S_i$ |
| $\langle[...]\rangle$, $\langle[...]\rangle_P$ | ensemble average |
| $\langle[...]\rangle_{\mathbb{E}}$ | average over the euclidian group |
| $\langle[...]\rangle_{\mathrm{SO(3)}}$ | average over the SO(3) group |
| $\langle[...]\rangle_{\Omega}$ | directional average |
| $P_{AB}(k)$ | power spectrum $\langle A(\mathbf{k})B^*(\mathbf{k}')\rangle = (2\pi)^3\delta^{(3)}(\mathbf{k}-\mathbf{k}')P_{AB}(k)$ |
| $\mathcal{P}_\zeta(k)$ | primordial curvature power spectrum $\mathcal{P}_\zeta = A_s(k/k_*)^{n_s-1}$ |
| $A_s$, $n_s$, $k_*$ | primordial amplitude, spectral index and pivot scale |
| $\xi(\theta, z_1, z_2)$ | two-point correlation function |
| $C_\ell(z_1, z_2)$ | angular power spectrum |
| $D_1(z)$ | matter growth function |
| $g(z)$ | Bardeen potentials growth function $g = D_1/a$ |
| $g_S(z)$ | scalar-induced vector modes growth function |
| $f(z)$ | velocity growth rate $f = d\ln D_1/d\ln a$ |
| $s_{\mathrm{hor}}$ | sound horizon |

| | |
|---|---|
| $b$ | galaxy bias |
| $s$ | magnification bias |
| $f_{\rm evo}$ | evolution bias |
| $L_p$ | size of the survey's pixel |
| $d\bar{N}$ | mean number of galaxies per pixel |
| $\mathrm{cov}^{(A)}$ | covariance matrix for the estimator $A$ |
| **mathematics** | |
| $\mathcal{P}_\ell(x)$ | Legendre polynomials |
| $Y_{\ell m}(\theta,\phi)$ | Spherical harmonics |
| $X^{JM}_{\ell\ell'}(\hat{a},\hat{b})$ | Bipolar Spherical harmonics |
| $J_n(x)$ | Bessel functions |
| $j_\ell(x)$ | spherical Bessel functions |
| ${}_2F_1(x,y,z,w)$ | hypergeometric function |
| $\delta^{(n)}(\mathbf{x})$ | $n-$dimensional Delta function |
| $\delta_{ij}$ | Kronecker delta |
| $\epsilon_{ijk}$ | Levi-Civita tensor |
| **abbreviations** | |
| (C)DM | (cold) dark matter |
| DE | dark energy |
| $\Lambda$ | cosmological constant |
| FLRW | Friedmann-Lemaître-Robertson-Walker |
| GR | general relativity |
| CMB | cosmic microwave background |
| LSS | large-scale structures |
| BAO | baryon acoustic oscillations |
| RSD | redshift-space distortion |
| 2pF | two-point function |
| 2FT | second feature |
| LOS | line-of-sight |
| (I)SW | (integrated) Sachs-Wolfe effect |
| S/N | signal-to-noise |
| $\vert_f$, fid | fiducial |
| PDF | probability distribution function |
| (S), (L)PT | (standard), (Lagrangian) perturbation theory |
| w.r.t. | with respect to |

# CHAPTER 1

## Introduction

> The story so far:
> In the beginning the Universe
> was created. This has made a lot
> of people very angry and been
> widely regarded as a bad move.
>
> *Douglas Adams*

*The vast ocean of space is full of starry islands called galaxies*[1]. Beside offering a peerless spectacle when we look into the night sky[2], galaxies are a valuable source of information and object of study of the science which deals with the origin, the history and the structure of the universe: cosmology. Since the dawn of time mankind has always tried to make sense of the world's origin: no human society has been found in which myths of creations are not part of its culture or its religion [91]. Science, on the other hand, took its time to contribute on this matter. Even with the advent of the scientific method in the 15th century, tools to properly deal with this subject were not developed until the beginning of the 20th century. It was Einstein's formulation of General Relativity (GR) that paved the way for a scientific understanding of the universe. If we consider that the dynamic of the universe is unlikely to be dominated by short-range interactions and that, on average, the universe is not electrically charged, it is not surprising that a theory of gravity was needed. General relativity is indeed a theory of gravity but the equivalence principle allows us to identify its action with the space-time itself. It was Einstein himself [136] that, two years after the completion of his theory, decided to apply it to the universe as a whole: assuming an homogeneous distribution of matter he found a solution to his field equations in which the universe is expanding or contracting

[1] Houjun Mo, Frank van den Bosch, Simon White "Galaxy formation and evolution" (2010) [231].

[2] We should point out that "look into the sky" is here intended by means of a powerful telescope: with the naked eye we can only see stars from our own galaxy, with few exceptions.

depending on its total energy density. Being convinced that the universe must be static, he introduced an additional term in the equations: the cosmological constant $\Lambda$ (we will come back to this issue later). A solution to the Einstein's equations which embrace the expansion of space was found, independently, a few years later by Friedmann and Lemaître [154, 205]. Robertson and Walker [262, 263, 264, 309] then proved that this was the unique solution compatible with the *cosmological principle* which assumes that the universe, on the largest scales, is spatially homogeneous and isotropic (see appendix A.1 for a technical introduction). The first experimental confirmation of the newborn idea of an expanding universe came in 1929 when Hubble [181] measured, from their redshift, the recession velocity of galaxies and found a relation between the velocity at which a galaxy moves away from us and its proper distance: $v = H_0 D$, where $H_0$ is the Hubble constant. This observation, together with the Friedmann-Lemaître-Robertson-Walker (FLRW) metric and equations laid the foundation for the prevailing *standard model* of cosmology, or *Big Bang* model. Success for this model was not immediate as in the '30 and '40 other concurring scenarios were proposed such as Hoyle's *steady state* model (which we mention here also to stress the irony of the fact that it was Hoyle himself who coined the term *Big Bang* in 1949 on BBC radio). Important theoretical work was carried on by Gamow, Alpher and Herman [21, 22] in the subject of the thermal history of the universe, but it was the 1964 discovery of the *cosmic microwave background* (CMB) radiation by Penzias and Wilson [243] to tip the balance in favor of the *Big Bang* model.

Today, after decades of theoretical research and a history of successful experimental observations, we believe the universe has existed for 13.8 billion years, it is nearly flat and it is composed by 26.5% of cold dark matter (CDM), a - still to be discovered - form of matter which does not interact electromagnetically, 68.6% of dark energy (DE), an unknown form of energy behaving like a cosmological constant and only 4.9% of "familiar" particles: baryons [11]. We call this model $\Lambda$CDM and, although other promising alternatives are available (e.g. [229, 48, 281, 180, 49]), we will stick to it for almost all the research presented in this thesis. The $\Lambda$CDM model has been uphold by numerous experimental evidence; however, we have already mentioned two puzzles that show how measuring something does not mean we understand it. The first one concerns the nature of dark matter. As we already pointed out, the simplest cosmological observation one can perform is look at galaxies. It turns out that galaxies are just the cherries on top of a cake we still have to get our hands on. Not interacting electromagnetically, dark matter is very elusive but we can still infer its presence by looking at its gravitational effect. In fact we have evidence of dark matter on a wide range of scale. The most famous piece of evidence that upholds the existence of a significant component of non-baryonic matter are galaxies' rotation curves and clusters' velocity dispersion measurements: variations in the orbital circular velocity of stars (in a galaxy) at different distances from the center and the velocity dispersion of galaxies (in a cluster). The shape of the rotation curves is linked with the amount and distribution of matter via Kepler's third law and it turns out that visible matter alone can not account for the mass distribution necessary to explain these curves. On the other hand if a dark matter halo envelops a galaxy (or cluster) it can provide the linear growth of total mass with distance from the center necessary to

explain a flat rotation curve or a high velocity dispersion. Observationally the velocity curve of stars in the Andromeda galaxy was first observed by Vera Rubin in 1970 [265] (see also later measurement such as [304]) while for galaxies in the Coma cluster velocity dispersion was famously measured by Fritz Zwicky in 1933 [329]. Another important evidence for dark matter is provided by gravitational lensing: matter bends and distorts light-paths traveling near it and this means, in turn, that we can infer the amount and distribution of matter that caused a deformation of some background object's image. Cosmologist and astrophysicist usually distinguish between two regimes: *strong* and *weak* lensing. On the one hand strong lensing occurs when the lens is very massive, the source is not too far away and both are roughly aligned with our line-of-sight. In this scenario strongly distorted multiple images of the source are visible and we can try to reconstruct the mass distribution in the lens plane, As this is a purely gravitational effect it is sensitive also to non-baryonic matter (see e.g. [301] for an example). On the other hand in the weak lensing regime we do not get multiple images or arcs but instead the image is slightly magnified (convergence) or deformed (shear). The underlying idea is again what we described before: link the lensing effect with the distribution of (dark) matter between the source and us. We usually look at the shape of galaxies, i.e. their ellipticity, (even though lensing in the CMB is extremely important [206, 12]) and as we of course know only the average properties of the un-lensed galaxies, weak lensing is treated with a statistical approach (see [118] for the latest result of the Dark Energy Survey). We also point out that weak lensing allowed for the reconstruction of the dark matter distribution in the *Bullet cluster* [107]: two colliding clusters of galaxies where the different ways in which interacting baryonic matter and non-interacting dark matter behave during a collision are clearly visible. On cosmological scales measurement of the dark matter density $\Omega_{\rm cdm}$ are the baryon acoustic oscillations (BAO) in galaxy clustering [137, 56, 61, 25, 47] and the photon acoustic oscillations in the CMB. In the galaxy correlation function, for example, we can relate the position of the BAO peak with the speed of sound $c_s$ before recombination which, in turn, is related to the baryon-to-photon density ratio $R \equiv 3\Omega_b/4\Omega_\gamma$: we expect a peak in the correlation function at a (comoving) position equal to the sound horizon $s_{\rm hor}$ at redshift $z \sim 1100$ [241, 286, 141]. If no dark matter is present, however, we would expect a feature in the 2-point function positioned at $\sim 2s_{\rm hor}$. We will come back to this argumentation in section 1.1 and in chapter 5. In the CMB we observe a similar pattern as photons are slightly hotter in over-dense regions and colder in under-dense regions; however, since we usually look at the CMB spectrum in angular space we see a number of succeeding peaks. The position (in angular space) and the relative heights of these peaks encode informations about $\Omega_{\rm cdm}$ and $\Omega_b$ (and of course all the other cosmological parameters). Following this brief excursus we should point out that beside the indirect observational evidence we have discussed, the debate on the nature of dark matter amongst particle physicist is still ongoing [53, 23] and DM still escapes direct (non-gravitational) detection.

We now turn our attention to the second troubling component of the ΛCDM model: dark energy. In its simplest form dark energy is identified with the cosmological constant $\Lambda$. The need for this additional component in the model surfaced in 1998 with the measurement of the distance-redshift relation for type Ia Supernovae (SNIa) by Riess, Schmidt and Perlmut-

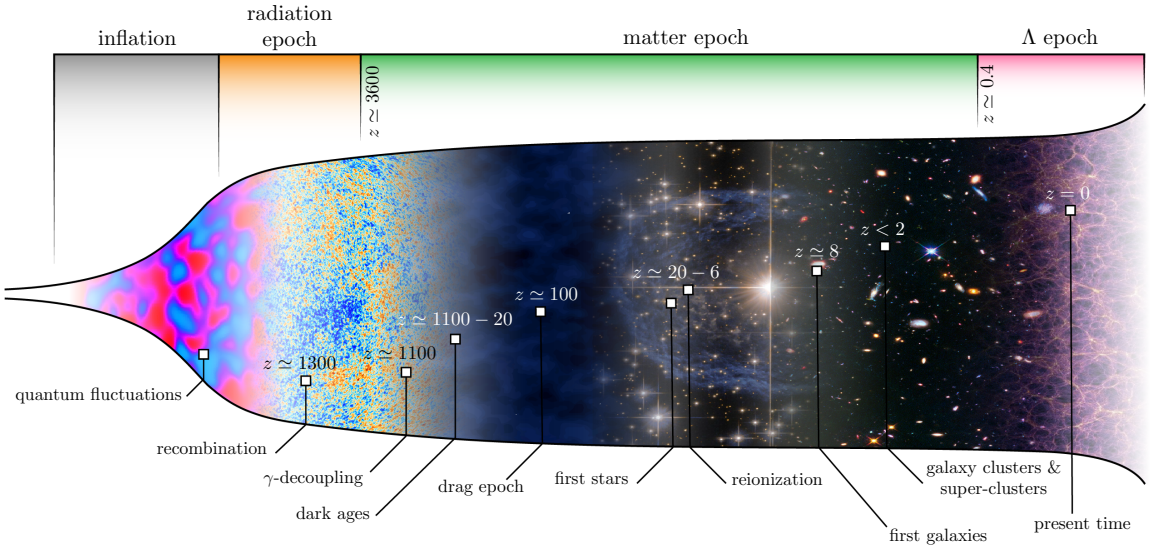


Figure 1.1: Sketch of the relevant phases in the evolution of the universe.

ter [260, 274, 244] (Nobel prize in 2011). The simple linear Hubble Law $v = H_0 D$ is only valid at small distances $D$ while at bigger distances the law is modified to account for the different components of the universe. Nowadays more evidence for $\Omega_\Lambda \neq 0$ has been gathered, mainly in the CMB power spectrum and with large scale structure (LSS) probes (DE modifies the clustering properties of the universe). So why is DE a problem? In its simplest realization, a cosmological constant, it is not very satisfactory from a theoretical point of view: in GR there is no formal reason to set it to zero nor to set it to any other value. Even if we allow $\Lambda \neq 0$ in the theory we are left with a fine tuning problem: the measured value differs from the vacuum expectation value predicted by quantum field theories (QFT) by a staggering 120 orders of magnitude: in other words to obtain an energy density $\rho_\Lambda$ as small as the one we observe we would need the contributions arising from QFT to cancel to better than a part in $10^{120}$ [96]. Possible solutions to this issue come in three flavors: i) modify the matter sector, ii) modify the gravity sector and iii) back-reaction. The line between point i) and ii) is sometimes blurry: consider, for example, an additional scalar field coupled to matter (e.g. massive gravity theories or *quintessence*). Are we modifying the gravity sector or the matter sector? In fairness we could also ask the same question regarding the cosmological constant: is it a modification of gravity or an additional matter field with constant energy-density and equation of state? The answer is somewhat arbitrary and some authors regard as modified gravity theories only theories in which the additional degrees of freedom (d.o.f.) are non-minimally coupled to the Einstein-Hilbert term in the action. A unified (effective) treatment of some class of DE and modified gravity models is possible via the effective field theory of DE [163]. The idea of modifying gravity to match theory and observations is a cornerstone of modern research in cosmology; however, as this subject is beyond the scope of this thesis we refer to the review [106] for a comprehensive discussion on this topic. We will limit ourself to

point out that probes which are sensitive to the DE behavior are extremely important as they could discriminate between possible deviations from a bare cosmological constant [185]. The third possible solution to the DE problem is back-reaction: the idea that inhomogeneities in the universe have an effect on its large-scale evolution. To state this idea in a more formal way let us introduce the Einstein field equations (EFE) for the first time:

$$G_{\alpha\beta}(g_{\mu\nu}) = 8\pi G\, T_{\alpha\beta}(g_{\mu\nu})\,. \tag{1.1}$$

Here $G_{\alpha\beta}$ is the Einstein tensor, $T_{\alpha\beta}$ is the energy-momentum tensor and they both depend on the metric tensor $g_{\mu\nu}$ (see appendix B.2). The back-reaction idea is based on the fact that due to the non-linearity of the EFE an averaging procedure is non-commutative: $\langle G_{\alpha\beta}(g_{\mu\nu})\rangle \neq G_{\alpha\beta}(\langle g_{\mu\nu}\rangle)$. The former is related to the average of the energy-momentum tensor $\langle T_{\alpha\beta}\rangle$ via the EFE; however, in cosmology we write down the FLRW equations using the latter $G_{\alpha\beta}(\langle g_{\mu\nu}\rangle)$. The difference between the two can potentially act as dark energy with the perk that this approach solves the *coincidence problem* (why are we living in a moment in cosmic history in which $\Omega_m \sim \Omega_\Lambda$?) by linking the late-time acceleration of the universe with the growth of structures. As of today this matter is still very much debated in the cosmology community (see [82, 85, 105, 142, 87, 86] and references therein).

Another topic that we ought to touch in this brief introduction is *inflation*: exponential expansion of the universe in its initial moments. The development of the inflationary theory began 25 years ago [165] to answer two[3] problems that were puzzling cosmologist: the *horizon problem* (why do we observe isotropic CMB radiation with a black body spectrum in patches of the sky that correspond to a distance much bigger than the causal horizon at the last scattering surface?) and the flatness problem (essentially a fine tuning problem: to obtain a flat model today $\Omega_{\rm tot} \simeq 1$ one needs to start with an extremely fine tuned value of $\Omega_{\rm tot} = 1 \pm 10^{-60}$ [97] as $\Omega_{\rm tot} - 1$ decreases going backwards with time). Inflation can solve both of these issues. As we said it consists of a period of exponential expansion, meaning that the scale factor grows as $a \sim e^{\mathcal{H}t}$ and this means that the causal horizon also grows exponentially while the Hubble horizon is constant: if inflation lasts long enough by the end of it the causal horizon is bigger than any sub-Hubble length scale, thus solving the first problem. The second issue is also solved as the quantity $\Omega_{\rm tot} - 1$ is exponentially suppressed during inflation and when inflation ends we are left (locally) with an almost perfectly flat model. In order to achieve accelerated expansion we need the pressure and energy density of the dominant component in the universe to satisfy $p < -\rho/3$. This condition can be satisfied by means of a simple scalar field: the inflaton, but many models of inflation have been proposed (see [208, 81, 261, 41] for reviews) as constrains in the parameter space get tighter [14]. As a "bonus" inflation not only explains why we experience an homogeneous universe but also explains the little inhomogeneities: the seed perturbations which allow the gravitational growth into structures. In the inflationary paradigm they are explained by quantum fluctuations of the inflaton, brought to cosmological scale during the exponential expansion phase. These perturbations are responsible for the temperature fluctuations observed in the CMB

[3] three problems if we include the *magnetic monopole problem* [255] which, in truth, was what inspired Guth in the first place [173].

spectrum [178, 11]: one of the biggest achievements of the hot big bang model. This observation somewhat closes the circle of our excursus in which we hope we have given the reader a feeling for the interesting topics covered in modern cosmology and its challenges.

As a last remark it is interesting to notice the interplay between theory and observations: like in others fields of physics cosmologists were sometimes in a situation in which theoretical arguments anticipated observations (e.g. the detection of CMB radiation or, possibly, the detection of primordial gravitational waves) while other times it is experimental evidence that awaits for theoretical understanding (e.g. the dark sector) and the community invests in new probes to find hints on the theoretical direction to follow. It is then often said that nowadays cosmology "is a data driven science" or that we "entered the precision era of cosmology"[4]. Let us try to put into numbers this argument for CMB experiments and galaxy surveys. The first measurement of the CMB anisotropies was carried out by the COBE satellite (1989) that reached an angular resolution of 7° with a sensitivity of 0.1mK; WMAP (2001) improved these figures to 0.2° and 35$\mu$K while Planck (2009) had a resolution of 5 arc-min and a sensitivity of $\sim 5\mu$K. The next generation satellites promise an order $\sim 10$ improvement [1, 117]. It is clear that these numbers translate into precision on the determination of cosmological parameters in a non-trivial way but the trend is clear. The same objection holds for galaxy survey but we could still quote the exponential improvement on the number of galaxies observed: cfA (completed 1982) gathered spectra for 2200 galaxies, cfA2 (1995) for 18000, 2dF (2002) observed $\sim$ 220000, SDSS (ongoing) roughly a million and Euclid (launch 2020) will have a catalog with 10 millions tracers. With this overwhelming amount of data coming (especially on the LSS side), will we understand what we measure? The goal of this work is, we hope, to contribute to this matter.

This thesis is organized as follows. The remainder of this chapter is dedicated to an introduction to the main subjects of this work: galaxy clustering (and perturbation theory) and light-cone effects. In chapter 2 we introduce the galaxy number counts and compute how projection effects modify this observable. We will follow Durrer & Tansella (2016), which computed the projection effects for vector and tensor perturbations, and integrate the results of this work with the well-known results for scalar perturbation as we will use them throughout this thesis. In chapter 3 we begin our study of the galaxy two-point function, presenting the theoretical framework developed in Tansella et.al. (2017). In chapter 4 we detail how the results of chapter 3 have been employed to write the code COFFE, presented in Tansella et.al. (2018a). We will also discuss some subtleties regarding the two-point function (further examined in chapter 7) and present forecast on the detectability of the lensing signal in the galaxy correlation function. Chapter 5 follows Tansella (2018) in which we point out the existence of a second feature in the matter two-point function, besides the acoustic peak, due to the baryon-baryon correlation in the early universe and positioned at twice the distance of the peak. In chapter 6, based on Tansella et.al. (2018b), we present a suitable decomposition to discuss the signal induced by anisotropic vector perturbation in the galaxy

[4]This sentence was actually used by the Nobel-prize committee for the 2006 prize (`https://www.nobelprize.org/nobel_prizes/physics/laureates/2006/press.html`).

two-point function and perform a Fisher forecast to determine the detectability of the parameters which characterise the anisotropy with planned or futuristic galaxy catalogs. Although part of this thesis, different chapters are thought to be self-contained.

## 1.1 Galaxy clustering

The definition of galaxies poses no difficulties in cosmology. They are easily identifiable objects as the density of stars inside them is roughly $\sim 10^7$ times the average density in the universe[5]. It is interesting to note however that at the beginning of the last century the debate on whether observed galaxies where part of the Milky way or external objects was very spirited. It was Hubble in 1920 that settled what went down in history as *the Great debate* [299]. From a cosmological point of view we essentially want to study how primordial fluctuations coming from inflation and imprinted in the CMB are amplified through gravitational instability to form the LSS of the universe. What seems like a simple task is however extremely complicated. Firstly, we need to deal with physics governing a very wide range of scales: from the size of the Hubble horizon $\mathcal{H}_0^{-1} \sim 4000\,\mathrm{Mpc}$ to the typical size of galaxies $\sim 10\,\mathrm{kpc}$ and secondly one in principle needs to solve the coupled Boltzmann-Liouville equations for each species in the universe. At early times perturbations enjoy, at least, some useful properties. As they come from quantum fluctuations of the inflaton field, their Fourier coefficients have a Gaussian probability distribution. Each coefficient is uncorrelated with the other, hence also the real space fluctuations are Gaussian. Furthermore the variance is independent of the direction of the wave-vector $\mathbf{k}$: for the primordial curvature perturbation we usually write $\mathcal{P}_\zeta \sim k^{n_s-1}$. If the spectral index $n_s$ is unity we have a scale-invariant spectrum while observations suggest $n_s \simeq 0.96$, a slightly red spectrum. When perturbations are small (as they are in the early universe) we can linearize the relevant equations and treat them in the regime of *linear* perturbation theory, where different Fourier modes evolve independently. The way in which curvature perturbations translate into late-time perturbations is usually encoded in the transfer function: for the matter density contrast we could for example write $\delta_{\mathbf{k}}(\eta) = S(k,\eta)\zeta_{\mathbf{k}}$ where $\zeta_{\mathbf{k}}$ is the value at horizon exit during inflation. The same equation can be written, with a different transfer function, for each species in the universe and for the metric perturbations (e.g. the gravitational potential $\Phi$). For a pressure-less, collision-less fluid (i.e. CDM), taking moments of the Liouville equation[6] we end up with a Boltzmann hierarchy with only two equations (continuity and Euler equations) which is closed by the Poisson equation. For other species, such as baryons and photons, the hierarchy is not naturally closed and to compute the transfer function we have to rely on numerical codes like CLASS [67] and CAMB [207] or on analytic approximations [139]. An important effect that early universe physics imprints on the matter correlation function (and power spectrum) are the BAO which originate in the primordial plasma when baryons are tightly coupled to photons via Thompson scattering. To heuristically explain this process let us focus on some

[5] This does not mean however that galaxies have well defined boundaries.

[6] In the case of a non-relativistic and collision-less fluid the mean-field limit of the Boltzmann-Liouville equation is called Vlasov equation.

initial over-dense patch of the plasma: if the fluctuations are adiabatic[7] the over-density will be shared by all species. In particular a region over-dense in photons will also have an over-pressure with respect to its surroundings. This pressure imbalance causes an acoustic wave in the baryon-photon plasma which travels at the speed of sound $c_s$ until recombination. When photons decouple from the plasma the baryon's speed of sound goes to zero and the wave is frozen: the initial over-density is now composed only of DM while baryons have created an over-dense spherical region around the initial point. Every over-density will behave as we just described and the net result is that matter is more likely to cluster with a correlation length corresponding to the sound horizon at recombination. It is clear that this process, as we have already anticipated, is responsible for the BAO peak: the correlation function is defined as the excess probability (over Poisson noise) of finding two tracers separated by a comoving distance $r$ and hence it peaks for $r \sim s_{\rm hor}$. We have also learned that after recombination, with photons out of the picture, baryons have essentially no pressure and we can treat them, together with CDM, as a pressure-less fluid (or *dust*). There are essentially two approaches to deal with the perturbation theory of dust: *Eulerian* and *Lagrangian*. The former (sometimes called standard perturbation theory, or SPT) relies on a perturbative expansion of the density and velocity fields of matter in fixed (comoving) coordinates [55, 80, 50, 131]. The latter (Lagrangian perturbation theory, or LPT) follows the trajectories of particles or fluid elements relating the Eulerian position to the initial Lagrangian position through a displacement vector [80, 135, 50, 256, 221, 33]. The main prediction of linear perturbation theory is the growth of matter density fluctuations with time, given by the function $D_1(\eta)$ called the growth function.

To complicate a bit this simple picture one needs to account for the *gauge freedom* in the theory: when we describe perturbations we are talking about two different manifolds. The physical manifold $(\mathcal{M}, g_{\mu\nu})$ and the fictitious background manifold $(\bar{\mathcal{M}}, \bar{g}_{\mu\nu})$ with respect to which the perturbations are defined. For a given coordinate system in the background there is no natural choice of coordinates in the perturbed space-time: different coordinates are related by a gauge transformation and fixing them corresponds to a gauge choice. With a gauge transformation we can introduce spurious degrees of freedom in the metric perturbations which are unphysical but still satisfy the linearized EFE, hence the need of developing perturbation theory in terms of gauge invariant variables. Pioneering work in this direction was first carried out by Lifshitz in 1946 [209] and later on by the other architects of the gauge invariant perturbation theory [35, 201, 144, 236, 284, 130]. The main idea of this approach is to write down perturbations of the metric tensor and the energy momentum tensor, study how they behave under a gauge transformation and then combine them into gauge invariant quantities such that the theory is no longer plagued by the gauge freedom and exhibit only the physical degrees of freedom. We can quickly count them: let us perturbe the metric around the FLRW solution as $g_{\mu\nu} = \bar{g}_{\mu\nu} + \delta g_{\mu\nu}$. The perturbation $\delta g_{\mu\nu}$, being a symmetric tensor, has 10 d.o.f. which can be split (via Helmholtz decomposition) into scalar (4 d.o.f.), vector

[7] We call the perturbations *adiabatic* if all the species are perturbed in the same way and the total curvature perturbation is space-dependent, as opposed to *isocurvature* fluctuations for which the ratio of different species varies in space but the total perturbation is constant.

(4 d.o.f.) and tensor (2 d.o.f.) components, with the advantage that the scalar, vector and tensor evolution equations are decoupled in linear theory. With a coordinate transformation we can "gauge away" 2 scalars and 2 vectors hence revealing the 6 physical d.o.f. of the theory (2 scalars, 1 transverse vector and 1 transverse trace-less tensor). A *gauge choice* essentially fixes how the physical d.o.f. are combined into $\delta g_{\mu\nu}$: in this thesis we will mainly work in *Poisson gauge* in which one scalar is described by $\delta g_{00}$, the transverse vector by $\delta g_{0i}$ and the other scalar together with the transverse trace-less tensor by $\delta g_{ij}$. The issue of gauge invariance unfolds in a similar way for the energy-momentum tensor $T_{\mu\nu}$. Let us finally point out that what we have sketched here is sometimes called the *metric approach* to perturbation theory and an important alternative to it is the *1+3 covariant approach* [174, 143, 146, 104]. For a technical discussion on linear perturbation theory we refer the reader to [131] or to appendix A.2.

Linear perturbation theory is able to describe a significant range of scales and most of the history of the universe but as all good things it must come to an end: it eventually breaks down. It is difficult to define a "non-linear scale" beyond which we cannot trust the linear predictions anymore but it is clear that as perturbations grow under the effect of gravity it will come a point where different techniques must be employed. Leaving the comfortable ground of linear physics, complications are quick to arise: as there is no general exact solution in the non-linear regime one must still rely on some expansion scheme, with the added complication of *mode coupling* (i.e. Fourier modes do not evolve independently anymore) and the subsequent loss of the Gaussian properties. Furthermore the convergence properties of some schemes are in question when higher order contributions get bigger than the lower order ones and do not improve agreement with N-body simulations [65, 64, 94]. Different techniques have been developed in the recent years; some straightforward, such as higher order SPT [289, 218, 188, 276] and LPT [84, 256, 222], some more involved such as *Time-RG* theory [245], *Renormalization group* perturbation theory [224], *Lagrangian resummation* theory [220, 219], *Effective field* theory [45, 95, 79], *Time sliced* perturbation theory [62] and others [296, 303]. These approaches are able to push the reach of perturbation theory in the so-called *quasi-linear* scales ($\gtrsim 0.1\ \mathrm{Mpc}^{-1}$ at $z = 0$) but eventually we enter the *non-linear* scales where a perturbation theory description is not at all suited. The best bet is then to rely on (time-consuming) N-body simulations to follow the growth of structure at small-scales ([283, 282, 8] among many others). To gain insight on non-linear collapse we can nevertheless construct oversimplified, heuristic models such as the Spherical collapse model, Secondary Infall Models [164, 149, 54] and the Zeldovich approximation [325] which help understanding the different phases of collapse until a *virialized*[8] structure is formed. The main result is that a region in which the (extrapolated) linear density field is bigger than the critical value $\delta(\mathbf{x}, \eta) > \delta_c \simeq 1.686$ will have collapsed to form a structure (dark matter halo) by time $\eta$. It is natural to wonder which is the probability that the Gaussian density field is bigger that $\delta_c$ or, a closely related question, which is the number of dark matter halos per comoving volume with a certain mass: the halo mass function. Theoretical understanding of this issue comes

[8]Virialized means a system of gravitationally interacting particles that is stable (i.e. self-gravitating or decoupled from the Hubble flow): its kinetic and potential energy satisfy the virial theorem $2K + U = 0$.

from the Press-Schechter formalism [246] or, in a more recent formulation, the Excursion Set Formalism [69, 277].

The reason for which we are interested in the properties of dark matter halos is because galaxies form (with a complex process of cooling of baryonic gas[9]) inside them. In fact it is generally assumed that galaxies follow the matter distribution within their host halo. The challenging task is then to relate the statistical properties of the matter field (given by the linear or beyond-linear perturbation theory) to the statistic of halos and hence of galaxies: this problem goes under the name of *galaxy bias*. This subject is both interesting from a theoretical point of view and crucial if we want to relate our theory with observations: it is in fact clear that in general we do not observe the matter field (with the notable exception of gravitational lensing as discussed above) but tracers of it. For example a galaxy is a tracer of the density field (although not the only one, we will sometimes use the word "tracer" as a synonym of "galaxy" in this work) but as galaxies are collapsed, non-linear objects the way in which they mirror the density field is non-trivial. In its simplest formulation the bias is linear and scale-independent: it can be defined as the ratio of the correlation function of the tracers with respect to the correlation function of matter $b = \sqrt{\xi_{\text{tracer}}/\xi_m}$. At large scale this is a good approximation [306, 156] (and we will stick to it for the purposes of this thesis), however at smaller scales (or if we want to profit from more precise surveys, e.g. [159]) a full *bias expansion* is required: a finite number of bias parameters is then needed to relate the galaxy density to the properties of the large-scale environment. For a comprehensive review of the concept presented in the last two paragraphs see [121].

## 1.2 Light-cone effects

Cosmological observations are restricted to objects and sources which are located on our past light-cone. Given a space-time $(\mathcal{M}, g_{\mu\nu})$ we can define the past light-cone for any point $x^\mu$ as the set of points $y^\mu$ for which exists a *null* geodesic joining $y^\mu$ to $x^\mu$. Essentially it contains all the events that can be observed at $x^\mu$ through light propagation[10]: in cosmology the light-cone is a 3-dimensional null surface parametrized by two angles $(\theta, \phi) \equiv \hat{n}$, which define the direction of observation, and the redshift $z$. This has an immediate consequence and a more subtle one. The immediate consequence is that our possibilities to probe the universe are fundamentally limited: we cannot observe something that lies outside our light-cone. The second consequence is a modification of the geometry of the light-cone due to the perturbations in the universe. As light-like geodesic are conformally invariant, the background universe has the light-cone geometry of Minkowski space. On the other hand if we introduce perturbations to

[9] See [231] sections 1.2.4 and 8.4 for details.

[10] It is clear from the definition that two different observers have distinct light-cones. This is in general not a practical concern in cosmology due to the time-scale of the processes it describes; however, an interesting possibility was envisioned in [271]: the *redshift drift*. The idea is to collect data from the two light cones at the observer space-position but separated by the time period $\Delta t$ and look for the change of redshift of a source given by $\Delta z \simeq [(1+z)H_0 - H(z)]\Delta t$.

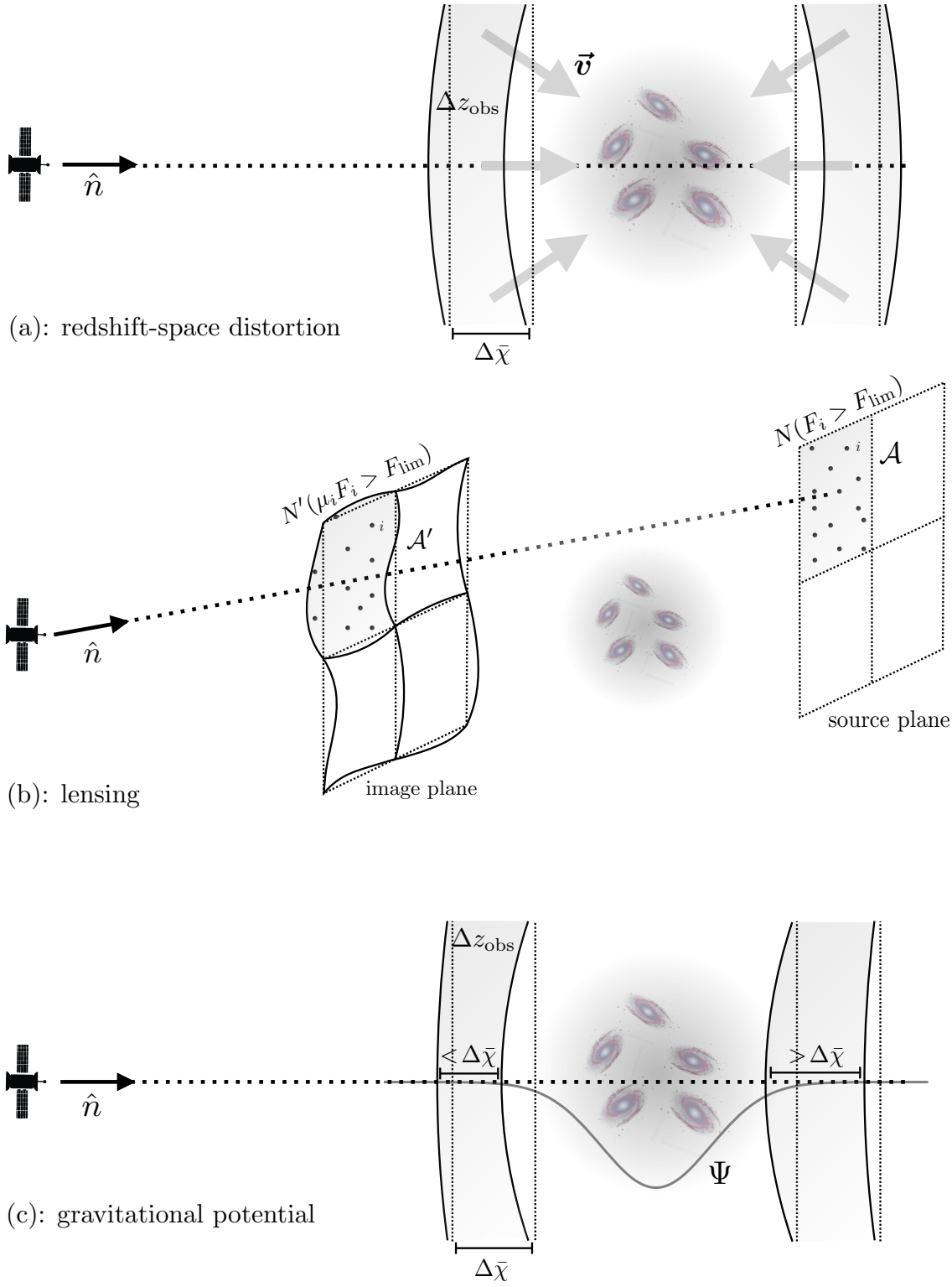


Figure 1.2: The effect of redshift-space distortion (*top*), lensing (*middle*) and the local gravitational potential (*bottom*) on the galaxy number counts. See text for the discussion.

the metric one needs to solve the perturbed null geodesic equation to follow the propagation of light. Since, as we said, we do not observe spatial hyper-surfaces but the past light-cone, this is an effect which must be taken into account when we compare theoretical predictions to observables: the coordinates $(\theta, \phi, z)$ will receive corrections due to the inhomogeneities in the universe $(\delta\theta, \delta\phi, \delta z)$, that, if not accounted for, will lead to misinterpretations of our measurements. We will take as an example the *galaxy number counts* as they represent the main measurement we will deal with in this thesis. This observable is constructed by *binning* a galaxy catalog into redshift slices of thickness $\Delta z$ and solid angle bins $\mathrm{d}\Omega$ and then counting the number of galaxies per bin $N(\hat{n}, z)$. The fluctuations in the number of tracers per bin with respect to the directional average $\langle N \rangle_\Omega(z)$ is denoted by $\Delta(\hat{n}, z)$ (we will give the proper definition in section 2.2) and can be related to the matter fluctuation in the same bin $\delta_m$, through the simple linear bias relation $\Delta \simeq b \cdot \delta_m$. Light-cone effects (often called relativistic effects or projection effects) enter this measurement as they modify the shape, the angular position, the radial distance and the number of tracers.

To gain intuition on how this happens we will give an heuristic description, with the help of figure 1.2, of three projection effects: redshift-space distortion (RSD), lensing and the local potential terms. The first formulation[11] of RSD was given by Kaiser in 1987 [198] (it is in fact sometimes called *Kaiser effect*): the idea is that the mapping from real space to redshift space is not only derived by considering the Hubble flow, but one also needs to account for the peculiar velocities of the tracers which induce an additional Doppler shift. In figure 1.2 (a) we sketch the typical situation in *real space*. Imagine an observer looking in direction $\hat{n}$ towards a spherical over-density: galaxies in front and behind the halo will have coherent peculiar velocities (grey arrows) in the direction of the over-dense region which will cause a perturbation $\delta z$ in the observed redshift. In particular galaxies in front, as they are moving away from the observer will appear redder than the Hubble flow would dictate and, vice versa, galaxies behind will appear blue-shifted. In the figure dashed lines are surfaces of constant distance $\bar{\chi}$ = const, and solid lines are iso$-z$ surfaces $z_{\mathrm{obs}}$ = const: as the change in redshift is proportional to the projection of the peculiar velocity $\hat{n} \cdot \vec{v}$ tracers closer to the line-of-sight will be more red-shifted (resp. blue-shifted) than the others and hence they have to be closer to us (resp. further away from us) to lay on the same iso$-z$ surface. When we bin a catalog into redshift slices and compute the correlation function this effect induces the famous *pancake* shape [257]. In the second panel (figure 1.2 (b)) we consider lensing: we already discussed how inhomogeneities in the universe bend the photons geodesics. In practice this means that a source with background position $\hat{n}$ will be seen by the observer at a different position $\hat{n} + \delta\hat{n}$. The effect of lensing is two-fold: firstly a solid angle bin $\mathcal{A}$ at the source position will be magnified and distorted so that in the image plane it describes a different area $\mathcal{A}'$. Secondly we must consider *flux magnification*: a galaxy survey can only observe sources with an intrinsic flux grater than some limiting

[11] Note that here we are discussing the "large scales" redshift space distortion, the *pancakes of God* effect, due to the coherent infall of galaxies towards a central mass. At smaller, non-linear scales the random velocity dispersions in galaxy clusters also induces RSD, elongating the observed structure along the line-of-sight: an effect know as *fingers of God* [186].

value $F_{\rm lim}$. If we start with a bin containing a number $N(F_i > F_{\rm lim})$ of tracers with this properties (i.e. we count only the galaxy with intrinsic flux $F_i$ big enough for our detector sensitivity), lensing will cause us to observe a higher (or lower) flux from the sources and we will actually detect a number $N'(\mu_i F_i > F_{\rm lim})$ of tracers, where $\mu$ is the magnification factor. Lensing is one of the so-called *integrated effects* as the calculation requires the integration of the photon geodesic along the line-of-sight. As a last example we consider the effect of the gravitational potential at the source position, in figure 1.2 (c). Our sketch is similar to the one we did for redshift-space distortion, except now the perturbation in the observed redshift is given by the gravitational redshift which adds to the Hubble flow as photons have to climb the potential well of the halo (grey solid line). Galaxies which are closer to the over-density will appear redder and hence the iso$-z$ surfaces are (in real space) "bent" towards the observer: redshift bins in the catalog $\Delta z_{\rm obs}$ will cover a bigger physical volume if they are behind the potential well rather than in front of it. Other projection effects include, notably, the *Shapiro time delay*, a perturbation in the radial distance due to the gravitational potentials that the photon encounters from the source to the observer, and the *Integrated Sachs-Wolfe* effect (ISW) [267], gravitational redshift effect that occurs when light travels through a time evolving potential. In summary galaxy number counts not only describe the matter density but also the light-cone effects: we will carefully derive the full expression in chapter 2. We will mainly deal with number counts and galaxy 2-point function in this thesis but relativistic effects also play a role in various LSS observables: higher order $n-$point functions such as the bispectrum [123, 127, 302, 195, 196], cross-correlations [158], the luminosity distance [73, 59], quasars and the Lyman$-\alpha$ forest [184], the Hubble diagram [152] and 21-cm intensity mapping [170].

# CHAPTER 2

## Vector perturbations of galaxy number counts

**Based on:**

[134] R. Durrer and V. Tansella, "*Vector perturbations of galaxy number counts*", **JCAP 1607** (2016) 037, [arXiv:1605.05974].

**Abstract.** In this chapter we derive the contribution to the relativistic galaxy number counts fluctuations from vector and tensor perturbations within linear perturbation theory. In this thesis we also detail the computation for the scalar contribution both for completeness and because we will make a large use of it in the following chapters. The result for vectors and tensors is consistent with the relativistic corrections to number counts due to scalar perturbations, where the Bardeen potentials are replaced with line-of-sight projection of vector and tensor quantities. Since vector and tensor perturbations do not lead to density fluctuations they do not contribute to the standard density term in the number counts. We apply our results to vector perturbations which are induced from scalar perturbations at second order and give numerical estimates of their contributions to the power spectrum of relativistic galaxy number counts.

## 2.1 Introduction

As promised in section 1.2, we review in this chapter the general relativistic description of galaxy clustering at linear order in perturbation theory. We introduce the observable *galaxy number counts* and discuss how projection effects must be taken into account if we want to compare theory with observations.

Within the last decade, cosmology has become a precision science, especially thanks to the very accurate measurements of the temperature fluctuations and the polarisation of the cosmic

microwave background with the Planck satellite [11]. These measurements have allowed us to determine cosmological parameters with a precision of 1% and better. Now we plan to continue this success story with very precise and deep large scale observations of the galaxies distribution. Several observational projects are presently under way or planned [2, 18, 129, 204, 116, 216].

In order to profit maximally from these future data, we have to understand very precisely what we are measuring. With perturbation theory and N-body simulations we compute the spatial matter density distribution in the Universe, while we observe galaxies in different directions on the sky and at different redshifts. The relation between the matter density and galaxies is the so called biasing problem. On large scales we expect biasing to be linear and in the simplest cases not scale dependent. Another problem is the fact that we observe redshifts and directions while the matter density fluctuations are calculated in real (physical) space. In order to convert angles and redshifts into physical distances we have to assume cosmological parameters. On the other hand, we would like to use the observed galaxy distribution to *infer* cosmological parameters. Therefore we have to calculate the density fluctuations in angular and redshift space (i.e. coordinates on the light-cone) to compare it directly with observations. This leads to several additional terms in the observed galaxy number counts due to the fact that also directions and redshifts are perturbed in the presence of fluctuations.

In the recent years, the truly observable density fluctuations have been determined in angle and redshift space [321, 72, 99]. In addition to the usual galaxy fluctuations there are contributions from redshift space distortions (RSD), lensing, Shapiro time delay, an integrated Sachs-Wolfe (ISW) term and several other contributions from the gravitational potential which are due to the perturbations of the observed direction and redshift. Additional effects such as galaxy bias and primordial non-gaussianities are discussed in [191, 193]. A generalisation to non-flat geometries is given in [126]. Galaxy number counts have recently also been calculated to second order [51, 324, 122] and the bispectrum has been determined [123]. Reviews on this topic can be found in [318, 70] and - with the general "cosmic rulers" and "cosmic clocks" formalism - in [192].

In this chapter we determine the galaxy number counts from vector and tensor perturbations (see also [100, 51]). This is relevant for different reasons. First of all, the non-linearities of structure formation induce vector and tensor fluctuations as first discussed in [232] and then further in [46, 214, 24]. The first estimate of the vector power spectrum was carried out in [215] and it has been shown recently [7] that the induced frame dragging can become quite substantial, of the order of 1%. For discussion on small scales non-linear effects see [83, 27]. Furthermore, if cosmology is not standard ΛCDM, e.g. if there is a contribution from cosmic strings, the presence of vector perturbations may be a very interesting diagnostic.

We also introduce the angular-redshift power spectrum $C_\ell(z_1, z_2)$. This quantity has been introduced in [72, 99], where it has also been shown that due to relativistic projection effects, the linear power spectrum is not simply given by density fluctuations and redshift-space distortions, but, as we said, it acquires several additional terms from lensing, ordinary and integrated Sachs Wolfe terms, gravitational redshift, Doppler terms, and Shapiro time delay. These projection effects had been previously identified in [321, 317].

Subsequently, linear Boltzmann codes like CAMB [207] and CLASS [66] have been general-

ized to calculate this galaxy count angular power spectrum [125, 124].

The remainder of this chapter is organised as follows. In the next section we derive the expression for perturbations of number counts from scalar, vector and tensor perturbations. Equations (2.47) and (2.48) are the main results of section 2.2. In particular we will make extensive use of (2.47) in this thesis. In section 2.3 we apply our result to second order vector perturbations. This gives a good indication of the order of magnitude of vector perturbations induced at second order in the number counts. In section 2.4 we summarise our findings and conclude.

We work with a flat Friedmann-Lemaître (FL) background using conformal time denoted by $\eta$, such that

$$\mathrm{d}s^2 = a^2(\eta)\left(-\mathrm{d}\eta^2 + \delta_{ij}\mathrm{d}x^i\mathrm{d}x^j\right) .$$

Spatial vectors are indicated by boldface symbols and by latin indices, while the 4 spacetime indices are greek. A photon geodesic in this background which arrives at position $\mathbf{x}_0$ at time $\eta_0$ and which has been emitted at affine parameter $\lambda = 0$ at time $\eta_s$, moving in direction $\mathbf{n}$ is then given by $(x^\mu(\lambda)) = (\eta_s + \lambda, \mathbf{x}_0 + (\lambda + \eta_s - \eta_0)\mathbf{n})$. Here $\lambda = \eta - \eta_s = \bar{\chi}_s - \bar{\chi}$, where $\bar{\chi}$ denotes the comoving distance $\bar{\chi} = |\mathbf{x}(\lambda) - \mathbf{x}_0|$, hence $d\bar{\chi} = -d\lambda$. We can of course choose $\mathbf{x}_0 = 0$. We denote the derivative w.r.t. conformal time $\eta$ by an overdot such that the conformal Hubble parameter is $\mathcal{H} = \dot{a}/a = aH$.

## 2.2 Relativistic galaxy number counts

Galaxy surveys provide a catalog which contains the redshift and the angular position for every observed galaxy. The mapping from the artificial FLRW background coordinates and the observed ones is non-trivial - as observed coordinates are affected by perturbations in the universe - and it gives rise to the projection effects. As we discussed in the Introduction, *gauge freedom* implies that the background-perturbations splitting is not uniquely determined; however, as number counts are observable and hence gauge invariant, we have the freedom to perform the derivation in an arbitrary gauge. We chose Poisson gauge (see Appendix A.2 for details) and write the metric as

$$\mathrm{d}s^2 = a^2\left[-(1+2\Psi)\mathrm{d}\eta^2 - 2S_i\,\mathrm{d}\eta\mathrm{d}x^i + \left[(1-2\Phi)\delta_{ij} + 2H_{ij}\right]\mathrm{d}x^i\mathrm{d}x^j\right] . \tag{2.1}$$

Here $\Psi, \Phi$ are the Bardeen potentials, $S_i$ is a transverse vector and $H_{ij}$ is a transverse-traceless tensor, i.e., $\partial^i S_i = 0$, $\partial^i H_{ij} = 0$ and $H^i_i = 0$.[1]

We follow the approach of [72, 233] generalising the derivation with the metric (2.1). We consider the number of galaxies in direction $-\mathbf{n}$ at redshift $z$, called $N(\mathbf{n}, z)d\Omega_{\mathbf{n}}dz$. The average over angles gives their redshift distribution, $\langle N\rangle_\Omega(z)dz$. The galaxy density perturbation

[1] Spatial indices of perturbed quantities are raised and lowered with $\delta^{ij}$.

at fixed redshift in direction $\mathbf{n}$ is given by

$$\begin{aligned}\delta_z(\mathbf{n},z) =& \frac{\rho_g(\mathbf{n},z)-\langle\rho_g\rangle_\Omega(z)}{\langle\rho_g\rangle_\Omega(z)} = \frac{\frac{N(\mathbf{n},z)}{V(\mathbf{n},z)}-\frac{\langle N\rangle_\Omega(z)}{V(z)}}{\frac{\langle N\rangle_\Omega(z)}{V(z)}} \\ =& \frac{N(\mathbf{n},z)-\langle N\rangle_\Omega(z)}{\langle N\rangle_\Omega(z)} - \frac{\delta V(\mathbf{n},z)}{V(z)}\,,\end{aligned} \tag{2.2}$$

where $V(\mathbf{n},z)$ is the physical survey volume density per redshift bin, per solid angle and $\rho_g$ denotes the galaxy density per comoving volume. The volume is also a perturbed quantity since the solid angle of observation as well as the redshift bin are distorted between the source and the observer. Hence $V(\mathbf{n},z) = V(z) + \delta V(\mathbf{n},z)$. The observed perturbation of the galaxy number density is

$$\frac{N(\mathbf{n},z)-\langle N\rangle_\Omega(z)}{\langle N\rangle_\Omega(z)} = \delta_z(\mathbf{n},z) + \frac{\delta V(\mathbf{n},z)}{V(z)} \equiv \Delta_g(\mathbf{n},z)\,. \tag{2.3}$$

The redshift density perturbation $\delta_z(\mathbf{n},z)$, the volume perturbation $\delta V(\mathbf{n},z)/V(z)$ and hence the galaxy number counts $\Delta_g(\mathbf{n},z)$ are gauge invariant quantities [72]. Note that the vector and tensor perturbations do not lead to density fluctuations, their contributions to the number counts fluctuation comes from two terms: the redshift perturbation $\delta z$ which contributes to $\delta_z(\mathbf{n},z)$ and the volume perturbation $\delta V$.
In the following two sections we never use Einstein equations, hence the results are valid for general theories of gravity as long as tracers follow geodesics.

### 2.2.1 Redshift perturbations

We start by relating the redshift density perturbation $\delta_z(\mathbf{n},z)$ to the metric and energy-momentum tensor perturbations. Note that in order to do this we assume ergodicity and we replace the directional averages in eq. (2.2) with ensemble averages, denoted by $\langle\rangle$. We will come back to this subtlety in section 4.2.2 and chapter 7. Expanding in Taylor series $\langle\rho_g\rangle_\Omega(z) \equiv \langle\rho_g\rangle(z) = \bar\rho_g(z) = \bar\rho_g(\bar z) + \partial_{\bar z}\bar\rho_g\,\delta z(\mathbf{n},z)$, where $z = \bar z + \delta z$, we obtain [72]:

$$\delta_z(\mathbf{n},z) = \delta_g(\mathbf{n},z) - \frac{\mathrm{d}\bar\rho_g(\bar z)}{\mathrm{d}\bar z}\frac{\delta z(\mathbf{n},z)}{\bar\rho(\bar z)} = \delta_g(\mathbf{n},z) - \frac{3}{1+\bar z}\delta z(\mathbf{n},z)\,, \tag{2.4}$$

where we have defined

$$\delta_g \equiv \frac{\rho(\mathbf{n},z)-\bar\rho(\bar z)}{\bar\rho(\bar z)}\,. \tag{2.5}$$

For the second equal sign of (2.4) we have used $a^3\bar\rho_g = \text{const.}$, so that

$$\partial_{\bar z}\bar\rho_g = 3\bar\rho_g/(1+\bar z)\,. \tag{2.6}$$

Note that at linear order we can evaluate first order quantities at the background position: for example the difference between $\delta_g(\mathbf{n},z)$ and $\delta_g(\bar{\mathbf{n}},\bar z)$ is second order small and we neglect it. Let us also stress that the density contrast $\delta_g$ is *not* gauge invariant.

In the perturbed universe a photon emitted by a galaxy, the source $s$, arrives at the observer $o$ with redshift

$$1+z=\frac{(n^\alpha u_\alpha)_s}{(n^\alpha u_\alpha)_o}. \tag{2.7}$$

Here we have introduced the perturbed photon momentum $n=a^{-2}(1+\delta n^0,\bar{\mathbf{n}}+\delta\mathbf{n})$, where $\bar{\mathbf{n}}$ is the unperturbed radial direction.[2] The observer 4-velocity is $u=a^{-1}(1-\Psi,\mathbf{v})$ and one should keep in mind that the peculiar velocity $\mathbf{v}$ is of the same order as the metric fluctuations. A brief first order calculation, ignoring unobservable contributions at the observer position, yields

$$(1+z)\simeq(1+\bar{z})\left(1+\delta n^0_s-\delta n^0_o+(S_iv^i)_s-(v_in^i)_s\right)=(1+\bar{z})\,(1+\delta z)\ . \tag{2.8}$$

Solving the (conformally related) geodesic equation $\frac{\mathrm{d}}{\mathrm{d}\lambda}\delta n^0=-\Gamma^0_{\alpha\beta}n^\alpha n^\beta$ we obtain

$$\delta n^0_o-\delta n^0_s=2\Psi_s+(S_iv^i)_s+\int_0^{\bar{\chi}_s}\mathrm{d}\chi\,(\dot{\Psi}+\dot{\Phi})+\int_0^{\bar{\chi}_s}\mathrm{d}\chi\,\dot{S}_in^i-\int_0^{\bar{\chi}_s}\mathrm{d}\chi\,\dot{H}_{ij}n^in^j\,. \tag{2.9}$$

Inserting this result in eqs. (2.8) we infer

$$\delta z=-(1+\bar{z})\left(\Psi_s+\int_0^{\bar{\chi}_s}\mathrm{d}\chi\,(\dot{\Psi}+\dot{\Phi})+\int_0^{\bar{\chi}_s}\mathrm{d}\chi\,\dot{S}_in^i-\int_0^{\bar{\chi}_s}\mathrm{d}\chi\,\dot{H}_{ij}n^in^j+(v_in^i)_s\right). \tag{2.10}$$

The redshift density perturbation in eq. (2.4) is then written as

$$\delta_z=\delta_g+3\Psi_s+3(v_in^i)_s+3\int_0^{\bar{\chi}_s}\mathrm{d}\chi\,(\dot{\Psi}+\dot{\Phi})+3\int_0^{\bar{\chi}_s}\mathrm{d}\chi\,\dot{S}_in^i-3\int_0^{\bar{\chi}_s}\mathrm{d}\chi\,\dot{H}_{ij}n^in^j\,. \tag{2.11}$$

The galaxy density fluctuation in Poisson gauge $\delta_g$ traces the matter density in the same gauge $\delta_{\rm poiss}$ via a bias relation. However it is most physical to assume that both the tracers and dark matter follow the same velocity field as they experience the same gravitational acceleration. We then expect that biasing should be applied to the density fluctuation in *comoving gauge*, $\delta_c$, not to $\delta_{\rm poiss}$. Therefore, we transform

$$\delta_c=\delta_{\rm poiss}+3\mathcal{H}v\,, \tag{2.12}$$

where we have introduced the velocity potential in Poisson gauge which appears in the decomposition of the velocity field in scalar and vector part:

$$v^i=-\partial^i v+v^{i,\mathrm{V}}\,. \tag{2.13}$$

With $\delta_g=b\cdot\delta_c-3\mathcal{H}v$ we can rewrite eq. (2.11) as

$$\begin{aligned}\delta_z=&b\cdot\delta_c+3\Psi_s+3(v_in^i)_s-3\mathcal{H}v+3\int_0^{\bar{\chi}_s}\mathrm{d}\chi\,(\dot{\Psi}+\dot{\Phi})\\&+3\int_0^{\bar{\chi}_s}\mathrm{d}\chi\,\dot{S}_in^i-3\int_0^{\bar{\chi}_s}\mathrm{d}\chi\,\dot{H}_{ij}n^in^j\,.\end{aligned} \tag{2.14}$$

[2] With this convention the direction of observation is $-\mathbf{n}$.

### 2.2.2 Volume perturbations

To compute the volume perturbation $\delta V(\mathbf{n}, z)/V(z)$, let us express the spatial volume element in terms of 'observable' quantities such as the angles at the observer position and the perturbed redshift. An observer moving with 4-velocity $u^\mu$ sees a spatial volume element

$$\begin{aligned} \mathrm{d}V &= \sqrt{-g}\,\epsilon_{\mu\nu\alpha\beta}u^\mu \mathrm{d}x^\nu \mathrm{d}x^\alpha \mathrm{d}x^\beta = \sqrt{-g}\,\epsilon_{\mu\nu\alpha\beta}u^\mu \frac{\partial x^\nu}{\partial z}\frac{\partial x^\alpha}{\partial \theta_s}\frac{\partial x^\beta}{\partial \phi_s}|\mathbf{J}|\,\mathrm{d}z\mathrm{d}\theta\mathrm{d}\phi \\ &\equiv \nu(z,\theta,\phi)\mathrm{d}z\mathrm{d}\theta\mathrm{d}\phi\,, \end{aligned} \tag{2.15}$$

where we have introduced the volume density $\nu$ such that $\delta V(\mathbf{n}, z)/V(z) = \delta\nu(\mathbf{n}, z)/\nu(z)$ and $|\mathbf{J}|$ is the determinant of the Jacobian matrix, $\mathbf{J}$, of the transformation from the angles at the source $(\theta_s, \phi_s)$ to the angles at the observer $(\theta, \phi)$. Given the unperturbed radial trajectory $(\theta, \phi) = (\theta_s, \phi_s)$ we can write, at first order, $\theta_s = \theta + \delta\theta$ and $\phi_s = \phi + \delta\phi$, so that $|\mathbf{J}| = \left(1 + \partial_\theta\delta\theta + \partial_\phi\delta\phi\right)$. The expression for the metric determinant is given by

$$\sqrt{-g} = a^4(1 + \Psi - 3\Phi)\chi^2 \sin\theta_s = a^4(1 + \Psi - 3\Phi)\bar{\chi}^2 \sin\theta\left(1 + \cot\theta\delta\theta + \frac{2}{\bar{\chi}}\delta\chi\right), \tag{2.16}$$

where we consider the fact that $\chi = \bar{\chi} + \delta\chi$ and we evaluate everything in terms of the observed redshift and angles at the observer. Note that vector and tensor perturbations do not contribute to the first equal sign in the expression for $\sqrt{-g}$ as at linear order $|\mathbf{J}| \simeq \mathrm{Tr}[\mathbf{J}]$. With this we can express $\nu$ as

$$\begin{aligned} \nu = a^3(1 + \Psi - 3\Phi)\bar{\chi}^2 \sin\theta\left(1 + \cot\theta\delta\theta + \frac{2}{\bar{\chi}}\delta\chi\right) \\ \times\left((1 - \Psi)\frac{\mathrm{d}\chi}{\mathrm{d}z} + \frac{a}{\mathcal{H}}v_i n^i\right)\left(1 + \frac{\partial\delta\theta}{\partial\theta} + \frac{\partial\delta\phi}{\partial\phi}\right). \end{aligned} \tag{2.17}$$

Since at lowest order, on a photon geodesic, $\mathrm{d}\eta = \mathrm{d}\lambda$, the derivative of comoving distance $\chi$ w.r.t. redshift, to first order, is given by

$$\frac{\mathrm{d}\chi}{\mathrm{d}z} = \frac{\mathrm{d}\bar{\chi}}{\mathrm{d}\bar{z}} + \frac{\mathrm{d}\delta\chi}{\mathrm{d}\bar{z}} - \frac{\mathrm{d}\delta z}{\mathrm{d}\bar{z}}\frac{\mathrm{d}\bar{\chi}}{\mathrm{d}\bar{z}} = \frac{a}{\mathcal{H}}\left(1 - \frac{\mathrm{d}\delta\chi}{\mathrm{d}\lambda} + \frac{a}{\mathcal{H}}\frac{\mathrm{d}\delta z}{\mathrm{d}\lambda}\right). \tag{2.18}$$

Inserting this in the volume element $\nu$ we obtain

$$\nu = \frac{a^4\bar{\chi}^2 \sin\theta}{\mathcal{H}}\left(1 - 3\Phi + \frac{\partial\delta\theta}{\partial\theta} + \cot\theta\,\delta\theta + \frac{\partial\delta\phi}{\partial\phi} - \frac{\mathrm{d}\delta\chi}{\mathrm{d}\lambda} + \frac{2}{\bar{\chi}}\delta\chi + \frac{a}{\mathcal{H}}\frac{\mathrm{d}\delta z}{\mathrm{d}\lambda} - v_i n^i\right). \tag{2.19}$$

We are interested in the fluctuation of the volume density $\delta\nu = \nu(z) - \bar{\nu}(z)$. The unperturbed volume element is simply $\bar{\nu}(\bar{z}) = \frac{a^4}{\mathcal{H}}\bar{\chi}^2 \sin\theta$ but we need to evaluate it at the observed (perturbed) redshift. We then expand $\bar{\nu}(z)$ around the background redshift $\bar{z}$ obtaining

$$\bar{\nu}(\bar{z}) = \bar{\nu}(z) + \frac{\mathrm{d}\bar{\nu}}{\mathrm{d}\bar{z}}\delta z\,, \tag{2.20}$$

and

$$\frac{\mathrm{d}\bar{\nu}}{\mathrm{d}\bar{z}} = -\bar{\nu}(\bar{z})\left(4 - \frac{2}{\bar{\chi}\mathcal{H}} - \frac{\dot{\mathcal{H}}}{\mathcal{H}^2}\right)\frac{1}{1+\bar{z}}\,. \tag{2.21}$$

Combining eq. (2.19) with eqs. (2.20–2.21) we find

$$\begin{aligned}\frac{\delta\nu}{\nu} = &-3\Phi - v_i n^i + (\cot\theta + \partial_\theta)\delta\theta + \partial_\phi\delta\phi - \frac{\mathrm{d}\delta\chi}{\mathrm{d}\lambda} + \frac{2}{\bar{\chi}}\delta\chi \\ &+ \frac{1}{(1+\bar{z})\mathcal{H}}\frac{\mathrm{d}\delta z}{\mathrm{d}\lambda} + \left(4 - \frac{2}{\bar{\chi}\mathcal{H}} - \frac{\dot{\mathcal{H}}}{\mathcal{H}^2}\right)\frac{\delta z}{1+\bar{z}}\,.\end{aligned} \tag{2.22}$$

Considering this equation, we are still missing the geodesic displacements $\delta x^j(\lambda)$ in order to express the volume fluctuation in terms of the metric potentials and the peculiar velocities. To find them we write

$$\frac{\mathrm{d}x^\alpha}{\mathrm{d}t} = \frac{\mathrm{d}x^\alpha}{\mathrm{d}\lambda}\frac{\mathrm{d}\lambda}{\mathrm{d}t} = \frac{n^\alpha}{1+\delta n^0}\,, \tag{2.23}$$

and we use the photon geodesic equation to find the $\delta n^i$. Together with eq. (2.9) we can express the integrals of (2.23) in terms of metric perturbations to find

$$\delta\chi = \int_0^{\bar{\chi}_s}\mathrm{d}\chi\,(\Psi+\Phi) + \int_0^{\bar{\chi}_s}\mathrm{d}\chi\,S_i n^i - \int_0^{\bar{\chi}_s}\mathrm{d}\chi\,H_{ij}n^i n^j\,, \tag{2.24}$$

$$\begin{aligned}(\cot\theta + \partial_\theta)\delta\theta + \partial_\phi\delta\phi = &-\int_0^{\bar{\chi}_s}\mathrm{d}\chi\,\frac{\bar{\chi}_s - \chi}{\bar{\chi}_s\chi}\Delta_\Omega\left(\Psi + \Phi + S_i n^i - H_{ij}n^i n^j\right) \\ &- \int_0^{\bar{\chi}_s}\mathrm{d}\chi\,\frac{1}{\chi}\left(\nabla_\Omega\cdot S_\Omega - \nabla_\Omega\cdot(H_{ij}n^j)_\Omega\right)\,,\end{aligned} \tag{2.25}$$

where the subscript $\Omega$ denotes the angular part of a vector $\vec{A}_\Omega = A_i\hat{e}^i_\theta + A_i\hat{e}^i_\phi$ and we denote the angular divergence and the angular Laplacian respectively by

$$\nabla_\Omega\cdot\vec{A}_\Omega = (\cot\theta + \partial_\theta)A_\theta + \partial_\phi A_\phi\,, \tag{2.26}$$

and

$$\Delta_\Omega = \left(\cot\theta\partial_\theta + \partial_\theta^2 + \frac{1}{\sin^2\theta}\partial_\phi^2\right)\,. \tag{2.27}$$

Combining eq. (2.22) with eqs. (2.24) and (2.25), and using the redshift perturbation given in eq. (2.14) which yields

$$\begin{aligned}\frac{1}{(1+\bar{z})\mathcal{H}}\frac{\mathrm{d}\delta z}{\mathrm{d}\lambda} = &\Psi_s + v_i n^i - \frac{1}{\mathcal{H}}\frac{\mathrm{d}}{\mathrm{d}\lambda}(v_i n^i) - \frac{1}{\mathcal{H}}\frac{\mathrm{d}\Psi}{\mathrm{d}\lambda} + \frac{1}{\mathcal{H}}\left(\dot{\Psi} + \dot{\Phi} + \dot{S}_i n^i - \dot{H}_{ij}n^i n^j\right) \\ &+ \int_0^{\bar{\chi}_s}\mathrm{d}\chi\left(\dot{\Psi} + \dot{\Phi} + \dot{S}_i n^i - \dot{H}_{ij}n^i n^j\right)\,,\end{aligned} \tag{2.28}$$

we find

$$\begin{aligned}\frac{\delta\nu}{\nu} =&\Psi - 2\Phi + S_i n^i - H_{ij}n^i n^j - v^i n_i + \frac{1}{\mathcal{H}}\left(\dot\Psi + \dot\Phi + \dot S_i n^i - \dot H_{ij} n^i n^j - \frac{\mathrm{d}\Psi}{\mathrm{d}\lambda} - \frac{\mathrm{d}}{\mathrm{d}\lambda}(v_i n^i)\right)\\ &+\left(-3 + \frac{2}{\bar\chi\mathcal{H}} + \frac{\dot{\mathcal{H}}}{\mathcal{H}^2}\right)\left(\Psi + v_i n^i + \int_0^{\bar\chi_s}\mathrm{d}\chi\left(\dot\Psi + \dot\Phi + \dot S_i n^i - \dot H_{ij} n^i n^j\right)\right)\\ &+\frac{2}{\bar\chi_s}\int_0^{\bar\chi_s}\mathrm{d}\chi\left(\Psi + \Phi + S_i n^i - H_{ij}n^i n^j\right) - \int_0^{\bar\chi_s}\mathrm{d}\chi\,\frac{\bar\chi_s - \chi}{\bar\chi_s\chi}\Delta_\Omega\left(\Psi + \Phi + S_i n^i - H_{ij}n^i n^j\right)\\ &-\int_0^{\bar\chi_s}\mathrm{d}\chi\,\frac{1}{\chi}\left(\nabla_\Omega\cdot S_\Omega - \nabla_\Omega\cdot(H_{ij}n^j)_\Omega\right).\end{aligned} \tag{2.29}$$

Adding the results given in eqs. (2.14) and (2.29) we finally obtain the galaxy number count fluctuations for scalar modes (S) and vector plus tensor modes (V,T) in a perturbed FLRW universe:

$$\begin{aligned}\Delta_g^{(\mathrm{S})}(\mathbf{n},z) =& b\delta_c + \Psi - 2\Phi + \frac{\dot\Phi}{\mathcal{H}} - 3\mathcal{H}v + \frac{1}{\mathcal{H}}\partial_\chi(v_i^{\mathrm{S}} n^i)\\ &+\left(\frac{2}{\bar\chi_s\mathcal{H}} + \frac{\dot{\mathcal{H}}}{\mathcal{H}^2}\right)\left(\Psi + v_i^{\mathrm{S}} n^i + \int_0^{\bar\chi_s}\mathrm{d}\chi\left(\dot\Psi + \dot\Phi\right)\right)\\ &-\int_0^{\bar\chi_s}\mathrm{d}\chi\,\frac{\bar\chi_s - \chi}{\bar\chi_s\chi}\Delta_\Omega(\Psi + \Phi) + \frac{2}{\bar\chi_s}\int_0^{\bar\chi_s}\mathrm{d}\chi\,(\Psi + \Phi)\\ \Delta_g^{(\mathrm{V,T})}(\mathbf{n},z) =& -H_{ij}n^i n^j - \frac{1}{\mathcal{H}}\dot H_{ij} n^i n^j + \frac{1}{\mathcal{H}}\partial_\chi(v_i^{\mathrm{V}} n^i)\\ &+\left(\frac{2}{\bar\chi_s\mathcal{H}} + \frac{\dot{\mathcal{H}}}{\mathcal{H}^2}\right)\left(v_i^{\mathrm{V}} n^i + \int_0^{\bar\chi_s}\mathrm{d}\chi\left(\dot S_i n^i - \dot H_{ij} n^i n^j\right)\right)\\ &-\int_0^{\bar\chi_s}\mathrm{d}\chi\,\frac{\bar\chi_s - \chi}{\bar\chi_s\chi}\Delta_\Omega\left(S_i n^i - H_{ij}n^i n^j\right) + \frac{2}{\bar\chi_s}\int_0^{\bar\chi_s}\mathrm{d}\chi\left(S_i n^i - H_{ij}n^i n^j\right)\\ &-\int_0^{\bar\chi_s}\mathrm{d}\chi\,\partial_\chi\left(S_i n^i - H_{ij}n^i n^j\right) - \int_0^{\bar\chi_s}\mathrm{d}\chi\left(\frac{2}{\chi}S_i n^i - \frac{3}{\chi}H_{ij}n^i n^j\right),\end{aligned} \tag{2.30}$$

where we have decomposed the velocity as in eq. (2.13): $v^i = -\partial^i v + v^{i,\mathrm{V}} = v^{i,\mathrm{S}} + v^{i,\mathrm{V}}$. For the last two equations we have used the fact that - with our normalization of the affine parameter $\mathrm{d}\eta = \mathrm{d}\lambda$ - the chain rule reads $\frac{\mathrm{d}A}{\mathrm{d}\lambda} = \dot A + \mathbf{n}\cdot\nabla A = \dot A - \partial_\chi A$. We have also exploited the transversality conditions, $\partial^i S_i = 0$ and $\partial^i H_{ij} = 0$ which imply $\frac{1}{\chi}\nabla_\Omega\cdot S_\Omega = \left(\frac{2}{\chi} + \partial_\chi\right)S_i n^i$ and equivalently for $H_{ij}$. Furthermore we have assumed that galaxies move along geodesic and use their geodesic equation, given respectively by:

$$\dot{\mathbf{v}}^{\mathrm{S}}\cdot\mathbf{n} + \mathcal{H}\mathbf{v}^{\mathrm{S}}\cdot\mathbf{n} - \partial_\chi\Psi = 0\,, \tag{2.31}$$

$$\dot{\mathbf{v}}^{\mathrm{V}}\cdot\mathbf{n} - \dot{\mathbf{S}}\cdot\mathbf{n} + \mathcal{H}(\mathbf{v}^{\mathrm{V}}\cdot\mathbf{n} - \mathbf{S}\cdot\mathbf{n}) = 0\,, \tag{2.32}$$

Equation (2.30) is the main result of this section. Let us comment on $\Delta^{(\mathrm{V,T})}$ before we move on to the study of a numerical application. We will comment in details on $\Delta^{(\mathrm{S})}$ in

chaper 3. We first notice that since vector and tensor perturbations do not produce density fluctuation we have no density term in the number counts which is the biggest contribution in the case of scalar perturbation. In the first line we have two terms coming from the tensor metric potential and the redshift-space distortion term:

$$\Delta^{\mathrm{P1}}(\mathbf{n}, z) = -H_{ij} n^i n^j \,, \tag{2.33}$$

$$\Delta^{\mathrm{P2}}(\mathbf{n}, z) = -\frac{1}{\mathcal{H}} \dot{H}_{ij} n^i n^j \,, \tag{2.34}$$

$$\Delta^{\mathrm{RSD}}(\mathbf{n}, z) = \frac{1}{\mathcal{H}} \partial_\chi (v_i n^i) \,. \tag{2.35}$$

The second line of eq. (2.30) contains the Doppler term and the Integrated Sachs-Wolfe term:

$$\Delta^{\mathrm{Dop}}(\mathbf{n}, z) = \left( \frac{2}{\bar{\chi}_s \mathcal{H}} + \frac{\dot{\mathcal{H}}}{\mathcal{H}^2} \right) v_i n^i \,, \tag{2.36}$$

$$\Delta^{\mathrm{ISW}}(\mathbf{n}, z) = \left( \frac{2}{\bar{\chi}_s \mathcal{H}} + \frac{\dot{\mathcal{H}}}{\mathcal{H}^2} \right) \int_0^{\bar{\chi}_s} \mathrm{d}\chi \left( \dot{S}_i n^i - \dot{H}_{ij} n^i n^j \right) . \tag{2.37}$$

We group the remaining contributions which account for distortions of the volume element into a lensing term and a radial distortion term:

$$\begin{aligned} \Delta^{\mathrm{Len}}(\mathbf{n}, z) &= -\int_0^{\bar{\chi}_s} \mathrm{d}\chi \, \frac{\bar{\chi}_s - \chi}{\bar{\chi}_s \chi} (2 + \Delta_\Omega) S_i n^i \\ &\quad + \int_0^{\bar{\chi}_s} \mathrm{d}\chi \, \frac{\bar{\chi}_s - \chi}{\bar{\chi}_s \chi} \Delta_\Omega H_{ij} n^i n^j \\ &\quad - \int_0^{\bar{\chi}_s} \mathrm{d}\chi \left( \frac{2}{\bar{\chi}_s} - \frac{3}{\chi} \right) H_{ij} n^i n^j \,, \end{aligned} \tag{2.38}$$

$$\Delta^{\mathrm{V}\chi}(\mathbf{n}, z) = -\int_0^{\bar{\chi}_s} \mathrm{d}\chi \, \partial_\chi \left( S_i n^i - H_{ij} n^i n^j \right) . \tag{2.39}$$

In the number counts all the terms that are not integrated are evaluated at the unperturbed source position (in direction $-\mathbf{n}$ at redshift $z(\bar{\chi}_s)$) while the terms inside integrals are evaluated along the unperturbed line of sight (Born approximation), from comoving distance $\bar{\chi}_s = 0$ to $\bar{\chi}_s$ and conformal time $\eta_0 - \bar{\chi}_s$.

### 2.2.3 Magnification bias & evolution bias

Up until now we have assumed that galaxy survey are volume-limited so that we can observe all the tracers in the survey's volume. However, surveys are characterised by a limiting flux below which we cannot detect sources hence galaxy survey are flux-limited. As sketched in figure 1.2 (b), because of projection effects (e.g. gravitational lensing) - which modify the observed flux of a source - a galaxy below the flux threshold can "make the cut" if its signal is magnified along the line-of-sight, and, *viceversa*, a galaxy below the flux threshold might become unobservable if its signal is de-magnified along the LOS. Including this effect, so

considering that the observed number counts depend also on the luminosity $L$, at a given fixed flux $F$, we write

$$\Delta_g(\mathbf{n}, z, F) = \Delta_g(\mathbf{n}, z) + \frac{\partial \bar{n}_g(L > L_*)}{\partial L} \frac{\delta L}{\bar{L}} \,. \tag{2.40}$$

Here $L_*$ is the limiting luminosity and $\bar{L}$ is the background luminosity corresponding to the flux $F$. Using the expression $L = 4\pi \mathcal{D}_L^2 F$ we can relate the fluctuation in the luminosity to the fluctuation in the luminosity distance $\mathcal{D}_L$ as

$$\frac{\delta L}{\bar{L}} = 2 \frac{\delta \mathcal{D}_L}{\bar{\mathcal{D}}_L} \,. \tag{2.41}$$

We introduced the dependence of the number density on the luminosity via the logarithmic derivative

$$s(z, L_*) \equiv \frac{\partial \log_{10} \bar{n}_g(L > L_*)}{\partial m} \,, \tag{2.42}$$

where we have defined the magnification bias $s$ as the slope of the luminosity function and $m = -2.5 \log_{10} F$ is the apparent magnitude so that

$$\frac{\partial \bar{n}_g(L > L_*)}{\partial L} = -\frac{5}{2} s \,. \tag{2.43}$$

The fluctuations in the luminosity distance are computed as

$$\begin{aligned} \left(\frac{\delta \mathcal{D}_L}{\bar{\mathcal{D}}_L}\right)^{(\mathrm{S})} = & -\left(1 - \frac{1}{\bar{\chi}_s \mathcal{H}}\right)\left(\Psi + v_i^{\mathrm{S}} n^i + \int_0^{\bar{\chi}_s} \mathrm{d}\chi \left(\dot{\Psi} + \dot{\Phi}\right)\right) - \Phi \\ & - \int_0^{\bar{\chi}_s} \mathrm{d}\chi \, \frac{\bar{\chi}_s - \chi}{2 \bar{\chi}_s \chi} \Delta_\Omega \left(\Psi + \Phi\right) + \frac{1}{\bar{\chi}_s} \int_0^{\bar{\chi}_s} \mathrm{d}\chi \left(\Psi + \Phi\right) , \end{aligned} \tag{2.44}$$

$$\begin{aligned} \left(\frac{\delta \mathcal{D}_L}{\bar{\mathcal{D}}_L}\right)^{(\mathrm{V,T})} = & -\left(1 - \frac{1}{\bar{\chi}_s \mathcal{H}}\right)\left(v_i^{\mathrm{V}} n^i + \int_0^{\bar{\chi}_s} \mathrm{d}\chi \left(\dot{S}_i n^i - \dot{H}_{ij} n^i n^j\right)\right) - \frac{1}{2} H_{ij} n^i n^j \\ & - \int_0^{\bar{\chi}_s} \mathrm{d}\chi \, \frac{\bar{\chi}_s - \chi}{2 \bar{\chi}_s \chi} \Delta_\Omega \left(S_i n^i - H_{ij} n^i n^j\right) + \frac{1}{\bar{\chi}_s} \int_0^{\bar{\chi}_s} \mathrm{d}\chi \left(S_i n^i - H_{ij} n^i n^j\right) \\ & - \int_0^{\bar{\chi}_s} \mathrm{d}\chi \left(\frac{2}{\chi} S_i n^i - \frac{3}{\chi} H_{ij} n^i n^j\right) . \end{aligned} \tag{2.45}$$

Before combining these expression to give the final form of $\Delta_g$, we must consider another additional effect. We have so far neglected any possible time evolution for $\bar{n}_g$ and we have used eq. (2.6). We can allow for a non-vanishing evolution term by introducing the evolution bias

$$f_{\mathrm{evo}}(z) \equiv \frac{d \ln(a^3 \bar{n}_g)}{\mathcal{H} d\eta} = -(1+z) \frac{d}{dz} \ln\left(\frac{\bar{n}_g}{(1+z)^3}\right) . \tag{2.46}$$

This modifies eq. (2.6) so that $\Delta_g$ in eq. (2.30) gains an additional factor $f_{\mathrm{evo}} \delta z / (1+z)$ and we must include it in the gauge transformation $\delta_g = b \cdot \delta_c - (3 - f_{\mathrm{evo}}) \mathcal{H} v$.

Including the evolution bias and combining eqs. (2.40), (2.43), (2.44) and (2.45) we obtain the final expressions:

$$\begin{aligned}\Delta_g^{(\mathrm{S})}(\mathbf{n},z) &= b\delta_c + \Psi + (5s-2)\Phi + \frac{\dot\Phi}{\mathcal{H}} + (f_{\mathrm{evo}}-3)\mathcal{H}v + \frac{1}{\mathcal{H}}\partial_\chi(v_i^{\mathrm{S}}n^i)\\ &+ \left(5s + \frac{2-5s}{\bar\chi_s\mathcal{H}} + \frac{\dot{\mathcal{H}}}{\mathcal{H}^2} - f_{\mathrm{evo}}\right)\left(\Psi + v_i^{\mathrm{S}}n^i + \int_0^{\bar\chi_s}\mathrm{d}\chi\left(\dot\Psi+\dot\Phi\right)\right)\\ &+ \frac{5s-2}{2}\int_0^{\bar\chi_s}\mathrm{d}\chi\,\frac{\bar\chi_s-\chi}{\bar\chi_s\chi}\Delta_\Omega(\Psi+\Phi) + \frac{2-5s}{\bar\chi_s}\int_0^{\bar\chi_s}\mathrm{d}\chi\,(\Psi+\Phi)\,,\end{aligned} \tag{2.47}$$

$$\begin{aligned}\Delta_g^{(\mathrm{V,T})}(\mathbf{n},z) &= \frac{5s-2}{2}H_{ij}n^in^j - \frac{1}{\mathcal{H}}\dot H_{ij}n^in^j + \frac{1}{\mathcal{H}}\partial_\chi(v_i^{\mathrm{V}}n^i)\\ &+ \left(5s + \frac{2-5s}{\bar\chi_s\mathcal{H}} + \frac{\dot{\mathcal{H}}}{\mathcal{H}^2} - f_{\mathrm{evo}}\right)\left(v_i^{\mathrm{V}}n^i + \int_0^{\bar\chi_s}\mathrm{d}\chi\left(\dot S_in^i - \dot H_{ij}n^in^j\right)\right)\\ &+ \frac{5s-2}{2}\int_0^{\bar\chi_s}\mathrm{d}\chi\,\frac{\bar\chi_s-\chi}{\bar\chi_s\chi}\Delta_\Omega\left(S_in^i - H_{ij}n^in^j\right)\\ &+ \frac{2-5s}{\bar\chi_s}\int_0^{\bar\chi_s}\mathrm{d}\chi\left(S_in^i - H_{ij}n^in^j\right) - \int_0^{\bar\chi_s}\mathrm{d}\chi\,\partial_\chi\left(S_in^i - H_{ij}n^in^j\right)\\ &+ \frac{5s-2}{2}\int_0^{\bar\chi_s}\mathrm{d}\chi\left(\frac{2}{\chi}S_in^i - \frac{3}{\chi}H_{ij}n^in^j\right).\end{aligned} \tag{2.48}$$

In the next section we set the magnification bias $s = 0$.

## 2.3 Application to second order perturbation theory

We now apply our main formula (2.48) to vector perturbations present in a standard ΛCDM universe. At first order the situation is not promising since standard inflationary scenarios do not produce vector perturbations and even if they would, vector perturbations decay without the presence of a non-standard source term, e.g. cosmic strings. However, at second order, non linearities in the scalar sector source vector modes and here we target these scalar-induced vector modes as a test of eq. (2.48).

We use the following perturbation scheme for the metric potentials

$$\begin{cases} g_{00} = -a^2\left(1 + 2\Psi^{(1)} + \Psi^{(2)}\right)\\ g_{0i} = -a^2(S_i^{(1)} + \frac{1}{2}S_i^{(2)})\\ g_{ij} = a^2\left(\left(1 - 2\Phi^{(1)} - \Phi^{(2)}\right)\delta_{ij} + H_{ij}^{(1)} + \frac{1}{2}H_{ij}^{(2)}\right),\end{cases} \tag{2.49}$$

for the energy-momentum tensor $\rho = \bar\rho + \delta\rho^{(1)} + 1/2\delta\rho^{(2)}$, $p = \bar p + \delta p^{(1)} + 1/2\delta p^{(2)}$ and for the 4-velocity $u^\mu = a^{-1}\left(1 + \delta u^0, \mathbf{v}^{(1)} + 1/2\mathbf{v}^{(2)}\right)$. Here we have used Newtonian gauge for the scalar perturbations which (locally) is well defined at every order. At first order, $\Psi^{(1)}$ and $\Phi^{(1)}$ are the usual Bardeen potentials. We neglect second order scalar and tensor fluctuations as well as first order vectors and tensors. The metric, up to second order, is then written

$$\mathrm{d}s^2 = a^2(\eta)\left(-(1+2\Psi^{(1)})\mathrm{d}\eta^2 - S_i^{(2)}\,\mathrm{d}\eta\mathrm{d}x^i + (1-2\Phi^{(1)})\delta_{ij}\mathrm{d}x^i\mathrm{d}x^j\right). \tag{2.50}$$

Within ΛCDM we can identify the two Bardeen potentials, $\Psi^{(1)} = \Phi^{(1)} = \Psi$. It is worth pointing out that our metric vector potential and the second order peculiar velocity are pure vector quantities: $\mathbf{S} = \mathbf{S}^V$ and $\mathbf{v}_{(2)} = \mathbf{v}^V_{(2)}$, where, following the notation used above, with $V$ we denote the transverse part of a vector that we can extract in Fourier space with the projection operator $P_{ij}$ which acts as

$$A^V_i = P_{ij}A^j = \left(\delta_{ij} - \frac{k_i k_j}{k^2}\right) A^j \,. \tag{2.51}$$

Following [215] we also define $\mathbf{\Omega}_{(2)} = \mathbf{v}_{(2)} - \mathbf{S} = \mathbf{\Omega}^V_{(2)}$. The covariant 4-velocity of the fluid is obtained via the normalisation condition $g_{\mu\nu}u^\mu u^\nu = -1$

$$u_\mu = a\left(-1 - \Psi + \frac{1}{2}\Psi^2 - \frac{1}{2}\mathbf{v}^{(1)}\cdot\mathbf{v}^{(1)}\,,\, \mathbf{v}^{(1)} - 2\Psi\,\mathbf{v}^{(1)} + \frac{1}{2}\mathbf{\Omega}^{(2)}\right). \tag{2.52}$$

With this, modelling matter as a perfect fluid, we can construct the energy momentum tensor $T_{\mu\nu} = (\rho + p)u_\mu u_\nu + p\, g_{\mu\nu}$. At first order, the Einstein constraint equations reduce to

$$4\pi G a^2 \delta\rho = \Delta\Psi - 3\mathcal{H}(\mathcal{H}\Psi + \dot\Psi)\,, \tag{2.53}$$

$$4\pi G(1+\omega)\,\bar\rho\, a^2 v^{(1)}_j = \partial_j(\mathcal{H}\Psi + \dot\Psi)\,, \tag{2.54}$$

where $\omega = p/\rho$ and $\Delta$ is the 3-dimensional Laplacian. At second order we use $T^{0(2)}_j = \frac{1}{2}\left(\bar\rho\,\Omega_j + 2v^{(1)}_j(\delta\rho - 3\bar\rho\Psi)\right)$ and the $0i$ Einstein equation is

$$\begin{aligned}\Omega_i &= \frac{1}{6(1+\omega)\mathcal{H}^2}\left(-\Delta S_i + \frac{16\Delta\Psi}{3\mathcal{H}^2}\partial_i(\mathcal{H}\Psi + \dot\Psi) - 8\mathcal{H}\Psi\partial_i\Psi - \frac{16}{\mathcal{H}}\dot\Psi\partial_i\dot\Psi - 8(3\dot\Psi\partial_i\Psi + 5\Psi\partial_i\dot\Psi)\right)^V \\ &= \frac{1}{6(1+\omega)\mathcal{H}^2}\left(-\Delta S_i + \frac{16\Delta\Psi}{3\mathcal{H}^2}\partial_i(\mathcal{H}\Psi + \dot\Psi) - 8(3\dot\Psi\partial_i\Psi + 5\Psi\partial_i\dot\Psi)\right)^V \,,\end{aligned}$$

where in the second line we ignored the pure gradient terms: $\Psi\partial_i\Psi \propto \partial_i\Psi^2$ and $\dot\Psi\partial_i\dot\Psi \propto \partial_i\dot\Psi^2$ which have vanishing vector projections. Since both the left hand side and the right hand side are pure vector terms, they are fixed by their curl. We can than write $\partial_{[i}\Omega_{j]} = \partial_{[i}(\cdots)_{j]}$, where ${}_{[i}(\cdots)_{j]}$ denotes anti-symmetrization, as

$$6(1+\omega)\mathcal{H}^2\partial_{[i}\Omega_{j]} = \partial_{[i}\left(-\Delta S_{j]} + 8\left(2\dot\Psi\partial_{j]}\Psi + \frac{2}{3\mathcal{H}^2}\Delta\Psi\partial_{j]}(\mathcal{H}\Psi + \dot\Psi)\right)\right), \tag{2.55}$$

and conclude that

$$6(1+\omega)\mathcal{H}^2\Omega_j = -\Delta S_j + 8\left(2\dot\Psi\partial_j\Psi + \frac{2}{3\mathcal{H}^2}\Delta\Psi\partial_j(\mathcal{H}\Psi + \dot\Psi)\right)^V \,, \tag{2.56}$$

in agreement with eq. (18) of [215].

The vorticity in the fluid is defined as $\omega_{\mu\nu} = F^\lambda_\mu F^\sigma_\nu(u_{\lambda;\sigma} - u_{\sigma;\lambda})$, with $F_{\mu\nu} = g_{\mu\nu} + u_\mu u_\nu$ [131]. In [215] it is shown that in a perfect fluid there is no generation of vorticity at any order. This allows us to set

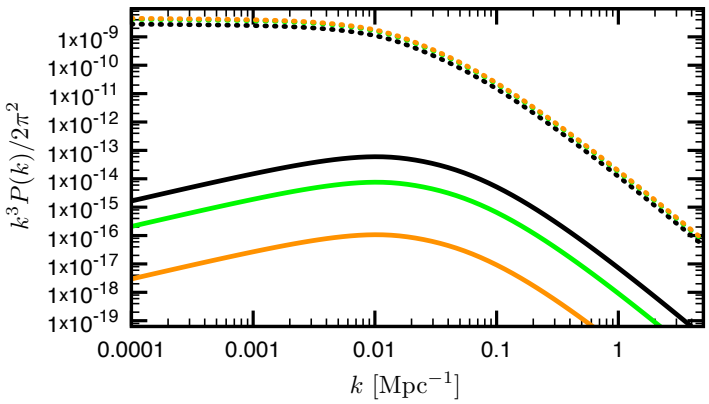


Figure 2.1: The dimensionless power spectra of the Bardeen potential $\mathcal{P}_\Psi$ (dashed) and of the scalar induced vectors $\mathcal{P}_S$ (solid), for different redshifts: $z = 0$ (black), $z = 1$ (green) and $z = 3$ (orange).

$$0 = \omega_{ij} = \partial_{[i}\Omega_{j]} + 6\, v^{(1)}_{[i}\partial_{j]}\Psi + 2\, v^{(1)}_{[i}\dot{v}^{(1)}_{j]} \,. \tag{2.57}$$

Inserting eqs. (2.54) and (2.56) in this expression we obtain

$$\Delta S_i = \frac{16}{3\mathcal{H}^2\Omega_m(1+\omega_m)} \left(\Delta\Psi\, \partial_i(\mathcal{H}\Psi + \dot{\Psi})\right)^V \,, \tag{2.58}$$

where $\omega_m = p_m/\rho_m$ and we shall set it to 0 in the following. Using the fact that for pressureless matter $\Psi(\mathbf{x},\eta) = g(\eta)\Psi(\mathbf{x},\eta_0)$, we find that $\dot{\Psi}\partial_i\Psi = (\dot{g}/g)\partial_i(\Psi^2/2)$ so that $(\dot{\Psi}\partial_i\Psi)^V = 0$. Inserting this and (2.58) in eq. (2.56) yields $\mathbf{\Omega} = 0$ and $\mathbf{v}_{(2)} = \mathbf{S}$.

From eq. (2.58) we can conclude that the scalar-induced vector power spectrum $P_S(k,z)$ is a convolution of the scalar power spectrum $P_\Psi(k,z)$ with itself. We can furthermore factorize the gravitational potential as $\Psi(k,z) = \Psi^{(\mathrm{in})}(k)T(k)g(z)$, where $T(k)$ is the transfer function, a good approximation to it can be found in [139], and $g(z)$ is the growth factor which, in a $\Lambda$CDM cosmology can be approximated as

$$g(z) = \frac{5}{2} g_\infty \Omega_m(z) \left(\Omega_m^{4/7}(z) - \Omega_\Lambda + \left(1 + \frac{1}{2}\Omega_m(z)\right)\left(1 + \frac{1}{70}\Omega_\Lambda\right)\right)^{-1} \,. \tag{2.59}$$

The pre-factor $g_\infty$ is chosen such that $g(0) = 1$. With this the dimensionless power spectrum of the Bardeen potential is given by, $\mathcal{P}_\Psi(k,z) = k^3/(2\pi^2)P_\Psi(k,z) = \mathcal{P}_\zeta(k)T^2(k)g^2(z)$, where we define the primordial power spectrum $\mathcal{P}_\zeta(k)$ by

$$\mathcal{P}_\zeta(k) = A_s \left(\frac{k}{k_*}\right)^{n_s - 1} \,, \tag{2.60}$$

where $k_*$ is an (arbitrary) pivot scale. In Fourier space eq. (2.58) becomes

$$S_i(\mathbf{k}) = -\frac{ik^{-2}}{(2\pi)^3}\frac{16}{3\mathcal{H}^2\Omega_m} \int \mathrm{d}^3\mathbf{q}\, q^2 P_{ij}(\mathbf{k})(q^j - k^j)\Psi(\mathbf{q}) \left(\mathcal{H}\Psi(\mathbf{k}-\mathbf{q}) + \dot{\Psi}(\mathbf{k}-\mathbf{q})\right) \,. \tag{2.61}$$

| | | |
|---|---|---|
| RSD | $\frac{1}{2\mathcal{H}}\partial_\chi(\mathbf{S}\cdot\mathbf{n})$ | green |
| Lensing | $-\frac{1}{2}\int_0^{\bar\chi_s} \mathrm{d}\chi\, \frac{\bar\chi_s-\chi}{\bar\chi_s\chi}(2+\Delta_\Omega)\,(\mathbf{S}\cdot\mathbf{n})$ | magenta |
| Volume distortion | $-\frac{1}{2}\int_0^{\bar\chi_s} \mathrm{d}\chi\, \partial_\chi\,(\mathbf{S}\cdot\mathbf{n})$ | orange |
| Doppler | $\frac{1}{2}\left(\frac{2}{\bar\chi_s\mathcal{H}}+\frac{\dot{\mathcal{H}}}{\mathcal{H}^2}\right)(\mathbf{S}\cdot\mathbf{n})$ | blue |
| ISW | $\frac{1}{2}\left(\frac{2}{\bar\chi_s\mathcal{H}}+\frac{\dot{\mathcal{H}}}{\mathcal{H}^2}\right)\left(\int_0^{\bar\chi_s}\mathrm{d}\chi\,(\dot{\mathbf{S}}\cdot\mathbf{n})\right)$ | red |

Table 2.1: The color coding used in the plots for the auto correlation angular power spectra $C_\ell(z_s,z_s')$ of the different contribution to $\Delta^{\rm vec}(\mathbf{n},z)$ in eq. (2.63).

Defining

$$\left\langle S_i(\mathbf{k})\,S_j^*(\mathbf{k}')\right\rangle = (2\pi)^3\frac{P_{ij}}{2}P_S(k)\delta(\mathbf{k}-\mathbf{k}')\,,$$

the power spectrum of vector perturbations, we find

$$\begin{aligned}P_S(k,z) &= \frac{4}{(2\pi)^3}\frac{64k^{-4}}{9\mathcal{H}^2\Omega_m^2}g(z)^2(g(z)-(1+z)g'(z))^2\\ &\times\int \mathrm{d}^3\mathbf{q}\,q^2(2k_iq^i-k^2)\left(q^2-\frac{(k_iq^i)^2}{k^2}\right)T^2(q)P_\Psi^{(\rm in)}(q)T^2(|\mathbf{k}-\mathbf{q}|)P_\Psi^{(\rm in)}(|\mathbf{k}-\mathbf{q}|)\,,\end{aligned}$$

which can be simplified to [215]

$$\mathcal{P}_S(k,z) = 4\frac{8A_s^2}{9\mathcal{H}^2\Omega_m^2}g(z)^2(g(z)-(1+z)g'(z))^2\,k^2\,\Pi(k)\,,\qquad\text{where}\tag{2.62}$$

$$\Pi(k) = \int_0^\infty \mathrm{d}x\int_{|x-1|}^{x+1}\mathrm{d}y\,\frac{(y^2-x^2)((x+y)^2-1)((y-x)^2-1)}{y^2}\left(\frac{k^2xy}{k_*^2}\right)^{n_s-1}T^2(kx)T^2(ky)\,.$$

We now go back to the galaxy number counts. With the results of this section we can rewrite the vector contributions to eq. (2.30) for a vorticity-free fluid as

$$\begin{aligned}\Delta_g^{(\rm V)}(\mathbf{n},z) &= \frac{1}{2\mathcal{H}}\partial_\chi(\mathbf{S}\cdot\mathbf{n})-\frac{1}{2}\int_0^{\bar\chi_s}\mathrm{d}\chi\,\frac{\bar\chi_s-\chi}{\bar\chi_s\chi}\Delta_\Omega\,(\mathbf{S}\cdot\mathbf{n})-\int_0^{\bar\chi_s}\mathrm{d}\chi\,\frac{\bar\chi_s-\chi}{\bar\chi_s\chi}\,(\mathbf{S}\cdot\mathbf{n})\\ &-\frac{1}{2}\int_0^{\bar\chi_s}\mathrm{d}\chi\,\partial_\chi\,(\mathbf{S}\cdot\mathbf{n})+\frac{1}{2}\left(\frac{2}{\bar\chi_s\mathcal{H}}+\frac{\dot{\mathcal{H}}}{\mathcal{H}^2}\right)\left(\mathbf{S}\cdot\mathbf{n}+\int_0^{\bar\chi_s}\mathrm{d}\chi\,(\dot{\mathbf{S}}\cdot\mathbf{n})\right).\end{aligned}\tag{2.63}$$

The first term is the vector-redshift space distortion, the second and third terms are the lensing contributions. In the second line the first term is the radial distortion of the volume

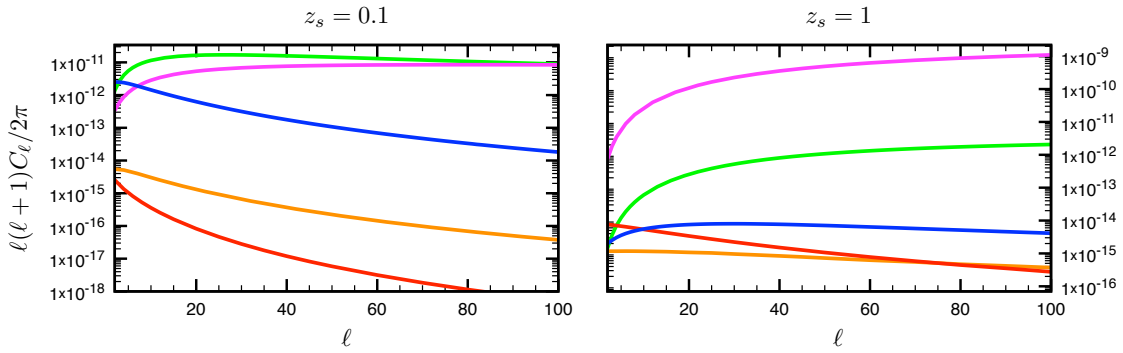


Figure 2.2: The angular power spectrum for the different terms at redshifts $z_s = z_s' = 0.1$ (left) and $z_s = z_s' = 1$ (right). We use the following color coding: redshift space distortion (green), lensing term (magenta), radial volume distortion term (orange), Doppler term (blue) and ISW effect term (red).

and the last two terms come from the redshift perturbation of the volume: a Doppler term and the vector-type integrated Sachs-Wolfe (ISW) term (see table 2.1). Since, at fixed redshift, (2.63) is a function on the sphere we expand it in spherical harmonics with redshift dependent amplitudes

$$\Delta_g^{(\mathrm{V})}(\mathbf{n}, z) = \sum_{\ell m} \delta_{\ell m}(z) Y_{\ell m}(\mathbf{n})\,, \tag{2.64}$$

and we denote the angular power spectrum of vector galaxy number counts by

$$\left\langle \delta_{\ell m}(z) \delta^*_{\ell' m'}(z') \right\rangle = C_\ell(z, z') \delta_{\ell\ell'} \delta_{mm'}\,. \tag{2.65}$$

The computation of the angular correlators is straightforward given that, with our Fourier convention,

$$\partial_\chi(\mathbf{S}\cdot\mathbf{n}) = -i \int \frac{\mathrm{d}^3\mathbf{k}}{(2\pi)^3} n^i k_i\, n^j S_j(k) e^{i\bar{\chi}\mathbf{k}\cdot\mathbf{n}}\,. \tag{2.66}$$

It is useful to factorise the scalar-induced vector power spectrum of eq. (2.62) as $\mathcal{P}_S(k, z, z') = g_S(z) g_S(z') k^2 \Pi(k)$ with

$$g_S(z) = \frac{4\sqrt{2} A_s}{3\mathcal{H}(z)\Omega_m(z)} g(z)\big(g(z) - (1+z)g'(z)\big)\,. \tag{2.67}$$

We present the angular power spectra for the auto-correlations of the different effects defined in eqs. (2.34)–(2.37). The expressions for the cross-correlations are given in Appendix 2.A. We denote the comoving distance to the source redshift $z_s$ by $\bar{\chi}_s$, $\mathcal{H}$ is the Hubble parameter at $z_s$ and $\mathcal{H}'$ is the Hubble parameter at $z_s'$.

$$C_\ell^{\mathrm{RSD}}(z_s, z_s') = \frac{\pi}{2} \frac{\ell(\ell+1)}{\bar{\chi}_s^2 \bar{\chi}_s'^2 \mathcal{H}\mathcal{H}'} \int \frac{\mathrm{d}k}{k^3} \Big[ \Big( (\ell-1) j_\ell(k\bar{\chi}_s) - k\bar{\chi}_s j_{\ell+1}(k\bar{\chi}_s) \Big) \\ \times \Big( (\ell-1) j_\ell(k\bar{\chi}_s') - k\bar{\chi}_s' j_{\ell+1}(k\bar{\chi}_s') \Big) \mathcal{P}_S(k, z_s, z_s') \Big]\,,$$

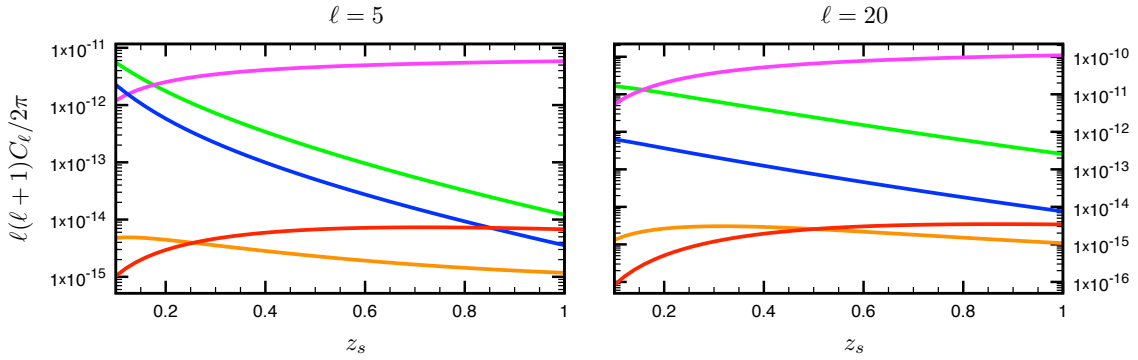


Figure 2.3: Different terms for the transversal power spectrum $C_\ell(z_s, z_s)$ at fixed multipoles $\ell = 5$ (left) and $\ell = 20$ (right) as a function of redshift. Color coding as in figure 2.2.

$$
\begin{aligned}
C_\ell^{\mathrm{Len}}(z_s, z_s') &= \frac{\pi}{2}\ell(\ell+1)(\ell^2+\ell-2)^2 \int_0^{\bar\chi_s} \mathrm{d}\chi \int_0^{\bar\chi_s'} \mathrm{d}\chi'\, W_L(\chi) W_L(\chi') \\
&\quad \times \int \frac{\mathrm{d}k}{k^3} \frac{j_\ell(k\chi)}{\chi} \frac{j_\ell(k\chi')}{\chi'} \mathcal{P}_S(k, z, z')\,, \\
C_\ell^{\mathrm{V}\chi}(z_s, z_s') &= \frac{\pi}{2}\ell(\ell+1) \int_0^{\bar\chi_s} \mathrm{d}\chi \int_0^{\bar\chi_s'} \mathrm{d}\chi' \int \frac{\mathrm{d}k}{k^3} \left[ \left( \frac{(\ell-1) j_\ell(k\chi) - k\chi j_{\ell+1}(k\chi)}{\chi^2} \right) \right. \\
&\quad \left. \times \left( \frac{(\ell-1) j_\ell(k\chi') - k\chi' j_{\ell+1}(k\chi')}{\chi'^2} \right) \mathcal{P}_S(k, z, z') \right], \\
C_\ell^{\mathrm{Dop}}(z_s, z_s') &= \frac{\pi}{2}\ell(\ell+1) \left( \frac{2}{\bar\chi_s \mathcal{H}} + \frac{\dot{\mathcal{H}}}{\mathcal{H}^2} \right) \left( \frac{2}{\bar\chi_s' \mathcal{H}'} + \frac{\dot{\mathcal{H}}'}{\mathcal{H}'^2} \right) \int \frac{\mathrm{d}k}{k^3} \frac{j_\ell(k\bar\chi_s)}{\bar\chi_s} \frac{j_\ell(k\bar\chi_s')}{\bar\chi_s'} \mathcal{P}_S(k, z_s, z_s')\,, \\
C_\ell^{\mathrm{ISW}}(z_s, z_s') &= \frac{\pi}{2}\ell(\ell+1) \left( \frac{2}{\bar\chi_s \mathcal{H}} + \frac{\dot{\mathcal{H}}}{\mathcal{H}^2} \right) \left( \frac{2}{\bar\chi_s' \mathcal{H}'} + \frac{\dot{\mathcal{H}}'}{\mathcal{H}'^2} \right) \int_0^{\bar\chi_s} \mathrm{d}\chi \int_0^{\bar\chi_s'} \mathrm{d}\chi' \\
&\quad \times \int \frac{\mathrm{d}k}{k^3} \left[ \frac{j_\ell(k\chi)}{\chi} \frac{j_\ell(k\chi')}{\chi'} \mathcal{P}_{\dot S}(k, z, z') \right],
\end{aligned}
$$

where $W_L(\chi) = \frac{\bar\chi_s - \chi}{\chi \bar\chi_s}$ and $\mathcal{P}_{\dot S}(k, z, z') = \dot g_S(z) \dot g_S(z') k^2 \Pi(k)$.

As vector perturbations do not affect the density of galaxies, all the contributions relate to gravitational effects on the propagation of light. We calculate these contributions numerically for a flat ΛCDM model with Planck [11] cosmological parameters. More precisely, we choose $\Omega_b h^2 = 0.022$, $\Omega_m h^2 = 0.12$, $n_s = 0.96$, $A_s = 2.21 \times 10^{-9}$ at the pivot scale $k_\star = 0.05\ \mathrm{Mpc}^{-1}$ . The Hubble constant at present time is $H_0 = h \times 100$ km/s/Mpc with $h = 0.67$. If we correlate perturbations at fixed redshift $C_\ell(z_s, z_s)$ we obtain the transversal power spectrum but we can also correlate perturbations at different redshifts to obtain the radial power spectrum $C_\ell(z_s, z_s')$. In figures 2.2–2.6 we plot the transversal and radial angular power spectra for the different terms. Comparing them with the effects induced by scalar perturbations we see in figure 2.7 that the amplitude of the corresponding vector terms is suppressed by 2 orders of

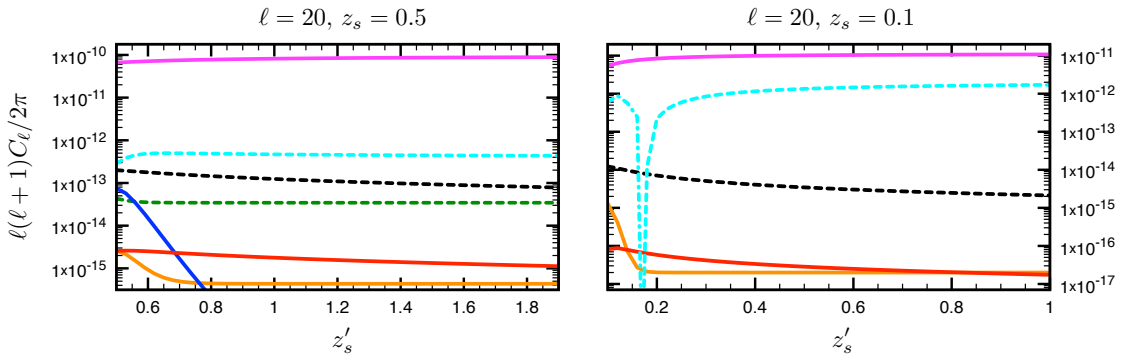


Figure 2.4: Most relevant terms for the radial power spectra $C_\ell(z_s, z_{S'})$ at $z_s = 0.5$ (left) and $z_s = 0.1$ (right), both for fixed multipole $\ell = 20$. The lensing term (magenta), the volume contribution (orange), the ISW effect (red). For the cross spectra: the correlation lensing-ISW (black, dashed), the RSD-lensing term (cyan, dashed) and the lensing-volume distortion (dashed, dark green). Cross spectra are dashed and negative contributions are dot-dashed.

magnitudes in the case of the relativistic terms and up to 4–5 orders of magnitudes in the case of RSD, see fig. 2.7. The standard density term is however absent and this means that, in total, the vector number counts amplitude can be suppressed up to 6 orders of magnitudes at low redshifts. The RSD is the dominant contribution only at low redshift while the lensing term starts to dominate for $z_s \gtrsim 0.2$. Like for scalar perturbations, the radial power spectra terms are largely dominated by the integrated terms, especially the lensing term. Therefore, in radial spectra with $z_s \neq z_s'$ the vector contribution is less suppressed.

Note also that all the results presented here have been obtained with a $\delta$-function window. Admitting a wider window function in redshift would significantly reduce the density term and the redshift space distortion without affecting integrated terms like lensing. [125, 235].

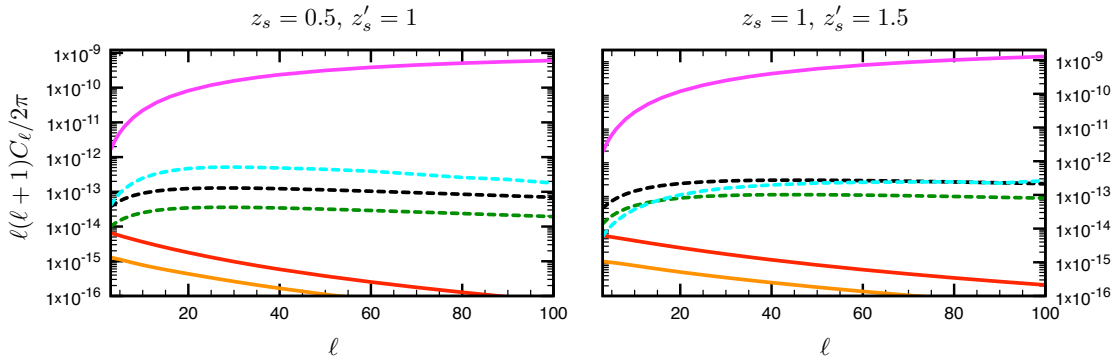


Figure 2.5: Most relevant terms for the radial power spectrum $C_\ell(z_s, z_{s'})$ as a function of multipoles for $z_s = 0.5$, $z_s' = 1$ (left) and $z_s = 1$, $z_s' = 1.5$ (right). Cross spectra are dashed. Color coding as in figure 2.4.

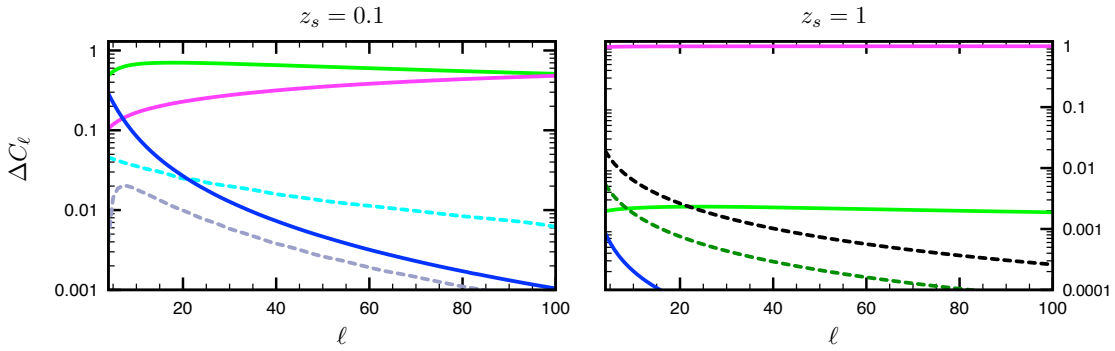


Figure 2.6: The dominant fractional contributions $\Delta C_\ell = (C_\ell - C_\ell^{\rm tot})/C_\ell^{\rm tot}$ to the total effect of vector perturbations due to the most relevant terms at $z_s = z_s' = 0.1$ (left) and $z_s = z_s' = 1$ (right). Color coding as in figures 2.2–2.4 and we also plot the RSD-doppler correlation (dashed, gray).

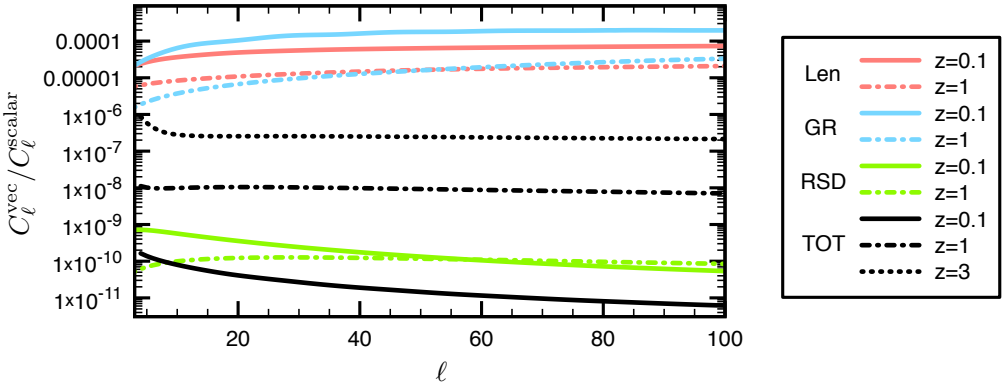


Figure 2.7: Comparison of the different terms in the case of scalar perturbation and in the case of scalar-induced vectors. If we refer to the CLASSgal terminolgy we have the lensing term (pink), the RSD term (green) and the GR terms (light blue). We also plot the total $C_\ell$ (black).

## 2.4 Conclusions

We have computed the galaxy number counts for vector and tensor fluctuations in linear perturbation theory. The well-known computation for the contribution from scalar modes has been also detailed since it represents the foundation upon which the following chapters are based. We have obtained a general expression which can be applied for all situations where linear cosmological perturbation theory is valid. We have employed it to compute the contribution to the galaxy number counts from vector perturbations which are induced from the usual scalar perturbations at second order in perturbation theory. While these terms are certainly present in the standard ΛCDM cosmology, they are very small.

Since within the perfect fluid approximation no vorticity is generated, the only 'standard term', the redshift space distortion is also very small. For intermediate to large redshifts, $z \gtrsim 0.2$, the lensing term dominates the result for both radial and transversal correlations. It is however 4 to 5 orders of magnitude smaller than the corresponding signal due to scalar perturbations. This means that only if the amplitude of the scalar lensing contribution can be measured to an accuracy of better than 1%, it might be feasible to see this vector contribution. This seems to be difficult, but the scalar lensing contribution by far dominates the radial correlation function and will probably be measured with good accuracy in the future. Furthermore, it has been found in simulations [7] that higher order non-linear contributions tend to enhance vector perturbations. However, this effect is strong only on small scales which are relevant in angular power spectra only at high multipoles [9].

Interestingly, when going to higher redshifts, up to redshift $z = 3$, the total vector to scalar ratio is increasing, see figure 2.7, even though the second order vectors are smaller at higher redshift. This is due to the fact that at higher redshift the lensing term increases while the density and redshift space distortions decrease [72]. Therefore the lensing term becomes more relevant and for this contribution vector perturbations are least suppressed.

Nevertheless, it seems not very promising to detect vector perturbations in the number counts with presently planned observations, if they are not larger than what is expected within ΛCDM. This probably stems from the fact that number counts are an inherently scalar quantity which is expected to be dominated by scalar perturbations. It has recently been suggested [275] that intrinsically spin-2 quantities like the alignment of the ellipticity of galaxies might be more promising. Another intriguing possibility might be measuring the alignment or the correlation of the spins of distant galaxies.

In chapter 6 we will come back to vector perturbations (with an anisotropic component) and we will see how an observable which is specifically designed can increase the chances of detection.

## 2.A Cross-correlations

For completeness we present here the results of eq. (2.65) also for the cross-correlations between the different terms of eqs. (2.34–2.37).

$$C_\ell^{\text{RSD-Len}}(z_s, z_s') = -\frac{\pi}{2}\frac{\ell(\ell+1)}{\bar{\chi}_s^2\mathcal{H}}(\ell^2+\ell-2)\int \frac{\mathrm{d}k}{k^3}\Bigg[\Big((\ell-1)j_\ell(k\bar{\chi}_s) - k\bar{\chi}_s j_{\ell+1}(k\bar{\chi}_s)\Big) \times \int_0^{\bar{\chi}_s'} \mathrm{d}\chi'\, W_L(\chi')\frac{j_\ell(k\chi')}{\chi'}\mathcal{P}_S(k, z_s, z')\Bigg]$$

$$C_\ell^{\text{RSD-V}\chi}(z_s, z_s') = -\frac{\pi}{2}\frac{\ell(\ell+1)}{\bar{\chi}_s^2\mathcal{H}}\int \frac{\mathrm{d}k}{k^3}\Bigg[\Big((\ell-1)j_\ell(k\bar{\chi}_s) - k\bar{\chi}_s j_{\ell+1}(k\bar{\chi}_s)\Big) \times \int_0^{\bar{\chi}_s'} \mathrm{d}\chi'\left(\frac{(\ell-1)j_\ell(k\chi') - k\chi' j_{\ell+1}(k\chi')}{\chi'^2}\right)\mathcal{P}_S(k, z_s, z')\Bigg]$$

$$C_\ell^{\text{RSD-Dop}}(z_s, z_s') = -\frac{\pi}{2}\frac{\ell(\ell+1)}{\bar{\chi}_s^2\mathcal{H}}\left(\frac{2}{\bar{\chi}_s'\mathcal{H}'} + \frac{\dot{\mathcal{H}}'}{\mathcal{H}'^2}\right)\int \frac{\mathrm{d}k}{k^3}\Bigg[\Big((\ell-1)j_\ell(k\bar{\chi}_s) - k\bar{\chi}_s j_{\ell+1}(k\bar{\chi}_s)\Big) \times \frac{j_\ell(k\bar{\chi}_s')}{\bar{\chi}_s'}\mathcal{P}_S(k, z_s, z_s')\Bigg]$$

$$C_\ell^{\text{RSD-ISW}}(z_s, z_s') = -\frac{\pi}{2}\frac{\ell(\ell+1)}{\bar{\chi}_s^2\mathcal{H}}\left(\frac{2}{\bar{\chi}_s'\mathcal{H}'} + \frac{\dot{\mathcal{H}}'}{\mathcal{H}'^2}\right)\int \frac{\mathrm{d}k}{k^3}\Bigg[\Big((\ell-1)j_\ell(k\bar{\chi}_s) - k\bar{\chi}_s j_{l+1}(k\bar{\chi}_s)\Big) \times \int_0^{\bar{\chi}_s'} \mathrm{d}\chi'\frac{j_\ell(k\chi')}{\chi'}\mathcal{P}_{S\dot{S}}(k, z_s, z')\Bigg]$$

$$
\begin{aligned}
C_\ell^{\text{Len-V}\chi}(z_s, z_s') &= \frac{\pi}{2}\ell(\ell+1)(\ell^2+\ell-2)\int_0^{\bar\chi_s}\mathrm{d}\chi\int_0^{\bar\chi_s'}\mathrm{d}\chi'\,W_L(\chi)\int\frac{\mathrm{d}k}{k^3}\Bigg[\frac{j_\ell(k\chi)}{\chi}\\
&\quad\times\left(\frac{(\ell-1)j_\ell(k\chi')-k\chi' j_{\ell+1}(k\chi')}{\chi'^2}\right)\mathcal{P}_S(k,z,z')\Bigg]\\
C_\ell^{\text{Len-Dop}}(z_s, z_s') &= \frac{\pi}{2}\ell(\ell+1)(\ell^2+\ell-2)\left(\frac{2}{\bar\chi_s'\mathcal{H}'}+\frac{\dot{\mathcal{H}}'}{\mathcal{H}'^2}\right)\int\frac{\mathrm{d}k}{k^3}\frac{j_\ell(k\bar\chi_s')}{\bar\chi_s'}\int_0^{\bar\chi_s}\mathrm{d}\chi\\
&\quad\times\Big[W_L(\chi)\frac{j_\ell(k\chi)}{\chi}\mathcal{P}_S(k,z,z_s')\Bigg]\\
C_\ell^{\text{Len-ISW}}(z_s, z_s') &= \frac{\pi}{2}\ell(\ell+1)(\ell^2+\ell-2)\left(\frac{2}{\bar\chi_s'\mathcal{H}'}+\frac{\dot{\mathcal{H}}'}{\mathcal{H}'^2}\right)\int_0^{\bar\chi_s}\mathrm{d}\chi\int_0^{\bar\chi_s'}\mathrm{d}\chi'\\
&\quad\times\left[W_L(\chi)\int\frac{\mathrm{d}k}{k^3}\frac{j_\ell(k\chi)}{\chi}\frac{j_\ell(k\chi')}{\chi'}\mathcal{P}_{S\dot S}(k,z,z')\right]\\
C_\ell^{\text{V}\chi\text{-Dop}}(z_s, z_s') &= \frac{\pi}{2}\ell(\ell+1)\left(\frac{2}{\bar\chi_s'\mathcal{H}'}+\frac{\dot{\mathcal{H}}'}{\mathcal{H}'^2}\right)\int\frac{\mathrm{d}k}{k^3}\Bigg[\frac{j_\ell(k\bar\chi_s')}{\bar\chi_s'}\\
&\quad\times\int_0^{\bar\chi_s}\mathrm{d}\chi\left(\frac{(\ell-1)j_\ell(k\chi)-k\chi j_{\ell+1}(k\chi)}{\chi^2}\right)\mathcal{P}_S(k,z,z_s')\Bigg]\\
C_\ell^{\text{V}\chi\text{-ISW}}(z_s, z_s') &= \frac{\pi}{2}\ell(\ell+1)\left(\frac{2}{\bar\chi_s'\mathcal{H}'}+\frac{\dot{\mathcal{H}}'}{\mathcal{H}'^2}\right)\int_0^{\bar\chi_s}\mathrm{d}\chi\int_0^{\bar\chi_s'}\mathrm{d}\chi'\int\frac{\mathrm{d}k}{k^3}\\
&\quad\times\left[\left(\frac{(\ell-1)j_\ell(k\chi)-k\chi j_{\ell+1}(k\chi)}{\chi^2}\right)\frac{j_\ell(k\chi')}{\chi'}\mathcal{P}_{S\dot S}(k,z,z')\right]\\
C_\ell^{\text{Dop-ISW}}(z_s, z_s') &= \frac{\pi}{2}\ell(\ell+1)\left(\frac{2}{\bar\chi_s\mathcal{H}}+\frac{\dot{\mathcal{H}}}{\mathcal{H}^2}\right)\left(\frac{2}{\bar\chi_s'\mathcal{H}'}+\frac{\dot{\mathcal{H}}'}{\mathcal{H}'^2}\right)\int\frac{\mathrm{d}k}{k^3}\frac{j_\ell(k\bar\chi_s)}{\bar\chi_s}\\
&\quad\times\int_0^{\bar\chi_s'}\mathrm{d}\chi'\Big[\frac{j_\ell(k\chi')}{\chi'}\mathcal{P}_{S\dot S}(k,z_s,z')\Big],
\end{aligned}
$$

where $\mathcal{P}_{S\dot S}(k,z,z') = g_S(z)\dot g_S(z')k^2\Pi(k)$.

# CHAPTER 3

## Correlation function I: Theoretical aspects

**Based on:**

[294] V. Tansella, C. Bonvin, R. Durrer, B. Ghosh and E. Sellentin, "*The full-sky relativistic correlation function and power spectrum of galaxy number counts. Part I: Theoretical aspects*",
**JCAP 1803** (2018) 019, [arXiv:1708.00492].

**Abstract.** In this chapter we derive an exact expression for the galaxy two-point function in redshift shells including all the relativistic contributions. This expression, which does not rely on the distant-observer or flat-sky approximation, is valid at all scales where linear PT holds and includes both local relativistic corrections and integrated contributions, like gravitational lensing. We present two methods to calculate this correlation function, one which makes use of the angular power spectrum $C_\ell(z_1, z_2)$, introduced in the previous chapter, and a second method which evades the costly calculations of the angular power spectra. In this work theoretical aspects of this procedure are presented, together with quantitative examples. In particular, we show that gravitational lensing modifies the multipoles of the correlation function and of the power spectrum by a few percent at redshift $z = 1$ and by up to 30% and more at $z = 2$. We also point out that large-scale relativistic effects and wide-angle corrections generate contributions of the same order of magnitude and have consequently to be treated in conjunction. These corrections are particularly important at small redshift, $z = 0.1$, where they can reach 10%. This means in particular that a flat-sky treatment of relativistic effects, using for example the power spectrum, is not consistent.

## 3.1 Introduction

In chapter 2 we have discussed the corrections induced by light-cone effects on the galaxy number counts, with an application to the angular power spectrum $C_\ell(z_1, z_2)$. We now move to the observable which will be the common thread for the rest of this thesis: the correlation function $\xi$. To define the correlation function $\xi$, let us recall that, as we have done in chapter 2, given a certain distribution of point galaxies, we can define the local number density in a small volume of size $V$. The point is that this may be regarded, after suitable normalisation, as the probability for finding a galaxy in the volume $V$. We treat the galaxy distribution as the result of a random process. If there was no correlation then we would simply have a distribution of randomly distributed, independent, point-like events, i.e. Poisson noise. In this sense the two-point function (2pF) $\xi(\mathbf{r})$ can be regarded as the excess probability, with respect to the Poisson distribution, to find two galaxies separated by a distance $\mathbf{r}$. In other words for an homogeneous Poisson process the probability of findings galaxies in two volumes $dV_1$, $dV_2$, separated by a distance $\mathbf{r}$ is given by

$$dP_{12} = \bar{n}^2 dV_1 dV_2 \,, \tag{3.1}$$

where $\bar{n}$ is the mean galaxy density. However, because of the underlying density field, clustering is not homogeneous and, as we anticipated, the excess probability w.r.t. Poisson noise is the two-point function

$$dP_{12} = \bar{n}^2 (1 + \xi(\mathbf{r})) dV_1 dV_2 \,. \tag{3.2}$$

If the probability is higher than Poisson noise then $\xi(\mathbf{r}) > 0$ (correlation), if it is smaller $\xi(\mathbf{r}) < 0$ (anti-correlation).

Theoretically the relevant field is the number count fluctuation $\Delta_g(\mathbf{x})$, which is a random field with vanishing expectation value $\langle \Delta_g \rangle = 0$. The excess probability is given by the field correlator, i.e. the expectation value of products of fields at different points

$$\xi(\mathbf{r}) = \xi(\mathbf{x} - \mathbf{y}) = \langle \Delta_g(\mathbf{x}) \Delta_g(\mathbf{y}) \rangle \,. \tag{3.3}$$

Notice that $\mathbf{x}$, $\mathbf{y}$ are spatial coordinates while redshift surveys generally associate (at least) two quantities to each galaxy they detect: the direction from which photons are received, $\mathbf{n}$, and the redshift $z$. It has therefore been argued in the past [175, 176, 290, 291, 254, 72], that galaxy correlation functions are truly functions of two redshifts and an angle. Essentially this comes from the fact that our observations are limited to our past light-cone: this means that the correlation function, in a similar way of the angular-redshift power spectrum $C_\ell(z_1, z_2)$, acquires corrections due to the projection effects. There is a simple way to obtain the two-point function starting from the $C_\ell$ and, as we have already determined the observed angular spectrum, this link will provide us with the general expression for the observable $\xi$. To determine the $C_\ell(z_1, z_2)$ observationally, one correlates the number of galaxies in a redshift bin around $z_1$ and in a small solid angle around direction $\mathbf{n}_1$ with those in a redshift bin around $z_2$ and in a small solid angle around direction $\mathbf{n}_2$. Due to statistical isotropy, the resulting correlation function only depends on the angle $\theta$ between $\mathbf{n}_1$ and $\mathbf{n}_2$, $\cos\theta = \mathbf{n}_1 \cdot \mathbf{n}_2$

(see appendix B.1) and is related to the angular power spectrum in the well known way,

$$\xi(\theta, z_1, z_2) = \frac{1}{4\pi}\sum_\ell (2\ell+1) C_\ell(z_1, z_2)\mathcal{P}_\ell(\cos\theta)\,, \tag{3.4}$$

where $\mathcal{P}_\ell$ denotes the Legendre polynomial of degree $\ell$.

Before the introduction of the $C_\ell(z_1, z_2)$'s, cosmologists have mainly concentrated on determining the correlation function and the power spectrum in Fourier space. In comoving gauge, on sub-horizon scales the latter is given by [199]

$$\begin{aligned} P_g(k,\nu,\bar{z}) &= D_1^2(\bar{z})\left[b(\bar{z}) + f(\bar{z})(\hat{\mathbf{k}}\cdot\mathbf{n})^2\right]^2 P(k) \\ &= D_1^2(\bar{z})\left[b^2 + \frac{2bf}{3} + \frac{f^2}{5} + \left(\frac{4bf}{3} + \frac{4f^2}{7}\right)\mathcal{P}_2(\nu) + \frac{8f^2}{35}\mathcal{P}_4(\nu)\right]P(k)\,. \end{aligned} \tag{3.5}$$

Here $\bar{z}$ is the mean redshift or the survey, $P(k)$ is the matter density power spectrum today, $D_1(\bar{z})$ is the growth factor normalised to $D_1(0) = 1$ and related to $g(z)$ in chapter 2 via $(1+z)D_1 = g$. Furthermore $b(\bar{z})$ is the galaxy bias and

$$f(\bar{z}) = -\frac{D_1'}{D_1}(1+\bar{z}) = \frac{d\ln D_1}{d\ln(a)}\,, \tag{3.6}$$

is the growth rate, where the prime denotes the derivative with respect to the redshift $\bar{z}$. The direction cosine $\nu$ is the cosine of the angle between $\mathbf{k}$ and the observation direction $\mathbf{n}$ (in the literature this direction cosine is often denoted as $\mu$ but here we reserve $\mu$ for the corresponding angle in real space and in order to avoid confusion we denote it by $\nu$ in Fourier space).

Equation (3.5) has an interesting property: projecting out the monopole, quadrupole and hexadecapole in $\nu$, one can directly measure the bias $b$ and the growth rate $f$. This has been exploited in previous observations and has led to the best determinations of $f$ so far (see [108, 239, 4, 10, 19, 272] and refs. therein). It is clear that the form (3.5) of the power spectrum can only be valid if the bins are not too far apart in the sky. Eq. (3.5) indeed implicitly assumes that the galaxies are observed in *one* single direction $\mathbf{n}$ so that a 'flat-sky approximation' with a well defined angle $\nu$ is a reasonably good approximation.

The correlation function $\xi(r, \mu, \bar{z})$ is an observable alternative to the power spectrum, which is routinely used in galaxy surveys. The separation between the galaxies is again denoted by $r$, while we have introduced a dependence on $\mu$, which is the orientation of the pair with respect to the direction of observation $\mathbf{n}$ and on $\bar{z}$, which is the mean redshift of the bin. The correlation function is observed in terms of $z_1, z_2$ and $\theta$. To express it in terms of $r, \mu$ and $\bar{z}$, the redshifts $z_1$ and $z_2$ have to be converted into comoving distances and a direction cosine $\mu$ has to be defined.

Neglecting spatial curvature we can use the cosine law to express $r$ in terms of the comoving distances to $z_1$ and $z_2$,

$$r(z_1, z_2, \theta) = \sqrt{\chi(z_1)^2 + \chi(z_2)^2 - 2\chi(z_1)\chi(z_2)\cos\theta}\,, \tag{3.7}$$

where

$$\chi(z) = \frac{1}{\mathcal{H}_0}\int_0^z \frac{dz}{\sqrt{\Omega_m(1+z)^3 + \Omega_X g_X(z)}}\,. \tag{3.8}$$

Here $\Omega_m$ is the matter density parameter and $\Omega_X g_X(z)$ is the dark energy density in units of the critical density today; $g_X$ is normalised to $g_X(0) = 1$ and accounts for the possible evolution of the equation of state parameter $w$. Hence the correlation function $\xi(r, \mu, \bar{z})$, as well as the power spectrum, are not directly observable: they both require the use of a fiducial cosmology to calculate $r$ and $\chi(z)$. If the redshift is small, $z \ll 1$, we can write $\chi(z) \simeq z/H_0$, and the dependence on $H_0$ is taken into account by measuring cosmological distances in units of Mpc/$h$, where Mpc denotes a megaparsec ($\simeq 3.1 \times 10^6$ light years) and $h = H_0/100\,\mathrm{km/s/Mpc}$. However, in present and upcoming catalogues which go out to $z = 2$ and more, this is no longer sufficient and $r$ depends in a non-trivial way on the dark matter and dark energy density, on the dark energy equation of state and on curvature (which is set to zero throughout this thesis for simplicity). Fortunately this dependence can be accounted for by introducing correction parameters, which allow for deviations from the fiducial cosmology, see e.g. [312]. Note that in this and in the following chapters we do not need to distinguish anymore between $\chi$ and $\bar{\chi}$: to avoid heavy notation we now set $\chi$ to be the background comoving distance as in eq. (3.8). Furthermore we sometimes use $\bar{\chi}$ as the mean distance of a pair of galaxies. In the flat-sky approximation, the standard correlation function takes the simple form [171]

$$\begin{aligned}\xi_{\text{flat-sky}}(r, \mu, \bar{z}) = D_1^2(\bar{z})\Bigg[&\left(b^2 + \frac{2bf}{3} + \frac{f^2}{5}\right) I_0^0(r) \\ &- \left(\frac{4bf}{3} + \frac{4f^2}{7}\right) I_2^0(r)\mathcal{P}_2(\mu) + \frac{8f^2}{35}\mathcal{P}_4(\mu) I_4^0(r)\Bigg],\end{aligned} \tag{3.9}$$

with

$$I_\ell^0(r) = \int \frac{dk}{2\pi^2}\, k^2 P(k) j_\ell(rk)\,, \tag{3.10}$$

(the reason for the superscript 0 will become clear in chapter 4). Note that the terms containing the growth factor $f$ come from the Jacobian transforming real space positions $\mathbf{x}$ into redshifts[1]. In Appendix 3.D we derive the general relation between the $I_\ell^0(r)$ and the corresponding pre-factors of the Legendre polynomials in the power spectrum.

Expressions (3.5) and (3.9) are currently used to analyse redshift surveys[2]. These expressions are sufficiently accurate to place meaningful constraints on cosmological parameters with

[1] We point out that the original derivation of redshift-space distortion from [199] contains a contribution proportional to $\mathbf{n} \cdot \mathbf{v} = v_r$. This term does contribute to the monopole and quadrupole and it consequently modifies (3.9). It is however neglected in most redshift-space distortion analysis and therefore we do not consider it as 'standard' and we do not include it in (3.9). We include it however in the relativistic corrections, along with the other Doppler corrections, which are of the same order of magnitude (see eq. (3.15)). Note that, as discussed in more detail in Section 3.2.2, this specific contribution has been studied in detail in [290, 291, 240, 254] and its impact on the correlation function was found to be important at small redshift and large separation.

[2] Note that these expressions are valid in the linear regime only. Theoretical models accounting for non-linearities have been developed and are used to extend the constraints to non-linear scales, see e.g. [151].

current data. They may however not be sufficient to analyse future surveys since they suffer from two important limitations: first they are based on the flat-sky (sometimes also called distant-observer) approximation. And second they take into account only density fluctuations and redshift-space distortions. They neglect lensing which is relevant especially at high redshifts. They also neglect all the relativistic projection effects which are relevant on large scales (close to horizon scale). These expressions are therefore only an approximate description of what we are observing, which is also reflected by the fact that they are gauge-dependent.

Due to these limitations, one would be tempted to use the angular power spectrum instead of eqs. (3.5) and (3.9) to analyse future redshift surveys. The gauge-invariant $C_\ell(z_1, z_2)$'s account indeed for all observable effects. They are directly observable and do not rely on the flat-sky approximation. And they can be determined numerically within a few seconds with sub-percent accuracy. Unfortunately they are not fully satisfactory for several reasons:

1. If we want to profit optimally from *spectroscopic* redshift information from a survey like the one that will be generated by Euclid [204], DESI [16] or the SKA [93], we need several thousand redshift slices leading to several million $C_\ell(z, z')$ spectra. For an MCMC parameter estimation this is simply prohibitive. Even if one spectrum is calculated within a few seconds, calculating the millions of spectra $\sim 10^5$ times would take months even if highly parallelised.

2. In each spectroscopic redshift bin we then only have a few 1000 galaxies, less than one per square degree, and the observed spectra would have very large shot noise $\propto 1/N$, allowing only computation up to very low $\ell$.

3. One of the big advantages of $\xi(r, \mu)$ and $P(k, \nu)$ is that the growth rate $f(z)$ can be simply determined by isolating the monopole, quadrupole and hexadecapole components in an expansion of $P$ and $\xi$ in Legendre polynomials in $\mu$ and $\nu$ respectively. With the $C_\ell$'s on the other hand there is no simple way to isolate redshift-space distortions since each multipole $\ell$ is a non-trivial combination of density and velocity.

Hence even though the $C_\ell$'s are very convenient theoretically, they are not fully satisfactory from an observational point of view. In this chapter we therefore derive general expressions for the correlation function and the power spectrum, that can be used as theoretical models for future surveys. Our work builds on the result of several papers, which have studied the impact of some of the relativistic effects on the correlation function and on the power spectrum. In [194, 322], expressions for the flat-sky power spectrum including all non-integrated relativistic effects have been derived. In [182, 213, 183] the lensing contribution to the flat-sky power spectrum and the flat-sky correlation function has been studied in detail. Refs. [290, 291, 240] have derived full-sky expressions for density and redshift-space (RSD) contributions to the correlation function, which have then be further developed in [254, 269, 52, 323]. These expressions have been re-derived using an alternative method in [90]. Ref. [259] has studied in detail the relation between the full-sky and flat-sky density and RSD for both the correlation function and the power spectrum. In [76] the full-sky calculation of [290, 291, 240] has been extended to include gravitational redshift and Doppler terms, which are especially relevant in the case of multiple populations of galaxies. Ref. [52]

further expands the formalism introduced in [290] by computing theoretical expressions for the wide-angle corrections including also the integrated terms and Ref. [250] numerically evaluates all the non-integrated relativistic terms in the full-sky. In [252] the integrated terms in the correlation function are plotted for the first time for two values of the angle $\theta$. The theoretical expressions in these works rely on an expansion of the correlation function in Tripolar Spherical Harmonics which on the one hand is a powerful tool to obtain simple expressions in the full-sky but on the other hand hides some properties of the correlation function enforced by isotropy.[3]

Here we generalise and complete these results. We first derive a full-sky expression for the correlation function including all local and integrated contributions, in which isotropy of the perturbations is explicit. In particular, we provide a detailed study of the gravitational lensing contribution to the correlation function which does not rely on the flat-sky or Limber approximation. We discuss how these full-sky contributions modify the simple multipole expansion of eq. (3.9). This represents the first analysis of the full-sky lensing contributions to the multipoles of the correlation function, which is most relevant when extracting the growth factor. In this aspect as in several other ways, this analysis goes beyond the work of [252].

In the last section of this chapter we use the correlation function to calculate the power spectrum, which we define as the Fourier transform of the full-sky correlation function. In this way the power spectrum does not rely explicitly on the flat-sky approximation. However, as we will explain in section 3.3, it has an unambiguous interpretation only in this limit. A comparison between the usual flat-sky derivation and the full-sky Fourier transform of the correlation function is not reported in this thesis but can be found in Tansella et.al. (2017), where we find that relativistic effects and wide-angle corrections[4] are of the same order of magnitude and they have therefore to be treated in conjunction. This leads us to the conclusion that relativistic effects cannot be consistently studied in the flat-sky approximation and that the correlation function is therefore more adapted than the power spectrum to investigate these effects.

This chapter is the first part of this study where we present the theoretical derivation and some numerical results. For an exhaustive numerical study we have written the public code COFFE which we present in the next chapter. Of course, there are many studies estimating cosmological parameters using the $C_\ell(z_1, z_2)$, see for example [124, 253, 235, 92, 126]. However as argued above, these can mainly be used for large, photometric redshift bins while within such bins, in order to profit optically from spectroscopic redshift information, a correlation function or power spectrum analysis is required.

The remainder of the chapter is structured as follows: in the next section we describe how we obtain the redshift-space correlation function from the angular correlation function. As already discussed above, the procedure of course depends on the cosmological model. We shall describe two possibilities: to go either over the $C_\ell(z_1, z_2)$ spectra or to obtain $\xi(r, \mu, \bar{z})$

[3] Whether in flat-sky or full-sky the correlation function depends on three variables: two distances and one angle ($\xi(\chi_1, \chi_2, \theta)$ or $\xi(\bar{\chi}, r, \cos\alpha)$ in this work), one distance and two angles ($\xi(\theta, \gamma, r)$ in [290], $\xi(\chi_2, \theta, \phi)$ in [250]) or three distances ($\xi(\chi_1, \chi_2, r)$). When $\xi$ is expanded in Tripolar Spherical Harmonics one obtains a function $\xi(\mathbf{x}_1, \mathbf{x}_2)$ and the three physical variables are in general not directly inferred.

[4] Here we call wide-angle corrections the difference between the flat-sky and full-sky expressions.

directly from the density fluctuations, velocity fluctuations and the Bardeen potentials in Fourier space. In Section 3.4 we discuss the implications of our findings for future surveys and we conclude. Several technical derivations are relegated to the appendices.

## 3.2 The correlation function

We have derived the galaxy number counts including relativistic corrections in eq. (2.47), with the following result

$$\Delta_g(\mathbf{n}, z) = \Delta^{\rm den} + \Delta^{\rm rsd} + \Delta^{\rm len} + \Delta^{\rm d1} + \Delta^{\rm d2} + \Delta^{\rm g1} + \Delta^{\rm g2} + \Delta^{\rm g3} + \Delta^{\rm g4} + \Delta^{\rm g5}\,, \tag{3.11}$$

where

$$\begin{aligned}
\Delta^{\rm den} &= b\delta_c(\chi(z)\mathbf{n}, z)\,, && (3.12)\\
\Delta^{\rm rsd} &= -\mathcal{H}^{-1}\partial_r v_r\,, && (3.13)\\
\Delta^{\rm len} &= \frac{5s-2}{2\chi}\int_0^{\chi(z)} d\lambda \frac{\chi-\lambda}{\lambda}\Delta_\Omega(\Phi+\Psi), && (3.14)\\
\Delta^{\rm d1} &= -\left(\frac{\dot{\mathcal{H}}}{\mathcal{H}^2} + \frac{2-5s}{\mathcal{H}\chi} + 5s - f_{\rm evo}\right) v_r\,, && (3.15)\\
\Delta^{\rm d2} &= -(3-f_{\rm evo})\mathcal{H}v\,, && (3.16)\\
\Delta^{\rm g1} &= \left(1 + \frac{\dot{\mathcal{H}}}{\mathcal{H}^2} + \frac{2-5s}{\mathcal{H}\chi} + 5s - f_{\rm evo}\right)\Psi\,, && (3.17)\\
\Delta^{\rm g2} &= (5s-2)\Phi\,, && (3.18)\\
\Delta^{\rm g3} &= \mathcal{H}^{-1}\dot{\Phi} && (3.19)\\
\Delta^{\rm g4} &= \frac{2-5s}{\chi}\int_0^{\chi(z)} d\lambda(\Phi+\Psi)\,, && (3.20)\\
\Delta^{\rm g5} &= \left(\frac{\dot{\mathcal{H}}}{\mathcal{H}^2} + \frac{2-5s}{\mathcal{H}\chi} + 5s - f_{\rm evo}\right)\int_0^{\chi(z)} d\lambda(\dot{\Phi}+\dot{\Psi})\,. && (3.21)
\end{aligned}$$

Here $\delta_c$ is the matter density fluctuation in comoving gauge, $v_r$ is the radial component of the velocity in longitudinal gauge, $v$ is the velocity potential such that $\mathbf{v} = -\nabla v$, $v_r = -\partial_r v$; hence $v$ has the dimension of a length (we later define $V$ via its Fourier transform, $\hat{v} = k^{-1}V(k)$, so that $V(\mathbf{x})$ is dimensionless). $\Phi$ and $\Psi$ are the Bardeen potentials and $\Delta_\Omega$ denotes the Lapacian on the sphere of directions $\mathbf{n}$. The galaxy bias is denoted by $b$, $s$ is the magnification bias and $f_{\rm evo}$ is the evolution bias. These biases generally depend on redshift. The magnification bias $s$ comes from the fact that in general we do not observe all galaxies but only those which are brighter than the flux limit of our instrument. Due to lensing and to some relativistic effects, some fainter galaxies may make it into our surveys. This is taken into account by $s$ which is proportional to the logarithmic derivative of the galaxy luminosity function at the flux limit of our survey, see [99, 125] or section 2.2.3, for more details.

The terms $\Delta^{\rm den}$ and $\Delta^{\rm rsd}$ are the density and redshift-space distortion terms usually taken into account. In the following we call the sum of these two terms the 'standard terms'. $\Delta^{\rm len}$

represents the lensing term, also often called magnification. This term has already been measured with quasars at large redshift, see e.g. [228], but it is usually neglected in galaxy surveys, since it is subdominant at low redshift. $\Delta^{\rm d1}$ is the Doppler contribution. Note that here we have used Euler's equation to derive this term. In all generality this term contains a contribution from gravitational redshift, proportional to $\partial_r\Psi/\mathcal{H}$, which can be rewritten in terms of the velocity $v_r$ using Euler equation, see e.g. [76]. $\Delta^{\rm d2}$ is a velocity term which comes from transforming the longitudinal gauge density into the comoving density. $\Delta^{\rm g1}, \Delta^{\rm g2}$ and $\Delta^{\rm g3}$ are relativistic effects, given by the gravitational potentials at the source. As such they are sometimes called 'Sachs-Wolfe' terms. $\Delta^{\rm g4}$ denotes the so-called Shapiro time-delay contribution and $\Delta^{\rm g5}$ is the integrated Sachs-Wolfe term.

In the following we will sometimes group together the relativistic non-integrated terms (d1, d2, g1, g2, g3). The lensing term is treated separately since its calculation is different. The relativistic integrated terms (g4 and g5) are neglected (for now, but are included in the COFFE code and discussed in chapter 4) in our numerical results since their contribution is largely subdominant with respect to the lensing term.

### 3.2.1 Using $C_\ell$'s

We start by deriving the correlation function of (3.11), using the angular power spectrum $C_\ell$. Using eqs. (3.4) and (3.7) we can write

$$\xi(r,\bar z,\theta) = \frac{1}{4\pi}\sum_\ell (2\ell+1) C_\ell(\bar z - \Delta z, \bar z + \Delta z)\mathcal{P}_\ell(\cos\theta)\,, \tag{3.22}$$

where $\Delta z$ is given by ($\bar H = H(\bar z)$, $\bar\chi = \chi(\bar z)$)

$$\Delta z(r,\bar z,\theta) = \frac{\bar H\sqrt{r^2 - 2\bar\chi^2(1-\cos\theta)}}{\sqrt{2(1+\cos\theta)}} \in \left[0, r\bar H/2\right]. \tag{3.23}$$

This is a simple consequence of (3.7) setting $z_{1,2} = \bar z \pm \Delta z$ and approximating $\chi_{1,2} = \chi(\bar z \pm \Delta z) \simeq \chi(\bar z) \pm \Delta z/H(\bar z)$. This function is the same full correlation function as the one given in eq. (3.4), but now expressed in terms of the variables $r, \bar z$ and $\theta$ instead of $z_1, z_2$ and $\theta$. We shall use the same symbol $\xi$ to denote it.

Usually, the correlation function is not considered as a function of $r, \bar z$ and the opening angle $\theta$ between the two directions which are correlated, but as a function of $r, \bar z$ and the angle with a fictitious but fixed line-of-sight between the two directions of observation. If $\theta$ is small enough, redshift-space distortions are proportional to the $\cos^2$ of the angle with this fictitious direction. To mimic this situation we introduce

$$r_\parallel = \chi_2 - \chi_1 \simeq 2\Delta z/H(\bar z) \le r\,, \tag{3.24}$$

$$\mu = \frac{r_\parallel}{r}\,, \qquad -1 \le \mu \le 1 \qquad \text{and} \qquad r_\perp = \sqrt{r^2 - r_\parallel^2}\,. \tag{3.25}$$

Writing $\bar\chi = (\chi_1+\chi_2)/2$ and using eq. (3.24) we obtain

$$\cos\theta = \frac{2\bar\chi^2 - r^2 + \frac{1}{2}\mu^2 r^2}{2\bar\chi^2 - \frac{1}{2}\mu^2 r^2} = \frac{2\bar\chi^2 - r_\perp^2 - \frac{1}{2}r_\parallel^2}{2\bar\chi^2 - \frac{1}{2}r_\parallel^2} \equiv c(\bar z, r, \mu)\,. \tag{3.26}$$

Note that $\bar{\chi}$ and $\chi(\bar{z})$ are not exactly the same but in what follows we neglect this difference which is of order $(\Delta z)^2/\mathcal{H}(\bar{z})$. With this, the correlation function, $\xi(r,\bar{z},\theta)$ can be written as a function of $\bar{z}$, $r_\parallel$ and $r_\perp$ (or, equivalently, $\bar{z}, r$ and $\mu$)

$$\xi(r_\parallel, r_\perp, \bar{z}) = \frac{1}{4\pi}\sum_\ell (2\ell+1) C_\ell \left(\bar{z} - \frac{r_\parallel \bar{H}}{2}, \bar{z} + \frac{r_\parallel \bar{H}}{2}\right) \mathcal{P}_\ell\left(c(\bar{z}, r, \mu)\right) \tag{3.27}$$

$$= \langle \Delta_g(\mathbf{x}_1, \bar{z} - \Delta z) \Delta_g(\mathbf{x}_2, \bar{z} + \Delta z)\rangle\,. \tag{3.28}$$

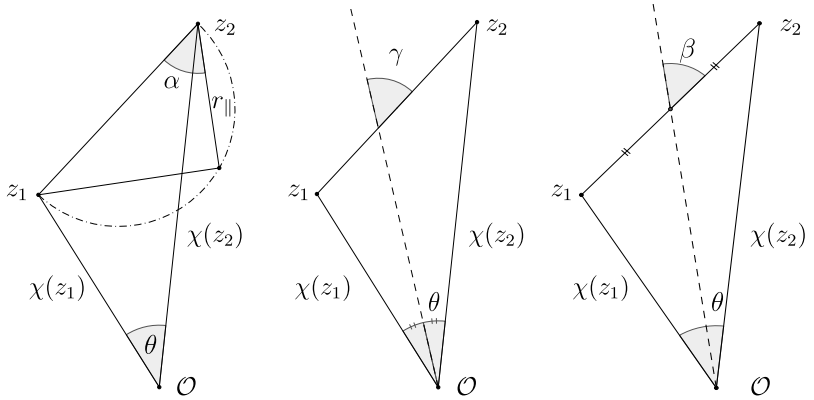


Figure 3.1: The definitions of the angles $\alpha$ (left panel, $r_\parallel = \chi_2 - \chi_1$), $\gamma$ (middle panel) and $\beta$ (right panel) as discussed in the text.

Expression (3.27) is valid as long as $\Delta z$ is small so that $\Delta z \simeq r_\parallel H(\bar{z})/2 = (\chi_2 - \chi_1)H(\bar{z})/2$ is a good approximation. Expression (3.28) however, is valid for all possible values of $r_\parallel = \chi(\bar{z} + \Delta z) - \chi(\bar{z} - \Delta z)$ and $r = \sqrt{(\mathbf{x}_1 - \mathbf{x}_2)^2}$, $r_\perp = \sqrt{r^2 - r_\parallel^2}$ where $\mathbf{x}_1 = \chi(\bar{z} - \Delta z)\mathbf{n}_1$, $\mathbf{x}_2 = \chi(\bar{z} + \Delta z)\mathbf{n}_2$ such that $c(\bar{z}, r, \mu) = \mathbf{n}_1 \cdot \mathbf{n}_2$. For a given cosmology, fixing $r_\parallel$ and $\bar{z}$ is therefore equivalent to fixing $z_1$ and $z_2$ while $r_\perp$ then fixes $\cos\theta$. Given a cosmological background model, there is a one-to-one correspondence between the model-independent angular correlation function (3.4) and the model-dependent correlation function (3.28).

The angle $\alpha$, given by $\mu = \cos\alpha$ defined by eq. (3.25), is the angle between the line $r$ connecting $\mathbf{x}_1$ and $\mathbf{x}_2$ and the line connecting the intersection of the circle around $\mathbf{x}_2$ with radius $r_\parallel = \mu r$ and the Thales circle over $r$ (see fig. 3.1, left panel). This angle is not very intuitive and it is not what observers use. In practice the angles used are either $\beta$, the angle between $r$ and the line dividing $r$ into two equal halves (see fig. 3.1, right panel) or $\gamma$, the angle between the line bisecting the angle $\theta$ and $r$ (see fig. 3.1, middle panel). Using elementary geometry we can express the angles $\beta$ and $\gamma$ in terms of $\theta$, $\chi_1$ and $\chi_2$ (see Appendix 3.A for a derivation):

$$\cos\beta = \mu f_\beta(\theta, \chi_1, \chi_2)\,, \qquad \cos\gamma = \mu f_\gamma(\theta, \chi_1, \chi_2)\,, \tag{3.29}$$

$$f_\beta = \frac{\chi_1 + \chi_2}{\sqrt{\chi_1^2 + \chi_2^2 + 2\chi_1\chi_2\cos\theta}}\,, \qquad f_\gamma = \frac{\sqrt{1+\cos\theta}}{\sqrt{2}}\,. \tag{3.30}$$

In the small angle approximation, $\theta \to 0$, both functions behave as

$$f_{\beta,\gamma} = 1 + \mathcal{O}(\theta^2)\,.$$

If $r_\parallel \neq 0$, i.e. $\chi_1 \neq \chi_2$, we can express $c(\bar{z}, r, \mu)$ in terms of $\bar{z}, r, \cos\beta$ as

$$c(\bar{z}, r, \cos\beta) = \frac{1}{2\chi_1\chi_2}\left[\frac{(\chi_1^2-\chi_2^2)^2}{r^2\cos^2\beta} - \chi_1^2 - \chi_2^2\right]. \tag{3.31}$$

Here $\chi_{1,2}$ are given in terms of $\bar{\chi}$ and $r$ by solving the equations

$$\bar{\chi} \;=\; (\chi_1+\chi_2)/2 \qquad \text{and} \qquad r^2 \;=\; \chi_1^2+\chi_2^2-2\chi_1\chi_2\cos\theta\,. \tag{3.32}$$

If we want to express the correlation function in terms of $\bar{z}$, $r$ and $\cos\beta$, we have to solve the system (3.31,3.32). A short calculation gives

$$\cos\theta \;=\; 1 - \frac{8r^2\bar{\chi}^2(1-\cos^2\beta)}{16\bar{\chi}^4 - r^2\cos^2\beta(8\bar{\chi}^2-r^2)}\,, \qquad \chi_{1,2} \;=\; \bar{\chi} \pm \sqrt{\bar{\chi}^2 - \frac{4\bar{\chi}^2-r^2}{2(1+\cos\theta)}}\,, \tag{3.33}$$

$$r_\parallel \;=\; \chi_2-\chi_1 = 2\sqrt{\bar{\chi}^2 - \frac{4\bar{\chi}^2-r^2}{2(1+\cos\theta)}}\,. \tag{3.34}$$

Inserting $\cos\theta$ from (3.33) and $r_\parallel$ from (3.34) in (3.27), we can express the correlation function as a function of $r, \bar{z}$ and $\cos\beta$. In terms of $\gamma$ we find

$$\cos\theta \;=\; 1 - \frac{r^2}{2\bar{\chi}^2}(1-\cos^2\gamma)\,. \tag{3.35}$$

In the small angle limit, all three angles, $\alpha$, $\beta$ and $\gamma$ coincide. In Section 3.2.2 we will see that the angle which gives the result closest to the flat-sky limit is the angle $\cos^{-1}(\mu)$. For this reason and due to its simplicity in what follows we express both, the correlation function and the power spectrum in terms of the projection along and transverse to the line-of-sight using the angle $\alpha$ with $\cos\alpha = \mu = (\chi_2-\chi_1)/r = r_\parallel/r$. As explained above, for small angles this is equivalent to choosing $\beta$ or $\gamma$, but for large angles, the expressions in terms of $\mu$ are simpler.

In fig. 3.2 we show the correlation function at $\bar{z} = 1$ as a function of $r_\parallel$ and $r_\perp$. In all figures, we use the cosmological parameters: $h^2\Omega_m = 0.14$, $h^2\Omega_b = 0.022$, $h = 0.676$, $A_s = 2.215\times10^{-9}$ at $k_* = 0.05\ \mathrm{Mpc}^{-1}$, $n_s = 0.961$, $b(z) = 1$, $f_{\rm evo} = 0$ and $s = 0$ unless otherwise stated. In the left panel of fig. 3.2 we include only the density, in the middle panel we also consider redshift-space distortions (RSD) and in the right panel we include also the lensing term. While the pure density term is spherically symmetric with a well visible baryon acoustic oscillation (BAO) feature at $r \sim 100\,\mathrm{Mpc}/h$, the RSD removes power for small $r_\perp$ and adds power at large $r_\perp$. Also the maximal amplitude has more than doubled due to RSD[5]. Finally the lensing term

[5]Note that we have chosen $b = 1$. For larger values of $b$, the importance of redshift-space distortion with respect to the density contribution is reduced.

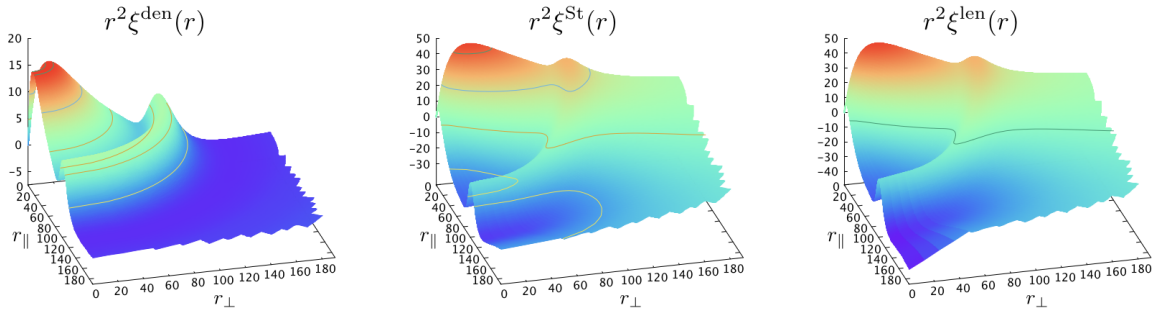


Figure 3.2: The correlation function at redshift $\bar{z} = 1$ as a function of $r_\parallel$ and $r_\perp$. The left panel contains only the density contribution, $\xi^{\rm den}$, the middle panel contains also RSD, $\xi^{\rm st}$, and the right panel contains also the lensing term, $\xi^{\rm st+len}$.

adds a very significant amount of power for large $r_\parallel$ and small $r_\perp$. This is the case when a foreground density fluctuations lenses a structure at higher redshift along its line of sight. The additional relativistic contributions are very small and become visible only on very large scales, as we shall see in the rest of this chapter and as has already been anticipated in several papers, e.g. Refs. [72, 99].

In fig. 3.3 we show fractional differences for $\mu = 0$ (left) and $\mu = 1$ (right)

$$\Delta\xi^A \equiv \frac{\xi^A - \xi^{\rm st}}{\xi^{\rm st}}\,, \tag{3.36}$$

where

$$\xi^A = \left\langle \left(\Delta^{\rm st} + \Delta^A\right)(\mathbf{n}_1, z_1)\left(\Delta^{\rm st} + \Delta^A\right)(\mathbf{n}_2, z_2)\right\rangle . \tag{3.37}$$

In this way we show separately the contribution of each correction $A$ with respect to the standard term, including its correlation with density and redshift-space distortion. The middle panel shows $\Delta\xi^A$ for $A$ = lensing and the lower panel for all the non-integrated relativistic effects, namely the terms d1, d2, g1, g2 and g3 (see eqs. (3.11) to (3.21) for a definition of the various relativistic terms). Note that the contribution d2, g1, g2 and g3 are infra-red divergent. Here we simply pick an infra-red cutoff in the computation $k_{\rm IR} \simeq \mathcal{H}_0$, while we will discuss and fix this problem in section 4.2.2. Finally, as reference, we plot in the top panel the fractional difference due to redshift-space distortion, namely $\Delta\xi^{\rm rsd} = (\xi^{\rm st} - \xi^{\rm den})/\xi^{\rm den}$.

Not surprisingly, for $\mu = 0$ the lensing term is very small apart from a small effect on the acoustic peaks. For $\mu = 1$ however, at large scales $r > 150\,$Mpc, lensing becomes the dominant term. As also noted in [213], it increases linearly with distance. Comparing our full-sky calculation of the lensing (orange) with the flat-sky expression (blue) derived in [213] and in Appendix 3.E (see eq. (3.111)) we see that for $\mu = 1$ the two expressions agree very well, which is not surprising because in this case $\mathbf{n}_1 = \mathbf{n}_2$ and flat-sky is a good approximation. The only source of difference in this case comes from the fact that the flat-sky result uses Limber approximation whereas the full-sky result is exact. This difference is very small, showing that Limber approximation for $\mu = 1$ is very good. For $\mu = 0$ on the other hand we see a

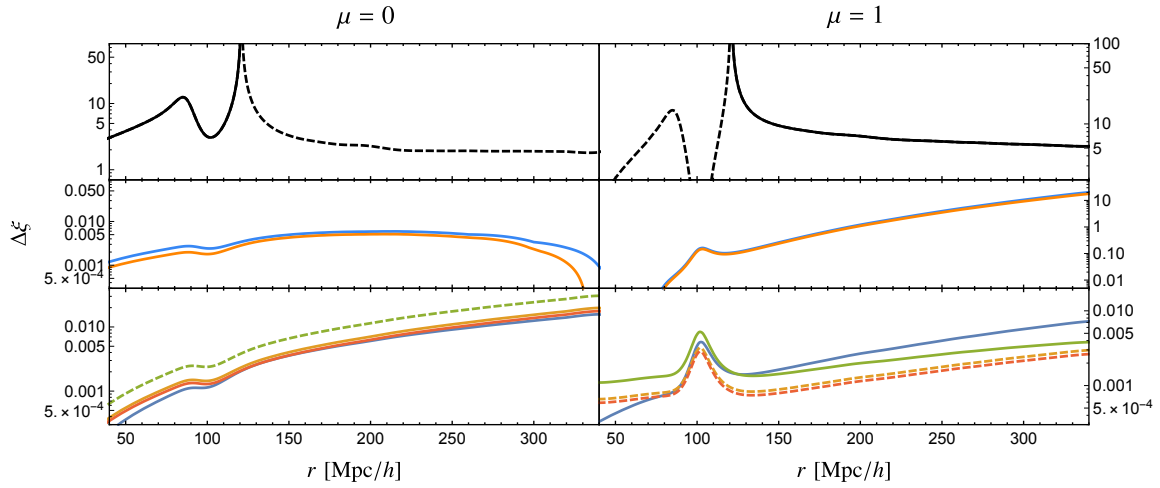


Figure 3.3: The relative difference $\Delta\xi$ at redshift $\bar{z} = 1$ for $\mu = 0$ (left panels) and $\mu = 1$ (right panels). *Top panels:* $\Delta\xi^{\rm rsd} = (\xi^{\rm st} - \xi^{\rm den})/\xi^{\rm den}$. *Middle panels:* fractional difference induced by lensing $\Delta\xi^{\rm lensing}$ (full-sky in orange and flat-sky in blue). *Bottom panels:* $\Delta\xi^A$ where $A =$: d1 (blue), d2 (orange), g1 (green) and g2 (red). The contribution g3 is subdominant (see eqs. (3.11) to (3.21) for a definition of the various relativistic terms). Negative contributions are dashed.

non-negligible difference between the flat-sky and full-sky result. We will discuss this in more detail in Section 3.2.2.

From the bottom panel, we see that the non-integrated relativistic terms generate a correction of the order of the percent at large separation $r \sim 350\,{\rm Mpc}/h$. Naively we would expect the Doppler term (d1: blue) to dominate over the other relativistic effects because it is proportional to the peculiar velocity and contains therefore one more factor $k/\mathcal{H}$ than the terms proportional to the potentials (see e.g. eqs. (3.39) to (3.48) below). However, as shown in [76] (see also Appendix 3.B), the correlation of this term with the standard term $\langle\Delta^{\rm d1}\Delta^{\rm st}\rangle$ exactly vanishes in the flat-sky because it is totally anti-symmetric. The contribution that we see in fig. 3.3 is therefore due to the correlation $\langle\Delta^{\rm d1}\Delta^{\rm d1}\rangle$, which is a factor $\mathcal{H}/k$ smaller, hence $\sim\langle\Delta^{\rm st}\Psi\rangle$ and to the full-sky contributions to $\langle\Delta^{\rm d1}\Delta^{\rm st}\rangle$, which are of the order $r/\chi\langle\Delta^{\rm d1}\Delta^{\rm st}\rangle \sim \langle\Delta^{\rm d1}\Delta^{\rm d1}\rangle \sim \langle\Delta^{\rm st}\Psi\rangle$. Consequently, with one population of galaxies the Doppler contribution to the correlation function is of the same order of magnitude as the gravitational potential contributions (d2, g1 and g2). Only in the case where one cross-correlates two populations of galaxies, the Doppler contribution strongly dominates over the other relativistic contributions, because in this case $\langle\Delta^{\rm d1}\Delta^{\rm st}\rangle$ does not vanish in flat-sky. At smaller redshift the Doppler d1 is nevertheless the dominant contribution amongst the relativistic effects as the flat-sky approximation fails at smaller separations.

For $\mu = 0$, the Sachs-Wolfe like term (g1) dominates over the other corrections at all scales. For $\mu = 1$ this term still dominates at small separation, but at large separation the full-sky corrections to the Doppler term become important and dominates over g1. Interestingly the

second Sachs-Wolfe like term (g2) and the second Doppler term (d2) are nearly equal for both values of $\mu$. It is easy to derive from the continuity and the Poisson equations that in a matter dominated Universe $(\mathcal{H}/k)V = -(2/3)\Phi$, hence $\Delta_\ell^{\rm d2} = \Delta_\ell^{\rm g2}$ if $s = 0$, see eqs. (3.43) and (3.45). At lower redshifts, when $\Lambda$-domination sets in, we expect this equality to be less precise. The relativistic terms not shown in fig. 3.3 are the Shapiro time delay (g4) and the integrated Sachs-Wolfe term (g5). These integrated terms are always subdominant with respect to the lensing term.

Let us also note that the difference between the flat-sky standard term and the full-sky standard term is of the same order of magnitude as the relativistic terms depicted in the bottom panel of fig. 3.3. It is therefore not consistent to use the flat-sky approximation for the standard terms when investigating relativistic effects.

Finally we should point out that in this chapter we present the *theoretical* contributions of relativistic effects on the correlation function (see figs. 3.3, 3.8, 3.11). To estimate the *observational* impact of these terms one should build a realistic estimator and proceed with signal-to-noise analysis, forecasts and constraints for a specific survey. Such studies have been performed for the angular power spectrum $C_\ell$ in [124, 253, 251, 92, 126, 212] and for the antisymmetric part of the correlation function $\xi_g$ in [77]. This would allow us to compare the observational impact of the relativistic effects on the angular power spectrum with their impact on the multipoles of the correlation function, which are one of the standard observables currently used in large-scale structure surveys to measure the growth rate $f$. A comprehensive study of this kind is currently planned. In chapter 4 however we will take the first steps in this direction by defining estimators of the multipoles of the correlation function, computing their covariance matrices and performing a signal-to-noise analysis of the lensing signal.

### 3.2.2 Direct determination of the correlation function

In the calculation of the correlation function presented in the previous section, we still need all the $C_\ell(z_1, z_2)$ for an accurate calculation. Hence the reason (1) given in the introduction for the use of the correlation function and the power spectrum is not satisfied: the calculation is not simplified. To compute the correlation function for thousands of spectroscopic redshifts in an MCMC would still take months even if very highly parallelised. In this section we show how to improve this. The method explained in this section reduces the calculation of several thousand $C_\ell(z_1, z_2)$'s into just several terms. This results in a very significant speed up so that the computation becomes feasible.

We expand on a method introduced in [90] which avoids the computation of $C_\ell(z_1, z_2)$ but requires integrations in $k$-space and over the line-of-sight, as we shall see. In this method, no flat-sky approximation is performed, and the correlation function is therefore exact, within linear perturbation theory. We start from expression (3.4) for the correlation function and use that the $C_\ell(z_1, z_2)$ are of the form (see e.g. [125]),

$$\begin{aligned} C_\ell(z_1, z_2) &= \sum_{A,B} C_\ell^{AB}(z_1, z_2)\,, \\ C_\ell^{AB}(z_1, z_2) &= 4\pi \int \frac{dk}{k} \mathcal{P}_\zeta(k) \Delta_\ell^A(k, z_1) \Delta_\ell^B(k, z_2)\,. \end{aligned} \tag{3.38}$$

Here $\mathcal{P}_\zeta$ denotes the primordial power spectrum, determined by the amplitude $A_s$ and the primordial spectral index $n_s$:

$$\mathcal{P}_\zeta(k) = A_s \left(\frac{k}{k_*}\right)^{n_s-1},$$

and $\Delta_\ell^A$, $\Delta_\ell^B$ are the Fourier-Bessel transforms of the terms defined in (3.12) to (3.21). More precisely

$$\Delta_\ell^{\rm den} = b(z) S_D j_\ell(k\chi)\,, \tag{3.39}$$

$$\Delta_\ell^{\rm rsd} = \frac{k}{\mathcal{H}} S_V j_\ell''(k\chi)\,, \tag{3.40}$$

$$\Delta_\ell^{\rm len} = \left(\frac{2-5s}{2}\right) \frac{\ell(\ell+1)}{\chi} \int_0^\chi {\rm d}\lambda \frac{\chi-\lambda}{\lambda} (S_\phi + S_\psi) j_\ell(k\lambda)\,, \tag{3.41}$$

$$\Delta_\ell^{\rm d1} = \left(\frac{\dot{\mathcal{H}}}{\mathcal{H}^2} + \frac{2-5s}{\chi\mathcal{H}} + 5s - f_{\rm evo}\right) S_V j_\ell'(k\chi)\,, \tag{3.42}$$

$$\Delta_\ell^{\rm d2} = -(3 - f_{\rm evo}) \frac{\mathcal{H}}{k} S_V j_\ell(k\chi) = \Delta^{\rm d2}(z,k) j_\ell(k\chi)\,, \tag{3.43}$$

$$\Delta_\ell^{\rm g1} = \left(1 + \frac{\dot{\mathcal{H}}}{\mathcal{H}^2} + \frac{2-5s}{\chi\mathcal{H}} + 5s - f_{\rm evo}\right) S_\psi j_\ell(k\chi) = \Delta^{\rm g1}(z,k) j_\ell(k\chi)\,, \tag{3.44}$$

$$\Delta_\ell^{\rm g2} = (-2 + 5s) S_\phi j_\ell(k\chi) = \Delta^{\rm g2}(z,k) j_\ell(k\chi)\,, \tag{3.45}$$

$$\Delta_\ell^{\rm g3} = \frac{1}{\mathcal{H}} \dot{S}_\phi j_\ell(k\chi) = \Delta^{\rm g3}(z,k) j_\ell(k\chi)\,, \tag{3.46}$$

$$\Delta_\ell^{\rm g4} = \frac{2-5s}{\chi} \int_0^\chi {\rm d}\lambda (S_\phi + S_\psi) j_\ell(k\lambda)\,, \tag{3.47}$$

$$\Delta_\ell^{\rm g5} = \left(\frac{\dot{\mathcal{H}}}{\mathcal{H}^2} + \frac{2-5s}{\chi\mathcal{H}} + 5s - f_{\rm evo}\right) \int_0^\chi {\rm d}\lambda (\dot{S}_\phi + \dot{S}_\psi) j_\ell(k\lambda)\,. \tag{3.48}$$

Here $j_\ell$ are the spherical Bessel functions and the functions $S_X(z,k)$ are the transfer functions for the variable $X$ which we specify in Appendix 3.B. Over-dots indicate derivatives with respect to conformal time. For the evolution bias $f_{\rm evo}$, the magnification bias $s$ and the galaxy bias $b$ we follow the conventions of [125], detailed in section 2.2.3. From these expressions one also infers the scaling of the different terms with respect to the density term. On sub-Hubble scales, $k > \mathcal{H}$, the scaling of these terms with powers of $\mathcal{H}/k$ is a simple consequence of Newtonian physics. The continuity equation implies $S_V \sim (\mathcal{H}/k) S_D$ and the Poisson equation yields $S_\phi \sim S_\psi \sim (\mathcal{H}/k)^2 S_D$, we see that the density, RSD and lensing terms dominate, while the Doppler term d1 is suppressed by one factor of $(\mathcal{H}/k)$, and all other terms are suppressed by $(\mathcal{H}/k)^2$. For this reason all relativistic terms apart from lensing are strongly suppressed on sub-horizon scales and we call them 'large-scale contributions'. Most of them are relevant only on very large scales close to $\mathcal{H}(z)^{-1}$. Exceptions to this rule are $\Delta_\ell^{\rm d1}$ and $\Delta_\ell^{\rm g1}$ which contain a pre-factor $1/(\chi\mathcal{H})$ which becomes large at very low redshift where $\chi$ is small. On super horizon scales all the transfer functions $S_X$ are typically of the same order but they become gauge dependent.

Using these expressions, the correlation function $\xi$ can be written as

$$\xi = \sum_{A,B} \xi^{AB} \qquad \text{with} \qquad \xi^{AB}(\theta, z_1, z_2) = \int \frac{dk}{k}\, \mathcal{P}_\zeta\, Q_k^{AB}(\theta, z_1, z_2)\,, \tag{3.49}$$

where we define

$$Q_k^{AB}(\theta, z_1, z_2) \equiv \sum_\ell (2\ell+1)\Delta_\ell^A(k, z_1)\Delta_\ell^B(k, z_2)\mathcal{P}_\ell(\cos\theta)\,. \tag{3.50}$$

In most of the terms $Q_k^{AB}$ we have a sum of the form

$$\sum_\ell (2\ell+1)\mathcal{P}_\ell(\cos\theta) j_\ell(k\chi_1) j_\ell(k\chi_2) \quad = \quad j_0(kr)\,, \tag{3.51}$$

where $r = \sqrt{\chi_1^2 + \chi_2^2 - 2\chi_1\chi_2\cos\theta}$ (see e.g. [3] (10.1.45)). Inserting (3.51) into (3.49) we can easily calculate the correlation function for these terms avoiding the numerically costly sum over the $C_\ell$'s. The redshift-space distortion and the Doppler term give rise to contributions that are slightly different because they contain first and second derivatives of the spherical Bessel functions with respect to $k\chi_1$ and $k\chi_2$. These terms can however be treated in a very similar way using recurrence relations for the spherical Bessel function. For this we define

$$\zeta^{ij} \equiv \sum_\ell (2\ell+1) j_\ell^{(i)}(k\chi_1) j_\ell^{(j)}(k\chi_2)\mathcal{P}_\ell(\cos\theta) = \sum_\ell (2\ell+1) j_\ell^{(i)}(x_1) j_\ell^{(j)}(x_2)\mathcal{P}_\ell(\cos\theta)\,, \tag{3.52}$$

where we have set $x_i = k\chi_i$ and $j_\ell^{(i)}(x) = \frac{\partial^i}{\partial x^i} j_\ell(x)$. Using

$$\zeta^{ij}(x_1, x_2) = \zeta^{ji}(x_2, x_1) \quad \text{and} \quad \frac{\partial^{n+m}}{\partial x_1^n \partial x_2^m}\zeta^{ij} = \zeta^{i+n, j+m},$$

we can determine explicit expressions for the $\zeta^{ij}$ for $i, j \in \{0, 1, 2\}$. They are all given in Appendix 3.B.

The only coefficients that do not fall into this category are the ones in $\Delta_\ell^{\rm len}$ which contain additional factors $\ell$ and $(\ell+1)$ (see eq. (3.41)). These terms can however be computed using the identity

$$\triangle_\Omega \mathcal{P}_\ell(\cos\theta) = -\ell(\ell+1)\mathcal{P}_\ell(\cos\theta)\,.$$

They are given by

$$\zeta^{\rm LL} \equiv \sum_\ell (2\ell+1)\ell^2(\ell+1)^2 j_\ell(x_1) j_\ell(x_2)\mathcal{P}_\ell(\cos\theta) = \triangle_\Omega^2\, \zeta^{00}\,, \tag{3.53}$$

$$\zeta^{i\rm L} \equiv \sum_\ell (2\ell+1)\ell(\ell+1) j_\ell^{(i)}(x_1) j_\ell(x_2)\mathcal{P}_\ell(\cos\theta) = -\triangle_\Omega\, \zeta^{i0}\,, \tag{3.54}$$

where LL denotes the correlation of lensing with itself and $i$L the cross-correlation of lensing with one of the other terms. With this we can build all the functions $Q_k^{AB}$ and hence, with eq. (3.49), the correlation function. The complete list of $Q_k^{AB}$ is given in Appendix 3.B. Here

we just report the dominant contributions, i.e. the contributions which are not suppressed with additional powers of $\mathcal{H}/k$ with respect to the density term:

$$
\begin{aligned}
Q^{\rm den}(\theta,z_1,z_2) &= b(z_1)b(z_2)S_D(z_1)S_D(z_2)\,\zeta^{00}(k\chi_1,k\chi_2)\,,\\
Q^{\rm rsd}(\theta,z_1,z_2) &= \frac{k^2}{\mathcal{H}_1\mathcal{H}_2}S_V(z_1)S_V(z_2)\,\zeta^{22}(k\chi_1,k\chi_2)\,,\\
Q^{\rm len}(\theta,z_1,z_2) &= \frac{(2-5s)^2}{4\chi_1\chi_2}\int_0^{\chi_1}\int_0^{\chi_2}{\rm d}\lambda{\rm d}\lambda'\left[\frac{(\chi_1-\lambda)(\chi_2-\lambda')}{\lambda\lambda'}S_{\phi+\psi}(\lambda)S_{\phi+\psi}(\lambda')\zeta^{LL}(k\lambda,k\lambda')\right],\\
Q^{\rm den\text{-}rsd}(\theta,z_1,z_2) &= \frac{kb(z_1)}{\mathcal{H}_2}S_D(z_1)S_V(z_2)\,\zeta^{02}(k\chi_1,k\chi_2)\,,\\
Q^{\rm den\text{-}len}(\theta,z_1,z_2) &= b(z_1)S_D(z_1)\left(\frac{2-5s}{2\chi_2}\right)\int_0^{\chi_2}{\rm d}\lambda\left[\frac{\chi_2-\lambda}{\lambda}\Big(S_\phi(\lambda)+S_\psi(\lambda)\Big)\zeta^{0L}(k\chi_1,k\lambda)\right],\\
Q^{\rm rsd\text{-}len}(\theta,z_1,z_2) &= \frac{k}{\mathcal{H}_1}S_V(z_1)\left(\frac{2-5s}{2\chi_2}\right)\int_0^{\chi_2}{\rm d}\lambda\left[\frac{\chi_2-\lambda}{\lambda}\Big(S_\phi(\lambda)+S_\psi(\lambda)\Big)\zeta^{2L}(k\chi_1,k\lambda)\right].
\end{aligned}
$$

Note that here and in the following we suppress the argument $\theta$ in the functions $\zeta^{\rm AB}(k\chi_1,k\chi_2,\theta)$ for simplicity. The correlation function is then given by eq. (3.49). For example, the correlation function including only the standard terms is given by

$$
\begin{aligned}
\xi^{\rm st} &= \int\frac{dk}{k}\,\mathcal{P}_\zeta\Big[Q^{\rm den}(\theta,z_1,z_2)+Q^{\rm den\text{-}rsd}(\theta,z_1,z_2)+Q^{\rm rsd\text{-}den}(\theta,z_1,z_2)+Q^{\rm rsd}(\theta,z_1,z_2)\Big]\\
&=\frac{2A_s}{9\pi^2\Omega_m^2}D_1(z_1)D_1z_2)\int\frac{dk}{k}\Big[b(z_1)b(z_2)\zeta^{00}(k\chi_1,k\chi_2)-b(z_1)f(z_2)\zeta^{02}(k\chi_1,k\chi_2)\\
&\quad-b(z_2)f(z_1)\zeta^{02}(k\chi_2,k\chi_1)+f(z_1)f(z_2)\zeta^{22}(k\chi_1,k\chi_2)\Big]\left(\frac{k}{H_0}\right)^4\left(\frac{k}{k_*}\right)^{n_s-1}T^2(k)\,.
\end{aligned}
\tag{3.55}
$$

For the second equal sign we made use of the transfer functions given in Appendix 3.B. Eq. (3.55) is expressed in terms of the redshift $z_1$ and $z_2$ and the angle $\theta$. It can however easily be written in terms of a mean redshift $\bar{z}$, the separation of the galaxies $r$ and the orientation of the pair using eqs. (3.24),(3.25),(4.7).

The correlation function obtained in this way agrees with the full-sky expressions derived in [290, 291, 240] for the standard terms and in [76] for the Doppler term. This method has however the advantage that it can be used to calculate also expressions for the integrated terms valid in full-sky. Since the lensing is the dominant correction, it is important to have an accurate expression for this term valid at all scales and not relying on the Limber approximation.

### $\mu$ and $r$ dependence of the correlation function

Let us first discuss the full-sky correlation function as a function of $\mu$ and $r$. In fig. 3.4 we show the lensing contribution

$$
\xi^L = \Big\langle\big(\Delta^{\rm st}+\Delta^{\rm len}\big)(\mathbf{n}_1,z_1)\big(\Delta^{\rm st}+\Delta^{\rm len}\big)(\mathbf{n}_2,z_2)\Big\rangle-\Big\langle\Delta^{\rm st}(\mathbf{n}_1,z_1)\Delta^{\rm st}(\mathbf{n}_2,z_2)\Big\rangle\,,
\tag{3.56}
$$

as a function of $\mu$ and $r$. We compare the full-sky result (solid lines) with the flat-sky result (dashed lines) derived in [182] and given in eq. (3.111). In the top left panel we show the cross-correlation between density and lensing, whereas in the top right panel we show the lensing-lensing correlation. We see that the flat-sky expression for the lensing-lensing agrees extremely well with the full-sky expression. The density-lensing cross-correlation is however significantly different in flat-sky and full-sky, even at small separation. This can be understood in the following way. The flat-sky result assumes not only that $\mathbf{n}_1 = \mathbf{n}_2$, but it also uses the Limber approximation, which implies that only correlations at the same redshift contribute to the correlation function. Hence instead of integrating the lensing along the line-of-sight as is done in the full-sky expression, the flat-sky expression correlates the density at position $z_2$ with the lensing from the same redshift. This can be seen by looking at eq. (3.103), where the integral along the line-of-sight has been replaced by the function $\delta(\chi_2 - \lambda)$. This approximation is quite good for values of $\mu$ close to 1, i.e. when the galaxies are behind each other, but it is very bad when $\mu$ becomes small and for small separations $r$. In such cases, the density $\delta$ is correlated with the gravitational potentials generated by that same density $\Phi$ and $\Psi$ and therefore the correlation is non-negligible even when the two redshifts are not exactly the same. As a result the flat-sky expression, which ignores this direct correlation, strongly underestimates the density-lensing correlation. Since the density-lensing cross-correlation is negative whereas the lensing-lensing is positive, this means that the flat-sky result overestimates the total correlation function, as shown in the bottom left panel of fig. 3.4. The bottom right panel shows the total lensing contribution as a function of separation for various values of $\mu$. In general we find that the relative difference between the flat-sky and full-sky result is of the order of 20 percents and it can become much larger in some configurations.

In all these plots we do not calculate the lensing contribution when $\mu$ is exactly equal to 1. This value is indeed not physical since it would correspond to a galaxy situated exactly behind the other, which we can of course not see. The largest value that we take is therefore $\mu = 0.9997895$. This value ensures us that the line-of-sight from the most distant galaxy passes sufficiently far away from the closest galaxy to avoid being absorbed by it. In the following when we discuss about the parallel correlation function or when we show plots for $\mu = 1$, this has to be understood as $\mu = 0.9997895$. Finally let us mention that we do not include the correlation between redshift-space distortion and lensing (it is however possible to obtain it with the COFFE code, see chapter 4). This correlation is exactly zero in the flat-sky approximation and we do expect it to remain very small in full-sky[6].

So far we have calculated all the flat-sky and full-sky correlation functions using the linear power spectrum. Since we are mainly interested in correlations at large separations, this is a very well motivated approximation for all the non-integrated terms. We have indeed checked that all the large-scale relativistic contributions change by at most 2-3 percents at small scales if we use the halo-fit power spectrum instead of the linear one to calculate the correlation function. For the lensing contribution on the other hand, non-linearities are important even at large separation, as already pointed out in [182, 213, 183]. This is due to the fact that

[6]We have checked numerically that at $\bar{z} \sim 1$ the RSD-lens contribution to the angular power spectrum is 3 to 4 orders of magnitude smaller than the $\delta$-lens term.

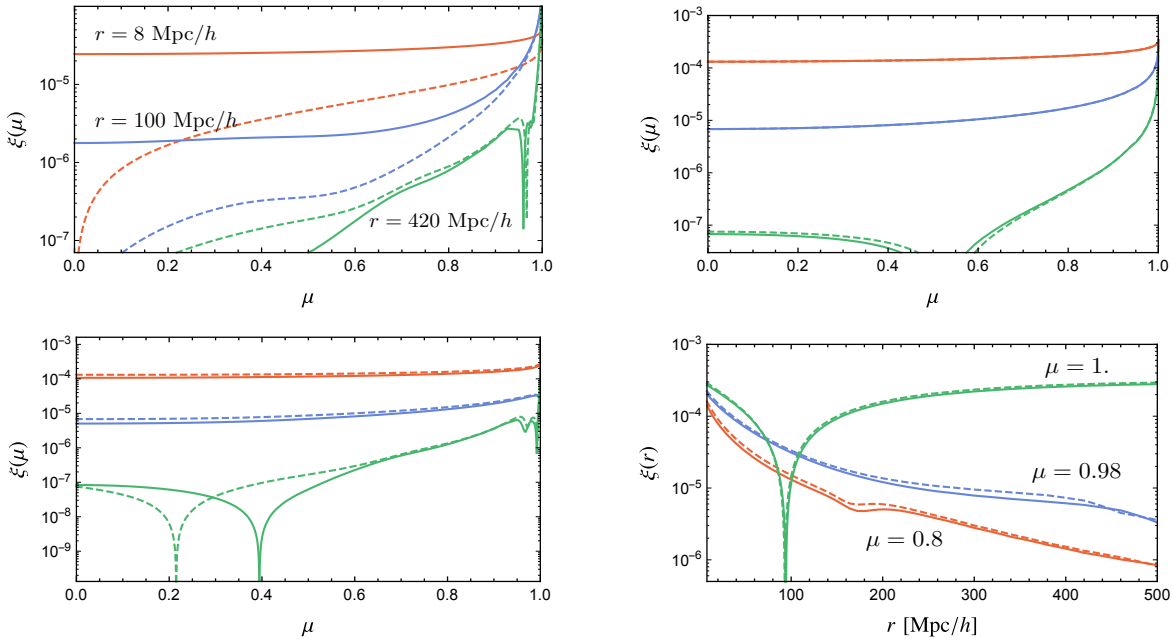


Figure 3.4: Top panels: correlation between density and lensing (left) and lensing-lensing (right) at $\bar{z} = 1$, as a function of $\mu$ and for fixed separation $r = 8\,\mathrm{Mpc}/h$ (orange), $r = 100\,\mathrm{Mpc}/h$ (blue) and $r = 420\,\mathrm{Mpc}/h$ (green). Solid lines show the full-sky result and dashed lines the flat-sky result using Limber approximation. Bottom panels: total lensing contribution as a function of $\mu$ (left) and $r$ (right) at $\bar{z} = 1$.

lensing is sensitive not only to correlations between the two positions of the galaxy, but also to all correlations between the two lines-of-sight from these galaxies. When $\mu$ is large, these two lines-of-sight are close to each other at least in the vicinity of the observer, even when $r$ is large, and consequently non-linear effects are important. Lensing has the property to mix large and small separations and a full-sky non-linear treatment is therefore necessary.

The simplest way to calculate the full-sky lensing non-linearly is to use the Poisson equation to relate the gravitational potentials along the line-of-sight to the density (this equation is indeed valid also in the non-linear regime) and to use halo-fit to calculate the non-linear density power spectrum. This procedure can however not be implemented exactly because the full-sky lensing requires the density power spectrum at different redshifts along the two lines-of-sight $P(k, z, z')$ where $z$ and $z'$ can take any values between 0 and $z_1$ and $z_2$. Halo-fit gives an expression for the power spectrum only when $z = z'$. Note that this problem does not arise in the calculation of the flat-sky expression which uses Limber approximation and therefore neglects correlations coming from $z \neq z'$. In order to overcome this problem we use the following approximate procedure: we calculate the non-linear power spectrum at a middle redshift along the line-of-sight $z_*$ and then evolve it using the linear growth rate $D_1(z)$ along the photon trajectory. This is of course not completely correct because in the non-linear regime density does not evolve with the linear growth rate, but it gives us a good

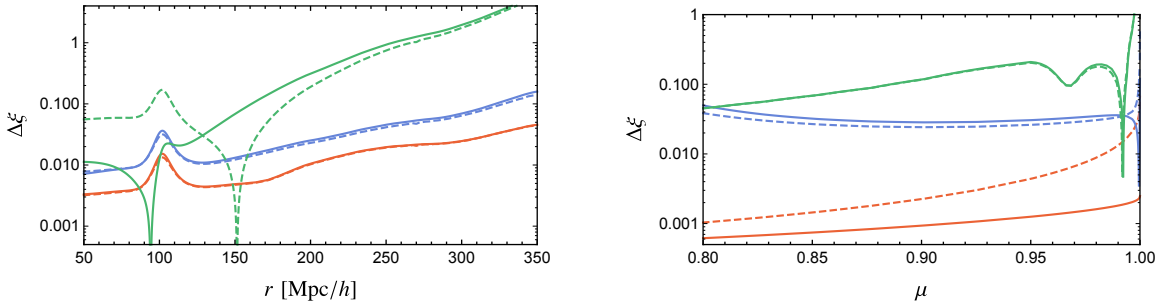


Figure 3.5: Fractional differences $\Delta\xi^L$ at redshift $\bar{z} = 1$ using the full-sky formalism. The solid lines show the fractional difference using the linear transfer function and the dashed line is using halofit. In the *left panel* we show $\Delta\xi^L$ as a function of separation $r$ for fixed values of $\mu$: $\mu = 1$ (green), $\mu = 0.98$ (blue) and $\mu = 0.8$ (orange), and in the *right panel* we show it as a function of $\mu$ for fixed separation: $r = 8\text{Mpc}/h$ (orange), $r = 100\text{Mpc}/h$ (blue) and $r = 420\text{Mpc}/h$ (green).

approximation of the true non-linear lensing contribution. To determine which $z_*$ is the most appropriate, we use the flat-sky approximation[7]. We checked that our result behaves in a consistent way when we vary $z_*$, which gives us confidence in this approximation (see fig. 3.C.1 in Appendix 3.C for more detail).

In fig. 3.5 we show the fractional difference with respect to the standard term due to the full-sky lensing in the linear and non-linear regime $\Delta\xi^L$. Contrary to fig. 3.3 where the fractional difference of all the terms was calculated with respect to the full-sky standard term, here we show the fractional difference with respect to the flat-sky standard term given in eq. (3.9). In this way fig. 3.5 can be directly interpreted as the fractional error that one makes when using the standard flat-sky correlation function instead of the full-sky observable correlation function containing lensing[8]. Clearly, lensing becomes very important at large separation and large $\mu$. Neglecting it in this regime can therefore impact the determination of cosmological parameters in a significant way. Comparing linear and non-linear results, we find that for $\mu = 1$, the non-linear result is very different from the linear one at all separations up to $250\,\text{Mpc}/h$. For $r \leq 150\,\text{Mpc}/h$, the non-linear lensing is significantly enhanced with respect to the linear regime. At larger separation however, the tendency is reversed. This reflects the fact that non-linearities move power from small to large $k$. On the right panel

[7]More precisely we do the following: we calculate the flat-sky contribution using the correct non-linear power spectrum integrated along the line-of-sight (remember that in the flat-sky we can do that since we have only one line-of-sight). Then we use the same approximation as in the full-sky to calculate also the flat-sky and we compare the correct flat-sky result with the approximate flat-sky result for various values of $z_*$. This allows us to find the best $z_*$. For $z = 1$ we find $z_* = 0.42$ and for $z = 2$, $z_* = 0.73$.

[8]Note that to calculate the flat-sky standard expression in the non-linear regime we use the linear continuity equation to relate the velocity to the density and then we use halo-fit for the density power spectrum. This procedure is not completely correct as the continuity equation is also modified in the non-linear regime. Current data analyses use a more sophisticated procedure to calculate the non-linear redshift-space distortions, based on [151]. Our procedure is however conservative since it tends to overestimate the impact of non-linearities on redshift-space distortions and therefore to underestimate the relative importance of lensing.

we see that at small separation, $r = 8\,\mathrm{Mpc}/h$, the non-linear lensing is significantly larger than the linear one for all $\mu$. In summary, fig. 3.5 shows that lensing cannot be neglected at redshift 1 and that it has to be calculated in the full-sky non-linear regime, because it mixes small scales (where non-linearities are important) and large scales (where full-sky effects are important).

### Multipole expansion of the correlation function

The correlation function is in general a function of separation $r$ and orientation $\mu$. However, the dependence in $\mu$ of the standard flat-sky expression (3.9) is very simple, since it is given by $\mathcal{P}_2(\mu)$ and $\mathcal{P}_4(\mu)$ only. This simple dependence has been exploited to measure directly the growth rate $f$. In practice this means that each pair of galaxies is weighted either by $\mathcal{P}_0(\mu) = 1$, $\mathcal{P}_2(\mu)$ or $\mathcal{P}_4(\mu)$. The average over all orientations is then performed, allowing one to measure the coefficient in front of each of the $\mathcal{P}_\ell$, i.e. the monopole, quadrupole and hexadecapole.

In the full-sky regime the dependence of redshift-space distortions on $\mu$ becomes more complicated, first due to the fact that $\mathbf{n}_1$ and $\mathbf{n}_2$ are not parallel (wide-angle effects) and second because the growth rate and bias are evolving with time $f(z_1) \neq f(z_2)$. In addition, the large-scale relativistic effects and the integrated effects have their own $\mu$-dependence, which cannot be simply expressed in terms of $\mathcal{P}_2(\mu)$ and $\mathcal{P}_4(\mu)$ as we saw in fig. 3.4. As a consequence the multipole expansion of the full-sky observable correlation function differs from the flat-sky standard expansion. Firstly the monopole, quadrupole and hexadecapole of the full-sky standard term differ from the flat-sky ones. Secondly, these multipoles get corrections from the relativistic and lensing contributions. And finally, due to wide-angle effects and lensing, the multipoles beyond $\ell = 4$ no longer vanish.

In fig. 3.6 we show the impact of wide-angle effects on the monopole, quadrupole and hexadecapole. Since the standard terms are almost not affected by non-linearities above $20\,\mathrm{Mpc}/h$, we calculate these multipoles using the linear power spectrum. In black we show the flat-sky multipoles from density and redshift-space distortions, that are simply given by the coefficients in front of $\mathcal{P}_\ell(\mu)$ in eq. (3.9). In blue, purple and green we show the full-sky multipoles from density and redshift-space distortions obtained from expression (3.55), which we multiply by the appropriate Legendre polynomial and numerically integrate over directions[9]

$$\xi_\ell(r, \bar{z}) = \frac{2\ell + 1}{2} \int_{-1}^{1} \xi(r, \bar{z}, \sigma) \mathcal{P}_\ell(\sigma) d\sigma \,. \tag{3.57}$$

As discussed in Section 3.2.1, in the full-sky there is no unique way to define the orientation of the pairs of galaxies. We therefore calculate the multipoles for different choices: $\sigma = \cos\beta$, $\sigma = \cos\gamma$ and $\sigma = \mu$. The amplitude of the multipoles depends on this choice, as can be seen from the different colours in fig. 3.6. At redshift $\bar{z} = 1$ (right), we find that the monopole differs only

[9]Note that the multipoles defined in eq. (3.57) completely differ from the multipoles defined in [252] (see their eq. (17)). The multipoles in (3.57) are defined at fixed galaxy separation $r$ and they correspond to what observers are measuring in redshift surveys. The multipoles in [252] are on the contrary defined at fixed angular separation $\theta$ (see their fig. 1). As a consequence they mix different separations $r$ and have completely different properties.

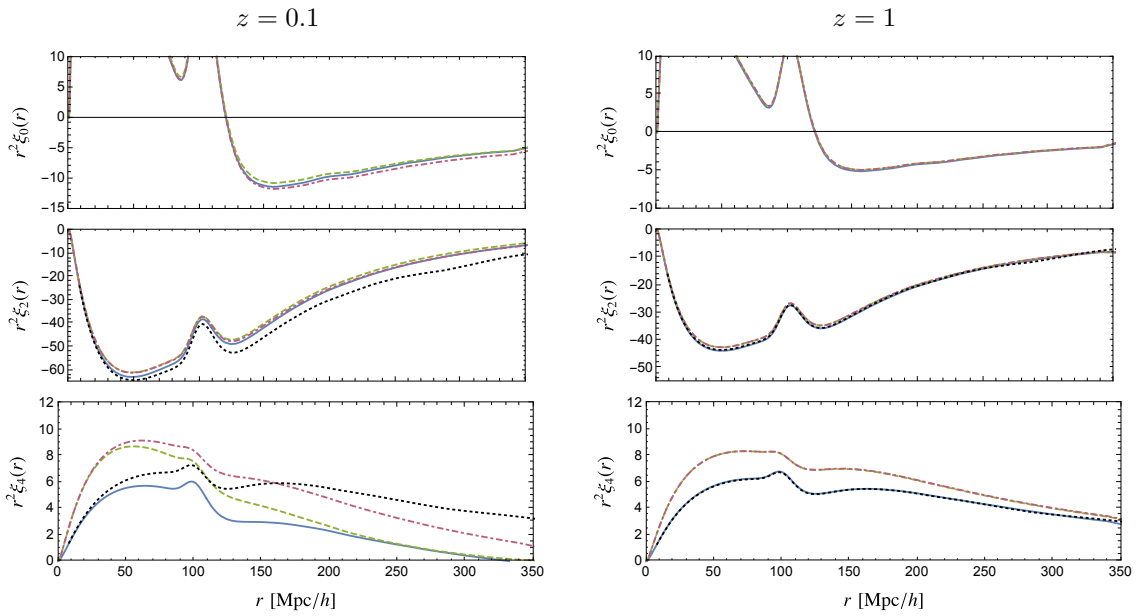


Figure 3.6: The multipoles from density and redshift-space distortions, $\xi^{\rm st}$, at redshift $\bar{z} = 0.1$ (left) and $\bar{z} = 1$ (right). We show the monopole (top) quadrupole (middle) and hexadecapole (bottom) for different definitions of the angle in the full-sky: $\mu$ (blue, solid), $\cos\gamma$ (purple, dash-dotted) and $\cos\beta$ (green, dashed) and we compare this with the flat-sky multipoles obtained from (3.9) (black, dotted).

at very large scales by a few percent, while the quadrupole also differs at intermediate scales by a few percent. The hexadecapole is significantly different at most scales. At redshift $\bar{z} = 0.1$ (left) the difference is much more important, up to 10% on the quadrupole at intermediate scales already. And the hexadecapole is very different at most scales. As already pointed out in [290, 291, 240, 254, 269, 52, 323] it is therefore important to account for wide-angle effects when interpreting the multipoles. We also see in Fig 3.6 that the angle which is closest to the flat-sky result is nearly always $\mu$ and especially it is always $\mu$ for $\bar{z} = 1$. Note that in [259], expressions for the dominant wide-angle corrections to the monopole, quadrupole and hexadecapole have been derived for various choices of angles.

In fig. 3.7 we show the multipoles from all the non-integrated contributions in the full-sky linear regime. We use the angle $\mu$ for this figure. Each plot represents a different relativistic contribution (see eqs. (3.12) to (3.21) for a definition of the terms). As in figs. 3.3 and 3.5, this encompasses the correlation of the term with itself as well as its cross-correlation with the standard term (density and redshift-space distortion). One would naively expect that the dominant contribution would come from the Doppler term d1 correlated with the standard term. However, as discussed in Section 3.2.1, this contribution exactly vanishes in the flat-sky approximation. It would contribute only to a dipole, which cannot be seen with one population of galaxies, due to its anti-symmetry (indeed only even multipoles exist in this case). As a consequence to measure the dominant dipole one needs to cross-correlate two

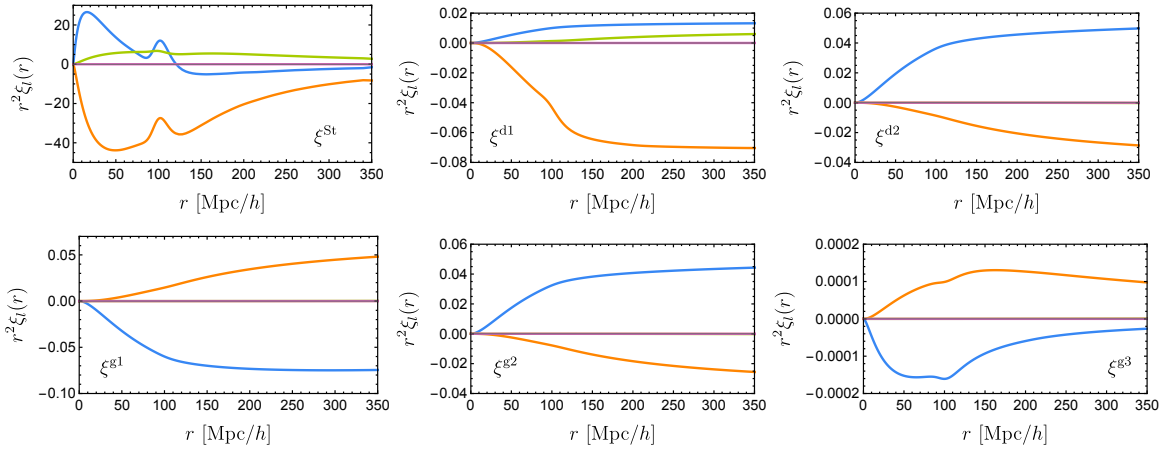


Figure 3.7: We show the multipoles of different contributions to the full-sky correlations function at $\bar{z} = 1$. The monopole (blue), quadrupole (orange), hexadecopole (green) and $\ell = 6$ purple.

populations of galaxies, as discussed in [76, 77, 155, 169].

However, as discussed in Section 3.2.1, in full-sky the Doppler-standard correlation does not exactly vanish and it contributes to the even multipoles. The amplitude of this term is then of the same order of magnitude as the d1-d1 correlation and as the other relativistic terms (for example g1 correlated with density). This is evident from the various panels in fig. 3.7, where we see that all the non-integrated relativistic terms generate multipoles of the same order of magnitude. The only exception is g3 which is much smaller. This is not surprising since at $z = 1$ the universe is still matter dominated and the gravitational potential is nearly constant. For the same reason also d2 and g2 are very similar. The Doppler contribution is the only one which generates a non-negligible hexadecapole. This comes from the correlation of d1 with redshift-space distortions which contains 3 gradient of the potential. In flat-sky this gives rise to a $\mu^3$-dependence, which again vanishes for symmetry reason, but in full-sky one obtains an additional factor $\mu \cdot r/\chi$ which leads to an hexadecapole[10]. In flat-sky the other relativistic terms (d2, g1, g2 and g3) generate only a monopole and quadrupole, due to their correlation with redshift-space distortion. In full-sky they do generate higher multipoles, but again those are suppressed by powers of $r/\chi$ and are consequently subdominant.

In fig. 3.8 we plot the fractional difference due to all non-integrated effects with respect to the standard flat-sky multipoles

$$\Delta\xi_\ell^{\rm rel} = \frac{\xi_\ell^{\rm rel}}{\xi_\ell^{\rm st,flat-sky}}\,, \tag{3.58}$$

where $\xi_\ell^{\rm rel}$ contains the correlation of all the non-integrated relativistic terms with themselves as well as their correlation with the standard term, i.e. they come from

$$\langle\Delta^{\rm st}\Delta^{\rm rel}\rangle + \langle\Delta^{\rm rel}\Delta^{\rm st}\rangle + \langle\Delta^{\rm rel}\Delta^{\rm rel}\rangle = \langle\Delta^{\rm st+rel}\Delta^{\rm st+rel}\rangle - \langle\Delta^{\rm st}\Delta^{\rm st}\rangle\,. \tag{3.59}$$

[10]This can been seen for example by expanding $\alpha_1 - \alpha_2$ in powers of $r/\chi$ in the expression $\zeta^{12}$ in Appendix 3.B.

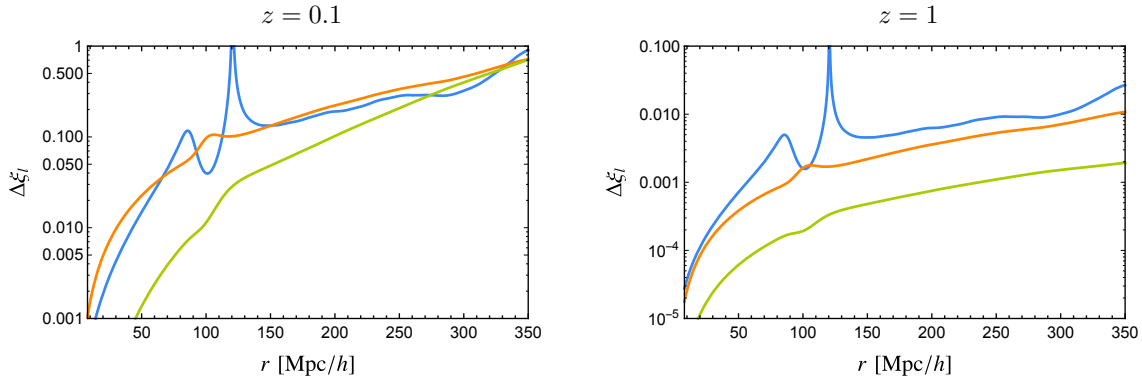


Figure 3.8: Fractional difference generated by the sum of the non-integrated relativistic effects on the monopole (blue), quadrupole (orange) and hexadecapole (green). The relativistic multipoles are calculated in the full-sky linear regime, whereas the standard multipoles are calculated in the flat-sky linear regime, to reproduce the theoretical prediction currently used.

At $\bar{z} = 1$ (right panel), the relativistic terms modify the monopole by a few percent at separations $\geq 300\,\mathrm{Mpc}/h$. The impact of these terms on parameter estimation is therefore probably negligible at high redshift. At $\bar{z} = 0.1$ however (left panel) the relativistic contribution to the multipoles is non-negligible at most scales. The contributions to the monopole and quadrupole are already of a few percent at $50\,\mathrm{Mpc}/h$. At $100\,\mathrm{Mpc}/h$ these contributions reach 10% and they quickly increase with separation.

The large amplitude of the relativistic terms at small redshift is due to one specific term in the Doppler contribution, namely the one proportional to $1/(\mathcal{H}\chi)$ (see eq. (3.15)). The correlation of the Doppler term with itself has roughly the following amplitude:

$$1/(\mathcal{H}\chi)^2(\mathcal{H}/k)^2\langle\Delta^{\mathrm{den}}\Delta^{\mathrm{den}}\rangle \sim (r/\chi)^2\langle\Delta^{\mathrm{den}}\Delta^{\mathrm{den}}\rangle\,,$$

where we have used that $k$ corresponds to $1/r$. At small redshift and large separation, this suppression is not very strong. For example at $\bar{z} = 0.1$, $\chi = 433\,\mathrm{Mpc}/h$ and therefore the amplitude of the Doppler term at $r = 200\,\mathrm{Mpc}/h$ is roughly $(r/\chi)^2\langle\Delta^{\mathrm{den}}\Delta^{\mathrm{den}}\rangle \sim 0.2\langle\Delta^{\mathrm{den}}\Delta^{\mathrm{den}}\rangle$, i.e. 20% of the standard term. The same argument applies to the full-sky Doppler-standard correlation which contributes at the same level. The other relativistic terms on the other hand are more strongly suppressed. For example, the correlation g1-standard has the following amplitude: $1/(\mathcal{H}\chi)(\mathcal{H}/k)^2\langle\Delta^{\mathrm{den}}\Delta^{\mathrm{den}}\rangle \sim (r/\chi)r\mathcal{H}\langle\Delta^{\mathrm{den}}\Delta^{\mathrm{den}}\rangle$. At $\bar{z} = 1$, $\mathcal{H} \sim 1/\chi$ and the Doppler contribution is similar to the g1 contribution, as already discussed. At $\bar{z} = 0.1$ however, $\mathcal{H}$ is significantly smaller than $1/\chi$ and therefore the Doppler contribution is enhanced with respect to the g1 contribution. Note that the importance of this Doppler effect on the correlation function has already been studied in detail in [240] and further discussed in [254, 269]. These references, however, do not include the other Doppler terms or lensing.

This result is especially relevant for a survey like the SKA that will cover wide parts of the sky from $z = 0$ to 2 and will therefore be strongly affected by the Doppler term at low redshift. In a forthcoming publication we will study the impact of this effect on the

measurement of cosmological parameters, in particular on the measurement of the growth rate $f$ from the monopole and quadrupole. Note that, as discussed above, such a study has to be performed using the full-sky formalism, since full-sky effects (from the Doppler-density correlation) contribute at the same level.

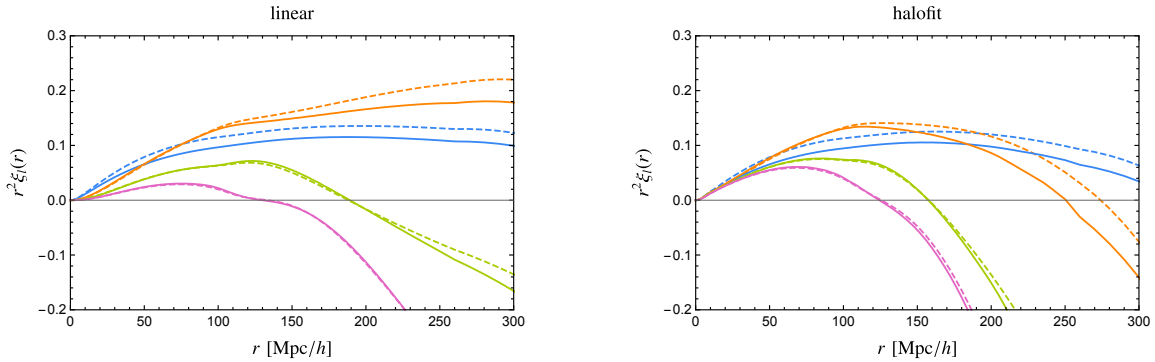


Figure 3.9: Multipoles of the lensing contribution (including its correlation with the standard term) at $\bar{z} = 1$. In the left panel we show the linear full-sky (solid) and linear flat-sky (dashed) result and in the right panel the non-linear full-sky (solid) and flat-sky (dashed) result. The monopole is shown in blue, the quadrupole in orange, the hexadecapole in green and the $\ell = 6$ in purple.

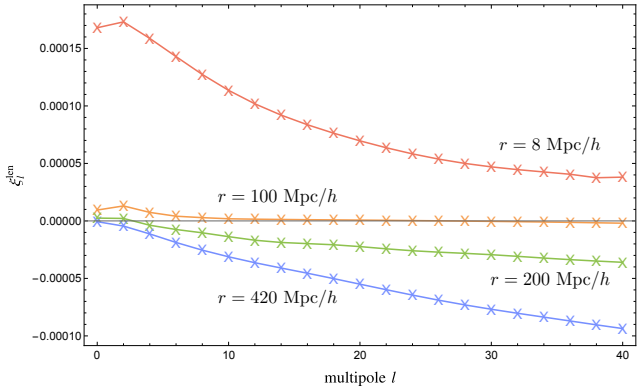


Figure 3.10: The full-sky non-linear lensing multipoles as a function of $\ell$ for different separations at $\bar{z} = 1$.

In fig. 3.9 we show the lensing contribution to the multipoles at $\bar{z} = 1$. In the left panel we show the linear result, using the flat-sky and Limber approximation (dashed) and the full-sky calculation (solid); and in the right panel we show the non-linear result. The flat-sky systematically overestimates the lensing contribution. As explained in Section 3.2.2 this is due to the fact that the Limber approximation underestimates the correlation between density and lensing, which is negative, and consequently it overestimates the total in most configurations.

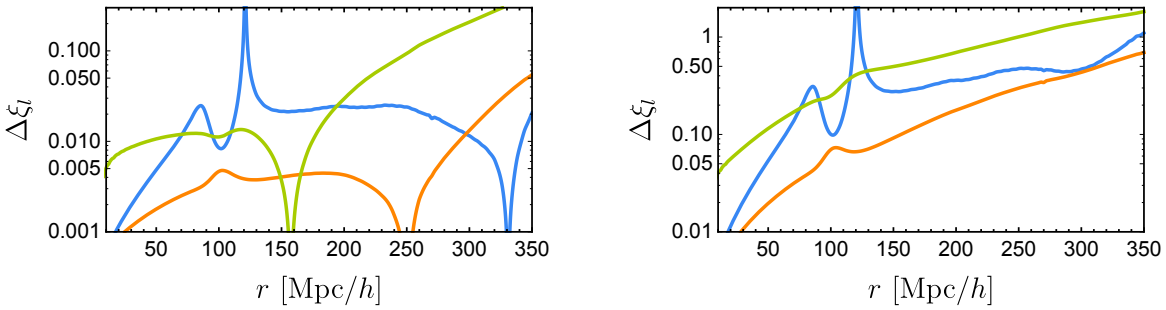


Figure 3.11: Fractional difference generated by lensing on the monopole (blue), quadrupole (orange) and hexadecapole (green). The lensing multipoles are calculated in the full-sky non-linear regime, whereas the standard multipoles are calculated in the flat-sky non-linear regime, to reproduce the theoretical prediction currently used. The left panel is for $\bar{z} = 1$ and the right panel for $\bar{z} = 2$.

Above $r \sim 50h^{-1}$Mpc the lensing contribution is 10% and more. Hence it has to be included for an accurate estimation of the growth rate $f$. Contrary to the non-integrated relativistic effects, lensing generates non-negligible $\ell = 4$ and $\ell = 6$. Actually, as is shown in fig. 3.10 the amplitude of the multipoles remains large for large values of $\ell$. Measuring $\ell > 4$ will therefore provide a way of isolating the lensing contribution from the standard terms.

In fig. 3.11 we show the fractional difference of the monopole, quadrupole and hexadecapole generated by lensing at $\bar{z} = 1$ and $\bar{z} = 2$. At $\bar{z} = 1$ we see that lensing modifies the monopole by a few percent at intermediate scales. The quadrupole is less affected, apart from at very large scales $r \sim 350\,\mathrm{Mpc}/h$ where lensing contributes by 5%. The hexadecapole is the one that is the most affected by lensing, up to 10-20% above $250\,\mathrm{Mpc}/h$. At $\bar{z} = 2$ the lensing contribution is significant for all multipoles. The monopole is modified by 30% already at a $150\,\mathrm{Mpc}/h$ and this increases to 50% at $300\,\mathrm{Mpc}/h$. The contribution to the quadrupole is slightly smaller, but it still reaches 10% at $150\,\mathrm{Mpc}/h$ and 40% at $300\,\mathrm{Mpc}/h$. And the hexadecapole is strongly affected at all scales. Surveys like Euclid and the SKA, that will observe up to high redshift should therefore include lensing in their modelling of the multipoles of the correlation function.

In this Section we have only discussed the contribution from even multipoles to the correlation function. As stated before, in the flat-sky approximation only even multipoles exist, even in the presence of relativistic effects and lensing[11]. This follows directly from the fact that the correlation function is symmetric $\xi(\mathbf{r}) = \xi(-\mathbf{r})$ and that the flat-sky angle goes from $\mu$ to $-\mu$ when $\mathbf{r}$ goes to $-\mathbf{r}$. In the full-sky, the existence of odd multipoles depend on the choice of angle used to measure them. If the cosine of the angle simply changes sign when $\mathbf{r}$ goes to $-\mathbf{r}$, then odd multipoles exactly vanish also in the full-sky. This is the case for the angles $\beta$, $\gamma$ and $\alpha$ defined in fig. 3.1. However if one uses instead the angle $\alpha_1$ (see fig. 3.A.1) to measure the multipoles, then the correlation function contains odd multipoles

[11]Note that this is not the case with the alternative definition of multipoles used in [250] which mixes different scales.

in the full-sky because $\alpha_1$ goes to $\pi + \alpha_1 - \theta$ when $\mathbf{r}$ goes to $-\mathbf{r}$. Hence even if the correlation function is symmetric, its expansion in terms of $\alpha_1$ contains odd multipoles due to the fact that the angle itself breaks the symmetry of the configuration [259]. Note that the dipole of the correlation function using the angle $\alpha_1$ has been measured in [155]. Finally let us stress that if we cross-correlate different populations of galaxies, then the correlation function is not symmetric anymore $\xi_{AB}(\mathbf{r}) \neq \xi_{BA}(-\mathbf{r})$ (where $A$ and $B$ denote the two populations under considerations) and it contains therefore odd multipoles already in the flat-sky approximation, as demonstrated in [76].

## 3.3 A word on the power spectrum

As discussed in the introduction, an alternative observable which is routinely used to analyse redshift surveys is the power spectrum. Here we discuss the impact of the large-scale relativistic effects and of lensing on this observable.

At the beginning of this chapter we pointed out that the power spectrum is consistently defined only in the flat-sky approximation. The reason for this is that $P(k)$ is not defined on the light-cone: to construct it one has to measure $\delta(\mathbf{k})$ on a spatial hyper-surface to which we do not have access observationally. In the flat-sky limit one can make the approximation that the patch of the sky he measures is a spatial hyper-surface but as the correlation length increases this becomes a bad approximation. Since, as we said, galaxies are seen on our background light-cone and not in 3D physical space, its positions are fixed by the redshift $z$ and the direction $\mathbf{n}$. We can however split the distance vector between two galaxies, $\mathbf{r}$ (which is the argument of the galaxy correlation function $\xi(\mathbf{r}, \bar{z})$) in a sufficiently small redshift bin into a radial, $r_\parallel$ and a transverse, $r_\perp$ component and express $\xi$ in the variables $\xi(r_\parallel, r_\perp, \bar{z})$. We can then define the power spectrum simply as the Fourier transform of the correlation function: this is an approach that was already advocate in [316], while a different approach based on the Spherical-Fourier analysis of the observed galaxy fluctuation is presented in [319]. We then write

$$P(k_\parallel, k_\perp, \bar{z}) = \int d^3r \xi(r_\parallel, r_\perp, \bar{z}) e^{i(r_\parallel k_\parallel + r_\perp k_\perp \cos\phi)} \tag{3.60}$$

$$= 2\pi \int_{-\infty}^{\infty} dr_\parallel \int_0^{\infty} dr_\perp \xi(r_\parallel, r_\perp, \bar{z}) e^{i(r_\parallel k_\parallel)} J_0(k_\perp r_\perp)\,. \tag{3.61}$$

In this expression $r_\parallel = r\sigma$ and $r_\perp = r\sqrt{1-\sigma^2}$ where

$$[-1, 1] \ni \sigma = \begin{cases} \mu = \cos\alpha \\ \cos\beta \\ \cos\gamma \\ \cos\alpha_2 \end{cases} \tag{3.62}$$

depending on the angle used to split the survey into a radial and a transversal component. Note that $\mathbf{r}_\perp = r_\perp(\cos\phi, \sin\phi)$ is a 2D vector in the plane normal to the parallel direction and we have performed the $\phi$ integration choosing the $x$-axis in the $\mathbf{r}_\perp$ plane parallel to $\mathbf{k}_\perp$. For the

case $\sigma = \mu$, $r_\parallel = \chi_2 - \chi_1$ the expression for the correlation function is given in Appendix 3.B and Section 3.2, (3.49). For the other angles, one has to use the relations given in Appendix 3.A.

However, we must consider that while the correlation function as given e.g. in eq. (3.27) can be defined for all values $r_\parallel \in [0, \chi(\infty)] \simeq [0, 14h^{-1}\text{Gpc}]$ and $r_\perp \in [0, 2\chi(\infty)]$, and is correct for $|r_\parallel H(\bar{z})| \ll 1$, this is no longer so for its Fourier transform[12]. To compute it we have to integrate the correlation function over all space, but as we just said, we cannot observe the correlation function outside of our horizon and the result is not reliable if $|r_\parallel H(\bar{z})| \gtrsim 1$. It is well defined only for a range of $(r_\parallel, r_\perp)$. This situation is further complicated by the fact that this range depends on redshift. Therefore, the simple Fourier transform given above gives a physically sensible result only for

$$k_\parallel \gg \frac{1}{\chi(\bar{z}+\Delta z) - \chi(\bar{z}-\Delta z)} \sim 2\Delta z H(\bar{z}) = \frac{1}{r_{\parallel\,\max}(\bar{z}, \Delta z)}\,, \qquad \Delta z \ll 1.$$

For these values of $k_\parallel$, contributions from radial distances such that the two galaxies are not in a thin shell around $\bar{\chi} = \chi(\bar{z})$ are cancelled by the rapid oscillations of the exponential in the Fourier transform.

With this word of caution we now simply Fourier transform the correlation function to obtain the power spectrum. We can either use the correlation function obtained via the $C_\ell(z_1, z_2)$'s or the one from the direct computation. Here we present the details for the latter.

As stated above, for the 'true' power spectrum, the integral over $r_\parallel$ should extend from $-\infty$ to $+\infty$ and the integral over $r_\perp$ should extend from 0 to $+\infty$. The correlation function is however not observable outside the horizon and the integral must therefore be truncated by a window function which removes these scales. In practice galaxy surveys do not observe the whole horizon but only part of it and therefore the range of integration is even more reduced. The true window function of the observation patch leads to a convolution in the correlation function and therefore to a multiplication of the Fourier transform of the window in the power spectrum

From eq. (3.61) we see that there is another reason to truncate the integral. The arguments $k_\parallel$ and $k_\perp$ (or equivalently $k$ and $\nu = \hat{\mathbf{k}} \cdot \hat{\mathbf{n}}$) of the power spectrum are parallel to $r_\parallel$ and $r_\perp$ respectively. Now the direction of $r_\parallel$, for example, depends on the direction of the pair of galaxies we consider. If the domain of integration in (3.61) is sufficiently small, then a mean direction $\mathbf{n}$ can be introduced and this splitting is well defined: one can identify one line-of-sight for the whole patch of sky we are observing and split parallel and transverse directions with respect to this line-of-sight. If the patch is too large however, this procedure is no longer valid [13]. The integral (3.61) can still be done mathematically, but its physical interpretation becomes unclear. This illustrates the fact that the power spectrum is truly well defined only in the flat-sky. In practice this means that we can consider the Fourier transform of the correlation function in a sphere of radius $\Delta z/\mathcal{H}(\bar{z})$ for values $k \gg \mathcal{H}(\bar{z})/\Delta z$.

Similar to what is done for the correlation function, in the standard analysis, the $\nu$ dependence of $P(k, \nu, \bar{z})$ is used to extract the growth rate $f(\bar{z})$. Indeed as seen in eq. (3.5),

[12] Here $\chi(\infty) \simeq 14h^{-1}$Gpc represents the comoving size of our horizon today.

[13] Note however the work of [315] which proposes methods to account for different lines-of-sight in the measurement of the power spectrum.

the standard power spectrum takes the simple form

$$P(k,\nu,\bar{z}) = p_0(k,\bar{z}) + p_2(k,\bar{z})\mathcal{P}_2(\nu) + p_4(k,\bar{z})\mathcal{P}_4(\nu)\,, \tag{3.63}$$

where the coefficients $p_n$ are given by:

$$p_0(k,\bar{z}) = D_1^2(\bar{z})P(k)\left[b^2 + \frac{2bf}{3} + \frac{f^2}{5}\right], \tag{3.64}$$

$$p_2(k,\bar{z}) = D_1^2(\bar{z})P(k)\left[\frac{4bf}{3} + \frac{4f^2}{7}\right], \tag{3.65}$$

$$p_4(k,\bar{z}) = D_1^2(\bar{z})P(k)\frac{8f^2}{35}\,. \tag{3.66}$$

The multipoles $p_0$ and $p_2$ contain different combinations of the bias and of the growth rate $f(\bar{z})$ and can be used to measure these two quantities. If $p_4$ can be measured as well it can be used as an additional consistency check. Furthermore, this quantity is independent of galaxy bias which renders it especially valuable.

The large-scale relativistic effects and the gravitational lensing are however expected to modify this simple multipole expansion. In principle to calculate the contribution of these effects to the multipoles, one would need to calculate eq. (3.61) for all values of $k_\parallel$ and $k_\perp$ and then integrate over all directions, weighting by the appropriate Legendre polynomial

$$p_\ell(k,\bar{z}) = \frac{2\ell+1}{2}\int_{-1}^{1} d\nu P(k,\nu,\bar{z})\mathcal{P}_\ell(\nu)\,. \tag{3.67}$$

As the correlation function is a symmetric function of $\mu$, $\xi(\mathbf{x}_1,\mathbf{x}_2) = \xi(\mathbf{x}_2,\mathbf{x}_1)$, the power spectrum will be symmetric in $\nu$ so that only even $\ell$'s are non-zero. This is no longer the case when one correlates different tracers, e.g. bright and faint galaxies [225, 322].

The procedure to obtain the multipoles of the power spectrum can however be simplified by using directly the multipoles of the correlation function $\xi_\ell(r)$ (see Appendix 3.D for a proof of this relation)

$$p_\ell(k) = 4\pi i^\ell \int_0^\infty dr r^2 j_\ell(kr)\xi_n(r)\,. \tag{3.68}$$

As discussed before, the integral over $r$ cannot run until infinity because the correlation function (and consequently its multipoles) is not observable over the whole space. For simplicity we assume that we observe galaxies within a sphere of radius $r_{\rm max}$, centred at redshift $\bar{z}$. This corresponds to introducing a window function in eq. (3.68) which removes scales larger than $r_{\rm max}$. For the standard terms, the multipoles $p_\ell(k)$ are relatively insensitive to the choice of $r_{\rm max}$ since $r^2\xi^{\rm st} \to 0$ as $r \to \infty$. The large-scale relativistic effects scale however as $r^2\xi^{\rm rel} \to$ constant as $r \to \infty$ and consequently their multipoles depend on the choice of $r_{\rm max}$. This reflects the fact that these terms diverge when $k \to 0$ as we will see in section 3.3.1. The situation for the lensing term is even worse: the correlation function scales as $r^2\xi^{\rm len} \to \infty$ and the dependence in $r_{\rm max}$ is even stronger. The lensing power spectrum is therefore strongly dependent on the geometry of the survey, as already noticed in [213].

### 3.3.1 The flat-sky approximation

In the previous section we obtained the power spectrum by integrating over the full-sky correlation function, weighted by a window function to restrict the range of integration to the observed patch of the sky. Here we would like to compare this procedure with a flat-sky direct calculation of the power spectrum[14]. The power spectrum for the non-integrated terms has been derived previously in [194, 322]. It can be easily obtained by Fourier transforming the non-integrated relativistic contributions to the number counts, namely $\Delta^{\rm d1}, \Delta^{\rm d2}, \Delta^{\rm g1}, \Delta^{\rm g2}$ and $\Delta^{\rm g3}$ (see eqs. (3.15) to (3.19)). Note that in principle this procedure does not generate an observable, because the Fourier transform of a function $f(\mathbf{k}, \eta)$ at a given conformal time $\eta$ requires the knowledge of the function over the whole hypersurface of constant $\eta$ [15]. An observer cannot observe this hypersurface, but only its intersection with her past light-cone. However, due to the statistical homogeneity and isotropy of our Universe, the properties of the function are the same everywhere, and the Fourier transform can be performed. We obtain (in agreement with [194] where only the non-integrated terms are considered)

$$P_\Delta^{\rm flat,\,non-int}(k,\nu,z) = \left| A + B\,\frac{\mathcal{H}}{k} + C\left(\frac{\mathcal{H}}{k}\right)^2 \right|^2 D_1^2(z) P(k)\,, \tag{3.69}$$

where

$$A(\nu,z) = (b - \nu^2 f)\,, \tag{3.70}$$

$$B(\nu,z) = -i\nu\left(\frac{\dot{\mathcal{H}}}{\mathcal{H}^2} + \frac{2-5s}{\mathcal{H}\chi} + 5s - f_{\rm evo}\right), \tag{3.71}$$

$$C(z) = \left[3f + \frac{3}{2}\Omega_m(1+z)\frac{H_0^2}{\mathcal{H}^2}\left(1 - 5s - \frac{\dot{\mathcal{H}}}{\mathcal{H}^2} - \frac{2-5s}{\mathcal{H}\chi} - 5s + f_{\rm evo}\right)\right]. \tag{3.72}$$

$A$ represents the standard terms, density and redshift space distortions. $B$ is the Doppler term which is suppressed by a factor $\mathcal{H}/k$ and $C$ represents the additional relativistic contributions which are suppressed by $(\mathcal{H}/k)^2$. To arrive at this result we have set $\Psi = \Phi$ and we have neglected the term containing the time derivative of the potential, since it is relevant only at late time and at very large angular scales where the flat sky approximation is not valid.

The contribution of the integrated terms to the flat-sky power spectrum are more complicated to calculate and have been neglected in [194, 322]. The reason is that integrated terms, like for example the lensing $\Delta^{\rm lens}(\mathbf{n}, \eta)$, depend on the value of the gravitational potential along the photon trajectory in direction $\mathbf{n}$. As a consequence $\Delta^{\rm lens}(\mathbf{n}, \eta)$ is well defined only on the past light-cone of the observer and not on the whole hypersurface of constant conformal time $\eta$. Calculating $\Delta^{\rm lens}(\mathbf{n}, \eta)$ for a point which is not on the past light-cone of the observer would require to calculate the lensing signal along arbitrary trajectories that have nothing to do with the trajectories followed by photons, as depicted in fig. 3.12.

[14] Note that the relation between the flat-sky and full-sky power spectrum of density and RSD has been studied in detail in [259].

[15] In principle we do not observe at constant conformal time $\eta$ but rather at constant redshift $z$. However the difference between $\eta$ and $z$ has been consistently included in the derivation of $\Delta_g$ so that a constant $z$ can now be seen as a constant $\eta$.

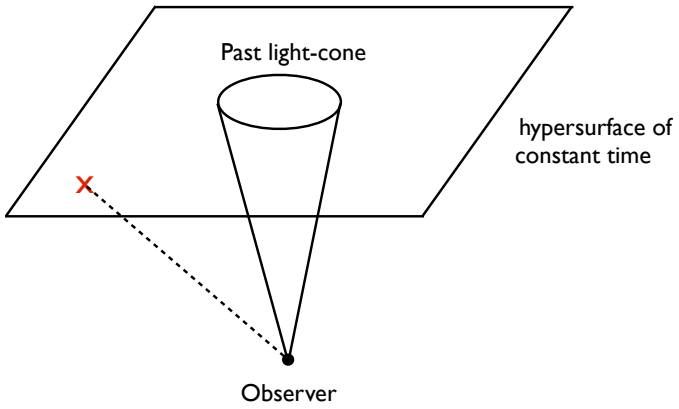


Figure 3.12: To calculate the Fourier transform of the lensing term $\Delta^{\rm lens}(\mathbf{k},\eta)$, one needs to know the value of $\Delta^{\rm lens}(\mathbf{x},\eta)$ for all $\mathbf{x}$ on the hypersurface of constant time $\eta$. However for a given observer, $\Delta^{\rm lens}(\mathbf{x},\eta)$ is well defined only on her past light-cone. Calculating $\Delta^{\rm lens}(\mathbf{x},\eta)$ outside of the past light-cone, like for example at the position of the cross would require to integrate the gravitational potential along the dashed trajectory, which is not physical, and would lead to wrong results.

To calculate the power spectrum of the integrated terms, we need therefore to go through the correlation function.

In Appendix 3.E we show how this can be done in the flat-sky approximation. To calculate the integrated terms in the flat sky approximation, we define a sky direction $\mathbf{n}_*$ and split the observation directions as $\mathbf{n}_1 = \mathbf{n}_* + \Delta\mathbf{n}/2$, $\mathbf{n}_2 = \mathbf{n}_* - \Delta\mathbf{n}/2$. We also split $\mathbf{r} = \mathbf{r}_\perp + \mathbf{n}_* r_\parallel$ with $\mathbf{r}_\perp = \chi(z)\Delta\mathbf{n}$. Representing the correlation function as the Fourier transform of the power spectrum, we can then perform the integral over $k_\parallel$ by neglecting the slow dependence of the power spectrum and taking into account only the fast oscillations of the exponential. This leads to the $\delta(k_\parallel)$ and $\delta^P(k_\parallel)$ defined below. All details are given in Appendix 3.E. We obtain

$$P_\Delta^{\rm flat,int}(k,\nu,z) = -3\pi\frac{\Omega_m H_0^2(1+z)D_1(z)(2-5s(z))}{\chi}P(k_\perp)\alpha(k_\perp,0,z)\left[\chi\delta^P(k_\parallel)+\frac{2}{k_\perp^2}\delta(k_\parallel)\right]$$
$$+\frac{\pi}{2}\left(\frac{3\Omega_m H_0^2(2-5s(z))}{\chi}\right)^2\delta(k_\parallel)\int_0^\chi d\lambda P(k\chi/\lambda)\left[\frac{(\chi-\lambda)\chi^2}{\lambda}+\frac{2}{k^2}\right]^2 D_1^2(z(\lambda))(1+z(\lambda))^2\,. \tag{3.73}$$

The first line comes from the correlation of the integrated terms with density and the second line is the correlation of the integrated terms with themselves. The distribution $\delta^P$ is defined by (see Appendix 3.E for more detail)

$$\delta^P(k) = \frac{1}{2\pi}\int_{-\infty}^{\infty} dx|x|e^{ikx}\,. \tag{3.74}$$

The lensing terms are proportional to the distributions $\delta(k_\parallel)$ and $\delta^P(k_\parallel)$. They have to be understood as formal expressions. Physical power spectra are obtained by smoothing

the signal with a longitudinal window function. Let us briefly explain this: we assume that our galaxies are all inside a radial window, $W(r_\parallel)$, with which the correlation function has to be convolved. Its Fourier transform, the power spectrum is then multiplied by the Fourier transform of the window, $\widehat{W}(k_\parallel)$. As an example, for the cross term involving $\delta^P(k_\parallel)$, denoting the pre-factor of $\delta^P(k_\parallel)$ by $P_\times$ and the result by $P_{\times\,\mathrm{obs}}$, we obtain an integral of the form

$$P_{\times\,\mathrm{obs}}(\mathbf{k},z) = P_\times(k_\perp,z)\frac{1}{2\pi}\int dr_\parallel dk_\parallel |r_\parallel| e^{ik_\parallel r_\parallel}|\widehat{W}(k_\parallel)|^2\,. \tag{3.75}$$

More details with examples of Gaussian and top hat windows can be found in [183].

## 3.4 Discussion and Conclusions

In this chapter we have studied the redshift-space correlation function and the power spectrum of galaxy number counts. Even though these functions depend on the cosmological model used to convert angles and redshifts into distances[16], they are useful for several reasons. First they are well adapted to describe the 3-dimensional information present in large-scale structure. This is not the case for the observable $C_\ell(z_1,z_2)$ angular-redshift power spectrum for which we cannot employ very fine redshift binning due to under-sampling. Second, the multipoles of the correlation function and of the power spectrum contain important information about the growth of perturbations which is difficult to isolate in the angular-redshift power spectrum. We therefore propose to use the redshift-space correlation function to analyse thin shells in redshift space, $\Delta z \sim 0.2$ and the power spectrum to analyse small (a few 100 Mpc) patches of sky.

Computing these quantities within linear perturbation theory and with the halofit approximation, we have shown how they are affected by large-scale relativistic effects and by lensing. The large-scale relativistic effects are important mainly at small redshifts. At $z = 0.1$ they introduce corrections to the monopole and quadrupole of the correlation function of the order of 10% at a separation of $100\,\mathrm{Mpc}/h$ and they quickly increase with separation. The hexadecapole is less affected at intermediate scales, but at large scales the correction becomes similar to the other multipoles. We have seen that this large correction is due to the Doppler effect, which contains a term proportional to $1/(\mathcal{H}\chi)$ which is enhanced at small redshift. This term has previously been identified in [240, 254, 269]. At large redshift however, this Doppler term contributes to the multipoles at the same level as the other relativistic effects and generates corrections that are never larger than about 1%. We have also seen that full-sky corrections to the correlation function are of the same order as relativistic corrections. It is hence inconsistent to take onto account only one or the other. They have to be discussed together as we do it in this work.

At large redshift the lensing term becomes much more relevant than the large-scale relativistic contributions. Furthermore, the importance of lensing strongly depends on the orientation of the pair of galaxies. In particular it is most important along the line-of-sight, when $\mu \sim 1$. In this case on large scales, $r > 200\,\mathrm{Mpc}/h$, the lensing term even dominates over the

[16]Note that deviations from the fiducial model can be accounted for in a consistent way by introducing correction parameters that rescale the correlation function, see e.g. [312].

standard terms (see fig. 3.3). We have also studied the contribution of lensing to the multipoles of the correlation function and of the power spectrum and we have seen that at $z = 1$ lensing modifies the monopole and quadrupole of the correlation function and of the power spectrum by a few percents. At larger redshift $z = 2$ these corrections amount to 10-30% at intermediate scales and quickly increase with separation. This clearly shows that lensing cannot be neglected in the analysis of future galaxy surveys at high redshift. Moreover we have seen that the hexadecapole of the correlation function and of the power spectrum are strongly affected by lensing at $z = 1$ and $z = 2$. This comes from the fact that the hexadecapole from the standard terms is significantly smaller than the monopole and quadrupole, whereas the hexadecapole of lensing is of the same order as the monopole and quadrupole (as can be seen from fig. 3.10). Measuring the hexadecapole is expected to provide a clean way of measuring the growth rate $f$ since it is independent of bias. Here we see however that such a measurement would require a careful modelling of the lensing contribution. Furthermore, we have found that lensing generates significant higher multipoles $\ell > 4$ in the correlation function , see figs. 3.9, 3.10 and 3.11.

In our work, contrary to previous studies on the subject, we have derived an expression for the lensing correlation function which is exact, i.e. which does not rely on the flat-sky and Limber approximation. By comparing our result with the flat-sky result, we have found that the flat-sky approximation is only good in forward direction, $\mu = 1$, see fig. 3.4. The full-sky lensing multipoles differ from the flat-sky one by 20-40%, see fig. 3.9. Finally, we have seen that due to the mixing of scales, non-linearities in the matter power spectrum are relevant for lensing even for large separations out to $r > 200\,\mathrm{Mpc}/h$ for $\mu \sim 1$ where lensing is most relevant, see fig. 3.5. A correct treatment of lensing requires therefore the use of the full-sky non-linear expressions.

The presence of higher multipoles in both, the correlation function and the power spectrum, might represent an ideal observational target to identify the lensing term. As it has been discussed previously [235], measuring the convergence $\kappa$ via the lensing of number counts is a promising alternative to shear measurements. On the other hand, it has been shown that neglecting lensing in the analysis of future surveys, at least for photometric surveys induces significant errors in parameter estimation [92]. It will be important to investigate whether this is also the case when precise spectroscopic redshifts are available.

# Appendices

## 3.A Relations between the angles

In this appendix we derive in detail the relation between the angles $\theta$, $\alpha$, $\beta$ and $\gamma$, see fig. 3.A.1. More precisely, we give expressions for $\cos\alpha$, $\cos\beta$ and $\cos\gamma$ in terms of $r$, $\cos\theta$ and $\bar{z} = (z_1 + z_2)/2$ or rather $\bar{\chi} = \chi(\bar{z})$. Note that $(\chi_1 + \chi_2)/2$ and $\chi(\bar{z})$ differ by a term of order $(\Delta z)^2/H(\bar{z})$ which we neglect.

As defined in the main text, $\alpha$ is the angle between the line of length $r$ connecting the two positions at redshifts $z_1$ and $z_2$ which span an angle $\theta$ at the observer and the line connecting $z_2$ and the intersection or the circle or radius $r_\parallel$ around $z_2$ with the Thales circle over $\mathbf{r}$ (see fig. 3.1, left panel). Evidently $\alpha$ is given by

$$\cos\alpha \;=\; r_\parallel/r = \frac{2}{r}\sqrt{\bar{\chi}^2 - \frac{4\bar{\chi}^2 - r^2}{2(1+\cos\theta)}}\,. \tag{3.76}$$

Here we have used eq. (3.34) to express $r_\parallel$ in terms of $(r, \bar{\chi}, \cos\theta)$.

The angle $\beta$ is obtained as follows: We denote by $s$ the length of the line from the observer $O$ to the middle of $r$ and by $\alpha_2$ the angle of the triangle $(O, z_2, z_1)$ at $z_2$, see fig. 3.A.1. The cosine law gives the following relations

$$\chi_2^2 \;=\; s^2 + (r/2)^2 + rs\cos\beta\,, \qquad s^2 \;=\; (r/2)^2 + \chi_2^2 - r\chi_2\cos\alpha_2 \tag{3.77}$$

Eliminating $s$ and solving for $\cos\beta$ we find

$$\cos\beta = \frac{-r^2/2 + r\chi_2\cos\alpha_2}{r\sqrt{(r/2)^2 + \chi_2^2 - r\chi_2\cos\alpha_2}} \tag{3.78}$$

Using furthermore

$$\cos\alpha_2 = \frac{\chi_2 - \chi_1\cos\theta}{r}$$

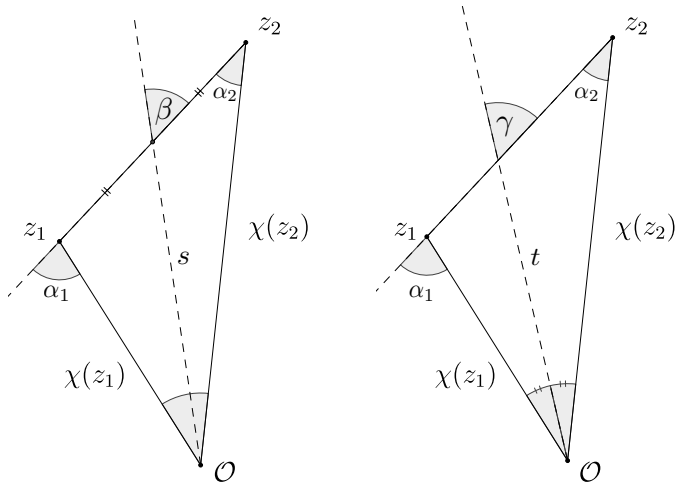


Figure 3.A.1: The angles $\alpha_1$, $\alpha_2$, $\beta$, $\gamma$ and the lengths $s$ and $t$ used to determine respectively $\beta$ and $\gamma$ are indicated.

we obtain after some simplifications

$$\cos\beta = \frac{\chi_2^2 - \chi_1^2}{r\sqrt{\chi_1^2 + \chi_2^2 + 2\chi_1\chi_2\cos\theta}} = \frac{2\bar{\chi}}{r}\sqrt{\frac{2r^2 - 4(1-\cos\theta)\bar{\chi}^2}{8\bar{\chi}^2\cos\theta^2 + (1\cos\theta)r^2}}\,. \tag{3.79}$$

For the second line we used expressions (3.33) for $\chi_{1,2}$.

Considering the angle $\gamma$ and using $t$ as indicated in fig. 3.A.1 and $\alpha_2$ as before we see that $\gamma = \theta/2 + \alpha_2$ hence

$$\cos\gamma = \cos(\theta/2)\cos\alpha_2 - (1-\cos^2\theta/2)^{1/2}(1-\cos^2\alpha_2)^{1/2}$$

Inserting

$$\cos\theta/2 = \left(\frac{1+\cos\theta}{2}\right)^{1/2}$$

and the expressions for $\cos\alpha_2$ we obtain

$$\cos\gamma \;=\; \frac{(1+\cos\theta)^{1/2}(\chi_2-\chi_1)}{\sqrt{2}r} \;=\; \frac{\sqrt{r^2 - 2(1-\cos\theta)\bar{\chi}^2}}{r}\,. \tag{3.80}$$

Again we have inserted the expressions (3.33) for $\chi_{1,2}$ in the last equal sign.

We shall also use the expressions for $\cos\alpha_i$ which are easily derived from the cosine theorem:

$$\cos\alpha_2 = \;\hat{\mathbf{r}}\cdot\mathbf{n}_2 \;=\; \frac{\chi_2 - \chi_1\cos\theta}{r}\,, \qquad \cos\alpha_1 = \;\hat{\mathbf{r}}\cdot\mathbf{n}_1 \;=\; -\,\frac{\chi_1 - \chi_2\cos\theta}{r}\,. \tag{3.81}$$

## 3.B The full angular–redshift correlation function

The 'full angular redshift correlation function' is $\xi(\theta, z_1, z_2)$ when we include all the relativistic terms. It can be computed as follows.
We first write down derivatives of eq. (3.51) wrt $\chi_1$ and $\chi_2$ which are encoded in the functions $\zeta^{ij}(k\chi_1, k\chi_2)$. Using $r = \sqrt{\chi_1^2 + \chi_2^2 - 2\chi_1\chi_2\cos\theta}$ and the recurrence relations for derivatives of spherical Bessel functions

$$j'_\ell = \frac{1}{2\ell+1}\left(\ell j_{\ell-1} - (\ell+1)j_\ell\right) \qquad \text{and} \qquad \frac{j_\ell(x)}{x} = \frac{1}{2\ell+1}\left(j_{\ell-1} + j_\ell\right)(x)$$

we find

$$\begin{aligned}
\zeta^{00} &= j_0(kr) \\
\zeta^{01} &= \frac{\chi_1\cos\theta - \chi_2}{r} j_1(kr) = -j_1(kr)\cos\alpha_2 \\
\zeta^{11} &= \left(\frac{2}{kr}j_1(kr) - j_0(kr)\right)\left(\frac{\chi_1 - \chi_2\cos\theta}{r}\right)\left(\frac{\chi_2 - \chi_1\cos\theta}{r}\right) + j_1(kr)\frac{\chi_1\chi_2\sin^2\theta}{kr^3} \\
&= -\frac{(\chi_2 - \chi_1\cos\theta)(\chi_1 - \chi_2\cos\theta)}{r^2} j_2(kr) + \frac{\cos\theta}{3}\left(j_0(kr) - j_2(kr)\right) \\
&= j_2(kr)\cos\alpha_2\cos\alpha_1 + \frac{\cos(\alpha_2 - \alpha_1)}{3}\left[j_0(kr) - j_2(kr)\right] \\
\zeta^{02} &= \left(\frac{2}{kr}j_1(kr) - j_0(kr)\right)\left(\frac{\chi_2 - \chi_1\cos\theta}{r}\right)^2 - j_1(kr)\frac{\chi_1^2\sin^2\theta}{kr^3} \\
&= \left(\frac{2}{3} - (1-\cos^2\theta)\frac{\chi_1^2}{r^2}\right) j_2(kr) - \frac{1}{3}j_0(kr) \\
&= \left(\frac{2}{3} - \sin^2\alpha_2\right) j_2(kr) - \frac{1}{3}j_0(kr) \\
\zeta^{12} &= \frac{(1+2\cos^2\theta)\chi_1 - 3\chi_2\cos\theta}{5r} j_1(kr) + \\
&\quad \frac{(1-3\cos^2\theta)\chi_1^3 + \cos\theta(5+\cos^2\theta)\chi_1^2\chi_2 - 2(2+\cos\theta^2)\chi_1\chi_2^2 + 2\chi_2^3\cos\theta}{5r^3} j_3(kr) \\
&= -\frac{\left[2\cos(\alpha_2 - \alpha_1)\cos\alpha_2 + \cos\alpha_1\right]}{5} j_1(kr) + \left[\cos\alpha_1\sin^2\alpha_2 - \frac{2}{5}\cos\alpha_2\cos(\alpha_1 - \alpha_2)\right] j_3(kr) \\
\zeta^{22} &= \frac{1+2\cos^2\theta}{15} j_0(kr) - \frac{1}{21}\left[1 + 11\cos^2\theta + \frac{18\cos\theta(\cos^2\theta - 1)\chi_1\chi_2}{r^2}\right] j_2(kr) + \\
&\quad \left[\frac{4(3\cos^2\theta - 1)(\chi_1^4 + \chi_2^4)}{35r^4} + \chi_1\chi_2(3+\cos^2\theta)\frac{3(3+\cos^2\theta)\chi_1\chi_2 - 8(\chi_1^2 + \chi_2^2)\cos\theta}{35r^4}\right] j_4(kr) \\
&= \frac{1+2\cos^2(\alpha_1 - \alpha_2)}{15} j_0(kr) - \frac{1}{42}\left[4 + 9\cos(2\alpha_1) + 9\cos(2\alpha_2) + 2\cos(2(\alpha_1 - \alpha_2))\right] j_2(kr) + \\
&\quad \frac{\left[3\cos(2(\alpha_1 - \alpha_2)) + 35\cos(2(\alpha_1 + \alpha_2)) + 10\cos(2\alpha_1) + 10\cos(2\alpha_2) + 6\right]}{280} j_4(kr)\,.
\end{aligned}$$

The coefficients $\zeta^{21}(x_1, x_2)$ etc. are obtained from $\zeta^{12}$ etc. via the symmetry relation

$$\zeta^{ij}(x, y) = \zeta^{ji}(y, x)\,.$$

The flat sky limit of the above function is obtained by setting $\alpha_1 = \alpha_2 \equiv \alpha$. In this case all the terms in front of a $j_\ell$ are a multiple of the Legendre polynomial $\mathcal{P}_\ell(\cos\alpha)$. More precisely, denoting the flat sky limit of $\zeta^{ij}$ by $\bar{\zeta}^{ij}$ we obtain

$$\begin{aligned}
\bar{\zeta}^{00} &= j_0(kr)\,,\\
\bar{\zeta}^{01} &= -L_1(\cos\alpha) j_1(kr)\,, \qquad \bar{\zeta}^{11} = \frac{2}{3}\mathcal{P}_2(\cos\alpha) j_2(kr) + \frac{1}{3} j_0(kr)\,,\\
\bar{\zeta}^{02} &= \frac{2}{3}\mathcal{P}_2(\cos\alpha) j_2(kr) - \frac{1}{3} j_0(kr)\,,\\
\bar{\zeta}^{12} &= -3L_1(\cos\alpha) j_1(kr) - \frac{2}{5} L_3(\cos\alpha)\,,\\
\bar{\zeta}^{22} &= \frac{8}{35}\mathcal{P}_4(\cos\alpha) j_4(kr) + \frac{4}{7}\mathcal{P}_2(\cos\alpha) j_2(kr) + \frac{1}{5} j_0(kr)\,.
\end{aligned}$$

The terms $\bar{\zeta}^{00}$, $\bar{\zeta}^{02}$ and $\bar{\zeta}^{22}$ give rise to the standard flat sky result (3.64) to (3.66). The flat sky results $\bar{\zeta}^{01}$ and $\bar{\zeta}^{12}$ are more subtle. Since we always have to add $\bar{\zeta}^{ij} + \bar{\zeta}^{ji}$ and $\bar{\zeta}^{ij}(\cos\alpha) = \bar{\zeta}^{ji}(\cos(\pi - \alpha)) = \bar{\zeta}^{ji}(-\cos\alpha)$ these odd terms actually cancel and do not contribute in the case of a single population of galaxies. They do contribute to a multi tracer signal, see [76].

The only coefficients that do not fall into this category, as explained in the main text, are the lensing terms which are computed using the identity

$$-\ell(\ell+1)\mathcal{P}_\ell(\cos\theta) = \triangle_\Omega \mathcal{P}_\ell(\cos\theta) = \frac{1}{\sin\theta}\partial_\theta\left(\sin\theta\partial_\theta \mathcal{P}_\ell(\cos\theta)\right)\,.$$

They are given explicitly by

$$\begin{aligned}
\zeta^{0\mathrm{L}} &= 2\frac{k\chi_1\chi_2\cos\theta}{r} j_1(kr) - \left(k^2\frac{\chi_1^2\chi_2^2\sin^2\theta}{r^2}\right) j_2(kr)\\
&= k^2\left[\frac{2}{3}\chi_1\chi_2\cos\theta j_0(kr) + \frac{\chi_1\chi_2}{3}\left(2\cos\theta - 3\chi_1\chi_2\frac{\sin^2\theta}{r^2}\right) j_2(kr)\right]\\
&= \frac{(kr)^2}{3}\Bigg[2\frac{\sin\alpha_1\sin\alpha_2\cos(\alpha_1-\alpha_2)}{\sin^2(\alpha_1-\alpha_2)} j_0(kr) + \frac{\sin\alpha_1\sin\alpha_2}{\sin^2(\alpha_1-\alpha_2)}\\
&\quad \times\left[\cos(\alpha_1-\alpha_2) + \cos\alpha_1\cos\alpha_2)\right] j_2(kr)\Bigg]\\
\zeta^{1\mathrm{L}} &= k^2\Bigg[\frac{2}{3}\chi_2 r\cos\theta j_{-1}(kr) + \frac{2\chi_2(\chi_1\cos\theta - \chi_2)(\chi_1 - 2\chi_2\cos\theta)}{5r} j_1(kr) -\\
&\quad \frac{1}{15r^3}\Big(\chi_2(4\chi_1^4\cos\theta - (9+\cos^2\theta)\chi_1^3\chi_2 + \cos\theta\left(\cos^2\theta + 5\right)\chi_1^2\chi_2^2 +
\end{aligned}$$

$$
\begin{aligned}
& 2(3-2\cos^2\theta)\chi_1\chi_2^3 - 2\chi_2^4\cos\theta)\Big) j_3(kr)\Big], \\
= \;& (kr)^2\left[\frac{2}{3}\frac{\cos(\alpha_1-\alpha_2)\sin\alpha_1}{\sin(\alpha_1-\alpha_2)} j_{-1}(kr) - \frac{2}{5}\frac{(2\sin\alpha_1-\sin\alpha_2)(\sin\alpha_1-\cos(\alpha_1-\alpha_2)\sin\alpha_2)}{\sin^3(\alpha_1-\alpha_2)}\times\right. \\
& \left. j_1(kr) - \frac{1}{120}\frac{\sin\alpha_1\left[6\sin(2\alpha_1)+\sin(2(\alpha_1-\alpha_2))-15\sin(2(\alpha_1+\alpha_2))\right]}{\sin^2(\alpha_1-\alpha_2)} j_3(kr)\right]
\end{aligned}
$$

$$
\begin{aligned}
\zeta^{2\mathrm{L}} = \;& -k^2\left\{\frac{2}{15}\chi_2\left(3\chi_1\cos\theta + (1-3\cos^2\theta)\chi_2\right) j_0(kr)\right. \\
& + \left[\frac{6\chi_1^3\chi_2\cos\theta - \left(9\cos^2\theta+11\right)\chi_1^2\chi_2^2}{21r^2} + \frac{2\cos\theta\left(3\cos^2\theta+8\right)\chi_1\chi_2^3 + 4\left(1-3\cos^2\theta\right)\chi_2^4}{21r^2}\right] j_2(kr) \\
& + \left[\frac{\chi_2\left(2\left(1-3\cos^2\theta\right)\chi_2^5 + 6\cos\theta(3-\cos^2\theta)\chi_1\chi_2^4 + (\cos^4\theta+12\cos^2\theta-21)\chi_1^2\chi_2^3\right)}{35r^4}\right. \\
& \left.\left. - \frac{\chi_2\left(2\cos\theta\left(\cos^2\theta+3\right)\chi_1^3\chi_2^2 - 12\chi_1^4\chi_2 + 4\chi_1^5\cos\theta\right)}{35r^4}\right] j_4(kr)\right\} \\
= \;& -(kr)^2\left\{\frac{1}{15}\frac{\sin\alpha_1(2\sin\alpha_1 - 3\sin(2(\alpha_1-\alpha_2))\cos\alpha_1)}{\sin^2(\alpha_1-\alpha_2)} j_0(kr) + \frac{\sin(\alpha_1)}{84\sin^4(\alpha_1-\alpha_2)}\times\right. \\
& \left[3\sin(3\alpha_1)(\cos(2\alpha_2)+3) - 12\cos^3\alpha_1\sin(2\alpha_2) - \sin\alpha_1(3\cos(2\alpha_2)+1)\right] j_2(kr) \\
& + \frac{\sin\alpha_1}{560\sin^2(\alpha_1-\alpha_2)}\left[5\sin(\alpha_1+2\alpha_2) - 35\sin(3\alpha_1+2\alpha_2)\right. \\
& \left.\left. + \sin(\alpha_1-2\alpha_2) + \sin(3\alpha_1-2\alpha_2) + 2\sin\alpha_1 + 10\sin(3\alpha_1)\right] j_4(kr)\right\} \qquad (3.82)
\end{aligned}
$$

$$
\begin{aligned}
\zeta^{\mathrm{LL}} = \;& -\sin^2\theta(k^2\chi_1\chi_2)^2\left[\left(\frac{6(r^2+5\chi_1\chi_2\cos\theta)}{35r^2} - \frac{\chi_1^2\chi_2^2\sin^2\theta}{r^4}\right) j_4(kr)\right. \\
& \left. + \frac{2\left(2r^2+3\chi_1\chi_2\cos\theta\right)}{7r^2} j_2(kr) \; + \frac{2}{5} j_0(kr)\right] \\
& + 4\cos\theta k^3\chi_1\chi_2\left[\left(\frac{r^2+6\chi_1\chi_2\cos\theta}{15r} - \frac{\chi_1^2\chi_2^2\sin^2\theta}{2r^3}\right) j_3(kr)\right. \\
& \left. + \frac{2\left(r^2+\chi_1\chi_2\cos\theta\right)}{5r} j_1(kr) + \frac{r}{3} j_{-1}(kr)\right] \qquad (3.83) \\
= \;& (kr)^3\left\{\frac{4}{3}\frac{\sin\alpha_1\sin\alpha_2\cos(\alpha_1-\alpha_2)}{\sin^2(\alpha_1-\alpha_2)} j_{-1}(kr)\right. \\
& - \frac{2}{5}\frac{\sin\alpha_1\sin\alpha_2\cot(\alpha_1-\alpha_2)[\cos(2(\alpha_1-\alpha_2))+\cos(2\alpha_1)+\cos(2\alpha_2)-3]}{\sin^3(\alpha_1-\alpha_2)} j_1(kr) \\
& \left. + \frac{\sin\alpha_1\sin\alpha_2\cos(\alpha_1-\alpha_2)}{60\sin^4(\alpha_1-\alpha_2)}\left[2+6\cos(2\alpha_1)+\cos(2(\alpha_1-\alpha_2))+6\cos(2\alpha_2)\right.\right.
\end{aligned}
$$

$$
\begin{aligned}
&-15\cos(2(\alpha_1+\alpha_2))\big]\, j_3(kr)\Big\}\\
&+(kr)^4\Big\{-\frac{2}{5}\frac{\sin^2\alpha_1\sin^2\alpha_2}{\sin^2(\alpha_1-\alpha_2)}j_0(kr)-\frac{2\sin^2\alpha_1\sin^2\alpha_2}{7\sin^4(\alpha_1-\alpha_2)}\\
&\times\big[2\sin^2(\alpha_1-\alpha_2)+3\cos(\alpha_1-\alpha_2)\sin\alpha_1\sin\alpha_2\big]\, j_2(kr)+\frac{\sin^2\alpha_1\sin^2\alpha_2}{280\sin^4(\alpha_1-\alpha_2)}\\
&\times\Big[35\cos(2(\alpha_1+\alpha_2))-10\cos(2\alpha_2)-\cos(2(\alpha_1-\alpha_2))-10\cos(2\alpha_1)-14\Big]j_4(kr)\Big\}\,.
\end{aligned}
$$

For the lensing terms the flat sky limit cannot be obtained by setting $\alpha_1 = \alpha_2$ since the terms $\xi^{iL}$ diverge in this limit. We discuss the flat sky approximation of lensing in Appendix 3.E.

We now give explicit expressions for the $Q_k^{AB}$ in terms of the $\zeta^{ij}$, to be inserted in eq. (3.49) to build the correlation function:

$$
\begin{aligned}
Q^{\rm den}(\theta,z_1,z_2) &= b(z_1)b(z_2)S_D(z_1)S_D(z_2)\,\zeta^{00}(k\chi_1,k\chi_2,\theta)\,,\\
Q^{\rm rsd}(\theta,z_1,z_2) &= \frac{k^2}{\mathcal{H}_1\mathcal{H}_2}S_V(z_1)S_V(z_2)\,\zeta^{22}(k\chi_1,k\chi_2,\theta)\,,\\
Q^{\rm len}(\theta,z_1,z_2) &= \frac{(2-5s)^2}{4\chi_1\chi_2}\int_0^{\chi_1}\!\!\int_0^{\chi_2}\mathrm{d}\lambda\mathrm{d}\lambda'\frac{(\chi_1-\lambda)(\chi_2-\lambda')}{\lambda\lambda'}S_{\phi+\psi}(\lambda)S_{\phi+\psi}(\lambda')\zeta^{LL}(k\lambda,k\lambda',\theta)\,,\\
Q^{\text{den-rsd}}(\theta,z_1,z_2) &= \frac{kb(z_1)}{\mathcal{H}_2}S_D(z_1)S_V(z_2)\,\zeta^{02}(k\chi_1,k\chi_2,\theta)\,,\\
Q^{\text{den-len}}(\theta,z_1,z_2) &= b(z_1)S_D(z_1)\left(\frac{2-5s}{2\chi_2}\right)\int_0^{\chi_2}\mathrm{d}\lambda\frac{\chi_2-\lambda}{\lambda}S_{\phi+\psi}(\lambda)\,\zeta^{0L}(k\chi_1,k\lambda,\theta)\,,\\
Q^{\text{rsd-len}}(\theta,z_1,z_2) &= \frac{k}{\mathcal{H}_1}S_V(z_1)\left(\frac{2-5s}{2\chi_2}\right)\int_0^{\chi_2}\mathrm{d}\lambda\frac{\chi_2-\lambda}{\lambda}S_{\phi+\psi}(\lambda)\,\zeta^{2L}(k\chi_1,k\lambda,\theta)\,,\\
Q^{\rm d1}(\theta,z_1,z_2) &= \left[\left(\frac{\dot{\mathcal{H}}}{\mathcal{H}^2}+\frac{2-5s}{\chi\mathcal{H}}+5s-f_{\rm evo}\right)S_V\right](z_1)\\
&\quad\times\left[\left(\frac{\dot{\mathcal{H}}}{\mathcal{H}^2}+\frac{2-5s}{\chi\mathcal{H}}+5s-f_{\rm evo}\right)S_V\right](z_2)\,\zeta^{11}(k\chi_1,k\chi_2,\theta)\,,\\
Q^{\rm X}(\theta,z_1,z_2) &= \Delta^{\rm X}(z_1,k)\Delta^{\rm X}(z_2,k)\zeta^{00}(k\chi_1,k\chi_2,\theta) \qquad\qquad X\in\{\mathrm{d2},\,\mathrm{g1},\,\mathrm{g2},\,\mathrm{g3}\}\,,\\
Q^{\rm g4}(\theta,z_1,z_2) &= \frac{(2-5s)^2}{\chi_1\chi_2}\int_0^{\chi_1}\mathrm{d}\lambda\int_0^{\chi_2}\mathrm{d}\lambda' S_{\phi+\psi}(\lambda,k)S_{\phi+\psi}(\lambda',k)\zeta^{00}(k\lambda,k\lambda',\theta)\,,\\
Q^{\rm g5}(\theta,z_1,z_2) &= \left(\frac{\dot{\mathcal{H}}}{\mathcal{H}^2}+\frac{2-5s}{\chi\mathcal{H}}+5s-f_{\rm evo}\right)(z_1)\left(\frac{\dot{\mathcal{H}}}{\mathcal{H}^2}+\frac{2-5s}{\chi\mathcal{H}}+5s-f_{\rm evo}\right)(z_2)\\
&\quad\times\int_0^{\chi_1}\mathrm{d}\lambda\int_0^{\chi_2}\mathrm{d}\lambda'\,\dot{S}_{\phi+\psi}(\lambda,k)\dot{S}_{\phi+\psi}(\lambda',k)\zeta^{00}(k\lambda,k\lambda',\theta)\,,
\end{aligned}
$$

$$Q^{\text{den-d1}}(\theta,z_1,z_2)=b(z_1)S_D(z_1)\left[\left(\frac{\dot{\mathcal{H}}}{\mathcal{H}^2}+\frac{2-5s}{\chi\mathcal{H}}+5s-f_{\text{evo}}\right)S_V\right](z_2)\zeta^{01}(k\chi_1,k\chi_2,\theta)\,,$$

$$Q^{\text{den-X}}(\theta,z_1,z_2)=b(z_1)S_D(z_1)\Delta^{\text{X}}(z_2,k)\zeta^{00}(k\chi_1,k\chi_2,\theta)\,,$$

$$Q^{\text{den-g4}}(\theta,z_1,z_2)=b(z_1)S_D(z_1)\frac{2-5s}{\chi_2}\int_0^{\chi_2}\mathrm{d}\lambda S_{\phi+\psi}(\lambda,k)\zeta^{00}(k\chi_1,k\lambda,\theta)\,,$$

$$Q^{\text{den-g5}}(\theta,z_1,z_2)=b(z_1)S_D(z_1)\left(\frac{\dot{\mathcal{H}}}{\mathcal{H}^2}+\frac{2-5s}{\chi\mathcal{H}}+5s-f_{\text{evo}}\right)(z_2)$$
$$\times\int_0^{\chi_2}\mathrm{d}\lambda\dot{S}_{\phi+\psi}(\lambda,k)\zeta^{00}(k\chi_1,k\lambda,\theta)\,,$$

$$Q^{\text{rsd-d1}}(\theta,z_1,z_2)=\frac{k}{\mathcal{H}_1}S_V(z_1)\left[\left(\frac{\dot{\mathcal{H}}}{\mathcal{H}^2}+\frac{2-5s}{\chi\mathcal{H}}+5s-f_{\text{evo}}\right)S_V\right](z_2)\zeta^{21}(k\chi_1,k\chi_2,\theta)\,,$$

$$Q^{\text{rsd-X}}(\theta,z_1,z_2)=\frac{k}{\mathcal{H}_1}S_V(z_1)\Delta^{\text{X}}(z_2,k)\zeta^{20}(k\chi_1,k\chi_2,\theta)\,,$$

$$Q^{\text{rsd-g4}}(\theta,z_1,z_2)=\frac{k}{\mathcal{H}_1}S_V(z_1)\frac{2-5s}{\chi_2}\int_0^{\chi_2}\mathrm{d}\lambda S_{\phi+\psi}(\lambda,k)\zeta^{20}(k\chi_1,k\lambda,\theta)\,,$$

$$Q^{\text{rsd-g5}}(\theta,z_1,z_2)=\frac{k}{\mathcal{H}_1}S_V(z_1)\left(\frac{\dot{\mathcal{H}}}{\mathcal{H}^2}+\frac{2-5s}{\chi\mathcal{H}}+5s-f_{\text{evo}}\right)(z_2)$$
$$\times\int_0^{\chi_2}\mathrm{d}\lambda\dot{S}_{\phi+\psi}(\lambda,k)\zeta^{20}(k\chi_1,k\lambda,\theta)\,,$$

$$Q^{\text{len-d1}}(\theta,z_1,z_2)=\left[\left(\frac{\dot{\mathcal{H}}}{\mathcal{H}^2}+\frac{2-5s}{\chi\mathcal{H}}+5s-f_{\text{evo}}\right)S_V\right](z_2)$$
$$\times\frac{2-5s}{2\chi_1}\int_0^{\chi_1}\mathrm{d}\lambda\frac{\chi_1-\lambda}{\lambda}S_{\phi+\psi}(\lambda)\zeta^{L1}(k\lambda,k\chi_2,\theta)\,,$$

$$Q^{\text{len-X}}(\theta,z_1,z_2)=\Delta^{\text{X}}(z_2,k)\frac{2-5s}{2\chi_1}\int_0^{\chi_1}\mathrm{d}\lambda\frac{\chi_1-\lambda}{\lambda}S_{\phi+\psi}(\lambda)\zeta^{L0}(k\lambda,k\chi_2,\theta)\,,$$

$$Q^{\text{len-g4}}(\theta,z_1,z_2)=\frac{(2-5s)^2}{2\chi_1\chi_2}\int_0^{\chi_1}\mathrm{d}\lambda\frac{\chi_1-\lambda}{\lambda}\int_0^{\chi_2}\mathrm{d}\lambda' S_{\phi+\psi}(\lambda,k)S_{\phi+\psi}(\lambda',k)\zeta^{L0}(k\lambda,k\lambda',\theta)\,,$$

$$Q^{\text{len-g5}}(\theta,z_1,z_2)=\left(\frac{\dot{\mathcal{H}}}{\mathcal{H}^2}+\frac{2-5s}{\chi\mathcal{H}}+5s-f_{\text{evo}}\right)(z_2)\frac{2-5s}{2\chi_1}$$
$$\times\int_0^{\chi_1}\mathrm{d}\lambda\int_0^{\chi_2}\mathrm{d}\lambda'\frac{\chi_1-\lambda}{\lambda}S_{\phi+\psi}(\lambda)\dot{S}_{\phi+\psi}(\lambda',k)\zeta^{L0}(k\lambda,k\lambda',\theta)\,,$$

$$Q^{\text{d1-X}}(\theta,z_1,z_2)=\left[\left(\frac{\dot{\mathcal{H}}}{\mathcal{H}^2}+\frac{2-5s}{\chi\mathcal{H}}+5s-f_{\text{evo}}\right)S_V\right](z_1)\Delta^{\text{X}}(z_2,k)\zeta^{10}(k\chi_1,k\chi_2,\theta)\,,$$

$$Q^{\text{d1-g4}}(\theta,z_1,z_2)=\left[\left(\frac{\dot{\mathcal{H}}}{\mathcal{H}^2}+\frac{2-5s}{\chi\mathcal{H}}+5s-f_{\text{evo}}\right)S_V\right](z_1)$$
$$\times\frac{2-5s}{\chi_2}\int_0^{\chi_2}\mathrm{d}\lambda S_{\phi+\psi}(\lambda,k)\zeta^{10}(k\chi_1,k\lambda,\theta)\,,$$

$$Q^{\text{d1-g5}}(\theta,z_1,z_2)=\left[\left(\frac{\dot{\mathcal{H}}}{\mathcal{H}^2}+\frac{2-5s}{\chi\mathcal{H}}+5s-f_{\text{evo}}\right)S_V\right](z_1)\left(\frac{\dot{\mathcal{H}}}{\mathcal{H}^2}+\frac{2-5s}{\chi\mathcal{H}}+5s-f_{\text{evo}}\right)(z_2)$$

$$\times \int_0^{\chi_2} \mathrm{d}\lambda \dot{S}_{\phi+\psi}(\lambda,k)\zeta^{20}(k\chi_1,k\lambda,\theta)\,,$$

$$Q^{\text{X-Y}}(\theta,z_1,z_2) = \Delta^{\text{X}}(z_1,k)\Delta^{\text{Y}}(z_2,k)\zeta^{00}(k\chi_1,k\chi_2,\theta) \qquad X\,,\,Y \in \{\text{d2, g1, g2, g3}\}\,,$$

$$Q^{\text{X-g4}}(\theta,z_1,z_2) = \Delta^{\text{X}}(z_1,k)\frac{2-5s}{\chi_2}\int_0^{\chi_2} \mathrm{d}\lambda S_{\phi+\psi}(\lambda,k)\zeta^{00}(k\chi_1,k\lambda,\theta)\,,$$

$$Q^{\text{X-g5}}(\theta,z_1,z_2) = \Delta^{\text{X}}(z_1,k)\left(\frac{\dot{\mathcal{H}}}{\mathcal{H}^2}+\frac{2-5s}{\chi\mathcal{H}}+5s-f_{\text{evo}}\right)(z_2)$$
$$\times \int_0^{\chi_2} \mathrm{d}\lambda \dot{S}_{\phi+\psi}(\lambda,k)\zeta^{10}(k\chi_1,k\lambda,\theta)\,,$$

$$Q^{\text{g4-g5}}(\theta,z_1,z_2) = \left(\frac{\dot{\mathcal{H}}}{\mathcal{H}^2}+\frac{2-5s}{\chi\mathcal{H}}+5s-f_{\text{evo}}\right)(z_2)\frac{2-5s}{\chi_1}$$
$$\times \int_0^{\chi_1} \mathrm{d}\lambda \int_0^{\chi_2} \mathrm{d}\lambda' S_{\phi+\psi}(\lambda,k)\dot{S}_{\phi+\psi}(\lambda,k)\zeta^{00}(k\lambda,k\lambda',\theta)\,.$$

The correlators $Q^{BA}(z_1,z_2)$ are obtained from $Q^{AB}(z_1,z_2)$ using the identity $Q^{BA}(z_1,z_2) = Q^{AB}(z_2,z_1)$. The functions $S_X$ and $\Delta^X$ are given in terms of the transfer function $T(k)$ and the density growth function $D_1(a)$ as

$$S_D = -\frac{3}{5}\frac{k^2}{\Omega_m\mathcal{H}_0^2}\frac{D_1(a)}{a}T(k)\,, \tag{3.84}$$

$$S_V = \frac{3}{5}\frac{k\mathcal{H}}{\Omega_m\mathcal{H}_0^2}\frac{dD_1(a)}{da}T(k) = -f\frac{\mathcal{H}}{k}S_D\,, \tag{3.85}$$

$$S_\phi = \frac{9}{10}\frac{D_1(a)}{a}T(k)\,, \qquad S_{\phi+\psi} = 2S_\phi\,, \tag{3.86}$$

$$\Delta^{\text{d2}} = -\frac{9}{5}\frac{\mathcal{H}^2}{\Omega_m\mathcal{H}_0^2}\frac{dD_1(a)}{da}T(k)\,, \tag{3.87}$$

$$\Delta^{\text{g1}} = \left(\frac{\dot{\mathcal{H}}}{\mathcal{H}^2}+\frac{2-5s}{\chi\mathcal{H}}+5s-f_{\text{evo}}\right)S_\phi\,, \tag{3.88}$$

$$\Delta^{\text{g2}} = -(2-5s)S_\phi\,, \qquad \Delta^{\text{g3}} = \mathcal{H}^{-1}\dot{S}_\phi\,. \tag{3.89}$$

Here we have set $\Phi = \Psi$ and the transfer function $T(k)$ as well as the growth function $D_1(a)$ have to be determined either with a Boltzmann solver like CLASS or using an analytic approximation like the one derived in Ref. [139]. We have normalized the growth function as well as the scale factor to unity today, $D_1(1) = 1$. For the numerical results shown in our figures we used the Boltzmann solver CLASS. We have checked analytically and numerically that our correlation functions for the standard and (d1)-terms agrees with the full sky results of [76].

## 3.C Approximation for the non-linear full-sky lensing

As discussed in Section 3.2.2, to calculate the non-linear full-sky lensing we calculate the halo-fit power spectrum at a fixed redshift $z_*$ and then evolve it along the line-of-sight using

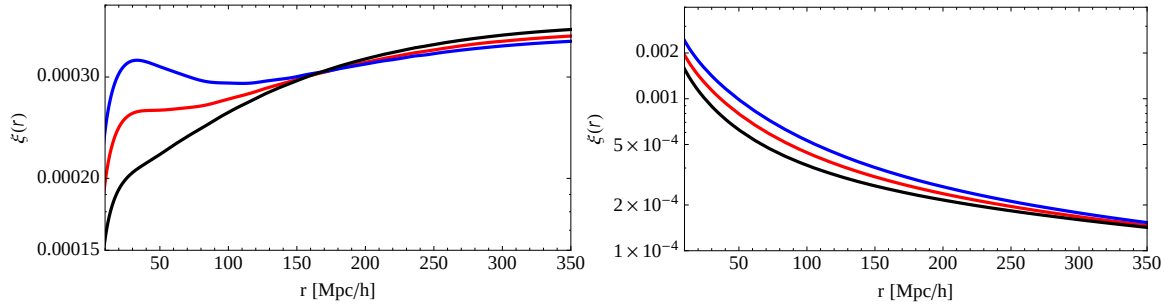


Figure 3.C.1: We show the full-sky non-linear density-lensing correlation function (left) and lensing-lensing correlation function (right) at $\bar{z} = 1$ as a function of separation, for $\mu = 1$. The black solid line shows the calculation with $z_* = 1$, the blue line with $z_* = 0$ and the red line with $z_* = 0.42$.

the linear growth rate. To choose $z_*$ we use the flat-sky non-linear result, that we calculate first without approximation and second with the same approximation as in the full-sky. We find that when $z_* = 0.42$ the approximate solution is in extremely good agreement with the correct solution. We use therefore the same $z_*$ to calculate the full-sky result, for which it is not possible to do an exact integration (see discussion in Section 3.2.2).

In fig. 3.C.1 we compare the non-linear full-sky lensing calculated with different values for $z_*$. In red we show the result for $z_* = 0.42$ (best fit from the flat-sky), and in black and blue we show the two extreme cases: $z_* = 1$ (black) and $z_* = 0$ (blue). We see that the lensing terms behave as expected: a smaller $z_*$ gives rise to a larger result, since in this case we overestimate the power spectrum along the line-of-sight. The curve $z_* = 0.42$ is well situated between the two extreme cases, as was the case in the flat-sky. This gives us confidence that the approximation works well also for the full-sky lensing.

## 3.D Direction dependent power spectra

In this appendix we prove a simple property of direction dependent power spectra which is often used. This result is of course not new but it is usually used without derivation and mainly in special cases. Here we prove it in full generality.

**Theorem** $\xi(\mathbf{r})$ *is a correlation function which depends on the orientation of* $\mathbf{r}$ *only via its scalar product with one fixed given direction* $\mathbf{n}$ *(e.g. the line of sight). Denoting the corresponding direction cosine by* $\mu$ *and expanding* $\xi$ *in Legendre polynomials, we have*

$$\xi(\mathbf{r}) = \sum_n \xi_n(r)\mathcal{P}_n(\mu)\,, \qquad \mu = \hat{\mathbf{r}}\cdot\mathbf{n}\,. \tag{3.90}$$

*In this situation the Fourier transform of* $\xi$*, the power spectrum, is of the form*

$$P(\mathbf{k}) \;=\; \sum_n p_n(k)\mathcal{P}_n(\nu)\,, \quad \nu = \hat{\mathbf{k}}\cdot\mathbf{n} \quad \textit{where} \tag{3.91}$$

$$p_n(k) = 4\pi i^n \int_0^\infty dr r^2 j_n(kr)\xi_n(r)\,, \quad \textit{and} \tag{3.92}$$

$$\xi_n(r) = \frac{(-i)^n}{2\pi^2}\int_0^\infty dk k^2 j_n(kr)p_n(k)\,. \tag{3.93}$$

**Proof** The Fourier transform of $\xi$ is defined as

$$P(\mathbf{k}) = \int d^3 r e^{i\mathbf{r}\cdot\mathbf{k}}\xi(\mathbf{r})\,. \tag{3.94}$$

We use that

$$e^{i\mathbf{r}\cdot\mathbf{k}} = \sum_\ell i^\ell(2\ell+1)j_\ell(kr)\mathcal{P}_\ell(\hat{\mathbf{k}}\cdot\hat{\mathbf{r}})$$

and

$$\mathcal{P}_\ell(\hat{\mathbf{k}}\cdot\hat{\mathbf{r}}) = \frac{4\pi}{2\ell+1}\sum_{m=-\ell}^{\ell} Y_{\ell m}(\hat{\mathbf{k}})Y^*_{\ell m}(\hat{\mathbf{r}}) = \frac{4\pi}{2\ell+1}\sum_{m=-\ell}^{\ell} Y_{\ell m}(\hat{\mathbf{r}})Y^*_{\ell m}(\hat{\mathbf{k}})\,.$$

Here $Y_{\ell m}$ are the spherical harmonics as given e.g. in [131]. Inserting these identities in (3.94) using the ansatz (3.90) for the correlation function, we obtain

$$P(\mathbf{k}) = \sum_{\ell m}\sum_{nm'}\frac{(4\pi)^2 i^\ell}{2\ell+1}\int d^3 r\xi_n(r)j_\ell(kr)Y_{\ell m}(\hat{\mathbf{k}})Y^*_{\ell m}(\hat{\mathbf{r}})Y_{nm'}(\hat{\mathbf{r}})Y^*_{nm'}(\mathbf{n})\,. \tag{3.95}$$

Using the orthogonality relation of spherical harmonics, the integration over directions gives

$$P(\mathbf{k}) = 4\pi\sum_n i^n\int_0^\infty dr r^2\xi_n(r)j_n(kr)\mathcal{P}_n(\nu)\,. \tag{3.96}$$

Identification of the expansion coefficients yields (3.92). Eq. (3.93) is obtained in the same way using the inverse Fourier transform,

$$\xi(\mathbf{r}) = \frac{1}{(2\pi)^3}\int d^3 k e^{-i\mathbf{k}\cdot\mathbf{r}}P(\mathbf{k})\,. \qquad \blacksquare$$

Clearly, if $\xi(\mathbf{r}) = \langle\Delta_g(\mathbf{x})\Delta_g(\mathbf{x}+\mathbf{r})\rangle$ is independent of $\mathbf{x}$ ($\Delta_g$ is statistically homogeneous), $\xi$ does not depend on the sign of $\mathbf{r}$ and in the sum above only $\xi_n$ with even $n$'s can contribute so that $P(\mathbf{k})$ is real.

Inserting the expressions for the $Q^{\rm AB}$ in (3.49) to obtain the correlation function, we realize that in the flat sky limit ($\mathbf{n}_1 \to \mathbf{n}_2$), all our terms $\xi^{AB}$ where the corresponding $Q^{AB}$ do not contain integrated terms, are actually of this form. This also shows that in this limit $\zeta^{01}+\zeta^{10}$ and $\zeta^{12}+\zeta^{21}$ must vanish since they contain $j_1(kr)$ and $j_3(kr)$ and would yield imaginary contributions to the power spectrum.

For wide angles $\mathbf{n}_1 \neq \mathbf{n}_2$ the correlation function depends on two directions. Furthermore, for large $\mathbf{r}$ it is not translation invariant as it depends on the redshift on our background light-cone at which $\mathbf{r}$ is placed. In this case, the Fourier transform of the correlation function is no longer simply given by the power spectrum of the fluctuations.

The theorem proven above has a simple but useful corollary which is sometimes called the *closure relation* of spherical Bessel functions [30]. Inserting the expression (3.92) into (3.93) and using that it holds for arbitrary functions $p_n(k)$, we find

$$\frac{2}{\pi}\int_0^\infty j_n(rk)j_n(rk')r^2dr = \delta(k-k')k^{-2}\,, \tag{3.97}$$

for positive $k$ and $k'$. Using

$$j_n(x) = \sqrt{\frac{\pi}{2x}}J_{n+1/2}(x)$$

we can convert (3.97) into an equation for ordinary Bessel functions $J_m$:

$$\int_0^\infty J_{n+1/2}(rk)J_{n+1/2}(rk')rdr = k^{-1}\delta(k-k')\,, \tag{3.98}$$

This identity also holds for $J_m$ with integer $m$, see [161], No 6.512-8.

## 3.E The flat sky approximation

To derive expression (3.73) we consider the observed galaxy density fluctuation in real space given in eq. (3.11). We neglect the integrated Sachs Wolfe term and the $\dot\Phi$ term in the first line; they are very small and relevant mainly on very large angular scales where the flat sky approximation breaks down. The remaining integrated term is then only the lensing term and the subdominant Shapiro time delay. Furthermore, we set $\Psi = \Phi$ which is a very good approximation in ΛCDM at late times. Denoting the power spectrum of the comoving density contrast $\delta_c$ at redshift $z = 0$ by $P_\delta$ and using the perturbed Einstein and continuity equations we find

$$\Phi = \Psi = -\frac{3}{2}\frac{\Omega_m H_0^2(1+z)D_1(z)}{k^2}\delta_c \tag{3.99}$$

$$V = -\frac{\mathcal{H}}{k}f(z)D_1(z)\delta_c\,, \tag{3.100}$$

where $f(z)$ is the growth rate as given in (4.3), $D_1(z)$ is the growth function such that $\delta_c(k,z) = D_1(z)\delta_c(k) \equiv D_1(z)\delta_c(k,0)$ and $\Omega_m$ is the matter density parameter today.

Neglecting first the integrated terms we can simply Fourier transform this expression from $\chi(z)\mathbf{n} \equiv \mathbf{x}$ to $\mathbf{k}$ and use that the power spectrum is the square of the Fourier transform amplitude. This yields

$$P_{n.i} = \left|A + B/(k\mathcal{H}) + C/(k\mathcal{H})^2\right|^2 P_\delta(k)\,, \tag{3.101}$$

where $A$, $B$ and $C$ are given in (3.70) and (3.72).

To derive the cross term of the non-integrated with the integrated terms, it is more useful to start with the correlation function. Let us denote $A + B/(k\mathcal{H}) + C/(k\mathcal{H})^2 = \alpha(k,\nu,z)$ and $\hat F(k,\nu,z) = \alpha(k,\nu,z)\delta_c(k)$ with Fourier transform $F(\mathbf{x},z)$ . Denoting

$$I(\chi(z)\mathbf{n},z) = \frac{2}{\chi(z)}\int_0^{\chi(z)} d\lambda\left[2 - \frac{\chi(z)-\lambda}{\lambda}\Delta_\Omega\right]\Phi\,, \tag{3.102}$$

we have

$$\begin{aligned}\xi_{\Delta\Delta}(\mathbf{r},z) &= \langle F(\chi_1\mathbf{n}_1,z_1)F(\chi_2\mathbf{n}_2,z_2)\rangle + \langle I(\chi_1\mathbf{n}_1,z_1)F(\chi_2\mathbf{n}_2,z_2)\rangle \\ &\quad +\langle F(\chi_1\mathbf{n}_1,z_1)I(\chi_2\mathbf{n}_2,z_2)\rangle + \langle I(\chi_1\mathbf{n}_1,z_1)I(\chi_2\mathbf{n}_2,z_2)\rangle\,,\end{aligned}$$

where $\chi_i = \chi(z_i)$ and $\mathbf{r} = \chi_2\mathbf{n}_2 - \chi_1\mathbf{n}_1$, $z = (z_1+z_2)/2$ and we assume both $\chi_i \gg r$ and the $z_i$ should not be very different. Using the relation between $\Phi$ and $\delta_c$, the contribution of the cross term to the correlation function is then given by

$$\begin{aligned}\xi_{IF}(\mathbf{r},z) = -\frac{3}{(2\pi)^3}\frac{\Omega_m H_0^2(2-5s(z))}{2\chi_1}\int\frac{d^3k}{k^2}P_\delta(k)e^{-i\mathbf{k}\mathbf{n}_2\chi_2}\alpha(k,\nu,z_2) \\ \times\int_0^{\chi_1}d\lambda\left[\lambda(\chi_1-\lambda)k_\perp^2+2\right]D_1(z(\lambda))(1+z(\lambda))e^{i\mathbf{k}\mathbf{n}_1\lambda}\,.\end{aligned}$$

In the spirit of the flat sky approximation we now set $\mathbf{n}_1 = \mathbf{n}_* + \Delta\mathbf{n}/2$ and $\mathbf{n}_2 = \mathbf{n}_* - \Delta\mathbf{n}/2$ assuming that $\Delta\mathbf{n}$ is very small. Splitting $\mathbf{r} = \mathbf{r}_\perp + \mathbf{n}_* r_\parallel$ with $\mathbf{r}_\perp = \chi(z)\Delta\mathbf{n}$ and $r_\parallel = r\cos\alpha_2$, see fig. 3.A.1, we then perform the $k$-integral in the direction parallel to $\mathbf{n}_*$, $dk_\parallel\exp(-ik_\parallel(\chi_2-\lambda))$. We neglect the slow dependence of the power spectrum on $k_\parallel$ and only consider the rapidly oscillating exponential which gives $2\pi\delta(\chi_2-\lambda)$. Hence the integral over $\lambda$ does not contribute if $\chi_2 > \chi_1$, otherwise it reduces to the integrand at $\chi_2$,

$$\begin{aligned}\xi_{IF}(\mathbf{r},z) = -\frac{3}{(2\pi)^2}\frac{\Omega_m H_0^2(2-5s(z))\Theta(\chi_1-\chi_2)}{2\chi_1}D_1(z_2)(1+z_2) \\ \times\int\frac{d^2k_\perp}{k_\perp^2}P_\delta(k_\perp)e^{-i\mathbf{k}_\perp\cdot\mathbf{r}_\perp}\alpha(k_\perp,0,z_2)\left[\chi_2(\chi_1-\chi_2)k_\perp^2+2\right]\,,\end{aligned} \tag{3.103}$$

where $\Theta$ is the Heaviside $\Theta$-function.

Using polar coordinates, $d^2\mathbf{k}_\perp = dk_\perp k_\perp d\varphi$ we can perform the $\varphi$ integration which yields a Bessel function, $2\pi J_0(k_\perp r_\perp) = 2\pi J_0(k_\perp r\sin\alpha_2)$. The term $\xi_{FI}(\mathbf{r},\bar{z})$ contributes in the same way with $z_1$ and $z_2$ exchanged. Setting $\chi_1-\chi_2 = r_\parallel = r\mu$ and neglecting the difference of $\chi_1$ and $\chi_2$ ($z_1$ and $z_2$) in all other places, we find for the sum of both mixed terms

$$\begin{aligned}\xi_{IF+FI}(\mathbf{r},z) = -\frac{3}{2\pi}\frac{\Omega_m H_0^2(2-5s(z))}{2\chi}D_1(z)(1+z) \\ \times\int\frac{dk_\perp}{k_\perp}P_\delta(k_\perp)J_0(k_\perp r\sqrt{1-\mu^2})\alpha(k_\perp,0,z)\left[\chi|\mu|rk_\perp^2+2\right]\,.\end{aligned} \tag{3.104}$$

Here we have also neglected the difference between $\cos\alpha_2$ and $\mu$. In the flat sky approximation all these angles are equal. (If we would want to be precise, actually in the case $z_1 \equiv z_2$, hence $\mu = 0$ the Shapiro time delay would obtain a factor 4, not 2, but we neglect this in the flat sky approximation.)

To obtain the Fourier transform of (3.104) which is the contribution n.i.-I to the power spectrum we first multiply the equation with $\int dk_\parallel\exp(-ik_\parallel r_\parallel)\delta(k_\parallel) = 1$. We then write the factor $|\chi_2-\chi_1| = |r_\parallel| = |\mu|r$ inside the integral,

$$\int dk_\parallel\exp(-ik_\parallel r_\parallel)|r_\parallel|\delta(k_\parallel) = |r_\parallel|$$

is the Fourier transform of

$$\delta^P(k_\parallel) \equiv \frac{1}{2\pi}\int dr_\parallel \exp(ik_\parallel r_\parallel)|r_\parallel|\,. \tag{3.105}$$

Note that without the absolute value $\delta^P$ would become $-i\delta'$. This distribution is purely imaginary while $\delta^P$ is real. However, like $\delta$ or $\delta'$ its support is on $k_\parallel = 0$, i.e. for a function $f$ which vanishes in a small neighborhood around $k_\parallel = 0$ we have $\delta^P \cdot f \equiv 0$.

Inserting (3.105), we can write the correlation function $\xi_{IF+FI}$ as the Fourier transform of

$$\begin{aligned} P_{\text{n.i.}-\text{I}}(\mathbf{k},z) = -3\pi\frac{\Omega_m H_0^2(2-5s(z))}{\chi}D_1(z)(1+z) \\ \times P_\delta(k_\perp)\alpha(k_\perp,0,z)\left[\delta^P(k_\parallel)+\frac{2}{k_\perp^2}\delta(k_\parallel)\right]. \end{aligned} \tag{3.106}$$

Note also that since $k_\parallel = 0$, in the flat sky limit, the integrated term is not correlated with redshift space distortions.

Let us finally compute the double integrated term,

$$\begin{aligned} \xi_{II}(\mathbf{r},z) = \frac{(3\Omega_m H_0^2(2-5s(z)))^2}{(2\pi)^3 4\chi^2}\int\frac{d^3k}{k^4}P_\delta(k)\int_0^{\chi_1}d\lambda\int_0^{\chi_2}d\lambda' \\ \times\left[\lambda(\chi_1-\lambda)k_\perp^2+2\right]\left[\lambda'(\chi_2-\lambda')k_\perp^2+2\right]D_1(z(\lambda))(1+z(\lambda)) \\ \times D_1(z(\lambda'))(1+z(\lambda'))e^{-i\mathbf{k}(\mathbf{n}_1\lambda-\mathbf{n}_2\lambda')}\,. \end{aligned} \tag{3.107}$$

Via the same procedure as above, the integration over $k_\parallel$ leads to $2\pi\delta(\lambda-\lambda')$ and we find

$$\begin{aligned} \xi_{II}(\mathbf{r},z) = \frac{(3\Omega_m H_0^2(2-5s(z)))^2}{(2\pi)^2 4\chi^2}\int\frac{d^2k_\perp}{k_\perp^4}P_\delta(k_\perp) \\ \times\int_0^{\chi}d\lambda\left[\lambda(\chi-\lambda)k_\perp^2+2\right]^2 D^2(z(\lambda))(1+z(\lambda))^2 e^{-i\mathbf{k}_\perp\mathbf{r}_\perp(\lambda/\chi))}\,. \end{aligned} \tag{3.108}$$

We now perform a change of variables, $\mathbf{k}_\perp \mapsto (\lambda/\chi)\mathbf{k}_\perp$. In terms of this new variable, the integral contribution to the correlation function becomes

$$\begin{aligned} \xi_{II}(\mathbf{r},z) = \frac{(3\Omega_m H_0^2(2-5s(z)))^2}{(2\pi)^2 4\chi^2}\int_0^{\chi}d\lambda\int\frac{d^2k_\perp}{k_\perp^4}P_\delta(k_\perp\chi/\lambda)e^{-i\mathbf{k}_\perp\mathbf{r}_\perp} \\ \times\left(\frac{\lambda}{\chi}\right)^2\left[\frac{(\chi-\lambda)\chi^2}{\lambda}k_\perp^2+2\right]^2 D^2(z(\lambda))(1+z(\lambda))^2\,. \end{aligned} \tag{3.109}$$

Again, performing the $\varphi$ integration we end up with

$$\begin{aligned} \xi_{II}(\mathbf{r},z) = \frac{(3\Omega_m H_0^2(2-5s(z)))^2}{8\pi\chi^2}\int_0^{\chi}d\lambda\int dk_\perp k_\perp P_\delta(k_\perp\chi/\lambda)J_0(k_\perp r\sqrt{1-\mu^2}) \\ \times\left(\frac{\lambda}{\chi}\right)^2\left[\frac{(\chi-\lambda)\chi^2}{\lambda}+\frac{2}{k_\perp^2}\right]^2 D^2(z(\lambda))(1+z(\lambda))^2\,. \end{aligned}$$

Inserting the same factor 1 as for the mixed term above, we can read off the flat sky power spectrum of the integrated contribution,

$$P_{II}(\mathbf{k},z) = \frac{\pi(3\Omega_m H_0^2(2-5s(z)))^2}{2\chi^2}\int_0^\chi d\lambda P_\delta(k\chi/\lambda)\delta(k_\parallel)\left(\frac{\lambda}{\chi}\right)^2 \times\left[\frac{(\chi-\lambda)\chi^2}{\lambda}+\frac{2}{k^2}\right]^2 D^2(z(\lambda))(1+z(\lambda))^2\,. \tag{3.110}$$

Adding (3.101, 3.106, 3.110) we obtain the result (3.73). For completeness, and since we use it for some of our results, we also write down the flat sky correlation function,

$$\begin{aligned}\xi_\Delta(\mathbf{r},z) = &\int dk_\perp k k_\perp P_\delta(k) J_0(k_\perp r\sqrt{1-\mu^2})\int_{-1}^1 d\nu|\alpha(k,\nu,z)|^2 e^{-ik\nu\mu r}\\ &-\frac{3\Omega_m H_0^2(2-5s(z))}{4\pi\chi}D_1(z)(1+z)\int\frac{dk_\perp}{k_\perp}P_\delta(k_\perp)J_0(k_\perp r\sqrt{1-\mu^2})\alpha(k_\perp,0,z)\left[\chi|\mu|rk_\perp^2+2\right]\\ &+\frac{(3\Omega_m H_0^2(2-5s(z)))^2}{8\pi\chi^2}\int_0^\chi d\lambda\int\frac{dk_\perp}{k_\perp^3}P_\delta(k_\perp\chi/\lambda)J_0(k_\perp r\sqrt{1-\mu^2})\\ &\times\left(\frac{\lambda}{\chi}\right)^2\left[\frac{(\chi-\lambda)\chi^2}{\lambda}k_\perp^2+2\right]^2 D^2(z(\lambda))(1+z(\lambda))^2\,.\end{aligned} \tag{3.111}$$

Since $\alpha$ only contains terms which are constant, linear or quadratic in $\nu$, the $\nu$-integration is easily performed analytically.

# CHAPTER 4

## Correlation function II: The COFFE code

**Based on:**

[295] V. Tansella, G. Jelic-Cizmek, C. Bonvin and R. Durrer "*COFFE: a code for the full-sky relativistic galaxy correlation function*"
**in publication**, [arXiv:1806.11090].

**Abstract.** In this chapter we continue our work on the 2pF presenting the public code COFFE (COrrelation Function Full-sky Estimator) available at `https://github.com/JCGoran/coffe`. The code computes the galaxy two-point correlation function and its multipoles in linear perturbation theory, including all relativistic and wide angle corrections, employing the results presented in chapter 3. COFFE also calculates the covariance matrix for two physically relevant estimators of the correlation function multipoles. We illustrate the usefulness of our code by a simple but relevant example: a forecast of the detectability of the lensing signal in the multipoles of the two-point function. In particular, we show that lensing should be detectable in the multipoles of the two-point function, with a signal-to-noise larger than 10, in future surveys like Euclid or the SKA.

## 4.1 Introduction

It is often argued, as we did in chapter 1, that cosmology has become a precision science thanks to the very accurate measurement of the Cosmic Microwave Background (CMB) temperature fluctuations and polarisation power spectra [6, 11]. It is now time for the observation of the galaxy distribution to contribute to this name. Measurements of the two-point correlation function (2pF) have been performed by different collaborations over the past years [197, 115, 17] and upcoming redshift surveys will probe the LSS of the universe at deeper redshift and

for larger volumes [20, 203, 216]. To correctly interpret and to profit maximally from the data that will soon be available we need robust theoretical predictions of the signal: this was the subject of the previous chapters. However, not only the signal has to be understood from a theoretical point of view, but it is necessary to find accurate and fast methods to compute it. For the CMB, we have at our disposal fast linear Boltzmann codes such as CAMB [207] and CLASS [66]. Recently, these codes have been extended to compute also the angular power spectrum of galaxy number counts, $C_\ell$, [98] and [125]. However, redshift surveys traditionally measure the 2pF and its multipoles (monopole, quadrupole and hexadecapole), rather than the $C_\ell$'s. In this chapter we present a public version of the code COFFE (COrrelation Function Full-sky Estimator) which computes the galaxy 2pF including all the relativistic projection effects and does not rely on the flat-sky approximation. The code builds on the results derived in the previous chapters to consider not only the density fluctuations and redshift-space distortions (RSD) but also several additional terms which we have already discussed: lensing, ordinary and integrated Sachs Wolfe effects, gravitational redshift, Doppler terms, and Shapiro time delay. These contributions arise in the expression of eq. (2.30) for the observed galaxy number counts $\Delta_g(\mathbf{n}, z)$ at redshift $z$ and direction $\mathbf{n}$ in the sky and of course they contribute also to the correlation function defined as in eq. (3.3)

$$\xi(\cos\theta, z_1, z_2) = \langle \Delta_g(z_1, \mathbf{n}_1)\Delta_g(z_2, \mathbf{n}_2)\rangle\,, \tag{4.1}$$

where $\cos\theta = \mathbf{n}_1 \cdot \mathbf{n}_2$. The brackets in eq. (4.1) are intended, from a theoretical point of view, as an ensemble average but if ergodicity holds (as it does for the case of a statistically homogeneous Gaussian random field), in observations, they can be replaced by a spatial average. The expression that is most commonly used in the literature for the 2pF is the Fourier transform of the Kaiser formula for the galaxy power spectrum [199]

$$P(\bar{z}, k, \nu)_{\,\mathrm{Kaiser}} = D_1^2(\bar{z})\left[b^2 + \frac{2bf}{3} + \frac{f^2}{5} + \left(\frac{4bf}{3} + \frac{4f^2}{7}\right)\mathcal{P}_2(\nu) + \frac{8f^2}{35}\mathcal{P}_4(\nu)\right]P(k)\,. \tag{4.2}$$

Here $\bar{z}$ is the mean redshift of the survey, $P(k)$ is the matter density power spectrum today, $D_1(\bar{z})$ is the growth factor normalised to 1 today, $\nu$ is the cosine of the angle between $\mathbf{k}$ and the line-of-sight direction (assumed fixed in the flat-sky limit), $\nu = \mathbf{n}\cdot\mathbf{k}$, and the $\mathcal{P}_\ell$ are the Legendre polynomials of degree $\ell$. We have also defined $b(\bar{z})$ as the galaxy bias which relates the galaxy density fluctuations to the matter perturbation in synchronous-comoving gauge: $\Delta^{\mathrm{den}} = b\cdot\delta_c$. Furthermore

$$f(\bar{z}) = -\frac{D_1'}{D_1}(1+\bar{z}) = \frac{d\ln D_1}{d\ln(a)}\,, \tag{4.3}$$

is the growth rate, where the prime denotes the derivative with respect to the redshift $\bar{z}$. Equation (4.2) relies on the flat-sky approximation and does not include all the projection effects we mentioned before. A simple way to write the 2pF in full generality is to use eq. (3.4):

$$\xi(\theta, z_1, z_2) = \frac{1}{4\pi}\sum_\ell (2\ell+1)C_\ell(z_1, z_2)\mathcal{P}_\ell(\cos\theta)\,, \tag{4.4}$$

where $C_\ell(z_1, z_2)$ is the number counts angular-redshift power spectrum introduced in [72, 99]. Even though fast and reliable codes such as CAMB and CLASS have been generalised

to calculate the number count angular power spectrum [125, 124], the use of eq. (4.4) to compute the 2pF is not advisable. As we anticipated in chapter 3 this approach has two relevant drawbacks:

- *Window function*: eq. (4.4) is essentially an inverse Fourier-Bessel transform. The sum over $\ell$ runs to infinity and we are forced to cut it at some $\ell_{\rm max}$. This is equivalent to introducing a top-hat window function $W_\ell$ in $\ell$-space which enforces $C_\ell = 0$ for $\ell > \ell_{\rm max}$. The inverse transform is then a convolution of $\xi$ with the inverse transform of $W_\ell$ (given usually in terms of spherical Bessel functions $j_\ell$): this introduces spurious oscillations in the result. A possible workaround is to introduce in the sum a decaying window function which ensures $(2\ell+1)C_\ell \simeq 0$ for $\ell \gtrsim \ell_{\rm max}$ but the result will then depend on the smoothing scale chosen.

- *Run time*: Typical values for $\ell_{\rm max}$ in order to reproduce the correct behaviour of $\xi$ are $\ell_{\rm max} > 3000$. This means that every point of the 2pF requires the computation of several thousands spectra $C_\ell$: CLASS is very fast but this quickly becomes unfeasible, especially when terms which require line-of-sight integrations are sought (i.e. lensing).

As argued in Ref. [294], this problems become especially relevant when we want to exploit the very high redshift resolution of spectroscopic surveys in a redshift bin $\Delta z$. For correlating only a small number of rather wide photometric redshift bins, the $C_\ell(z_1, z_2)$ probably remain the method of choice.

The code COFFE performs a direct calculation of the 2pF which does not need the angular power spectra $C_\ell(z_1, z_2)$. For the standard and one of the Doppler terms this has already been done in [90], with an implementation in the public code `AngPow` [89]. Here we extend this work to include lensing and all other relativistic effects in full sky. In particular, our code computes: 1) the 2pF as a function of redshift, separation and orientation, 2) the multipoles of the 2pF, which is the output directly delivered by redshift surveys, and 3) the covariance matrix, necessary e.g. to assess the detectability of lensing and relativistic effects and their information content. In the next section we summarise the theoretical results which allow for a direct calculation and we deal with the problem of Infra-Red (IR) divergence which afflicts some terms in the correlation function. In section 4.3 we illustrate the usefulness of our code through one simple example. In section 4.4 we present the code and in section 4.5 we conclude and discuss future implementation to expand its functionalities.

## 4.2 The relativistic full-sky correlation function

### 4.2.1 The formalism

In the spirit of having self-contained chapters in this thesis, we summarise in this section the results obtained in chapter 3. The reader familiar with the formalism can jump to section 4.2.2, taking however note of the change in notation we present here.

Let us start with the set up for computing the two-point correlation function. The 2pF is usually not regarded as a function of two redshifts and one angle as in eq. (4.1) but as a function of the separation between the two points $r$, the mean redshift $\bar{z}$ and the cosine

$\mu$ of the angle between the separation vector $\mathbf{r}$ and a line-of-sight (LOS) between the two directions of observation, determined by convention. There is not a unique way to define this angle. In the flat-sky limit common definitions coincide, but in full sky they lead to differences in the multipoles, which are potentially of the same order of magnitude as the relativistic effects. It is therefore crucial to clearly specify the chosen angle. It is common practice to split $\mathbf{r}$ into its parallel component $r_\parallel$ (i.e. parallel to the LOS) and transverse component $r_\perp$ (i.e. perpendicular to the LOS) so that $r = \sqrt{r_\parallel^2 + r_\perp^2}$. In the full-sky regime, where we take into account that the two points do not share the same LOS, we chose to define the parallel separation as the difference between the comoving distance of the two points

$$r_\parallel = \chi_2 - \chi_1 \,, \tag{4.5}$$

where $\chi_i = \chi(z_i)$. We also define $\mu$ in the usual way as $\mu = r_\parallel / r$, which reduces to the standard definition in the flat-sky limit. Assuming vanishing spatial curvature $\Omega_K = 0$ (as this first release of COFFE does) the separation between the two points is given by

$$r(\theta, z_1, z_2) = \sqrt{\chi_1^2 + \chi_2^2 - 2\chi_1\chi_2 \cos\theta} \,, \tag{4.6}$$

and $\cos\theta$ can be related to $r$, $\mu$ and $\bar{z}$ by

$$\cos\theta = \frac{2\bar{\chi}^2 - r^2 + \frac{1}{2}\mu^2 r^2}{2\bar{\chi}^2 - \frac{1}{2}\mu^2 r^2} \,, \tag{4.7}$$

where we have introduced[1] $\bar{\chi} = (\chi_1 + \chi_2)/2 \simeq \chi(\bar{z})$. We point out that when writing the correlation function $\xi(r, \mu, \bar{z})$ (considering physical distances) a cosmology must be assumed to convert the observed redshifts to $\chi_1$ and $\chi_2$, while $\xi(\theta, z_1, z_2)$ can be directly measured in observations. However the former approach allows us to compute the multipoles of the correlation function which are often useful to break the degeneracy between cosmological parameters [102, 103, 111, 179, 310, 101, 326]. One then has to be careful when estimating cosmological parameters, taking into account that the data $\xi(r, \mu, \bar{z})$ itself depends on them. This is usually done by introducing rescaling parameters in the correlation function, which are fitted at the same time as cosmological parameters, see e.g. [313].

Having clarified the setup, we can now turn to the computation of the 2pF. Including all the relativistic corrections, the galaxy number counts can be written as in eqs. (3.12)-(3.21):

$$\Delta_g(\mathbf{n}, z) = \Delta^{\rm den} + \Delta^{\rm rsd} + \Delta^{\rm len} + \Delta^{\rm d1} + \Delta^{\rm d2} + \Delta^{\rm g1} + \Delta^{\rm g2} + \Delta^{\rm g3} + \Delta^{\rm g4} + \Delta^{\rm g5} \,. \tag{4.8}$$

Let us go through the physical meaning of each term once more: the standard terms, i.e. the density fluctuations and the RSD term, denoted respectively by $\Delta^{\rm den}$ and $\Delta^{\rm rsd}$, are usually taken into account in galaxy clustering analyses. $\Delta^{\rm len}$ represents the lensing term. $\Delta^{\rm d1}$ is the Doppler contribution, $\Delta^{\rm d2}$ is a velocity term which comes from transforming the longitudinal gauge density into the comoving density. $\Delta^{\rm g1}, \Delta^{\rm g2}$ and $\Delta^{\rm g3}$ are relativistic effects, given by

[1] Note that $\bar{\chi}$ and $\chi(\bar{z})$ are not exactly the same but in what follows we neglect this difference which is of order $(\Delta z)^2/\mathcal{H}(\bar{z})$.

the gravitational potentials at the source. As such they are sometimes called 'Sachs-Wolfe' terms. $\Delta^{g4}$ denotes the so-called Shapiro time-delay contribution and $\Delta^{g5}$ is the integrated Sachs-Wolfe term. Redshift-space expressions for the contributions in eq. (4.8) can be found in eqs. (3.12)-(3.21), here we will only use the Fourier-Bessel transform of these terms given by eqs. (3.39)-(3.48):

$$\Delta_\ell^{\rm den} = b(z) S_D j_\ell(k\chi)\,, \tag{4.9}$$

$$\Delta_\ell^{\rm rsd} = \frac{k}{\mathcal{H}} S_V j_\ell''(k\chi)\,, \tag{4.10}$$

$$\Delta_\ell^{\rm len} = \left(\frac{2-5s}{2}\right)\frac{\ell(\ell+1)}{\chi}\int_0^\chi {\rm d}\lambda \frac{\chi-\lambda}{\lambda}(S_\phi + S_\psi) j_\ell(k\lambda)\,, \tag{4.11}$$

$$\Delta_\ell^{\rm d1} = \left(\frac{\dot{\mathcal{H}}}{\mathcal{H}^2} + \frac{2-5s}{\chi\mathcal{H}} + 5s - f_{\rm evo}\right) S_V j_\ell'(k\chi)\,, \tag{4.12}$$

$$\Delta_\ell^{\rm d2} = -(3 - f_{\rm evo})\frac{\mathcal{H}}{k} S_V j_\ell(k\chi)\,, \tag{4.13}$$

$$\Delta_\ell^{\rm g1} = \left(1 + \frac{\dot{\mathcal{H}}}{\mathcal{H}^2} + \frac{2-5s}{\chi\mathcal{H}} + 5s - f_{\rm evo}\right) S_\psi j_\ell(k\chi)\,, \tag{4.14}$$

$$\Delta_\ell^{\rm g2} = (-2 + 5s) S_\phi j_\ell(k\chi)\,, \tag{4.15}$$

$$\Delta_\ell^{\rm g3} = \frac{1}{\mathcal{H}} \dot{S}_\phi j_\ell(k\chi)\,, \tag{4.16}$$

$$\Delta_\ell^{\rm g4} = \frac{2-5s}{\chi}\int_0^\chi {\rm d}\lambda (S_\phi + S_\psi) j_\ell(k\lambda)\,, \tag{4.17}$$

$$\Delta_\ell^{\rm g5} = \left(\frac{\dot{\mathcal{H}}}{\mathcal{H}^2} + \frac{2-5s}{\chi\mathcal{H}} + 5s - f_{\rm evo}\right)\int_0^\chi {\rm d}\lambda (\dot{S}_\phi + \dot{S}_\psi) j_\ell(k\lambda)\,. \tag{4.18}$$

We define the matter transfer function $S_D$, which relates the primordial power spectrum $\mathcal{P}_\zeta(k) = A_s(k/k_*)^{n_s-1}$ to the matter power spectrum at redshifts $z_1$ and $z_2$, via

$$\mathcal{P}_\zeta(k) S_D(k,z_1) S_D(k,z_2) = \frac{k^3}{2\pi^2} D_1(z_1) D_1(z_2) P(k)|_{z=0} = \frac{k^3}{2\pi^2} P(k,z_1,z_2)\,. \tag{4.19}$$

In standard ΛCDM, the velocity and potentials transfer functions are related to $S_D$ through

$$S_V = -(\mathcal{H}f)/k\, S_D\,, \tag{4.20}$$

$$S_\Phi = S_\Psi = -\frac{3\Omega_m}{2a}\left(\frac{\mathcal{H}_0}{k}\right)^2 S_D\,, \tag{4.21}$$

$$S_{\dot\Phi} = S_{\dot\Psi} = -\frac{3\Omega_m}{2a}\left(\frac{\mathcal{H}_0}{k}\right)^2 (\dot{S}_D - \mathcal{H} S_D)\,. \tag{4.22}$$

Furthermore $s$ denotes the magnification bias and $f_{\rm evo}$ is the evolution bias.

The basic idea upon which the direct calculation is performed is based on eq. (4.4) and the explicit expression for the contributions of the correlation of the terms $A$ and $B$ in the angular power spectrum

$$C_\ell^{AB}(z_1,z_2) = 4\pi\int \frac{dk}{k}\mathcal{P}_\mathcal{R}(k)\Delta_\ell^A(k,z_1)\Delta_\ell^B(k,z_2)\,, \tag{4.23}$$

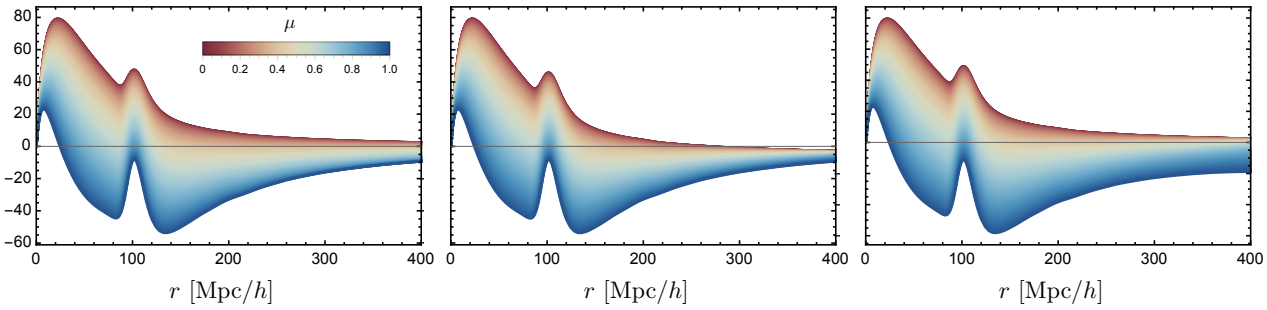


Figure 4.1: A possible output of the COFFE code. The correlation function $r^2\xi(r,\mu)$ is plotted at $\bar{z} = 0.1$ for different values of $\mu$ (color coded): the *left* panel is the flat-sky result of eq. (4.32), the *middle* panel the full-sky result considering only density and redshift-space distortion, while the *right* panel also considers the "d1" doppler term (the most relevant relativistic contribution at low redshift). Note that the full sky result for the standard terms is negative at large distances while the flat sky result can be positive depending on the orientation $\mu$. Including the relativistic terms (in this case only d1 contributes visibly), the correlation function becomes again positive for almost transverse orientations. For large $\mu$ and large $r$ it is significantly more negative than the standard flat sky result.

where we set schematically $\{A, B\} \in \{\text{den}, \text{rsd}, ..., \text{g5}\}$. Combining eqs. (4.4) and (4.23) we can exchange the sum over $\ell$ and the integral over the wavenumber: we then need to evaluate sums of the form

$$\sum_\ell (2\ell+1)\Delta_\ell^A(k,z_1)\Delta_\ell^B(k,z_2)\mathcal{P}_\ell(\cos\theta)\,. \tag{4.24}$$

The $\Delta_\ell^A$ depend on $\ell$ only via a spherical Bessel function or derivatives of it and hence we can perform the infinite sum over $\ell$ analytically, leading to simple functions of $\theta$, $z_1$, $z_2$ multiplying $j_L(kr)$ with $L \in \{0,1,2,3,4\}$. We refer the interested reader to section 2.2 of [294] for details of this calculation. Here we report the results with a somewhat different notation w.r.t. chapter 3, to present the expressions in a way which is closer to what is implemented in COFFE. It is useful to split the discussion between non-integrated terms $\{\text{den}, \text{rsd}, \text{d1}, \text{d2}, \text{g1}, \text{g2}, \text{g3}\}$ and integrated terms $\{\text{len}, \text{g4}, \text{g5}\}$, which require a LOS integration.

For the non-integrated terms we define[2]

$$\xi^{AB}(\theta,\chi_1,\chi_2) = D_1(\chi_1)D_1(\chi_2)\sum_{\ell,n}\left(X_\ell^n\big|_A + X_\ell^n\big|_{AB} + X_\ell^n\big|_{BA} + X_\ell^n\big|_B\right)I_\ell^n(r)\,, \tag{4.25}$$

where the $X_\ell^n\big|_{AB} = X_\ell^n(\theta,\chi_1,\chi_2)\big|_{AB}$, $\{A,B\} = \{\text{den}, \text{rsd}, \text{d1}, \text{d2}, \text{g1}, \text{g2}, \text{g3}\}$ are listed in Appendix 4.B. Note that a single tag means autocorrelation: $X_\ell^n\big|_A \equiv X_\ell^n\big|_{AA}$. The sum is intended

[2]Note that since we have assumed a cosmological model we write $\xi(\theta,\chi_1,\chi_2) = \xi(\theta,z_1,z_2) = \xi(r,\mu,\bar{z}) = \xi(r,\mu,\bar{\chi})$ with no distinction. In fact we can use $\chi_i = \chi(z_i)$, $\mu = (\chi_2-\chi_1)/r$ and eqs. (4.6),(4.7) to switch between the different variables in which we express the correlation function. We neglect the difference between $\bar{\chi}$ and $\chi(\bar{z})$.

over all the values of $\ell, n \in \{0,1,2,3,4\}$ for which the coefficients (given in the appendix) are non-zero. Note that the symmetry of the 2pF implies

$$X_\ell^n\big|_{AB}(\theta,\chi_1,\chi_2) = X_\ell^n\big|_{BA}(\theta,\chi_2,\chi_1)\,, \tag{4.26}$$

and we have defined[3]

$$I_\ell^n(r) = \int \frac{dk\,k^2}{2\pi^2}\,P(k)\,\frac{j_\ell(kr)}{(kr)^n}\,. \tag{4.27}$$

The use of this notation is justified in two ways: firstly it is now clear that the integrals $I_\ell^n(r)$ need to be computed only once for every separation, independently of the orientation (i.e. $\mu$). This fact was somewhat hidden in the notation of chapter 3 and we make it explicit here. Secondly we have isolated the integrals $I_\ell^n(r)$: a fast and accurate computation of these integrals is crucial for the precision of the 2pF. We have implemented the 2-FAST [162] algorithm in C and included it in our code[4]. In eq. (4.25), $\xi^{AB}$ means $\xi^{AB} = \langle (A+B)(A+B)\rangle$ and in general we define

$$\xi^{ABCD...} = \langle (A+B+C+D+...)(A+B+C+D+...)\rangle\,, \tag{4.28}$$

where in this case the sum in eq. (4.25) is done over all possible combinations.

For the integrated terms we define

$$\xi^{AB}(\theta,\chi_1,\chi_2) = \left(Z\big|_A + Z\big|_{AB} + Z\big|_{BA} + Z\big|_B\right), \tag{4.29}$$

where $Z = Z(\theta,\chi_1,\chi_2)$, $\{A,B\} = \{\mathrm{den},\mathrm{rsd},...,\mathrm{len},\mathrm{g4},\mathrm{g5}\}$ and a single tag means autocorrelation. We again have

$$Z\big|_{AB}(\theta,\chi_1,\chi_2) = Z\big|_{BA}(\theta,\chi_2,\chi_1)\,, \tag{4.30}$$

and the full list is given in Appendix 4.B. Examples of the correlation function are shown in fig. 4.1.

For completeness we also give the definition of the multipoles of the correlation function:

$$\xi_\ell(z,r) \equiv \frac{2\ell+1}{2}\int_{-1}^{1} d\mu\,\xi(z,r,\mu)\mathcal{P}_\ell(\mu)\,, \tag{4.31}$$

and we remind the reader that in the flat-sky approximation, redshift-space distortions are included by Fourier transforming eq. (4.2), which simply yields eq. (3.9):

$$\xi(\bar{z},r,\mu)_{\text{flat-sky}} = D_1^2(\bar{z})\Big[c_0(\bar{z})I_0^0(r) - c_2(\bar{z})I_2^0(r)\mathcal{P}_2(\mu) + c_4(\bar{z})I_4^0(r)\mathcal{P}_4(\mu)\Big], \tag{4.32}$$

[3] It is now clear that the superscript 0 in eq. (3.10) is to uniform the notation.

[4] The original, publicly available, 2-FAST code (`https://github.com/hsgg/twoFAST`) is implemented in the high-level language **julia**.

with

$$c_0 = b^2 + \frac{2}{3}bf + \frac{f^2}{5}\,, \tag{4.33}$$

$$c_2 = \frac{4}{3}bf + \frac{4}{7}f^2\,, \tag{4.34}$$

$$c_4 = \frac{8}{35}f^2\,. \tag{4.35}$$

### 4.2.2 IR divergence

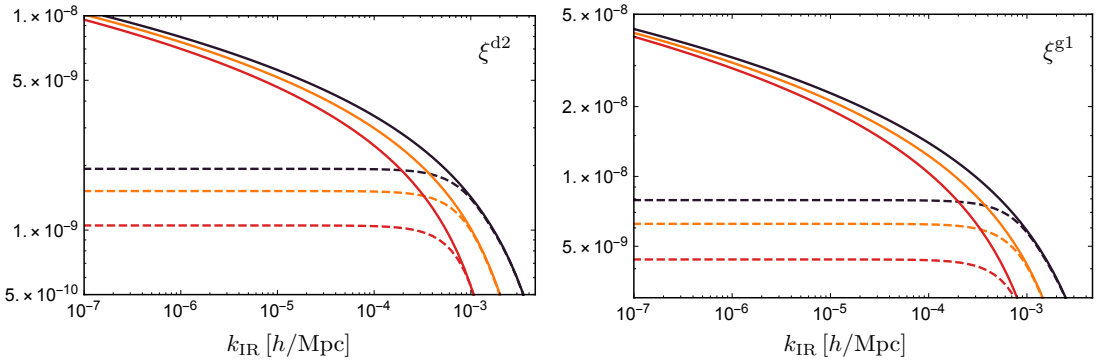


Figure 4.2: The divergent (*solid*) and convergent (*dashed*) correlation function for two potential terms as a function of the IR cut-off $k_{\rm IR}$. It is shown how eq. (4.40) regularise the Infra-Red behaviour of the correlation function. Different colours are different choices of $(r, \mu)$.

We now turn to a problem which afflicts the 2pF contributions coming from the auto-correlation and cross-correlation of potentials terms, namely $\xi^{AB}$ with $\{A, B\} = \{\mathrm{d2}, .., \mathrm{g5}\}$. The issue is essentially that the integral $I_0^4$ has an Infra-Red divergence. It is in fact known that the variance of the curvature has an IR divergence [34, 157, 52, 60]:

$$\langle\zeta^2(x)\rangle = \int_{k_{\rm IR}}^{\infty}\frac{dk}{k}\mathcal{P}_\zeta(k) \sim \left(\frac{k_{\rm IR}}{k_*}\right)^{n_s-1} \xrightarrow{k_{\rm IR}\to 0} \infty \quad \text{for } n_s \leq 1\,. \tag{4.36}$$

This is a problem for the integral $I_0^4$. Recall that $\Phi_k \sim \zeta_k S_\Phi(k) \sim k^{-2}\zeta_k S_D(k)$ which, with the large scale behavior $S_\Phi(k) \to 1$, gives $S_D(k) \sim k^2$ for $k \to 0$. This implies

$$I_0^4(r) = \int \frac{dk\,k^2}{2\pi^2}\,P(k)\,\frac{j_0(kr)}{(kr)^4} \sim \int \frac{dk}{k^5}S_D(k)^2\mathcal{P}_\zeta(k) \sim \int \frac{dk}{k}\mathcal{P}_\zeta(k) \to \infty\,. \tag{4.37}$$

This means that the auto- and cross-correlations of potential terms (d2,..,g5) grow indefinitely as $k_{\rm IR} \to 0$ (as they all depend on $I_0^4$, see appendix 4.B). It is clear that this is an unphysical divergence as $\Delta_g(\mathbf{n}, z)$ and its 2pF, $\xi(\theta, z_1, z_2)$, are observables and they can therefore not diverge.

To understand why the divergence in (4.36) does not contribute to the observable, let us go back to the definition of $\Delta_g(\mathbf{n}, z)$:

$$\Delta_g(\mathbf{n}, z) = \frac{N(\mathbf{n}, z) - \langle N\rangle_\Omega(z)}{\langle N\rangle_\Omega(z)}\,, \tag{4.38}$$

where $N(\mathbf{n}, z)$ is the number of galaxies in direction $\mathbf{n}$ at redshift $z$ and $\langle N\rangle_\Omega(z)$ is the directional average of $N(\mathbf{n}, z)$:

$$\langle N\rangle_\Omega(z) = \frac{1}{4\pi}\int d\Omega_{\mathbf{n}}\, N(\mathbf{n}, z)\,. \tag{4.39}$$

It is clear from eq. (4.38) that $\langle\Delta_g\rangle_\Omega = 0$. This simply reflects the fact that $\Delta_g$ is the departure from the average number of galaxies. Since in linear perturbation theory directional average and ensemble average commute [71], we also have $\langle\xi(\theta, z_1, z_2)\rangle_\Omega = 0$, meaning that the correlation function does not have a monopole contribution. Physically this comes from the fact that an observer will include into $\langle N\rangle_\Omega$ not only the background but also all the IR modes which he *cannot* distinguish from the background. This includes super-horizon modes as well as terms at the observer, which we have neglected in this chapter specifically for this reason. All these modes contribute only to the monopole[5] and as they are included in the directional average they are subtracted in eq. (4.38), leading to $C_0 = 0$. If we apply these considerations to eq. (4.4) we see that we are able to cure the divergence by explicitly removing the monopole

$$\xi_g \longrightarrow \xi_g - C_0/4\pi\,. \tag{4.40}$$

In principle this line of reasoning could be applied to all the contributions to the 2pF, however we only regularise in this way the contributions for which the monopole $C_0$ is divergent (auto- and cross-correlations of potential terms (d2,..,g5)). For the other terms this correction is negligible. Equation (4.40) can be easily implemented in the code as it amounts to a redefinition of $I_0^4(r)$:

$$I_0^4(r) \longrightarrow \frac{1}{r^4}\int \frac{dk}{2\pi^2}k^{-2}P(k)\Big(j_0(kr) - j_0(k\chi_1)j_0(k\chi_2)\Big)\,. \tag{4.41}$$

The result of this procedure is shown in figures 4.2 and 4.3.

We point out that from a theoretical point of view the regularisation of the divergence can be achieved by consistently keeping track of the terms at the observer [60, 59]. The resulting 2pF will be gauge invariant, consistent with the equivalence principle[6] and free of divergences. However to achieve this result one has to ensemble average over different realisations of the

[5]The peculiar velocity at the observer also induces a dipole contribution [321], which is irrelevant for this regularisation discussion.

[6]Inconsistency with the equivalence principle can be regarded as the reason for which the divergence arises: a term like $\Delta^{g2}$, for example, is given by the value of the gravitational potential at the source $\Phi_s$. This is not observable, while considering a counter term at the observer $\Phi_s - \Phi_o$ does not only agree with the equivalence principle but it also regularises the divergence.

perturbation fields at the observer. As we will explain in chapter 7, this procedure leads to a result which is not linked with the observable correlation function: although the ergodic hypothesis can be applied on fields at the observer position, their contribution is relegated to the monopole for which the ergodic approximation fails.

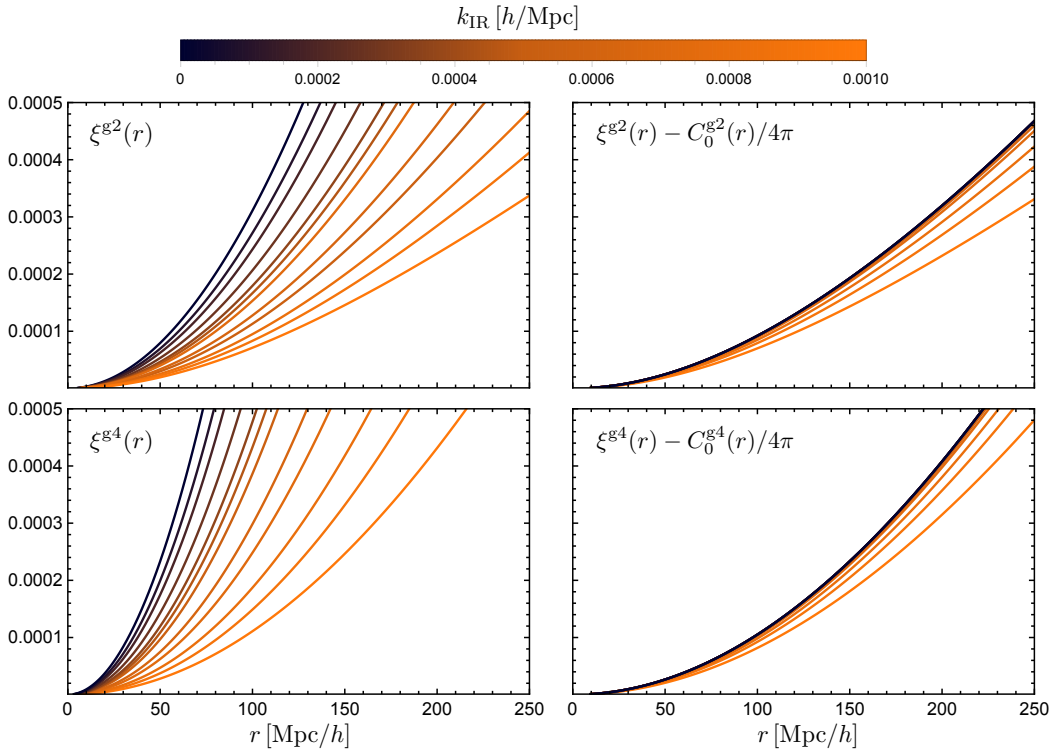


Figure 4.3: *Left*: the divergent correlation function for two potential terms as a function of separation $r$ for different values of the IR cut-off. *Right*: subtracting the unobservable monopole the correlation function converges for "reasonable" values of $k_{\rm IR} \lesssim 10^{-4}$.

### 4.2.3 Estimators and the covariance matrix

The correlation function can be estimated in several ways from a given galaxy catalog. In this section we present the two estimators for the multipoles of the 2pF that we consider in COFFE and we compute their covariance matrix. We start by splitting a catalog covering a fraction of the sky $f_{\rm sky}$ and a redshift interval $(\bar{z} - \delta z, \bar{z} + \delta z)$, amounting to a total volume $V$, into pixels of comoving size $L_p$. We then count the number of galaxies $N_i$ in each pixel $i$ at redshift $z_i$ in the sky and we define $\Delta_i \equiv \Delta_g(\mathbf{x}_i)$ as in eq. (4.38):

$$\Delta_i = \frac{N_i - \langle N \rangle_\Omega(z_i)}{\langle N \rangle_\Omega(z_i)}\,, \tag{4.42}$$

where the directional average $\langle N\rangle_\Omega$ is performed over all the pixels at redshift $z_i$. The simplest estimator we can construct for the multipoles is then

$$\hat{\xi}_\ell(r,\bar{z}) = \beta_\ell \sum_{ij} \Delta_i\Delta_j \mathcal{P}_\ell(\mu_{ij})\delta_K(r_{ij}-r)\,, \tag{4.43}$$

where $r_{ij} = |\mathbf{x}_i - \mathbf{x}_j|$ is the distance between the two pixels and $\mu_{ij} = r_\parallel/r = (\chi(z_1)-\chi(z_2))/r$ represents the orientation of the pixels. The function $\delta_K$ denotes the (dimensionless) Kronecker delta representing the fact that in a binned catalog the values $r_{ij}$ are discrete. The normalisation factor $\beta_\ell$ is obtained by imposing that in the continuum limit the ensemble average of the estimator satisfies $\langle\hat{\xi}_\ell\rangle = \xi_\ell$. One finds (more details are given in appendix 4.A)

$$\beta_\ell = \frac{2\ell+1}{4\pi}\frac{L_p^5}{r^2 V}\,. \tag{4.44}$$

Equation (4.43) is the estimator which is usually used in redshift surveys[7]. However to obtain this result we have made one important approximation, which is to neglect time-evolution in our redshift shell. We have indeed assumed that all pairs of pixels $(i,j)$ in eq. (4.43) have the same mean redshift $\bar{z}$. It is only under this assumptions that the estimator (4.43) is unbiased, i.e. that $\langle\hat{\xi}_\ell\rangle = \xi_\ell$. In practice however, we know that the galaxy distribution evolves with redshift, so that each pair of pixels $(i,j)$ contributes in a slightly different way to the sum. This is especially relevant when computing the multipoles of the correlation function at large separation $r$, for which thick redshift bins must be used[8]. In this case, the mean of (4.43) can be different from the theoretical predictions $\xi_\ell$ and the estimator is therefore biased. For this reason we propose a second estimator, which distinguishes between different mean redshifts $z_{ij} = (z_i+z_j)/2$ inside the redshift bin, and which is therefore unbiased also in the full sky regime

$$\hat{\Xi}_\ell(r,\bar{z},\delta z) = \gamma_\ell \sum_{\{z_k\}} W(z_k) \sum_{i,j} \frac{1+\cos\theta_{ij}}{2r_j^2}\Delta_i\Delta_j\,\mathcal{P}_\ell(\mu_{ij})\,\delta_K(r_{ij}-r)\delta_K(z_{ij}-z_k)\,, \tag{4.45}$$

which sums all the pairs at fixed separation $r$ and at fixed mean redshift $z_k$ and then sums over all the different redshifts in the bin $\{z_k\}$ so that no pair in the catalog is lost. Here $\theta_{ij}$ is the angle between $\mathbf{x}_i$ and $\mathbf{x}_j$ (note that this is not $\mu_{ij} = 2(|\mathbf{x}_i|-|\mathbf{x}_j|)/(|\mathbf{x}_i|+|\mathbf{x}_j|)$. The expectation value of this new estimator is the quantity $\Xi_\ell$ (which we can compute with COFFE) defined as

$$\Xi_\ell(r,\bar{z},\delta z) = \mathcal{H}_0 \int_{\bar{z}-\delta z}^{\bar{z}+\delta z} dz\,\frac{W(z)}{\mathcal{H}(z)(1+z)}\xi_\ell(r,z)\,. \tag{4.46}$$

Here $W(z)$ denotes the redshift distribution (normalised to unity) and the normalisation factor $\gamma_\ell$ has to be chosen as

$$\gamma_\ell = \frac{2\ell+1}{(4\pi)^2}\frac{L_p^5\mathcal{H}_0}{r^2 f_{\rm sky}}\,. \tag{4.47}$$

[7]Note that in practice the Landy-Szalay estimator [202] is used, in order to account for the geometry of the surveys and for irregularities in the galaxy distribution.

[8]In order to measure the multipoles at large separation $r$, we need indeed a redshift bin thicker than $r$ in order to include pairs with all orientations in the average over $\mu$.

Details of the derivation of this result are given in appendix 4.A, where we show that $\hat{\Xi}_\ell$ is an unbiased estimator of $\Xi_\ell$ at all separations. Note that the non-trivial factor

$$\frac{1+\cos\theta_{ij}}{2r_j^2}\,, \tag{4.48}$$

that we have introduced in eq. (4.45) is necessary to find eq. (4.46). It accounts for the geometry of the average over pairs in the full-sky regime. It can be expanded as

$$\frac{1+\cos\theta_{ij}}{2r_j^2} \simeq \frac{1}{\bar{\chi}^2}\left(1 \pm \mu\frac{r}{\bar{\chi}} + O\left(\frac{r}{\bar{\chi}}\right)^2\right), \tag{4.49}$$

and it reduces to $1/\bar{\chi}^2$ in the flat-sky approximation.

Let us finally address one important subtlety in the definition of eq. (4.46). Equation (4.46) is a weighted average of $\xi_\ell(r,z)$, with $z$ running over the size of the redshift bin, i.e. from $z(\chi_1) = \bar{z}-\delta z$ to $z(\chi_2) = \bar{z}+\delta z$. In practice however, the mean redshift of the pair of galaxies $z$ cannot take all the values between $z(\chi_1)$ and $z(\chi_2)$. The calculation of the multipoles defined in eq. (4.31) contains indeed a sum over all orientations $\mu$. However, for a given separation $r$ and orientation $\mu$ not all values of $z$ are permitted. More precisely, the allowed values are $z \in [z(\chi_1 + r/2), z(\chi_2 - r/2)]$. If we want to take care of this subtlety theoretically, we have to make the limits of integration and the redshift distribution $W(z)$ in eq. (4.46) $r$-dependent. For a simple top-hat distribution, COFFE computes

$$\Xi_\ell(r,z_1,z_2) = \frac{\mathcal{H}_0}{z_2(r)-z_1(r)}\int_{z_1(r)}^{z_2(r)} dz\,\frac{\xi_\ell(r,z)}{\mathcal{H}(z)(1+z)}\,, \tag{4.50}$$

where $z_1(r) = z(\chi_1 + r/2)$ and $z_2(r) = z(\chi_2 - r/2)$.

We can now compare our two estimators. In figure 4.4 we show the fractional difference, at $\bar{z} = 1$, between the mean of the two estimators: $\xi_\ell(r)$ and $\Xi_\ell(r,\delta z)$ for different values of the half-width of the bin $\delta z$. The main difference between the two estimators is a different normalisation: this is because the $\xi_\ell$ are computed exactly at $\bar{z} = 1$, while the $\Xi_\ell$ are averaged over the redshift bin. The wider the bin, the larger is the deviation from the multipole at the mean redshift. The second difference is more fundamental since it is directly due to the evolution of the galaxy number counts with redshift. This effect is slightly scale-dependent and it can be isolated in the following way: let us define a flat-sky $\Xi_\ell$ starting from the flat-sky $\xi_\ell$. In this case, as evolution is neglected in the flat-sky limit, the only difference between the two estimators would be due to their different normalisation. In particular, in the flat-sky limit we can separate the $z$- and $r$-dependence of the multipoles, as in eq. (4.32), to obtain

$$\Xi_\ell(\bar{z})_{\text{flat-sky}} = \left(\frac{\mathcal{H}_0}{2\delta z}\frac{1}{c_\ell(\bar{z})D_1^2(\bar{z})}\int_{\bar{z}-\delta z}^{\bar{z}+\delta z} dz\,\frac{c_\ell(z)D_1^2(z)}{\mathcal{H}(z)(1+z)}\right)\xi_\ell(\bar{z})_{\text{flat-sky}}\,, \tag{4.51}$$

where the $c_\ell$'s are defined in eqs. (4.33)-(4.35). In the full-sky regime, at large separations, we expect a deviation from this simple behaviour. In figure 4.4 we therefore normalise the

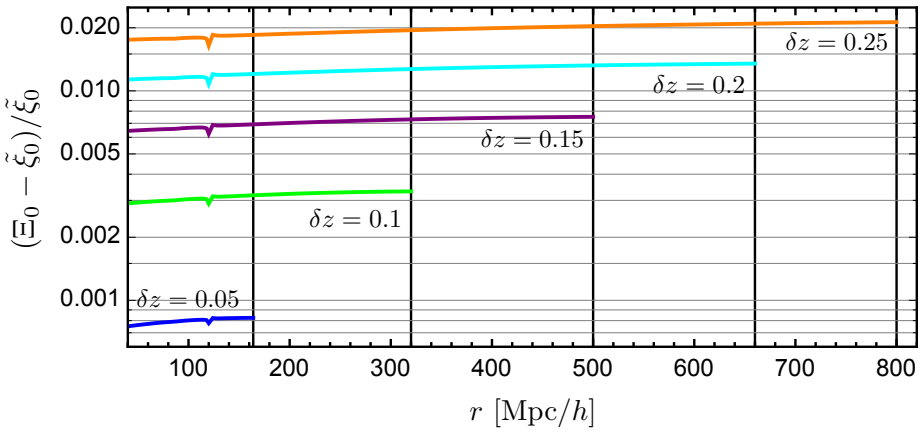


Figure 4.4: The fractional difference $(\Xi_\ell(r) - \tilde{\xi}_\ell(r))/\tilde{\xi}_\ell(r)$ for the monopole $\ell = 0$ at redshift $\bar{z} = 1$. The $\Xi_\ell$ are computed in redshift bins with different half-widths $\delta z$. The monopole at $\bar{z}$ can only be calculated out to $r \sim 2\delta z/H(z)$. The 'glitch' at $r \simeq 120\,\mathrm{Mpc}/h$ comes from the monopole going through zero. The result for $\ell = 2, 4$ is similar.

multipoles $\xi_\ell$ with

$$\tilde{\xi}_\ell \equiv \left( \frac{\mathcal{H}_0}{2\delta z} \int_{\bar{z}-\delta z}^{\bar{z}+\delta z} dz \, \frac{1}{\mathcal{H}(z)(1+z)} \right) \xi_\ell \,. \tag{4.52}$$

In this way, we get rid of the difference due to the normalisation and we show only the intrinsic difference due to evolution. Overall the difference between the estimators is small, but it can be substantial (of order 1%) if a thick redshift bin is considered. Finally, let us emphasise again that whereas $\Xi_\ell$ is an unbiased estimator of $\hat{\Xi}_\ell$ at all separations, $\xi_\ell$ is biased at large separations due to evolution. The order of magnitude of this bias is related to the difference plotted in figure 4.4. For very thick redshift bins, $\xi_\ell$ is therefore not a reliable estimator of the multipoles and $\Xi_\ell$ should be used instead.

We can now compute the covariance matrix for the two estimators:

$$\mathrm{cov}^{(\xi)}_{\ell\ell'}(r, r') \equiv \left\langle \hat{\xi}_\ell(r) \hat{\xi}_{\ell'}(r') \right\rangle - \left\langle \hat{\xi}_\ell(r) \right\rangle \left\langle \hat{\xi}_{\ell'}(r') \right\rangle , \tag{4.53}$$

$$\mathrm{cov}^{(\Xi)}_{\ell\ell'}(r, r') \equiv \left\langle \hat{\Xi}_\ell(r) \hat{\Xi}_{\ell'}(r') \right\rangle - \left\langle \hat{\Xi}_\ell(r) \right\rangle \left\langle \hat{\Xi}_{\ell'}(r') \right\rangle . \tag{4.54}$$

The variance of the number counts has two contributions

$$\langle \Delta_i \Delta_j \rangle = \frac{1}{d\bar{N}} \delta_{ij} + C_{ij} \,. \tag{4.55}$$

The first term accounts for shot noise, where $d\bar{N}$ is the average number of tracers per pixel. It comes from the fact that we Poisson sample from the underlying smooth density distribution. Shot noise contributes only to the correlation function at zero separation, i.e. when $i = j$. The second term is the cosmic variance contribution. For simplicity we perform the covariance

calculation in the flat-sky approximation (which means we stop at the $0^{\text{th}}$-order term in eq. (4.49)) and we consider only the density and redshift-space distortion contributions. Since this is by far the dominant term, it is a good approximation to the full result. Assuming Gaussianity (i.e. we write 4-point functions as products of 2-point functions), we can express the covariance matrix in terms of Wigner's 3j-symbols as

$$\begin{aligned}\mathrm{cov}^{(\xi)}_{\ell\ell'}(r_i,r_j) = \frac{i^{\ell-\ell'}}{V}\Bigg[&\frac{2\ell+1}{2\pi\bar{n}^2L_p r^2}\delta_{ij}\delta_{\ell\ell'} + \frac{1}{\bar{n}}\mathcal{G}_{\ell\ell'}(r_i,r_j,\bar{z})\sum_\sigma c_\sigma\begin{pmatrix}\ell & \ell' & \sigma\\ 0 & 0 & 0\end{pmatrix}^2\\ &+\mathcal{D}_{\ell\ell'}(r_i,r_j,\bar{z})\sum_\sigma \tilde{c}_\sigma\begin{pmatrix}\ell & \ell' & \sigma\\ 0 & 0 & 0\end{pmatrix}^2\Bigg],\end{aligned} \tag{4.56}$$

$$\begin{aligned}\mathrm{cov}^{(\Xi)}_{\ell\ell'}(r_i,r_j) = \frac{i^{\ell-\ell'}}{4\pi f_{\rm sky}}\int_{\bar{z}-\delta z}^{\bar{z}+\delta z}dz\,\frac{W^2(z)}{\mathcal{H}(z)\chi^2(z)(1+z)}\Bigg[&\frac{2\ell+1}{2\pi\bar{n}^2L_p r^2}\delta_{ij}\delta_{\ell\ell'}\\ &+\frac{1}{\bar{n}}\mathcal{G}_{\ell\ell'}(r_i,r_j,z)\sum_\sigma c_\sigma\begin{pmatrix}\ell & \ell' & \sigma\\ 0 & 0 & 0\end{pmatrix}^2+\mathcal{D}_{\ell\ell',z}(r_i,r_j,z)\sum_\sigma \tilde{c}_\sigma\begin{pmatrix}\ell & \ell' & \sigma\\ 0 & 0 & 0\end{pmatrix}^2\Bigg],\end{aligned} \tag{4.57}$$

where $\bar{n}$ is the mean number density[9] in the redshift bin and we have defined

$$\mathcal{G}_{\ell\ell'}(r,r',z) = \frac{2(2\ell+1)(2\ell'+1)}{\pi^2}\int dk\,k^2P(k,z)j_\ell(kr)j_{\ell'}(kr')\,, \tag{4.58}$$

$$\mathcal{D}_{\ell\ell'}(r,r',z) = \frac{(2\ell+1)(2\ell'+1)}{\pi^2}\int dk\,k^2P^2(k,z)j_\ell(kr)j_{\ell'}(kr')\,, \tag{4.59}$$

together with the modified coefficients

$$\tilde{c}_0 = c_0^2+\frac{c_2^2}{5}+\frac{c_4^2}{9}\,, \tag{4.60}$$

$$\tilde{c}_2 = \frac{2}{7}c_2(7c_0+c_2)+\frac{4}{7}c_2c_4+\frac{100}{693}c_4^2\,, \tag{4.61}$$

$$\tilde{c}_4 = \frac{18}{35}c_2^2+2c_0c_4+\frac{40}{77}c_2c_4+\frac{162}{1001}c_4^2\,, \tag{4.62}$$

$$\tilde{c}_6 = \frac{10}{99}c_4(9c_2+2c_4)\,, \tag{4.63}$$

$$\tilde{c}_8 = \frac{490}{1287}c_4^2\,. \tag{4.64}$$

These results are also derived in appendix 4.A, while in fig. 4.5 we show the covariance matrix for the monopole, the quadrupole and their cross-correlation.

[9] In the covariance we ignore the redshift dependence of $\bar{n}$ and set $\bar{n}\equiv n(\bar{z})$ inside a given redshift bin. A method to include $\bar{n}(z)$ consistently can be found in [313].

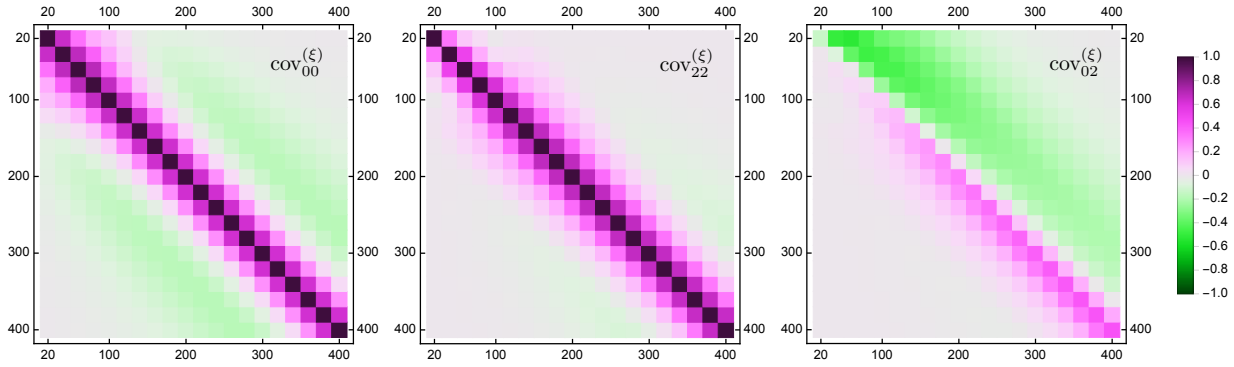


Figure 4.5: The covariance matrix for the monopole, the quadrupole and their cross-correlation, normalised as $\mathrm{cov}_{\ell\ell',ij}/(\mathrm{cov}_{\ell\ell,ii}\mathrm{cov}_{\ell'\ell',ii}\mathrm{cov}_{\ell\ell,jj}\mathrm{cov}_{\ell'\ell',jj})^{1/4}$. SKA2 specifications are used here and we plot the covariance for the middle bin of the 5-bin configuration, i.e. $L_p = 20\,\mathrm{Mpc}/h$.

## 4.3 A simple application: is lensing detectable?

As a first, simple application of COFFE we want to discuss the feasibility of measuring the lensing contribution in the correlation function with future galaxy surveys. In order to do so, we introduce an artificial parameter $A_L$, encoding the amplitude of the lensing signal, in the multipoles of the two-point function. Schematically, with the notation of eq. (4.28) we write (neglecting the Doppler and potential terms)

$$\xi_\ell = \xi_\ell^{\mathrm{st}} + A_L\,\xi_\ell^{L}\,, \tag{4.65}$$

where

$$\xi_\ell^{\mathrm{st}} = \langle \mathrm{den} + \mathrm{den}\rangle_\ell + \langle \mathrm{den} + \mathrm{rsd}\rangle_\ell + \langle \mathrm{rsd} + \mathrm{den}\rangle_\ell + \langle \mathrm{rsd} + \mathrm{rsd}\rangle_\ell\,, \tag{4.66}$$

represent the standard density and redshift-space distortion term, and

$$\xi_\ell^{L} = \langle \mathrm{den} + \mathrm{len}\rangle_\ell + \langle \mathrm{len} + \mathrm{den}\rangle_\ell + \langle \mathrm{rsd} + \mathrm{len}\rangle_\ell + \langle \mathrm{len} + \mathrm{rsd}\rangle_\ell + \langle \mathrm{len} + \mathrm{len}\rangle_\ell\,, \tag{4.67}$$

is the lensing contribution. Clearly the physical value of the lensing amplitude is $A_L = 1$ and we want to forecast the precision with which we can measure it. In figure 4.6, we show the monopole, quadrupole and hexadecapole with ($A_L = 1$) and without ($A_L = 0$) the lensing contribution. The shadowed regions show the size of the error-bars for an SKA2-like survey (specification givenbelow).

The Fisher matrix is defined as

$$F_{\alpha\alpha'} \equiv \frac{\partial^2\chi^2}{\partial\alpha\partial\alpha'} = \sum_{\ell,\ell',i,j} \left.\frac{\partial\langle\hat{\xi}_\ell\rangle(r_i)}{\partial\alpha}\right|_{\mathrm{f}} \mathrm{cov}^{-1}_{\ell\ell'}(r_i,r_j) \left.\frac{\partial\langle\hat{\xi}_{\ell'}\rangle(r_j)}{\partial\alpha'}\right|_{\mathrm{f}}, \tag{4.68}$$

where $\alpha$ and $\alpha'$ are the parameters we want to constrain and $|_{\mathrm{f}}$ means evaluation at some fiducial values of the parameters. The sum runs over all pixels' separations $r_i, r_j$ in the

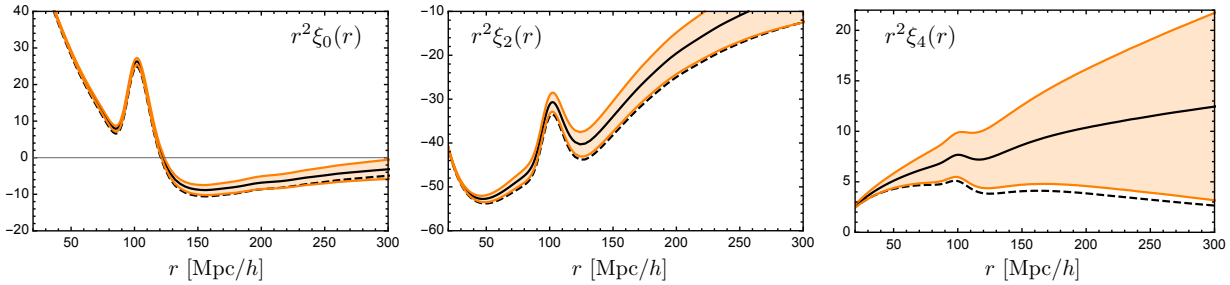


Figure 4.6: The monopole (*left*), the quadrupole (*middle*) and the hexadecapole (*right*) at $\bar{z} = 1.5$. Solid lines have $A_L = 1$ while dashed lines have no lensing contribution $A_L = 0$. Specifications, in particular biases, are for an SKA2-like survey.

survey as well as over the even multipoles $\ell, \ell' = 0, 2, 4, 6$. Note that the covariance matrices account for both correlations between different pixels' separations, $r_i \neq r_j$, and correlations between different multipoles, $\ell \neq \ell'$. The Cramér-Rao bound states that we can assign the $1\sigma$ uncertainty as

$$\sigma_\alpha = \sqrt{(F^{-1})_{\alpha\alpha}}\,, \tag{4.69}$$

and this gives the smallest possible achievable error on $\alpha$. We assume that the thickness of the redshift bins in which we split our catalog is big enough so that we can treat them as uncorrelated, implying

$$F^{\rm tot}_{\alpha\alpha'} = \sum_{\{\bar{z}_i\}} F_{\alpha\alpha'}(\bar{z}_i)\,. \tag{4.70}$$

Furthermore, for simplicity, we consider only the parameter $A_L$ and, instead of marginalizing over the remaining cosmological parameters, we fix them to: $\Omega_{\rm cdm} = 0.26$, $\Omega_b = 0.048$, $h = 0.676$, $A_s = 2.22 \times 10^{-9}$ and $n_s = 0.96$. In this case we only have

$$\begin{aligned} F_{A_L A_L} \equiv F &= \sum_{\ell,\ell',i,j} \frac{\partial\langle\hat{\xi}_\ell\rangle(r_i)}{\partial A_L}\bigg|_{\rm f} {\rm cov}^{-1}_{\ell\ell'}(r_i, r_j) \frac{\partial\langle\hat{\xi}_{\ell'}\rangle(r_j)}{\partial A_L}\bigg|_{\rm f} \\ &= \sum_{\ell,\ell',i,j} \xi^L_\ell(r_i)\bigg|_{\rm f} {\rm cov}^{-1}_{\ell\ell'}(r_i, r_j)\xi^L_\ell(r_j)\bigg|_{\rm f}\,. \end{aligned} \tag{4.71}$$

Note that the parameter $A_L$ does not have a direct physical interpretation; however, it allows us to estimate the signal-to-noise (S/N), a measure of the sensitivity to the lensing signal in galaxy clustering. This is an important information, especially as a high S/N is needed to test deviations from general relativity, for example with the widely used $(\Sigma, \mu)$ parametrization (see e.g. [163, 279, 148] and references therein): $\mu \neq 1$ represents a modification to Poisson equation while $\Sigma \neq 1$ represents a modification to the gravitational slip relation (see eqs. (4.81),(4.82)). The standard terms constrain $\mu$, while one needs to be sensitive to the lensing potential to constrain also $\Sigma$.

In this analysis we make one optimistic assumption and one conservative assumption. The optimistic one, as we mentioned, is to neglect the parameter degeneracies that will increase

the actually achievable error bar on $A_L$. A forecast study on all the cosmological parameters is left as future work. The conservative one is to treat the lensing term within linear perturbation theory, while non-linearities increase the lensing signal [294]: COFFE is for the moment a fully linear code and, as we discuss it in section 4.5, pushing its capabilities beyond the linear treatment is amongst our priorities.

The forecast (4.71) is easily done with COFFE and we compute the result for the signal-to-noise, which is simply given by

$$\mathrm{S/N} = \sqrt{\mathrm{F}} = 1/\sigma_{\mathrm{A_L}} \,, \tag{4.72}$$

with $A_L|_{\mathrm{f}} = 1$.

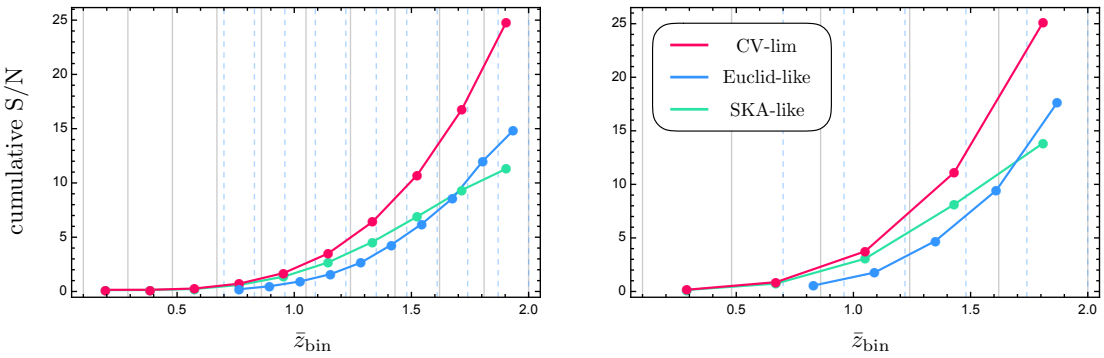


Figure 4.7: The cumulative signal-to-noise on the parameter $A_L$ for three different survey specifications and two different choice of binning, as explained in the text.

In Figure 4.7 we show the results for the signal-to-noise for three different spectroscopic survey specifications: an Euclid-like survey (specifications given in [203]), an SKA2-like survey (specifications given in [307]) and a survey limited only by cosmic variance, in which shot noise is neglected (essentially performing the limit $\bar{n} \to \infty$ in eq. (4.56)). We split the surveys into 5 bins (right panel of figure 4.7) or 10 bins (left panel of figure 4.7) to accommodate the full redshift range: $z \in [0.1, 2.0]$ for the SKA2 and the CV-limited survey and $z \in [0.7, 2.0]$ for Euclid (respectively solid and dashed vertical lines in fig. 4.7). For the 5-bins configuration we chose $L_p = 20\,\mathrm{Mpc}/h$ while for the 10-bins configuration we set $L_p = 10\,\mathrm{Mpc}/h$. We include separations from $r_{\mathrm{min}} = L_p$ to $r_{\mathrm{max}} = \chi(\bar{z}_{\mathrm{bin}} + \delta z) - \chi(\bar{z}_{\mathrm{bin}} - \delta z)$. The redshifts $\bar{z} < 1$ contribute very little to the signal. Only for $\bar{z} > 1$ sufficient lensing has accumulated to be truly visible in the correlation function. The S/N for the 5-bin configuration is somewhat larger than the one for the 10 bin. This is due to the fact that lensing dominates for large radial separation. Since we neglect correlations between different bins in the calculation of the Fisher matrix, we include more correlations at large separations when we have 5 bins than when we have 10 bins. The results for the cumulative S/N of eq. (4.72) on the lensing amplitude $A_L$ are

summarised as follows: for the 5-bins splitting we obtain

$$\begin{aligned} \mathrm{S/N}\big|_{\text{CV-lim}} &\simeq 25.2\,, \\ \mathrm{S/N}\big|_{\text{Euclid-}} &\simeq 17.6\,, \\ \mathrm{S/N}\big|_{\text{SKA}} &\simeq 13.8\,, \end{aligned} \tag{4.73}$$

while for the 10-bins splitting they are slightly lower. Note that the monopole alone contributes to ~ 45% of the total $S/N$, the quadrupole to ~ 30%, the hexadecapole to ~ 15% while, interestingly, the $\ell = 6$ multipole contributes to roughly 10% of the total signal-to-noise. This can be explained as the balance between two different effects: on the one hand the lensing contribution is more relevant for higher multipoles, but on the other hand, as seen in fig. 4.6, the covariance also gets bigger for higher $\ell$. We therefore conclude that upcoming galaxy surveys will be able to detect the lensing signal in the 2pF. This will open the possibility to put constraints in the $(\Sigma, \mu)$ plane from the clustering signal alone.

Note that here we have used the $\xi_\ell$ for the forecasts. Since we split the survey in bins of half-width $\delta z = 0.05$ and $\delta z = 0.1$, given the discussion in section 4.2.3, we do not expect these results to change if we use the $\Xi_\ell$ instead.

## 4.4 Structure of the code

COFFE is entirely written in C and the code can be divided into several key `structs` and functions. The main flow of the program can be summarized as follows:

1. Read the settings file containing all of the necessary parameters: cosmological parameters, the input $P(k)$ and desired output.
2. Compute and store the background quantities.
3. Calculate all of the $I^n_\ell(r)$ using an implementation of the 2-FAST algorithm for a fixed number of separations, specified by the user; $I^4_0$ is only computed if one of the following contributions is requested: d2, g1, g2, g3, g4, g5.
4. Compute one of the following, depending on input:
   - angular correlation function $\xi(\theta, \bar{z})$
   - full sky correlation function $\xi(\mu, r, \bar{z})$
   - multipoles of the correlation function $\xi_\ell(r, \bar{z})$
   - redshift averaged multipoles $\Xi_\ell(r, \bar{z}, \delta z)$
   - covariance of multipoles $\mathrm{cov}^{(\xi)}_{\ell\ell'}$
   - covariance of redshift averaged multipoles $\mathrm{cov}^{(\Xi)}_{\ell\ell'}$
5. Save the necessary output.

6. Perform a memory cleanup and exit.

In the next sections we will go over the structure in more detail. For more information, the interested reader can consult the user manual, available at
`https://cosmology.unige.ch/content/coffe` or at `https://github.com/JCGoran/coffe`.
The manual also contains detailed instructions on how to run the code.

### 4.4.1 The parser & background modules

The parser module is used for the parsing of the structured settings file and making sure all of the values in the input are valid. The library used for parsing is the LIBCONFIG library[10].

The background module is responsible for calculating all of the derived redshift dependent quantities in a ΛCDM or $w$CDM cosmology with zero curvature, such as the Hubble rate $H(z)$, growth rate $f(z)$, comoving distance $\chi(z)$, etc. All of the quantities are computed at equally spaced intervals up to redshift $z = 30$, with a user defined sampling rate, and are stored in `interpolation` structures. We have compared our results with CLASS and have found an agreement of order $10^{-4}$.

### 4.4.2 The integrals $I_\ell^n(r)$

For the integrals $I_\ell^n(r)$ we have created a native implementation of the 2-FAST algorithm introduced in [162]. We have tested it against the original implementation in **julia**, and have found a negligible discrepancy of the order $10^{-5}$. As they are computed only for a discrete number of points, we again use interpolation to find their values for arbitrary $r$.

Note that for the non-integrated terms we have to deal with the $r \to 0$ limit of the $I_\ell^n(r)$ only if the value of the correlation function at zero separation is required. On the other hand the expressions for the integrated terms contain integrals of the type (see appendix 4.B)

$$\int_0^{\chi_1} d\lambda \, [...] \, I_\ell^n(r) \,, \qquad \int_0^{\chi_1} d\lambda \int_0^{\chi_2} d\lambda' \, [...] \, I_\ell^n(r) \,, \tag{4.74}$$

where inside the integrals we have, respectively,

$$r = \sqrt{\lambda^2 + \chi_2^2 - 2\lambda\chi_2 \cos\theta} \,, \tag{4.75}$$

$$r = \sqrt{\lambda^2 + \lambda'^2 - 2\lambda\lambda' \cos\theta} \,. \tag{4.76}$$

When we compute the 2pF along the line-of-sight (i.e. $\mu = 1$ or $\theta = 0$) the integrand evaluates at $r = 0$ and hence we have to deal with this limit. We treat the following three cases separately:

[10] described in `https://hyperrealm.github.io/libconfig/`

1. For $\boldsymbol{\ell < n}$ we have $\lim_{r\to 0} I_\ell^n(r) = \infty$; however, these terms always appear in the correlation function multiplied by the appropriate power $r^{n-\ell}$, so that

$$\lim_{r\to 0} r^{n-\ell} I_\ell^n(r) \sim \int \frac{dk\, k^2}{2\pi^2} P(k) k^{\ell-n}\,. \tag{4.77}$$

   Assuming that the linear power spectrum behaves in the IR and UV as

$$P(k) \sim \begin{cases} k^{n_1} & \text{for } k/k_{\rm eq} \ll 1 \\ k^{n_2-4} & \text{for } k/k_{\rm eq} \gg 1 \end{cases} \tag{4.78}$$

   the condition for which the integral in eq. (4.77) converges is $-3 - n_1 < \ell - n < 1 - n_2$, which is always satisfied for ΛCDM cosmologies[11] for the values of $\ell, n$ needed (except for $I_0^4$ in the IR as we discussed in section 4.2.2). We use 2-FAST to interpolate $r^{n-\ell} I_\ell^n$ until a small separation $r_{\rm min} \simeq 1\,{\rm Mpc}/h$. As the 2-FAST algorithm cannot be pushed to $r \to 0$ we use the standard GSL integrator for $r \lesssim 1\,{\rm Mpc}/h$, where the very oscillatory behaviour of the integrands is less pronounced, and GSL gives a reliable result.

2. For $\boldsymbol{\ell = n}$ we have $\lim_{r\to 0} I_\ell^n(r) = {\rm const}$, and we can simply switch to GSL from $r \lesssim 1\,{\rm Mpc}/h$ to $I_\ell^n(r = 0)$.

3. For $\boldsymbol{\ell > n}$ the limit gives $\lim_{r\to 0} I_\ell^n(r) = 0$ and the $I_\ell^n$ go to zero as $r^{\ell-n}$. The behaviour close to $r = 0$ is again captured with the GSL integrator. Note however that capturing the overall behaviour would be really important only if the coefficients by which the $I_\ell^n$ are multiplied diverge at zero like $r^{n-\ell}$. As all the coefficients are well behaved at zero, our procedure causes no concern.

The $I_0^4(r)$ integral of eq. (4.41) is not in a form suitable for the 2-FAST algorithm and it is therefore integrated using standard GSL integration for a predefined number of separations, and then interpolated. In this case, we have the further complication that we also need the counter term to renormalise $I_0^4(r)$ which is a function of both comoving distances $\chi_1$ and $\chi_2$. This term is calculated for a fixed number of points (200×200) and is then 2D interpolated for all other points.

### 4.4.3 Outputs

To calculate the correlation function $\xi$, its multipoles $\xi_\ell$ and the redshift averaged multipoles $\Xi_\ell$, we use the $X_\ell^n$ and $Z_\ell^n$ coefficients defined in appendix 4.B and build the desired quantities using eqs. (4.25),(4.29),(4.31) and (4.46) respectively. The $I_\ell^n$ integrals are computed with our implementation of the 2-FAST algorithm. Integrated terms have a structure as in eq. (4.74). To compute them, depending on the number of integrations required, we use either standard GSL integration (1 integration) or one of the following options:

- GSL Monte Carlo methods, using either importance sampling or stratified sampling
- the CUBA library [166], using a deterministic integrator employing cubature rules

[11] The values obtained for the linear $P(k)$ used in the figures of this chapter are $n_1 \simeq n_s \simeq 0.96$ and $n_2 \simeq 1$.

| **output** | | | **time** |
|---|---|---|---|
| $\xi(r,\mu)$ | (den+rsd) | up to $\sim 1000\,\mathrm{Mpc}/h$ | $\sim 0.5$ s |
| $\xi(r,\mu)$ | (den+rsd+len) | up to $\sim 1000\,\mathrm{Mpc}/h$ | $\sim 17$ s |
| $\xi_\ell(r)$ | (den+rsd) | up to $\sim 1000\,\mathrm{Mpc}/h$ | $\sim 9$ s |
| $\xi_\ell(r)$ | (den+rsd+len) | up to $\sim 1000\,\mathrm{Mpc}/h$ | $\sim 2$ min |
| $\Xi_\ell(r)$ | (den+rsd) | $\delta z = 0.3$ | $\sim 1.5$ s |
| $\Xi_\ell(r)$ | (den+rsd+len) | $\delta z = 0.3$ | $\sim 3$ min |
| $\mathrm{cov}^{(\xi)}_{\ell\ell'}(r_i,r_j)$ | $(N_p = 50)$ | $N_p \times N_p$ | $\sim 20$ s |
| $\mathrm{cov}^{(\Xi)}_{\ell\ell'}(r_i,r_j)$ | $(N_p = 50)$ | $N_p \times N_p$ | $\sim 20$ s |

Table 4.1: Run time of COFFE calculating the correlation function at fixed $\mu$ (for $\sim 200$ separations), one multipole $\ell$ for $\xi_\ell$ and $\Xi_\ell$ or the covariance matrices on one Intel(R) Core(TM) i7-7700 CPU @ 3.60GHz core. COFFE is however parallelized using the `openMP` standard.

The user can select which one to use at compile time, as well as the number of iterations at run time.

The covariance is built from eqs. (4.56),(4.57). The challenging part of the computation are clearly the integrals $\mathcal{D}_{\ell\ell'}$ and $\mathcal{G}_{\ell\ell'}$. As the 2-FAST algorithm is not optimised to compute covariances[12] it is (at the moment) too slow to be implemented in the public version of the code. We therefore choose to release COFFE `v.1.0` with the covariance implemented in GSL, which is much faster but less precise. Note that this trade of precision for speed has sometimes important drawbacks: for thick redshift bins the GSL covariance might not be positive definite because of numerical fluctuations. For this reason the results reported in section 4.3 have been obtained with the 2-FAST algorithm: in future versions of COFFE we will optimize this for covariance calculation and release it to the public.

For reference, in table 4.1 we list the run time of COFFE for the different possible outputs.

## 4.5 Conclusion and outlook

In this chapter we have presented a code to calculate the relativistic full-sky correlation function and its covariance matrix. As we have shown previously [294], relativistic effects and wide-angle contributions are of the same order and it is therefore inconsistent to consider one

[12]To be precise, 2-FAST allows for the computation of integrals with two Bessel functions such as $\mathcal{D}_{\ell\ell'}$ and $\mathcal{G}_{\ell\ell'}$. However the algorithm is structured to output them for a list of $r_i$ but fixed $R = r_j/r_i$. In the covariance we however need $N_p^2$ pairs of $(r_i, r_j)$, where $N_p = r_{\max}/L_p$ is the number of pixels in the covariance. To get them, with no modification of the algorithm, we need to run 2-FAST $N_p^2$ times, with a runtime not suitable for a public code. The covariance in section 4.3 is nevertheless computed in this way: with our implementation of the 2-FAST double-Bessel algorithm (we use the main principle of the algorithm, i.e. an Hankel transform of the integrand, but not their specific hyper geometric function ${}_2F_1$ implementation).

but not the other. Presently, the code uses the linear matter power spectrum and therefore is most relevant on large scales. This will be important for the many planned future deep wide-angle surveys. We have argued that the correlation function is a better tool than the –in principle equivalent– angular power spectrum $C_\ell(z_1, z_1)$ for spectroscopic surveys. As an example of how to use the code we have computed the signal-to-noise of the lensing term for some near-future galaxy surveys. The code is publicly available at `https://cosmology.unige.ch/content/coffe` or at `https://github.com/JCGoran/coffe`.

We finally discuss some features that we plan to implement in upcoming versions of COFFE:

- CLASS *integration*: We will integrate CLASS on top of COFFE so that with only one parameter file it will be possible to generate the matter power spectrum necessary for the 2pF computation and to obtain the desired correlation function output. This integration will be particularly useful for forecasts.

- *Non-linearities*: COFFE `v.1.0` is a fully linear code. On the one hand this is justified by the fact that wide-angles and relativistic projections effects are most relevant at large scales. On the other hand it will be important in future versions to include the effects of non-linearities on the 2pF. Especially lensing, which is an integrated effect where non-linearities close to the observer contribute, is always affected by non-linearities. One can of course, already in the present version, use the halo-fit matter power spectrum for non-integrated effects to mimic these non-linearities. But this is not really consistent as long as the linearized continuity equation is used to infer velocities. At small-scales the velocity dispersion is responsible for the *fingers-of-god* effect which can be modeled as a convolution of the real-space 2pF with the probability distribution for velocity along the LOS [150, 258, 58]. Also at intermediate scales, both the position and the shape of the BAO peak are affected by non-linearities [141, 110, 280]. In this sense a promising formalism is the one developed in [223] as it is mostly based on quantities already computed in the code.

- *Bias*: Another important feature that ought to be implemented in future versions of the code is the generalisation of the simple redshift-dependent bias $b(z)$ to different contributions of the bias expansion and scale-dependent bias, as they are known to have important effects on the 2pF [119].

- *Curvature*: A generalisation of the code functionality which seems trivial at first sight is to allow for non-zero curvature $\Omega_K \neq 0$; however, from a technical point of view it has some challenges. As we discussed in section 4.2, the way the code computes the correlation function is based on the fact that we can analytically re-sum eq. (4.24) via the addition theorem for spherical Bessel functions. The $j_\ell$'s appear in the Fourier-Bessel transform $\Delta_\ell$ as they are the radial part of the eigenfunctions $\mathcal{Q}_k(\mathbf{x})$ of the flat-space laplacian (i.e. $\mathcal{Q}_k(\mathbf{x}) = \text{Exp}(i\mathbf{k}\cdot\mathbf{x})$). The addition theorem can then be derived from the identity

$$e^{i\mathbf{k}\cdot\mathbf{r}} = e^{i\mathbf{k}\cdot\mathbf{x}_2} e^{-i\mathbf{k}\cdot\mathbf{x}_1} \tag{4.79}$$

  where $\mathbf{r} = \mathbf{x}_2 - \mathbf{x}_1$. For a manifold with constant curvature, expressions for the eigenfunctions can be obtained (one finds expressions equivalent to the plane wave expansion

of the flat case but with the spherical Bessel replaced by hyperspherical Bessel function [126]) and they do satisfy

$$\mathcal{Q}_k(\mathbf{x}_2 - \mathbf{x}_1) = \mathcal{Q}_k(\mathbf{x}_2)\mathcal{Q}_k(-\mathbf{x}_1) \tag{4.80}$$

from which the addition theorem can be derived. Therefore, including curvature in COFFE is in principle straight forward, but it will require additional theoretical and coding efforts.

- *EFT of DE*: An interesting application of the code will be to study the effect of dark energy and modified gravity on the galaxy 2pF beyond the cosmological constant behaviour. On the one hand the code heavily relies on the ΛCDM equations and modifying it to account for a different model will require a substantial rewriting of some portions of it. On the other hand we can explore all the dark energy and modified gravity models that contain one additional scalar degree of freedom with the *effective field theory of dark energy* (EFT of DE) [109, 163, 68]. We can in fact describe a range of models only using an handful of couplings, making it a very useful approach to constrain deviations from GR. If we limit ourself to Horndeski theories and fix a background history close to ΛCDM we can parametrise the changes to the Poisson and the anisotropy equations by introducing two scale- and time-dependent quantities $\mu$ and $\Sigma$:

$$k^2\Psi = -\mu(z,k)\frac{3\Omega_m\mathcal{H}^2}{2a}\delta_c\,, \tag{4.81}$$

$$\Phi/\Psi = \Sigma(z,k)\,. \tag{4.82}$$

A simple suitable parametrisation for the two couplings and applications of this idea for the CMB and the galaxies angular power spectrum can be found in [268, 327].

- *Multi-tracer observables*: it has been shown that by combining different tracers of the density field (e.g. two populations of galaxies with different biases), one can reduce cosmic variance [226] and improve the detectability of relativistic effects in the power spectrum [322] and in the $C_\ell$'s [212]. In the 2pF, correlating two populations of galaxies has the particularity to generate a dipole and octupole contribution [76, 77, 155, 169], which for symmetry reasons are absent in the case of one tracer. This dipole can be used to test the equivalence principle in a model-independent way and constrain modifications of gravity with relativistic effects [75]. An extension of the code to multiple tracers is therefore planed in the future. This will require the computation of odd multipoles and their covariance matrices.

Appendices

## 4.A Estimators and Covariances

In this appendix we give some more details on the estimators used and we derive their covariances. We especially derive our estimator $\hat{\Xi}_\ell$ which is new.

### 4.A.1 Estimators

Let us start with the estimator of the multipole of the correlation function averaged of the redshift bin $[\bar{z}-\delta z, \bar{z}+\delta z]$ given in eq. (4.43),

$$\hat{\xi}_\ell(r,\bar{z}) = \beta_\ell \sum_{ij} \Delta_i \Delta_j \mathcal{P}_\ell(\mu_{ij}) \delta_K(r_{ij}-r)\,. \tag{4.83}$$

Here $\Delta_i \equiv \Delta_g(\mathbf{x}_i, z_i)$ is the number counts per pixel of size $L_p^3$ and $\mu_{ij} = r_\parallel/r_{ij}$ where $\mathbf{r}_{ij} = \mathbf{x}_i - \mathbf{x}_j$ and $r_\parallel = \chi(z_i) - \chi(z_j)$. We want to normalise this estimator such that in the continuum limit, $N = V/L_p^3 \to \infty$, its expectation value is the multipole of the correlation function. Let us compute its expectation value,

$$\langle \hat{\xi}_\ell(r,\bar{z}) \rangle = \beta_\ell \sum_{ij} \langle \Delta_i \Delta_j \rangle \mathcal{P}_\ell(\mu_{ij}) \delta_K(r_{ij}-r)\,. \tag{4.84}$$

We now perform the continuum limit and set $\mathbf{x}_i = \mathbf{y} + \mathbf{r}/2$, $\mathbf{x}_j = \mathbf{y} - \mathbf{r}/2$ and $\mu_{ij} = \mu$. The volume of a ring of radius $r$ with direction cosine $\mu$ to the outward direction is $2\pi r dr\, r d\mu = 2\pi r^2 dr d\mu$. In our discrete sample we have to replace the infinitesimal scale $dr$ by the pixel size $L_p$. Hence one of the sums can by replaced by $\int d^3y/L_p^3$ while the other becomes $2\pi r^2 \int d\mu/L_p^2$. Since at fixed mean redshift $\bar{z}$ the correlation function does not depend on $\mathbf{y}$, the $y$-integration just contributes a volume factor. Putting it all together we obtain

$$\langle \hat{\xi}_\ell(r,\bar{z}) \rangle = \beta_\ell \frac{2\pi r^2 V}{L_p^5} \int_{-1}^{1} d\mu \xi(r,\mu,\bar{z}) \mathcal{P}_\ell(\mu)\,. \tag{4.85}$$

Inserting the expansion

$$\xi(r,\mu,\bar{z}) = \sum_{\ell=0}^{\infty} \xi_\ell(r,\bar{z})\mathcal{P}_\ell(\mu) \tag{4.86}$$

and making use of the orthogonality relation

$$\int_{-1}^{1} d\mu \mathcal{P}_\ell(\mu)\mathcal{P}_{\ell'}(\mu) = \frac{2}{2\ell+1}\delta_{\ell,\ell'}\,,$$

we find

$$\langle\hat{\xi}_\ell(r,\bar{z})\rangle = \beta_\ell \frac{4\pi r^2 V}{L_p^5(2\ell+1)}\ \xi_\ell(r,\bar{z})\,. \tag{4.87}$$

In order for this to estimate $\xi_\ell$ we must choose

$$\beta_\ell = \frac{2\ell+1}{4\pi}\frac{L_p^5}{r^2 V}\,. \tag{4.88}$$

Let us now turn to the more sophisticated estimator $\hat{\Xi}_\ell$ which does not just assign a global mean redshift inside our redshift bin but instead assigns to each pair its correct mean redshift. Since the redshift resolution of a spectroscopic survey can be very high, $10^{-3}$ or better, it may well be that there are only a few galaxy pairs with a fixed distance and the precise mean redshift in a bin (of width $2\delta z \sim 0.1$ or so). Therefore we shall integrate over the bin with a given redshift distribution $W(z)$. If one wants to select a fixed redshift one can simply choose $W$ to be a delta function.

The quantities $\Delta_i$ are again the number counts per pixel of size $L_p^3$. For the continuum limit of eq. (4.45) we therefore have to replace

$$\sum_{ij}\Delta_i\Delta_j \longrightarrow \int \frac{d^3x_i d^3x_j}{L_p^6}\Delta_g(\mathbf{x}_i)\Delta_g(\mathbf{x}_j)\,,$$

where now $\Delta_g(\mathbf{x})$ is the continuum density contrast. We also replace the sum over discrete redshifts $z_k$ by an integral, $\int dz$. With this, the continuum limit of $\hat{\Xi}_\ell$ is

$$\begin{aligned}\hat{\Xi}_\ell(r,\bar{z},\delta z) \to \gamma_\ell \int_{\bar{z}-\delta z}^{\bar{z}+\delta z} dz\, W(z) \int \frac{d^3x_i d^3x_j}{L_P^6}\Bigg[\frac{1+\cos\theta_{ij}}{2r_j^2} \\ \times \Delta_g(x_i,z_i)\Delta_g(x_j,z_j)\,\mathcal{P}_\ell(\mu_{ij})\,L_p\delta(r_{ij}-r)\delta(z_{ij}-z)\Bigg],\end{aligned} \tag{4.89}$$

Note that we have replaced the Kronecker delta for the relative distance $r_{ij}$ by a Dirac delta multiplied by the pixel size. This not only has the right dimension but also takes care of the fact that we do not distinguish distances within one pixel.

We now make the coordinate transformation

$$\mathbf{x}_i \to \mathbf{r} = \mathbf{x}_i - \mathbf{x}_j \quad \text{and} \quad \mathbf{x}_j \to \left(\chi_{ij} = \frac{|x_i|+|x_i|}{2}, \theta_j, \phi_j\right).$$

Here $\theta_j$ and $\phi_j$ are the polar angles of $\mathbf{x}_j$, and we do not distinguish between $\chi((z_i+z_j)/2)$ and $(|x_i|+|x_i|)/2$. The Jacobian of the transformation is readily calculated and amounts to

$$J = \mathrm{Det}\left[\frac{\partial(\mathbf{x}_i,\mathbf{x}_j)}{\partial(\chi_{ij},\theta_j,\phi_j)}\right] = \frac{2x_j^2\sin\theta_j}{1+\cos\theta_{ij}}\,, \tag{4.90}$$

where as above $\theta_{ij}$ is the angle between $\mathbf{x}_i$ and $\mathbf{x}_j$. To eliminate this $x_j$ and $x_i$ dependent factor, we had to define our estimator as the density pair multiplied by the inverse of the factor. After this coordinate transformation the integration over $(\theta_j,\phi_j)$ can readily be performed and simply gives a factor $4\pi$. As above, the integral $d^3r$ can be written as $2\pi r^2 dr d\mu$. We then obtain, for the expectation value of our estimator,

$$\langle\hat{\Xi}_\ell(r,\bar{z},\delta z)\rangle = \gamma_\ell\frac{(4\pi)^2r^2}{2L_p^5}\int_{\bar{z}-\delta z}^{\bar{z}+\delta z}dz\frac{W(z)}{H(z)}\int_{-1}^{1}d\mu\,\xi(r,\mu,z)\mathcal{P}_\ell(\mu)\,. \tag{4.91}$$

Here we have performed the $\chi_{ij}$-integration using the redshift delta-function and the identity $\delta(z_{ij}-z) = \delta(\chi_{ij}-\chi)/H(z)$. Like above, the $\mu$-integration now yields the moment $\xi_\ell$,

$$\langle\hat{\Xi}_\ell(x,\bar{z},\delta z)\rangle = \gamma_\ell\frac{(4\pi)^2r^2}{(2\ell+1)L_p^5}\int_{\bar{z}-\delta z}^{\bar{z}+\delta z}dz\frac{W(z)}{H(z)}\xi_\ell(r,z)\,. \tag{4.92}$$

Hence in order to obtain the desired estimator for

$$\Xi_\ell(r,\bar{z},\delta z) = H_0\int_{\bar{z}-\delta z}^{\bar{z}+\delta z}dz\frac{W(z)}{H(z)}\xi_\ell(r,z)\,, \tag{4.93}$$

we have to choose

$$\gamma_\ell = \frac{2\ell+1}{(4\pi)^2}\frac{L_p^5H_0}{r^2f_{\mathrm{sky}}}\,. \tag{4.94}$$

The factor $f_{\mathrm{sky}}$ has been introduced here to account also for partial sky coverage. Note that the normalization factor $\gamma_\ell$ has the correct dimension $(\mathrm{length})^2$ to compensate for the dimensions of the factor $1/r_j^2$ in the sum of (4.89) which therefore yields a dimensionless estimator. For the formula to hold, we also have assumed that the redshift window function is normalized to unity.

The estimators discussed here are optimal for the unrealistic case of a nearly full and homogeneous sky coverage. If there are certain parts of the sky where observations are better, more complete and or more precise, this can be taken into account by multiplying with an inhomogeneous weighting function in order to enhance the weight of these regions. Furthermore, for a complicated fractional sky coverage a simple multiplicative factor $f_{\mathrm{sky}}$ is also not optimal. In this thesis we do not discuss these subtleties which, however are part of every real observation.

### 4.A.2 Covariance matrix

Here we briefly derive the expressions for the covariance matrices, eqs. (4.56) and (4.57).

In this calculation we only include the dominant terms: density and redshift space distortion. Even though at very large distance the correlation function is dominated by lensing, the covariance matrix $C(\mathbf{r},\mathbf{r}')$ includes contributions from distances much smaller than $r$ and $r'$ where the standard terms largely dominate. This means that the density and RSD are the main contribution to the covariance matrix also at large distances. We also neglect redshift evolution and wide angle effects in the covariance matrix such that our estimator for the correlation function is

$$\hat{\xi}(\mathbf{r}) = \frac{1}{V}\int_V d^3x \hat{\Delta}_g(\mathbf{x})\hat{\Delta}_g(\mathbf{x}+\mathbf{r})\,. \tag{4.95}$$

Including Poisson noise the observed two-point correlation function is given by

$$\langle\hat{\Delta}_g(\mathbf{x})\hat{\Delta}_g(\mathbf{x}')\rangle = \xi(\mathbf{x}-\mathbf{x}') + \frac{1}{\bar{n}}\delta(\mathbf{x}-\mathbf{x}')\,, \tag{4.96}$$

where $\bar{n}$ is the mean number density in the redshift bin under consideration.

Assuming Gaussianity the covariance matrix of $\hat{\xi}$ is then becomes

$$\begin{aligned} C(\mathbf{r},\mathbf{r}') &= \langle\hat{\xi}(\mathbf{r})\hat{\xi}(\mathbf{r}')\rangle - \langle\hat{\xi}(\mathbf{r})\rangle\langle\hat{\xi}(\mathbf{r}')\rangle \\ &= \frac{1}{V^2}\int_{V\times V} d^3x d^3x' \left[\xi(\mathbf{x}-\mathbf{x}')\xi(\mathbf{x}+\mathbf{r}-\mathbf{x}'-\mathbf{r}') + \xi(\mathbf{x}+\mathbf{r}-\mathbf{x}')\xi(\mathbf{x}-\mathbf{x}'-\mathbf{r}')\right] \\ &\quad + \frac{2}{V\bar{n}}\left[\xi(\mathbf{r}-\mathbf{r}') + \xi(\mathbf{r}+\mathbf{r}')\right] + \frac{1}{\bar{n}^2}\left[\delta(\mathbf{r}-\mathbf{r}') + \delta(\mathbf{r}+\mathbf{r}')\right]. \end{aligned}$$

Here we have used that the correlation function (for one population of galaxies) is symmetric, $\xi(\mathbf{r}) = \xi(-\mathbf{r})$. The first line is the cosmic variance term, the second line contains terms which mix cosmic variance and Poisson noise and the last term is a pure Poisson noise term. Note that - as we have already anticipated - even if both $\mathbf{r}$ and $\mathbf{r}'$ are very large, the covariance matrix contains the correlation function at very small arguments, maybe in $\xi(\mathbf{r}-\mathbf{r}')$ but surely in the pure cosmic variance term, and these terms dominate the covariance. This has disadvantages, namely the covariance becomes much larger than $\xi(\mathbf{r})$ and $\xi(\mathbf{r}')$ for large $r$ and $r'$ leading to a small signal with large noise, but it also means that it is a good approximation to neglect wide angle effects and lensing in the covariance matrix as these are subdominant for small separation.

After a change of variables, $(\mathbf{x},\mathbf{x}') \to (\mathbf{x},\mathbf{y})$ with $\mathbf{y} = \mathbf{x}-\mathbf{x}'$, the $\mathbf{x}$-integration of the cosmic variance term becomes trivial. Inserting the Fourier representation

$$\xi(\mathbf{y}) = (2\pi)^{-3}\int d^3k P(\mathbf{k})\exp[i\mathbf{k}\cdot\mathbf{y}]\,,$$

the $y$-integration of the cosmic variance term can be performed leading to a Dirac delta of the two Fourier variables. Representing also the Dirac delta of the Poisson term in Fourier space, we end up with

$$C(\mathbf{r},\mathbf{r}') = \frac{1}{V(2\pi)^3}\int d^3k\left[P^2(\mathbf{k}) + \frac{2}{\bar{n}}P(\mathbf{k}) + \frac{1}{\bar{n}^2}\right]\left(e^{i\mathbf{k}\cdot(\mathbf{r}-\mathbf{r}')} + e^{i\mathbf{k}\cdot(\mathbf{r}+\mathbf{r}')}\right). \tag{4.97}$$

We now use the fact that (in the flat sky approximation) $P(\mathbf{k}) = P(k,\nu)$ where $\nu$ is the direction cosine between the observation direction $\mathbf{n}$ and $\mathbf{k}$. Furthermore, we write the exponentials

in terms of Bessel functions, $j_\ell$, and Legendre polynomials $\mathcal{P}_\ell$ as

$$\exp(i\mathbf{k}\cdot\mathbf{r}) = \sum_{\ell=0}^{\infty} i^\ell (2\ell+1)\mathcal{P}_\ell(\mu) j_\ell(kr)\,,$$

where $\mu$ is the direction cosine between $\mathbf{k}$ and $\mathbf{r}$. With this for example the pure cosmic variance term becomes

$$\frac{1}{V(2\pi)^3}\int d^3k P^2(k,\nu)\sum_{\ell,\ell'}\mathcal{P}_\ell(\mu)\mathcal{P}_{\ell'}(\mu')j_\ell(kr)j_{\ell'}(kr')\left[i^{\ell-\ell'}+i^{\ell+\ell'}\right](2\ell+1)(2\ell'+1)\,.$$

Since $P(\mathbf{k})$ is even in $\mathbf{k}$, we obtain non-vanishing results only if both, $\ell$ and $\ell'$ are even. Therefore $i^{\ell-\ell'} + i^{\ell+\ell'} = 2i^{\ell-\ell'}$. We expand also $P$ and $P^2$ in Legendre polynomials using $P(k,\nu) = P(k)(c_0 + c_2\mathcal{P}_2(\nu) + c_4\mathcal{P}_4(\nu))$ and

$$P^2(k,\nu) = P^2(k)\sum_{\ell=0}^{4}\tilde{c}_{2\ell}\,\mathcal{P}_{2\ell}(\nu)\,, \tag{4.98}$$

where the coefficients $\tilde{c}_L$ are obtained by expanding the square $(P(k,\nu)/P(k))^2$ in Legendre polynomials,

$$(c_0\mathcal{P}_0 + c_2\mathcal{P}_2 + c_4\mathcal{P}_4)^2 = \sum_{L=0}^{8}\tilde{c}_L\mathcal{P}_L\,. \tag{4.99}$$

The values $c_L$ and $\tilde{c}_L$ are given in (4.33) to (4.35) and (4.60) to (4.64).

Employing the addition theorem of spherical harmonics for $\nu = \hat{\mathbf{k}}\cdot\mathbf{n}$, $\mu = \hat{\mathbf{k}}\cdot\hat{\mathbf{r}}$ and $\mu' = \hat{\mathbf{k}}\cdot\hat{\mathbf{r}}'$ we convert the Legendre polynomials into products of spherical harmonics. The angular integral of the pure covariance and of the mixed term leads to an angular integral of a product of three spherical harmonics which can be performed exactly using

$$\int d\Omega_{\mathbf{k}} Y_{LM}(\hat{\mathbf{k}})Y_{\ell'm'}(\hat{\mathbf{k}})Y_{\ell m}(\hat{\mathbf{k}}) = \sqrt{\frac{(2L+1)(2\ell'+1)(2\ell+1)}{4\pi}}\begin{pmatrix}L & \ell' & \ell\\ 0 & 0 & 0\end{pmatrix}\begin{pmatrix}L & \ell' & \ell\\ M & m' & m\end{pmatrix}.$$

This yields

$$\begin{aligned}\int d\Omega_{\mathbf{k}}\mathcal{P}_L(\nu)\mathcal{P}_\ell(\mu)\mathcal{P}_{\ell'}(\mu') = &\sqrt{\frac{(4\pi)^5}{(2L+1)(2\ell'+1)(2\ell+1)}}\begin{pmatrix}L & \ell' & \ell\\ 0 & 0 & 0\end{pmatrix}\\ &\times\sum_{M,m,m'}\begin{pmatrix}L & \ell' & \ell\\ M & m' & m\end{pmatrix}Y^*_{LM}(\mathbf{n})Y^*_{\ell'm'}(\hat{\mathbf{r}}')Y^*_{\ell m}(\hat{\mathbf{r}})\,.\end{aligned}$$

We now choose $\mathbf{n} = \mathbf{e}_z$ so that $Y_{LM}(\mathbf{n}) = \sqrt{(2L+1)/4\pi}\delta_{M,0}$. Inserted this in (4.97) we find

$$\begin{aligned}C(\mathbf{r},\mathbf{r}') = &\frac{2(4\pi)^2}{V(2\pi)^3}\sum_{L,\ell,\ell',m,m'}\sqrt{(2\ell'+1)(2\ell+1)}\begin{pmatrix}L & \ell' & \ell\\ 0 & 0 & 0\end{pmatrix}i^{\ell-\ell'}\begin{pmatrix}L & \ell' & \ell\\ 0 & m' & m\end{pmatrix}\\ &\times Y^*_{\ell'm'}(\hat{\mathbf{r}}')Y^*_{\ell m}(\hat{\mathbf{r}})\int dk k^2\left[\tilde{c}_L P^2(\mathbf{k}) + c_L\frac{2}{\bar{n}}P(\mathbf{k}) + \delta_{0L}\frac{1}{\bar{n}^2}\right]j_\ell(kr)j_{\ell'}(kr')\,.\end{aligned}$$

The covariance matrix for the multipoles $n$ and $n'$ is given by

$$\mathrm{cov}^{(\xi)}_{n,n'}(r,r') = \frac{(2\ell+1)(2\ell'+1)}{4}\int_{-1}^{1}d\mu\int_{-1}^{1}d\mu'\mathcal{P}_n(\mu)\mathcal{P}_{n'}(\mu')C(\mathbf{r},\mathbf{r}')\,, \tag{4.100}$$

where now $\mu = \mathbf{n}\cdot\hat{\mathbf{r}} = \cos\theta$ and $\mu' = \mathbf{n}\cdot\hat{\mathbf{r}}' = \cos\theta'$. Using that $\mathcal{P}_n(\mu) = \sqrt{4\pi/(2n+1)}Y_{n0}(\hat{\mathbf{r}})$ together with the orthonormality of the spherical harmonics we can write

$$\begin{aligned}\mathrm{cov}^{(\xi)}_{\ell,\ell'}(r,r') = {}& \frac{1}{V\pi^2}(2\ell'+1)(2\ell+1)\sum_L\begin{pmatrix}L & \ell' & \ell\\ 0 & 0 & 0\end{pmatrix}^2 i^{\ell-\ell'}\\ &\times\left(\int dk k^2\left[\tilde{c}_L P^2(\mathbf{k}) + c_L\frac{2}{\bar{n}}P(\mathbf{k}) + \delta_{0L}\frac{1}{\bar{n}^2}\right]j_\ell(kr)j_{\ell'}(kr')\right).\end{aligned}$$

Integrating the last term with

$$\int_0^\infty dk k^2 k j_\ell(kr)j_{\ell'}(kr') = \delta_{\ell\ell'}\frac{\pi}{2r^2}\delta(r-r')\,,$$

and using $\begin{pmatrix}0 & \ell' & \ell\\ 0 & 0 & 0\end{pmatrix} = (-)^\ell\sqrt{1/(2\ell+1)}\delta_{\ell\ell'}$, we finally obtain

$$\begin{aligned}\mathrm{cov}^{(\xi)}_{\ell,\ell'}(r,r') = \frac{i^{\ell-\ell'}}{V}\Bigg[&\frac{(2\ell+1)}{2\pi\bar{n}^2r^2}\delta(r-r')\delta_{\ell\ell'} + \frac{1}{\bar{n}}\mathcal{G}_{\ell\ell'}(r,r',\bar{z})\sum_\sigma c_\sigma\begin{pmatrix}\ell & \ell' & \sigma\\ 0 & 0 & 0\end{pmatrix}^2\\ &+\mathcal{D}_{\ell\ell'}(r,r',\bar{z})\sum_\sigma\tilde{c}_\sigma\begin{pmatrix}\ell & \ell' & \sigma\\ 0 & 0 & 0\end{pmatrix}^2\Bigg],\end{aligned} \tag{4.101}$$

where $\mathcal{G}_{\ell\ell'}$ and $\mathcal{D}_{\ell\ell'}$ are given in eqs. (4.58) and (4.59). This is simply the continuum limit of eq. (4.56).

In order to find the corresponding expressions for $\Xi$ we integrate the result obtained for $\xi$ over the redshift interval with the weight given in (4.46). This is of course not very precise since it does not take into account the exact mean redshift of the points $\mathbf{x}$, $\mathbf{x}+\mathbf{r}$ and $\mathbf{x}'$, $\mathbf{x}'+\mathbf{r}'$, but these redshifts depend also on the directions of $\mathbf{r}$ and $\mathbf{r}'$ which would lead to very complicated expressions. Furthermore, since the covariance matrix is dominated by small distances, we expect only very minor changes which we neglect.

## 4.B $X^n_\ell$ and $Z^n_\ell$ list

The full list of $X^n_\ell$ is given (where $b_1 = b(z_1)$, $f_2 = f(z_2)$ etc.):

$$\begin{aligned}X^0_0\big|_{\mathrm{den}} &= b_1b_2\,,\\ X^0_0\big|_{\mathrm{rsd}} &= f_1f_2\frac{1+2\cos^2\theta}{15}\,,\\ X^0_2\big|_{\mathrm{rsd}} &= -\frac{f_1f_2}{21}\left[1+11\cos^2\theta+\frac{18\cos\theta(\cos^2\theta-1)\chi_1\chi_2}{r^2}\right],\end{aligned}$$

$$X_4^0\big|_{\rm rsd} = f_1 f_2 \left[ \frac{4(3\cos^2\theta - 1)(\chi_1^4 + \chi_2^4)}{35 r^4} + \chi_1\chi_2(3+\cos^2\theta)\frac{3(3+\cos^2\theta)\chi_1\chi_2 - 8(\chi_1^2+\chi_2^2)\cos\theta}{35 r^4} \right],$$

$$X_0^2\big|_{\rm d1} = \mathcal{H}_1\mathcal{H}_2 f_1 f_2 G_1 G_2 \frac{r^2\cos\theta}{3},$$

$$X_2^2\big|_{\rm d1} = -\mathcal{H}_1\mathcal{H}_2 f_1 f_2 G_1 G_2 \left( (\chi_2 - \chi_1\cos\theta)(\chi_1 - \chi_2\cos\theta) + \frac{r^2\cos\theta}{3} \right),$$

$$X_0^4\big|_{\rm d2} = (3 - f_{\rm evo1})(3 - f_{\rm evo2})\, r^4 \mathcal{H}_1^2\mathcal{H}_2^2 f_1 f_2,$$

$$X_0^4\big|_{\rm g1} = \frac{9\, r^4\Omega_m^2}{4a_1a_2}(1+G_1)(1+G_2)\mathcal{H}_0^4,$$

$$X_0^4\big|_{\rm g2} = \frac{9\, r^4\Omega_m^2}{4a_1a_2}(5s_1 - 2)(5s_2 - 2)\mathcal{H}_0^4,$$

$$X_0^4\big|_{\rm g3} = \frac{9\, r^4\Omega_m^2}{4a_1a_2}(f_1 - 1)(f_2 - 1)\mathcal{H}_0^4$$

$$X_0^0\big|_{\rm den\text{-}rsd} = \frac{b_1 f_2}{3},$$

$$X_2^0\big|_{\rm den\text{-}rsd} = -b_1 f_2 \left( \frac{2}{3} - (1-\cos^2\theta)\frac{\chi_1^2}{r^2} \right),$$

$$X_1^1\big|_{\rm den\text{-}d1} = -b_1 f_2 \mathcal{H}_2 G_2 (\chi_1\cos\theta - \chi_2),$$

$$X_0^2\big|_{\rm den\text{-}d2} = (3 - f_{\rm evo2})\, r^2 b_1 f_2 \mathcal{H}_2^2,$$

$$X_0^2\big|_{\rm den\text{-}g1} = -b_1 \frac{3\Omega_m}{2a_2}(1+G_2) r^2 \mathcal{H}_0^2,$$

$$X_0^2\big|_{\rm den\text{-}g2} = -b_1 \frac{3\Omega_m}{2a_2}(5s_2 - 2) r^2 \mathcal{H}_0^2,$$

$$X_0^2\big|_{\rm den\text{-}g3} = -b_1 \frac{3\Omega_m}{2a_2}(f_2 - 1) r^2 \mathcal{H}_0^2,$$

$$X_1^1\big|_{\rm rsd\text{-}d1} = f_1 f_2 \mathcal{H}_2 G_2 \frac{(1+2\cos^2\theta)\chi_2 - 3\chi_1\cos\theta}{5},$$

$$X_3^1\big|_{\rm rsd\text{-}d1} = f_1 f_2 \mathcal{H}_2 G_2 \frac{(1-3\cos\theta)\chi_2^3 + \cos\theta(5+\cos^2\theta)\chi_2^2\chi_1 - 2(2+\cos\theta^2)\chi_2\chi_1^2 + 2\chi_1^3\cos\theta}{5r^2},$$

$$X_0^2\big|_{\rm rsd\text{-}d2} = \frac{3 - f_{\rm evo2}}{3} f_1 f_2 r^2 \mathcal{H}_2^2,$$

$$X_2^2\big|_{\rm rsd\text{-}d2} = -(3 - f_{\rm evo2}) f_1 f_2 \mathcal{H}_2^2 \left( \frac{2}{3} r^2 - (1-\cos^2\theta)\chi_2^2 \right),$$

$$X_0^2\big|_{\rm rsd\text{-}g1} = -\frac{\Omega_m}{2a_2} f_1 (1+G_2) r^2 \mathcal{H}_0^2,$$

$$X_2^2\big|_{\rm rsd\text{-}g1} = \frac{3\Omega_m}{2a_2} f_1 (1+G_2)\mathcal{H}_0^2 \left( \frac{2}{3} r^2 - (1-\cos^2\theta)\chi_2^2 \right),$$

$$X_0^2\big|_{\rm rsd\text{-}g2} = -\frac{\Omega_m}{2a_2} f_1 (5s_2 - 2) r^2 \mathcal{H}_0^2,$$

$$X_2^2\big|_{\text{rsd-g2}} = \frac{3\Omega_m}{2a_2} f_1(5s_2-2)\mathcal{H}_0^2\left(\frac{2}{3}r^2 - (1-\cos^2\theta)\chi_2^2\right),$$
$$X_0^2\big|_{\text{rsd-g3}} = -\frac{\Omega_m}{2a_2} f_1(f_2-1)r^2\mathcal{H}_0^2,$$
$$X_2^2\big|_{\text{rsd-g3}} = \frac{3\Omega_m}{2a_2} f_1(f_2-1)\mathcal{H}_0^2\left(\frac{2}{3}r^2 - (1-\cos^2\theta)\chi_2^2\right),$$
$$X_1^3\big|_{\text{d1-d2}} = -(3-f_{\text{evo2}})\mathcal{H}_1\mathcal{H}_2^2 f_1 f_2\, r^2(\chi_2\cos\theta-\chi_1),$$
$$X_1^3\big|_{\text{d1-g1}} = \frac{3\Omega_m}{2a_2}\mathcal{H}_0^2\mathcal{H}_1 f_1(1+G_2)\, r^2(\chi_2\cos\theta-\chi_1),$$
$$X_1^3\big|_{\text{d1-g2}} = \frac{3\Omega_m}{2a_2}\mathcal{H}_0^2\mathcal{H}_1 f_1(5s_2-2)\, r^2(\chi_2\cos\theta-\chi_1),$$
$$X_1^3\big|_{\text{d1-g3}} = \frac{3\Omega_m}{2a_2}\mathcal{H}_0^2\mathcal{H}_1 f_1(f_2-1)\, r^2(\chi_2\cos\theta-\chi_1),$$
$$X_0^4\big|_{\text{d2-g1}} = -\frac{3(3-f_{\text{evo1}})\, r^4\Omega_m}{2a_2}\mathcal{H}_0^2\mathcal{H}_1^2 f_1(1+G_2),$$
$$X_0^4\big|_{\text{d2-g2}} = -\frac{3(3-f_{\text{evo1}})\, r^4\Omega_m}{2a_2}\mathcal{H}_0^2\mathcal{H}_1^2 f_1(5s_2-2),$$
$$X_0^4\big|_{\text{d2-g3}} = -\frac{3(3-f_{\text{evo1}})\, r^4\Omega_m}{2a_2}\mathcal{H}_0^2\mathcal{H}_1^2 f_1(f_2-1),$$
$$X_0^4\big|_{\text{g1-g2}} = \frac{9\, r^4\Omega_m^2}{4a_1a_2}\mathcal{H}_0^4(1+G_1)(5s_2-2),$$
$$X_0^4\big|_{\text{g1-g3}} = \frac{9\, r^4\Omega_m^2}{4a_1a_2}\mathcal{H}_0^4(1+G_1)(f_2-1),$$
$$X_0^4\big|_{\text{g2-g3}} = \frac{9\, r^4\Omega_m^2}{4a_1a_2}\mathcal{H}_0^4(5s_1-2)(f_2-1).$$

where

$$G(z) = \frac{\dot{\mathcal{H}}}{\mathcal{H}^2} + \frac{2-5s}{\chi\mathcal{H}} + 5s - f_{\text{evo}}. \tag{4.102}$$

The full list of $Z_\ell^n$ is given (note that inside the integral: $r = r(\lambda,\lambda')$ as defined in eqs. (4.75),(4.76)):

$$\begin{aligned} Z\big|_{\text{len}} = {} & \frac{9\Omega_m^2}{4}\mathcal{H}_0^4\frac{(2-5s_1)(2-5s_2)}{\chi_1\chi_2}\int_0^{\chi_1}d\lambda\int_0^{\chi_2}d\lambda'\frac{(\chi_1-\lambda)(\chi_2-\lambda')}{\lambda\lambda'}\frac{D_1(\lambda)D_1(\lambda')}{a(\lambda)a(\lambda')} \\ & \times\left\{\frac{2}{5}(\cos^2\theta-1)\lambda^2\lambda'^2 I_0^0(r) + \frac{4r^2\cos\theta\lambda\lambda'}{3}I_0^2(r)\right. \\ & + \frac{4\cos\theta\lambda\lambda'(r^2+6\cos\theta\lambda\lambda')}{15}I_1^1(r) + \frac{2(\cos^2\theta-1)\lambda^2\lambda'^2(2r^4+3\cos\theta r^2\lambda\lambda')}{7r^4}I_2^0(r) \\ & \left. + \frac{2\cos\theta\lambda\lambda'\left(2r^4+12\cos\theta r^2\lambda\lambda'+15(\cos^2\theta-1)\lambda^2\lambda'^2\right)}{15r^2}I_3^1(r)\right. \end{aligned}$$

$$+\frac{(\cos^2\theta-1)\lambda^2\lambda'^2\left(6r^4+30\cos\theta r^2\lambda\lambda'+35(\cos^2\theta-1)\lambda^2\lambda'^2\right)}{35r^4}I_4^0(r)\Bigg\},$$

$$Z\big|_{\mathrm{g4}}=9\Omega_m^2\mathcal{H}_0^4\frac{(2-5s_1)(2-5s_2)}{\chi_1\chi_2}\int_0^{\chi_1}d\lambda\int_0^{\chi_2}d\lambda'\frac{D_1(\lambda)D_1(\lambda')}{a(\lambda)a(\lambda')}r^4I_0^4(r)\,,$$

$$Z\big|_{\mathrm{g5}}=9\Omega_m^2\mathcal{H}_0^4G_1G_2\int_0^{\chi_1}d\lambda\int_0^{\chi_2}d\lambda'\frac{D_1(\lambda)D_1(\lambda')}{a(\lambda)a(\lambda')}\mathcal{H}(\lambda)\mathcal{H}(\lambda')(f(\lambda)-1)(f(\lambda')-1)r^4I_0^4(r)\,,$$

$$Z\big|_{\text{den-len}}=-\frac{3\Omega_m}{2}b_1\mathcal{H}_0^2\frac{2-5s_2}{\chi_2}D_1(z_1)\int_0^{\chi_2}d\lambda\frac{\chi_2-\lambda}{\lambda}\frac{D_1(\lambda)}{a(\lambda)}\Bigg\{2\chi_1\lambda\cos\theta I_1^1(r)$$
$$-\frac{\chi_1^2\lambda^2(1-\cos^2\theta)}{r^2}I_2^0(r)\Bigg\},$$

$$Z\big|_{\text{rsd-len}}=\frac{3\Omega_m}{2}f_1\mathcal{H}_0^2\frac{2-5s_2}{\chi_2}D_1(z_1)\int_0^{\chi_2}d\lambda\frac{\chi_2-\lambda}{\lambda}\frac{D_1(\lambda)}{a(\lambda)}\Bigg\{\frac{\lambda}{15}(\lambda-6\chi_1\cos\theta+3\lambda\cos2\theta)I_0^0(r)$$
$$-\lambda\frac{6\chi_1^3\cos\theta-\chi_1^2\lambda\left(9\cos^2\theta+11\right)+\chi_1\lambda^2\cos\theta(3\cos2\theta+19)-2\lambda^3(3\cos2\theta+1)}{21r^2}I_2^0(r)$$
$$-\frac{\lambda}{35r^4}\Bigg[-4\chi_1^5\cos\theta-\chi_1^3\lambda^2\cos\theta(\cos2\theta+7)+\chi_1^2\lambda^3\left(\cos^4\theta+12\cos^2\theta-21\right)$$
$$-3\chi_1\lambda^4\cos\theta(\cos2\theta-5)-\lambda^5(3\cos2\theta+1)+12\chi_1^4\lambda\Bigg]I_4^0(r)\Bigg\},$$

$$Z\big|_{\text{d1-len}}=\frac{3\Omega_m}{2}\mathcal{H}_0^2\mathcal{H}_1f_1G_1\frac{2-5s_2}{\chi_2}D_1(z_1)\int_0^{\chi_2}d\lambda\frac{\chi_2-\lambda}{\lambda}\frac{D_1(\lambda)}{a(\lambda)}$$
$$\times\Bigg\{2\lambda\frac{\cos\theta\left(\lambda^2-2\chi_1^2\right)+\chi_1\lambda(2\cos2\theta-1)}{15}I_1^1(r)+\frac{2}{3}r^2\lambda\cos\theta I_0^2(r)$$
$$-\lambda\frac{4\chi_1^4\cos\theta-\chi_1^3\lambda\left(\cos^2\theta+9\right)+\chi_1^2\lambda^2\cos\theta\left(\cos^2\theta+5\right)-2\chi_1\lambda^3(\cos2\theta-2)-2\lambda^4\cos\theta}{15r^2}I_3^1(r)\Bigg\},$$

$$Z\big|_{\text{d2-len}}=-\frac{3\Omega_m}{2}(3-f_{\mathrm{evo1}})f_1\mathcal{H}_1^2\mathcal{H}_0^2\frac{2-5s_2}{\chi_2}D_1(z_1)\int_0^{\chi_2}d\lambda\frac{\chi_2-\lambda}{\lambda}\frac{D_1(\lambda)}{a(\lambda)}\Bigg\{2\chi_1\lambda r^2\cos\theta I_1^3(r)$$
$$-\chi_1^2\lambda^2(1-\cos^2\theta)I_2^2(r)\Bigg\},$$

$$Z\big|_{\text{g1-len}}=\frac{9\Omega_m^2}{4}(1+G_1)\mathcal{H}_0^4\frac{2-5s_2}{\chi_2}D_1(z_1)\int_0^{\chi_2}d\lambda\frac{\chi_2-\lambda}{\lambda}\frac{D_1(\lambda)}{a(\lambda)}\Bigg\{2\chi_1\lambda r^2\cos\theta I_1^3(r)$$
$$-\chi_1^2\lambda^2(1-\cos^2\theta)I_2^2(r)\Bigg\},$$

$$Z\Big|_{\text{g2-len}} = \frac{9\Omega_m^2}{4}(5s_1-2)\mathcal{H}_0^4\frac{2-5s_2}{\chi_2}D_1(z_1)\int_0^{\chi_2}d\lambda\frac{\chi_2-\lambda}{\lambda}\frac{D_1(\lambda)}{a(\lambda)}\Big\{2\chi_1\lambda r^2\cos\theta I_1^3(r)$$
$$-\chi_1^2\lambda^2(1-\cos^2\theta)I_2^2(r)\Big\},$$

$$Z\Big|_{\text{g3-len}} = \frac{9\Omega_m^2}{4}(f_1-1)\mathcal{H}_0^4\frac{2-5s_2}{\chi_2}D_1(z_1)\int_0^{\chi_2}d\lambda\frac{\chi_2-\lambda}{\lambda}\frac{D_1(\lambda)}{a(\lambda)}\Big\{2\chi_1\lambda r^2\cos\theta I_1^3(r)$$
$$-\chi_1^2\lambda^2(1-\cos^2\theta)I_2^2(r)\Big\},$$

$$Z\Big|_{\text{g4-len}} = \frac{9\Omega_m^2}{2}\mathcal{H}_0^4\frac{(2-5s_1)(2-5s_2)}{\chi_1\chi_2}\int_0^{\chi_1}d\lambda\int_0^{\chi_2}d\lambda'\frac{\chi_2-\lambda'}{\lambda'}\frac{D_1(\lambda)D_1(\lambda')}{a(\lambda)a(\lambda')}\Big\{2\lambda\lambda' r^2\cos\theta I_1^3(r)$$
$$-\lambda^2\lambda'^2(1-\cos^2\theta)I_2^2(r)\Big\},$$

$$Z\Big|_{\text{g5-len}} = \frac{9\Omega_m^2}{2}\mathcal{H}_0^4G_1\frac{2-5s_2}{\chi_2}\int_0^{\chi_1}d\lambda\int_0^{\chi_2}d\lambda'\mathcal{H}(\lambda)(f(\lambda)-1)\frac{\chi_2-\lambda'}{\lambda'}\frac{D_1(\lambda)D_1(\lambda')}{a(\lambda)a(\lambda')}\Big\{2\lambda\lambda' r^2\cos\theta I_1^3(r)$$
$$-\lambda^2\lambda'^2(1-\cos^2\theta)I_2^2(r)\Big\},$$

$$Z\Big|_{\text{den-g4}} = -3\Omega_m\mathcal{H}_0^2b_1\frac{2-5s_2}{\chi_2}D_1(z_1)\int_0^{\chi_2}d\lambda\frac{D_1(\lambda)}{a(\lambda)}r^2I_0^2(r)\,,$$

$$Z\Big|_{\text{den-g5}} = -3\Omega_m\mathcal{H}_0^2b_1G_2D_1(z_1)\int_0^{\chi_2}d\lambda\mathcal{H}(\lambda)(f(\lambda)-1)\frac{D_1(\lambda)}{a(\lambda)}r^2I_0^2(r)\,,$$

$$Z\Big|_{\text{rsd-g4}} = 3\Omega_m\mathcal{H}_0^2f_1\frac{2-5s_2}{\chi_2}D_1(z_1)\int_0^{\chi_2}d\lambda\frac{D_1(\lambda)}{a(\lambda)}\left\{\left(\frac{2r^2}{3}+(\cos^2\theta-1)\lambda^2\right)I_2^2(r)-\frac{r^2}{3}I_0^2(r)\right\},$$

$$Z\Big|_{\text{rsd-g5}} = 3\Omega_m\mathcal{H}_0^2f_1G_2D_1(z_1)\int_0^{\chi_2}d\lambda\mathcal{H}(\lambda)(f(\lambda)-1)\frac{D_1(\lambda)}{a(\lambda)}\left\{\left(\frac{2r^2}{3}+(\cos^2\theta-1)\lambda^2\right)I_2^2(r)-\frac{r^2}{3}I_0^2(r)\right\},$$

$$Z\Big|_{\text{d1-g4}} = 3\Omega_m\mathcal{H}_0^2\mathcal{H}_1f_1\frac{2-5s_2}{\chi_2}D_1(z_1)\int_0^{\chi_2}d\lambda\frac{D_1(\lambda)}{a(\lambda)}\Big\{r^2(\lambda\cos\theta-\chi_1)I_1^3(r)\Big\},$$

$$Z\Big|_{\text{d1-g5}} = 3\Omega_m\mathcal{H}_0^2\mathcal{H}_1f_1G_2D_1(z_1)\int_0^{\chi_2}d\lambda\mathcal{H}(\lambda)(f(\lambda)-1)\frac{D_1(\lambda)}{a(\lambda)}\Big\{r^2(\lambda\cos\theta-\chi_1)I_1^3(r)\Big\},$$

$$Z\Big|_{\text{d2-g4}} = -3\Omega_m\mathcal{H}_0^2(3-f_{\text{evo1}})f_1\mathcal{H}_1^2\frac{2-5s_2}{\chi_2}D_1(z_1)\int_0^{\chi_2}d\lambda\frac{D_1(\lambda)}{a(\lambda)}r^4I_0^4(r)\,,$$

$$Z\big|_{\text{d2-g5}} = -3\Omega_m\mathcal{H}_0^2(3-f_{\text{evo1}})f_1\mathcal{H}_1^2G_2D_1(z_1)\int_0^{\chi_2}d\lambda\mathcal{H}(\lambda)(f(\lambda)-1)\frac{D_1(\lambda)}{a(\lambda)}r^4I_0^4(r)\,,$$

$$Z\big|_{\text{g1-g4}} = \frac{9\Omega_m^2}{2a_1}\mathcal{H}_0^4(1+G_1)\frac{2-5s_2}{\chi_2}D_1(z_1)\int_0^{\chi_2}d\lambda\frac{D_1(\lambda)}{a(\lambda)}r^4I_0^4(r)\,,$$

$$Z\big|_{\text{g1-g5}} = \frac{9\Omega_m^2}{2a_1}\mathcal{H}_0^4(1+G_1)G_2D_1(z_1)\int_0^{\chi_2}d\lambda\mathcal{H}(\lambda)(f(\lambda)-1)\frac{D_1(\lambda)}{a(\lambda)}r^4I_0^4(r)\,,$$

$$Z\big|_{\text{g2-g4}} = \frac{9\Omega_m^2}{2a_1}\mathcal{H}_0^4(5s_1-2)\frac{2-5s_2}{\chi_2}D_1(z_1)\int_0^{\chi_2}d\lambda\frac{D_1(\lambda)}{a(\lambda)}r^4I_0^4(r)\,,$$

$$Z\big|_{\text{g2-g5}} = \frac{9\Omega_m^2}{2a_1}\mathcal{H}_0^4(5s_1-2)G_2D_1(z_1)\int_0^{\chi_2}d\lambda\mathcal{H}(\lambda)(f(\lambda)-1)\frac{D_1(\lambda)}{a(\lambda)}r^4I_0^4(r)\,,$$

$$Z\big|_{\text{g3-g4}} = \frac{9\Omega_m^2}{2a_1}\mathcal{H}_0^4(f_1-1)\frac{2-5s_2}{\chi_2}D_1(z_1)\int_0^{\chi_2}d\lambda\frac{D_1(\lambda)}{a(\lambda)}r^4I_0^4(r)\,,$$

$$Z\big|_{\text{g3-g5}} = \frac{9\Omega_m^2}{2a_1}\mathcal{H}_0^4(f_1-1)G_2D_1(z_1)\int_0^{\chi_2}d\lambda\mathcal{H}(\lambda)(f(\lambda)-1)\frac{D_1(\lambda)}{a(\lambda)}r^4I_0^4(r)\,,$$

$$Z\big|_{\text{g4-g5}} = 9\Omega_m^2\mathcal{H}_0^4G_2\frac{2-5s_1}{\chi_1}\int_0^{\chi_1}d\lambda\int_0^{\chi_2}d\lambda'\mathcal{H}(\lambda')(f(\lambda')-1)\frac{D_1(\lambda)D_1(\lambda')}{a(\lambda)a(\lambda')}r^4I_0^4(r)\,.$$

# CHAPTER 5

## Correlation function III: The 2nd feature

**Based on:**

[292] V. Tansella "*On the $2^{nd}$ feature of the matter two-point function*"
**Phys.Rev. D97** (2018) 10, [arXiv:1804.05826].

**Abstract.** In this chapter we point out the existence of a second feature in the matter two-point function, besides the acoustic peak, due to the baryon-baryon correlation in the early universe and positioned at twice the distance of the peak. We discuss how the existence of this feature is implied by the well-known heuristic argument that explains the baryon bump in the correlation function. A standard $\chi^2$ analysis to estimate the detection significance of the second feature is mimicked. We conclude that for realistic values of the baryon density, an SKA-like galaxy survey will not be able to detect this feature with a standard correlation function analysis.

## 5.1 Introduction

The main subject of this thesis is the two-point function of galaxies. It is one of the most important probes of the large scale structures (LSS) of the universe and measurements of the two-point function (2pF) have been reported by different collaborations in the past years [197, 115, 17, 179, 31, 20]. In the future, upcoming redshift surveys will probe the LSS of the universe at deeper redshift and for larger volumes [203, 216], with unprecedented precision.

With these surveys we can nicely link late-time measurements to early-time physics. The most striking example are the acoustic oscillations in the primordial plasma – first predicted

in [288, 287, 242] – which leave their imprint on cosmological observables. Their measurement is considered as one of the most important successes of the ΛCDM model. In the cosmic microwave background, the scale of the baryon acoustic oscillations (BAO) is a probe of the sound horizon at decoupling and it manifests itself as a series of peaks in the angular spectrum [11]. A similar feature can also be seen in the matter power spectrum [227], while, in the 2pF, the same physics is responsible for a single peak located at a comoving distance slightly bigger – as we will explain in section 5.2 – than the sound horizon at decoupling.

The BAO peak in the correlation function has been first measured in [137]. Since then it has been systematically used as a standard ruler to probe the distance-redshift relation [57, 61, 25], in order to constrain the cosmic expansion history [140]. The peak is also sensitive to other cosmological parameters [305, 44, 42, 43]. A complication arises as the position of the peak measured with data cannot be fitted with linear theory: non-linearities affect both the position and the shape of the BAO feature [141, 110, 280, 223, 308, 29].

Here we consider a second feature: a trough in the correlation function positioned at twice the distance of the peak. The existence of this feature is implied by the well-known heuristic argument that is commonly used to explain the BAO peak (see section 5.2), but never mentioned in the literature. In section 5.3 we mimic the fitting procedure – used by galaxy surveys to measure the peak position – to study the expected detection significance of the second feature for an SKA-like survey.

## 5.2 The $2^{\text{nd}}$ feature

We outline in this section the heuristic argument given in the seminal paper [141] and summarized in the review [40]. This will give us insight on how this argument implies a second feature in the correlation function. The technical foundations can be found in [38, 39, 234].

Let us focus on some initial over-dense point in the primordial plasma – when baryons are tightly coupled to photons via Thomson scattering. If the fluctuations are adiabatic the over-density will be shared by all species: in particular a region over-dense in photons will also have an over-pressure with respect to its surroundings. This pressure imbalance causes an acoustic wave in the baryon-photon plasma which travels at the speed of sound $c_s$ until baryons decouple from the photons. When this happens the baryon's speed of sound goes to zero and the wave is frozen: the initial over-density is now composed only of dark matter while baryons have created an over-dense spherical region around the initial point. Every over-density will behave as we just described and the net result is that matter is more likely to cluster with a correlation length corresponding to the sound horizon at decoupling. It is clear that this process, as we have already anticipated, is responsible for the BAO peak: according to our discussion in section 3.1, the correlation function is defined as the excess probability (over Poisson noise) of finding two tracers separated by a comoving distance $s$

and hence it peaks for $s \sim s_{\rm hor}$, where the comoving sound horizon is defined as

$$s_{\rm hor} = \int_0^{t_{\rm drag}} dt\, c_s(t)(1+z)\,. \tag{5.1}$$

and $t$ is cosmic time. The end of the Compton drag epoch $t_{\rm drag}$ is the time at which the baryons are released from the drag of photons. It is the moment at which the baryons velocity decouples from the photons. Baryons decoupling takes place at a later time than photon-decoupling, roughly at $z_{\rm drag} \simeq 100$. In fact, even if radiation decoupling epoch is $z \simeq 1100$, the mean-free path of electrons and photons is given respectively by $\ell_e = (\sigma_T n_\gamma)^{-1}$, $\ell_\gamma = (\sigma_T n_e)^{-1}$, where $\sigma_T$ is the Thomson cross-section and $n_{e,\gamma}$ the energy densities. As $n_\gamma \gg n_e$ we have $\ell_e \ll \ell_\gamma$ and the scattering rate of electrons is sufficient to keep the baryons temperature $T_b$ equal to radiation temperature $T_\gamma$ down to redshifts $z_{\rm drag}$. One must however be careful to solve eq. (5.1) analytically up to $z_{\rm drag}$ as the tight-coupling approximation fails below $z \simeq 850$, where $s_{\rm hor}$ essentially stops to grow since the baryons sound speed drops dramatically. Here we do not solve for $s_{\rm hor}$ analytically but using the Boltzmann code CLASS [66].

If we go back to our idealistic picture of a dark matter perturbation surrounded by a spherical shell of baryons we see that the correlation will not only be enhanced at $s_{\rm hor}$ but, as all the baryons are in the shell, we will also get a trough when the correlation length reaches the diameter of the shell: $2s_{\rm hor}$. In other words – in our idealized picture – as long as the correlation length is $< 2s_{\rm hor}$ the baryon-baryon correlation contributes to the matter 2pF as it is always likely to 'find' two baryons in the shell. On the other hand, when the correlation length reaches the diameter of the shell, the baryon-baryon contribution has a sharp trough. This $2^{\rm nd}$ feature (2FT) is illustrated in figure 5.1: we can clearly see the drop in the 2pF at $2s_{\rm hor}$ for high values of $\Omega_b$, while the feature is less pronounced when baryons contribute less to the energy-density budget.

One might notice that, even in linear theory, the position of the acoustic peak is not exactly centered on $s_{\rm hor}$: this is a known effect due to imperfect baryon-photon coupling, which allows photons to diffuse out of the perturbation and drag the baryons with them[1], and velocity overshoot – both discussed in detail in [270]. Note that the dark matter over-density does not remain at the center of the shell as it is gravitationally bound to the outgoing species, this does however not change the position of the peak. Despite these complications the peak is an extremely interesting cosmological observable as it is sensitive to a range of cosmological parameters. For example $s_{\rm hor}$ is directly related to the sound speed $c_s$ via eq. (5.1) which, in turn, is related to the $\Omega_b$ and $\Omega_\gamma$ ratio. The positions of the features are also sensitive to the expansion history prior to decoupling as the propagation time of the sound wave depends on the expansion rate, introducing for example a subtle dependence on $\Omega_\nu$ (see [298] for a comprehensive treatment). Finally, measuring the positions of the features as a function of redshift – using them as statistical standard rulers – constrains the late-time expansion rate and gives informations on $\Omega_m$, $\Omega_\Lambda$ and the equation of state of dark energy $w$.

[1] In Fourier– and angular– space this effect is responsible for the *Silk damping*.

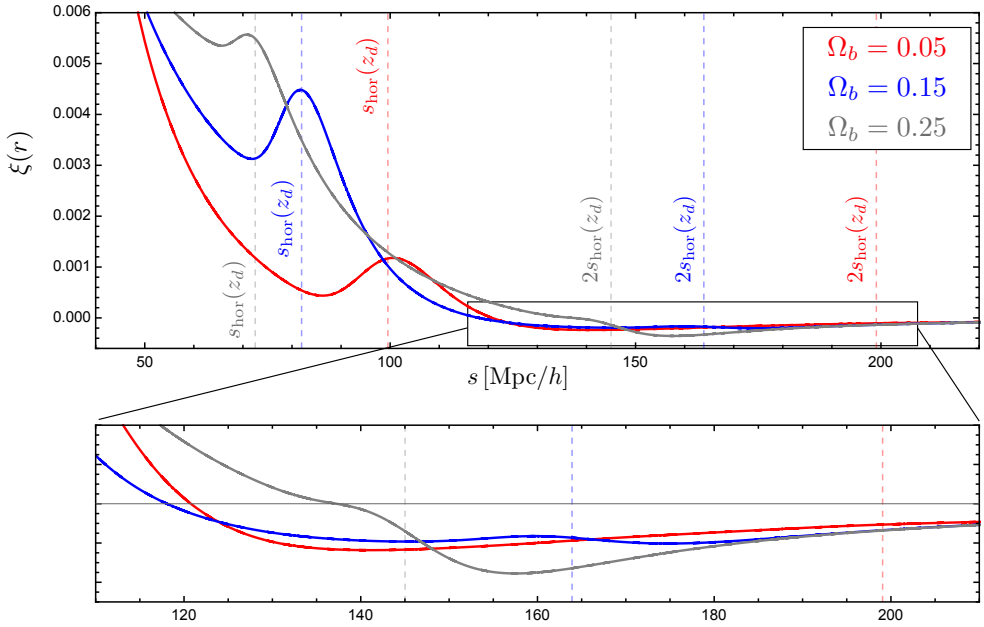


Figure 5.1: The angle-averaged matter correlation function at $\bar{z} = 1$ for three different cosmologies with $\Omega_b = 0.25$ (gray), $\Omega_b = 0.15$ (blue) and $\Omega_b = 0.05$ (red). The total matter density is fixed to $\Omega_m = 0.31$ and the sound horizon at the drag epoch for the different models is shown.

We could naively think that, since we are searching for a feature at twice the separation of the BAO peak, we are safe from non-linear effects at these very large scales. This is only partially correct. Non-linear effects on the BAO peak come in two aspects: a broadening of the feature and a shift of the peak position. The damping effect is easily understood in real space, where non-linear physics can move the tracers around, on the scale of $\sim 10\,$Mpc, pulling them out of the $100\,$Mpc$/h$ shell and hence broadening the peak feature [223]. In Fourier space this effect is responsible for the smoothing of the subsequent peaks in the power spectrum (see e.g. [28]). The fact that we are looking at two galaxies at a distance where linear physics should give an adequate description is not important in this case: the local non-linearities around the two tracers have an observable (and important) effect. For this reason we expect the 2FT to suffer from the same non-linear correction to its shape as it is not protected from non-linear broadening. We stick to the linear description of the 2pF in this work where the feature is sharper and therefore we will overestimate the detection significance in section 5.3. This does not change our conclusions. On the other hand, in order to induce a shift in the position of the feature, non-linear physics has to coherently and systematically move tracers separated by $s_{\rm hor}$ or $2s_{\rm hor}$ either closer or further away from each other. The small shift of the BAO peak has been widely investigated [280, 120, 32, 29, 238, 63] and in this sense the fact the 2FT is located at larger scales means it will be less affected, as the position is only sensible to non-linear effects at the $\sim 200\,$Mpc$/h$ scale.

**Fourier space**

Let us now discuss how the simple picture depicted in this section is translated in Fourier space[2]. The matter transfer function can be written as

$$S_D(k) = f_{\rm cdm} S_{\rm cdm}(k) + f_b S_b(k)\,, \tag{5.2}$$

where $f_{\rm cdm} = \Omega_{\rm cdm}/\Omega_m$, $f_b = \Omega_b/\Omega_m$ and we drop the redshift-dependence here. $S_{\rm cdm}$ is the smooth contribution of cold dark matter to the transfer function while $S_b \sim \sin(s_{\rm hor}k)$ contains the 'sine-wave' oscillations of the BAO (note that $S_{\rm cdm}$ and $S_b$ are intended as contributions to the matter transfer function at late time but they are no transfer functions themselves). The power spectrum is then proportional to

$$k^3 P(k) \sim f_{\rm cdm}^2 S_{\rm cdm}^2 + 2 f_{\rm cdm} f_b S_{\rm cdm} S_b + f_b^2 S_b^2\,. \tag{5.3}$$

For $f_b \ll f_{\rm cdm}$ the last term is subdominant and $P(k)$ has the familiar shape of a superposition of a smooth function and a 'sine-wave'. On the other hand for $f_b \gtrsim f_{\rm cdm}$ the squared oscillations start to dominate, increasing both the frequency of the BAO and their amplitude (see fig. 5.2). When we Fourier transform to obtain the 2pF, the 'sine-wave' part of $P(k)$ contributes to the BAO peak while the 'sine-square' part from $S_b^2$ is responsible for the feature at twice the peak distance as it oscillates with twice the frequency. Hence, also in Fourier space, bigger values of $f_b$ correspond to a more pronounced 2FT.

## 5.3 Fitting Methodology

We now want to gain insight on the ability of galaxy surveys to detect the second feature in the matter two-point function. The procedure to detect the BAO peak is now well-established (as described in [314] and used e.g. in [217]) and we follow it here for the 2FT. The BAO detection is usually quoted as the $\chi^2$ difference between the best fit model and the model with no features. In other words we study how reliably we can reject a no-feature model. We do not deal with real data here but generate a fake 'data' vector $\boldsymbol{\xi}$ from our fiducial model and compute the $\chi^2$ from the standard definition

$$\chi^2_{\rm fit}(\alpha) = (\boldsymbol{\xi}_{\rm fit}(\alpha) - \boldsymbol{\xi})^{\rm T} \mathbf{C}^{-1} (\boldsymbol{\xi}_{\rm fit}(\alpha) - \boldsymbol{\xi})\,, \tag{5.4}$$

where $\mathbf{C}$ is the covariance matrix for the fiducial model, which we have computed in section 4.2.3. The quantity $\alpha$ is the scale dilatation parameter which measures the position of the feature (being the BAO peak or the 2FT) with respect to the fiducial model. In real data analyses $\alpha$ is a measure of

$$\alpha = \frac{D_V(z) s_{*,\rm fid}}{D_V^{\rm fid}(z) s_*} \tag{5.5}$$

[2]This argument is discussed in `https://www.cfa.harvard.edu/~deisenst/acousticpeak/spherical_acoustic.pdf`: a short but vey nice essay which, to our knowledge, is the only place where the 2FT is briefly mentioned for the purely-baryonic case.

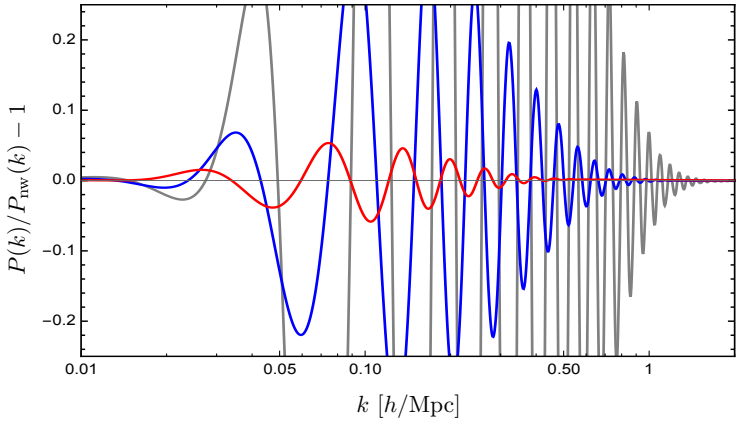


Figure 5.2: The residual BAO oscillations $P(k)/P_{\rm nw}(k) - 1$ once the broadband shape is factored out with the no-wiggle power spectrum $P_{\rm nw}$, defined in eq. (5.14). Color coding as in fig. 5.1.

where the subscript 'fid' means 'fiducial', $s_*$ is the comoving position of the feature and $D_V$ is the spherically averaged[3] distance defined as

$$D_V(z) = \left[cz(1+z)D_A^2(z)\mathcal{H}(z)\right]^{1/3} . \tag{5.6}$$

The parameter $\alpha$ is the measurement of the 2FT scale in the sense that it characterises any observed shift in the relative position of the acoustic feature in the data versus the model. The value of $\alpha$ which minimises $\chi^2$ is related to the feature position via eq. (5.5), and the feature position roughly marks $2s_{\rm hor}$.

In this work the fiducial model is generated starting from the linear matter power spectrum $P(k)$ obtained from CLASS (multiplied by the large-scale galaxy bias $b^2(z)$) and converted into the full-sky correlation function [294] using the COFFE [295] code[4]. To mimic most BAO analyses we include the effect of redshift-space distortion in the 2pF but neglect other relativistic effects (such as lensing and the Doppler effect). We also neglect non-linear damping[5] and set the streaming scale to zero as our fiducial model – from which we draw data – is fully linear. To improve the signal-to-noise, galaxy surveys measure the spherically averaged two-point function $\xi_0(r)$ (the monopole) and the quadrupole $\xi_2(r)$ defined as

$$\xi_\ell(r) = \frac{2\ell+1}{2}\int d\mu\, \xi(r,\mu)\mathcal{P}_\ell(\mu)\,, \tag{5.7}$$

[3]Note that in real data situations both the angle averaged parameter $\alpha$ and an additional parameter $\varepsilon$ are considered: $\varepsilon$ parametrises the anisotropic clustering due to redshift-space distortions and due to an analysis where an incorrect cosmology is assumed.

[4]Available at `https://github.com/JCGoran/coffe`.

[5]We also do not consider a Gaussian damping term which is commonly introduced in the Fourier transform $P(k) \to \xi(r)$ to improve numerical convergence as the COFFE code is based on the very reliable 2-FAST algorithm [162].

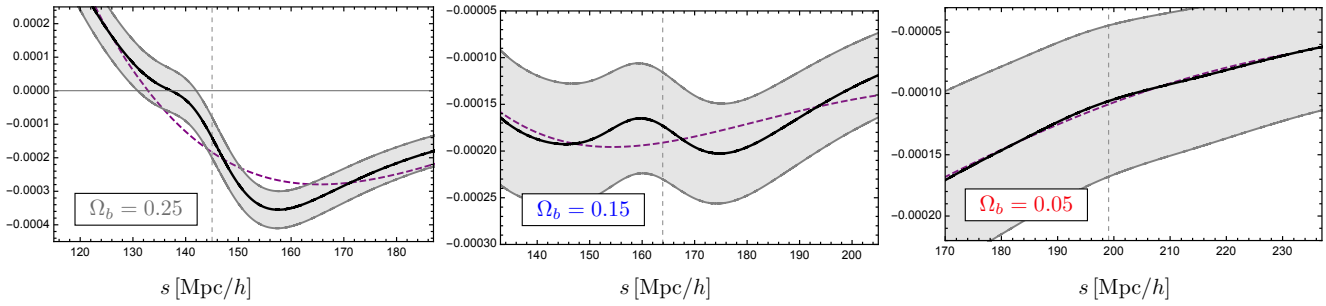


Figure 5.3: A zoom of fig. 5.1 for the range used in the $\Delta\chi^2$ estimation, where the 2$^{\text{nd}}$ feature is clearly visible for high-baryon models. The gray region marks the error bars given by the covariance for an SKA-like survey and the purple dashed line is the best-fit non BAO (de-wiggled) model.

where $\mathcal{P}_\ell$ is the Legendre polynomial of degree $\ell$ and $\mu$ is the orientation with respect to the line of sight at which we measure the 2pF. Our data vector is then given by

$$\boldsymbol{\xi} = \begin{pmatrix} \boldsymbol{\xi}_0 \\ \boldsymbol{\xi}_2 \end{pmatrix} . \tag{5.8}$$

Fake 'data' are generated for three different cosmologies: the fiducial *Planck2015*[6] cosmology and two unrealistic toy models with $\Omega_b = 0.25$ and $\Omega_b = 0.15$ – keeping $\Omega_m$ and all the other parameters fixed – to illustrate the procedure in models where the 2FT is more pronounced. The binning of the data vectors ($\boldsymbol{\xi}_0$ and $\boldsymbol{\xi}_2$) is chosen in a range of $\sim 75\,\mathrm{Mpc}/h$ around the value $2s_{\mathrm{hor}}$ for each fiducial model and with a bin size $L_p = 3\,\mathrm{Mpc}/h$, for 25 bins in total. The covariance matrix is computed for an SKA-like survey, with parameters taken from [88] (Table 3). We consider a single redshift-bin centred at $\bar{z} = 1$ with thickness $\Delta z = 0.2$, sky-coverage $f_{\mathrm{sky}} \simeq 0.72$, mean number density $\bar{n} \simeq 8.7 \times 10^{-4}\,\mathrm{Mpc}^{-3}$ and bias $b \simeq 1.3$. Given our data vector in eq. (5.8) the covariance is written as

$$\mathbf{C} = \begin{pmatrix} \mathbf{cov}_{00} & \mathbf{cov}_{02} \\ \mathbf{cov}_{20} & \mathbf{cov}_{22} \end{pmatrix} , \tag{5.9}$$

where $\mathbf{cov}_{\ell\ell',ij} = \mathrm{cov}^{(\xi)}_{\ell\ell'}(x_i, x_j)$, defined in eq. (4.56).

### Fitting models

To fit the correlation function we adopt two template models, one with the BAO peak and the 2FT and the other with no baryonic features. The fit is performed, as in recent BAO data analyses, with 5 parameters: a multiplicative bias $B$, the scale dilatation $\alpha$ and (as we

[6] We set $h = 0.676$, $\Omega_{\mathrm{cdm}} = 0.26$, $\Omega_b = 0.048$, $\Omega_\Lambda = 0.68$. The primordial spectrum has $n_s = 0.96$ and $A_s = 2.22 \times 10^{-9}$ at $k_{\mathrm{pivot}} = 0.05\,\mathrm{Mpc}^{-1}$ .

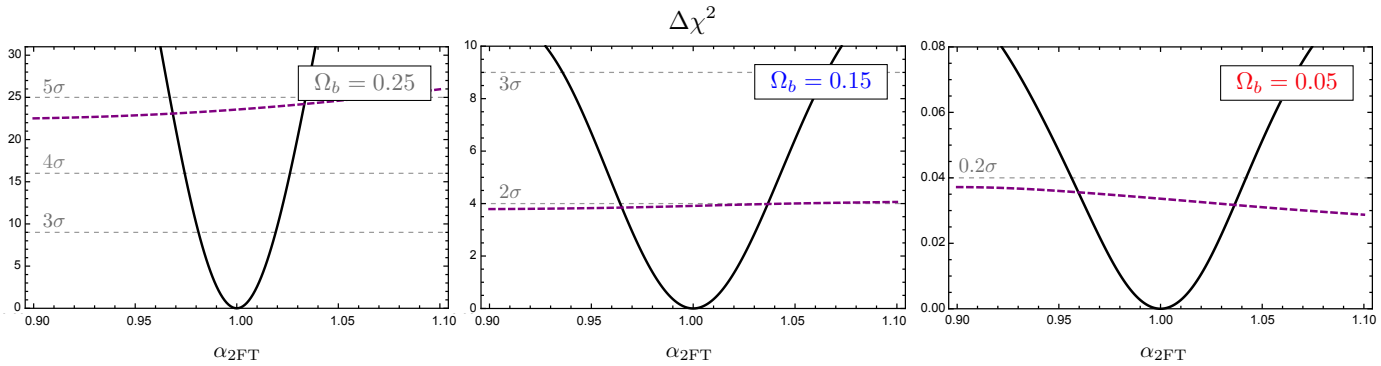


Figure 5.4: The $\Delta\chi^2(\alpha) = \chi^2(\alpha) - \chi^2_{\rm min}$ as a function of the BAO-parameter $\alpha_{2FT}$. The solid line is the model of eq. (5.12) while the dashed curve displays the same information for a no BAO model (eq. (5.15)), where $\Delta\chi^2$ is determined by subtracting the minimum $\chi^2_{\rm min}$ from the BAO model.

are only interested in the position of the 2FT) a $2^{\rm nd}$ order polynomial to marginalise over the broad-band shape of the multipoles. We then write

$$\begin{aligned} \xi_0^{\rm fit}(r) &= B^2\xi_0^{\rm mod}(\alpha, r) + A_0(r)\,, \\ \xi_2^{\rm fit}(r) &= \xi_2^{\rm mod}(\alpha, r) + A_2(r)\,, \end{aligned} \tag{5.10}$$

where we define

$$A_\ell(r) = \frac{a_{1,\ell}}{r^2} + \frac{a_{2,\ell}}{r} + a_{\ell,3} \quad ;\ \ell = 0, 2\,, \tag{5.11}$$

with three nuisance parameters per multipole $(a_1, a_2, a_3)$, to account for the overall unknown shape of the correlation function. A difference with the standard approach is that we set here $B = 1$ for two reasons. Firstly, as we are not dealing with real data, we have full control on the linear bias parameter when we generate fake data from our fiducial model. Secondly we are not comparing different cosmologies (for which the amplitude of the feature might change) but the same cosmology with and without the feature. This also prevents the data to be fitted only by the quadratic polynomial $A_\ell$.

The first template model is simply given by

$$\xi_\ell^{\rm mod}(\alpha, r) = \xi_\ell^{\rm fid}(\alpha r)\,. \tag{5.12}$$

Note that when performing the BAO analysis in real space, it is standard practice to shift the all model as in eq. (5.12). A different approach is usually employed in the Fourier space analysis where only the BAO oscillations are shifted. As the nuisance parameters $a_{i,\ell}$ are marginalizing over the broadband shape of the multipoles, this has no effect [26].

The second template is the *de-wiggled* model. It is a phenomenological prescription widely used in BAO analysis: it consists in generating a correlation function starting from a power

spectrum $P_{\rm nw}(k)$ in which the BAO features have been erased. To obtain $P_{\rm nw}(k)$ we start with the Eisenstein&Hu [138, 139] approximated power spectrum $P_{\rm EH}(k)$ and perform a Gaussian smoothing on the ratio $P(k)/P_{\rm EH}(k)$:

$$P_{\rm nw}(k) = P_{\rm EH}(k)\,\mathcal{S}[P(k)/P_{\rm EH}(k)]\,, \tag{5.13}$$

where $\mathcal{S}$ schematically represents the smoothing. The no-wiggle spectrum is then given by [308]

$$\frac{P_{\rm nw}(10^{k_{log}})}{P_{\rm EH}(10^{k_{log}})} = \frac{1}{\sqrt{2\pi}\lambda}\int dq_{log}\left[\frac{P(10^{q_{log}})}{P_{\rm EH}(10^{q_{log}})}{\rm Exp}\left(-\frac{1}{2\lambda^2}(k_{log}-q_{log})^2\right)\right], \tag{5.14}$$

where $\lambda$ is a parameter that controls the size of the smoothing. We found the best results for $\lambda = 0.14\,{\rm Mpc}/h$. In figure 5.2 we plot the fractional difference of the no-wiggle power spectrum and the linear one. The multipoles of the correlation function with no feature $\xi_\ell^{\rm nw}(r)$ are then generated by feeding COFFE with $P_{\rm nw}$ and the second template model is given by

$$\xi_\ell^{\rm mod}(\alpha, r) = \xi_\ell^{\rm nw}(\alpha r)\,. \tag{5.15}$$

For every value of $\alpha$ we fit the remaining parameters to minimise the $\chi^2$ for both models. We chose only one fiducial redshift $z = 1$, hence we require the size of the redshifts bin of the survey to be $\Delta z \gtrsim 0.2$. We focus here only on one redshift bin as the shape of the correlation function is nearly constant at large scales for the depth accessible by galaxy surveys and the analysis is trivially extended to more bins, given also the fact that we can treat them as uncorrelated to a good approximation (see e.g. the analysis we perform in section 4.3). In figure 5.3 we show the fiducial model monopole $\xi_0^{\rm fid}(r)$ with the error bars obtained from eq. (4.56), together with the best fit no-feature model of eq. (5.15). Clearly as $\Omega_b$ decreases the feature is less and less pronounced and the no-feature model is an increasingly better fit to the data. For a realistic model with $\Omega_b \simeq 0.05$ the 2FT is barely visible and lies completely within the error bars. This situation is reflected when we compare the $\Delta\chi^2(\alpha) = \chi^2(\alpha) - \chi^2_{\rm min}$ for the two templates. We can read off the detection significance for the 2FT in fig. 5.4. In the two toy models – with an unrealistically high baryon fraction – the no-feature templates are disfavored at $\sim 5\sigma$ and $\sim 2\sigma$ respectively. The realistic model *Planck2015* shows no preference for the template which correctly describes the 2FT compared to the smoothed template. We have checked that these results marginally change when we vary the order of the polynomial fit in eq. (5.11). Note that the no-BAO model has a broad $\chi^2$ as the lack of features makes the scale less constrainable.

## 5.4 Conclusions

In this chapter we have introduced a second feature in the matter correlation function. This feature, positioned at twice the distance of the BAO peak, is understood – in the early universe – as a trough in the baryon-baryon correlation for separations bigger than twice the sound horizon at $t_{\rm drag}$. The feature is clearly visible in models with an high baryon fraction but in a realistic cosmological model it is a very small effect. We proved this with a $\chi^2$ analysis that

showed how – in an SKA-like survey – it is not possible to distinguish between the models with and without the feature. We have considered only one redshift bin and it is possible to increase the detection significance by a factor $\sim \sqrt{N}$ by considering $N$ bins; however, the analysis requires $\Delta z_{\rm bin} \gtrsim 0.2$ hence limiting the number of bins $N$ in which we can split a galaxy catalog. Furthermore, the fact that at $2s_{\rm hor}$ the error is cosmic variance dominated suggests that the two-point function is not the best observable to detect this feature.

In a Fourier space analysis the effect described here is correctly modeled if the template $P(k)$ is generated from a Boltzmann code such as CLASS [66, 125] or CAMB [207].

It is nevertheless interesting to study if other observable – e.g. intensity mapping – are more sensitive to this feature which, if detected, would provide an additional probe for early-time cosmology. We leave this matter for future work.

# CHAPTER 6

## Correlation function IV: Anisotropic signal

**Based on:**

[293] V. Tansella, C. Bonvin, G. Cusin, R. Durrer, M. Kunz and I. Sawicki "*Redshift-space distortions from vector perturbations II: Anisotropic signal*"
**submitted for publication**, [arXiv:1807.00731].

**Abstract.** In this chapter we study the impact on the galaxy correlation function of the presence of a vector component in the tracers' peculiar velocities, in the case in which statistical isotropy is violated. We present a general framework – based on the bipolar spherical harmonics expansion – to study this effect in a model independent way, without any hypothesis on the origin or the properties of these vector modes. We construct six new observables, that can be directly measured in galaxy catalogs in addition to the standard monopole, quadrupole and hexadecapole, and we show that they completely describe any deviations from isotropy. We then perform a Fisher analysis in order to quantify the constraining power of future galaxy surveys. As an example, we show that SKA2 would be able to detect anisotropic rotational velocities with amplitudes as low as 1% of that of the vorticity generated during shell-crossing in standard dark matter scenarios.

## 6.1 Introduction

Mechanisms such as topological defects [133, 114, 211], magnetic fields [132], inflation with vector fields [153, 160], or vector-field-based models of modified gravity [187, 328, 177, 297], the shell-crossing present in concordance cosmology, but also non-linear effects (as discussed e.g. in chapter 2) can generate vector perturbations throughout the history of the Universe and on a wide range of scales. It is important to properly characterize the signature of these

vector degrees of freedom on the observables of large scale galaxy surveys. The reason for this is twofold. On the one hand, the presence of such vector perturbations – if not properly taken into account – will 'pollute' (i.e. bias) the measurement of the scalar degrees of freedom and act as a source of systematic error. On the other hand vector degrees of freedom can leave their imprint on observables which, in turn, can be used to constrain their properties and to study the mechanism that generated them.

Various approaches exist in the literature with the aim of constraining vector-type deviations of the metric and they have mostly focused on the Cosmic Microwave Background (CMB). They can be grouped into three categories: (i) introducing dynamical vector degrees of freedom in the early universe while maintaining isotropy and homogeneity at the background level. Then, one can either maintain statistical isotropy and homogeneity of the perturbations or allow for statistically anisotropic perturbations [210, 237]. Alternatively (ii), one can deform the isotropy of the cosmological background and therefore constrain its anisotropy, while keeping the matter content standard, making sure that this anisotropy decays with time [266]. Finally (iii), one can introduce an anisotropy directly in the primordial power spectrum (through some interactions in the early universe, e.g. [5, 36]). One then tries to look for 'anomalies' in the CMB, such as in, for example, [13]. Signatures of this primordial signal in galaxy surveys have been analyzed in [248, 190, 278, 285].

Additionally, late time non-linear evolution, as simulated in N-body codes, is found to generate vector perturbations of both the metric [7, 8] and the fluid vorticity [247, 189]. It is interesting to develop statistical tools to measure these vector modes, which are present also in standard ΛCDM cosmology, and to distinguish them, e.g. from an intrinsic, global anisotropy.

In [74] the authors considered the impact of statistically isotropic vector modes in the peculiar velocity field of galaxies and in particular on the redshift-space distortion (RSD) observed in galaxy surveys. We have found that vector contributions to RSD enter in the monopole, quadrupole and hexadecapole of the galaxy correlation function. While the impact of vector perturbations from topological defects is very small, those from non-linear clustering affect especially the hexadecapole quite strongly, contributing up to 20% of the total signal on scales smaller than $5h^{-1}$Mpc. This additional contribution should in principle be detectable with next generation surveys, such as Euclid or the SKA.

In this chapter we consider a vector component of the peculiar velocities, which violates statistical isotropy, and study its impact on the galaxy correlation function. This is a natural generalization of the study in [74]. We present a general framework suitable specifically to study this effect, with no assumptions on the origin or properties of these vector modes. We show that the anisotropic signal can be completely characterised by six new observables, that can be directly extracted from galaxy catalogs. General results regarding the Fisher analysis of these types of models are also discussed. We investigate the detectability of these contributions, for a specific example, with planned or futuristic galaxy surveys.

In particular we want to develop tests of statistical isotropy using large-scale structure (LSS) observations. While it is clear that our Universe is not strongly anisotropic, a small anisotropy is still compatible with, if not favoured by the analysis of CMB anisotropies and polarisation [13]. This might be due to e.g. a small global magnetic field or some slight

anisotropy which remained after inflation. In this work we do not make assumptions on the model responsible for the global anisotropy in the vector sector but we want to investigate its observational consequences. We study the situation where scalar perturbations are still statistically isotropic but vector perturbations are not. It will be interesting not only to study whether LSS also favours a slight anisotropy of the Universe but whether the characteristics of any such anisotropy are in agreement with the one of the CMB. Furthermore, LSS observations allow for a tomographic approach, i.e. we can observe many different redshifts, making it easier to overcome limitations from cosmic variance.

This chapter is structured as follows: In section 6.2 we detail the general anisotropic structure of vector perturbations. In 6.3 we study the effects of a vector component in the velocity field on the two-point function and present a suitable decomposition to describe it. Finally, in section 6.4, we forecast the constraints on the anisotropic parameters for upcoming clustering surveys.

## 6.2 Vector Contribution to Galaxy Velocities

We assume here that our Universe shows signs of a violation of statistical isotropy, manifesting itself by the presence of vector modes in the peculiar velocity of tracers. We investigate how galaxy catalogs can be used, independently from other probes, to constrain the amplitude of these anisotropies. We therefore model our Universe as a perturbed Friedman-Lemaître universe, with a metric given by eq. (2.50):

$$\mathrm{d}s^2 = a^2\Big[-(1+2\Psi)\mathrm{d}\eta^2 - S_i\mathrm{d}\eta\mathrm{d}x^i + (1-2\Phi)\mathrm{d}x_i\mathrm{d}x^i\Big]. \tag{6.1}$$

Here $\Phi$ and $\Psi$ are the standard Newtonian-gauge scalar potentials, and $S_i$ is a pure vector fluctuation, $\partial_i S^i = 0$, related to frame dragging[1]. We define $\mathcal{H} = \dot{a}/a = aH$ to be the conformal Hubble parameter.

The general velocity field for galaxies located at position $\mathbf{x}$ at conformal time $\eta$, $v^i(\mathbf{x},\eta)$, can be decomposed into a scalar (potential) part, $v$, and a pure vector part, $\Sigma^i$, with $\partial_i\Sigma^i = 0$,

$$v^i \equiv \partial^i v + \Sigma^i\,. \tag{6.2}$$

The gauge-invariant relativistic vorticity [131] can be obtained by lowering the index of $\Sigma^i$ with the perturbed metric. The relativistic vorticity is often denoted $\Omega_i$ (e.g. in [215, 131] and chapter 2) and it is an additional rotational velocity on top of the frame-dragging effect. We also denote it by $\Omega_i \equiv g_{ij}\Sigma^j/a = a\delta_{ij}(\Sigma^j - S^j)$.[2] We mainly concentrate on $\Sigma^i$ as it is the velocity with an upper index that is relevant for us and we use the notation $\Sigma_i = \delta_{ij}\Sigma^j \equiv \Sigma^i$.

We assume that galaxies move on time-like geodesics of the metric, i.e. they obey the Euler equation. Then, to first order in perturbation theory we can write, for perfect fluids, eq. (2.32):

$$\dot{\Sigma}_i - \dot{S}_i + \mathcal{H}(\Sigma_i - S_i) = 0\,, \tag{6.3}$$

[1] We have fixed the gauge such that the $0i$ component of the metric has no scalar contribution and the vector part of the $ij$ component vanishes. We also neglect gravitational waves (tensor perturbations).

[2] The difference between $a\Sigma^j$ and $\Omega_j$ is only relevant on large scales.

which is equivalent to $\partial_\eta \Omega_i = 0$. Hence vorticity is conserved. This is not only true within linear perturbation theory but also in full General Relativity as long as matter can be described as a perfect fluid [215]. The $0i$ component of the energy momentum tensor of a perfect fluid is given by

$$T^i_{0\,(V)} = \left[(\rho + P)v^i\right]_{(V)} = T^i_0 - T^i_{0\,(S)} \,. \tag{6.4}$$

Taking the curl of this equation the scalar part vanishes and we obtain

$$\begin{aligned} \epsilon_{ijk}(T^j_0)_{,k} &= \epsilon_{ijk}\left[(\rho + P)v^j\right]_{,k} \\ &= \left(\mathbf{v} \wedge \boldsymbol{\nabla}(\rho + P)\right)_i + (\rho + P)(\boldsymbol{\nabla} \wedge \mathbf{v})_i \,. \end{aligned} \tag{6.5}$$

Only the vector velocity $\Sigma^j$ contributes to the second term, while the first term is non-vanishing when the gradient of the density fluctuations in not parallel to the velocity. This also happens in perfect fluids at second order in perturbation theory, see e.g. [8]. At second order therefore, despite vorticity conservation, vector perturbations of the metric are generated, which induce effects like frame dragging. It has been shown recently [189] that the vector potential found in relativistic numerical simulations is actually mainly due to the first term of (6.5) and not to vorticity which is also induced in N-body simulations.

The perfect fluid description is just an approximation when we want to describe the motion of dark matter (or galaxies). In the real Universe, dark matter particles are free-streaming, i.e. they move on geodesics. As soon as shell crossing occurs, velocity dispersion can no longer be neglected and vorticity is generated. In [113], the vorticity generation from large-scale structure was modelled by including velocity dispersion using a perturbative approach.

Clearly, even if in the standard ΛCDM model vector perturbations are generated by non-linearities, they are statistically isotropic. In this work we assume that the vectorial part of the peculiar velocity in eq. (6.2) acquires an anisotropic component.

### 6.2.1 Tensor structure of vector perturbations

In order to compute the two-point correlation function of galaxies, we need a model for the two-point auto-correlation of the vector velocity, $\langle \Sigma_i \Sigma_j \rangle$ and its cross-correlation with the dark matter overdensity $\langle \delta_{\rm m} \Sigma_i \rangle$. We will characterise their structure in Fourier space:

1. The auto-correlation of the vector field takes the general form

$$\left\langle \Sigma_i(\mathbf{k}) \Sigma_j(\mathbf{k}') \right\rangle = (2\pi)^3 \delta^{(3)}(\mathbf{k} + \mathbf{k}') \left[ W_{ij}(\mathbf{k}) P_\Sigma(k) + i\alpha_{ij}(\mathbf{k}) P_A(k) \right] , \tag{6.6}$$

where $P_\Sigma(k)$ and $P_A(k)$ contain information about the amplitude of the vector field. The Dirac delta function appearing in the above equation, $\delta^{(3)}(\mathbf{k}+\mathbf{k}')$, is a consequence of statistical homogeneity, and if we assume that scalar spectra are isotropic, the amplitudes, $P_\Sigma(k)$ and $P_A(k)$, depend on $\mathbf{k}$ only through its absolute value $k \equiv |\mathbf{k}|$. One might think it would be more natural for an anisotropic spectrum to show an anisotropy also in $P_\Sigma(\mathbf{k})$. However, in a real observation, the power spectrum is usually obtained by averaging the squared Fourier modes over directions. Here we mimic this by considering $P_\Sigma$ and $P_A$ to be functions of the modulus $k$ only. In practice, these are the direction averaged spectra. For scalar perturbations, this averaging removes all signs of

an anisotropy, for vector perturbations this is, interestingly, not the case as we show in this chapter.

The tensors $W_{ij}$ and $\alpha_{ij}$ are, respectively, symmetric and anti-symmetric tensors, that encode the dependence on direction. Since $\Sigma_i$ is a pure vector field, $W_{ij}$ and $\alpha_{ij}$ must satisfy $k^i W_{ij} = k^j W_{ij} = k^i \alpha_{ij} = k^j \alpha_{ij} = 0$. The $P_A$-term is parity odd while the $P_\Sigma$-term is parity even. If no parity violating processes occur in the Universe we may set $P_A = 0$. The tensorial form for $\alpha_{ij}$ is completely fixed by anti-symmetry and transversality,

$$\alpha_{ij} = \alpha \varepsilon_{ijm} \hat{k}^m \,. \tag{6.7}$$

The most general form for $W_{ij}$ is then

$$W_{ij} = \frac{\omega}{2}\left(\delta_{ij} - \hat{k}_i \hat{k}_j\right) + \omega^A_{ij} \,, \tag{6.8}$$

where we have decomposed the tensor into its trace $\omega$ and trace-free part

$$\omega^A_{ij} = \omega_{ij} - \omega_{il}\hat{k}^l \hat{k}_j - \omega_{lj}\hat{k}^l \hat{k}_i + \omega_{lm}\hat{k}^l \hat{k}^m \hat{k}_i \hat{k}_j \,, \tag{6.9}$$

with $\omega^i_i = 0$. As usual $\hat{\mathbf{k}}$ denotes the unit vector in the direction of the vector $\mathbf{k}$. The first term of (6.8) respects statistical homogeneity and isotropy, whereas the second one is non-zero only when isotropy is violated. In what follows, we absorb the trace $\omega$ into the normalisation of the power spectrum $P_\Sigma$ in eq. (6.6). Note that in general the isotropic and anisotropic contribution do not need to have the same amplitude $P_\Sigma(k)$: in this sense one can use $\omega(k)$ to parametrise the difference between $P_\Sigma^{(\mathrm{iso})}$ and $P_\Sigma^{(\mathrm{ani})}$. Interestingly, the only possible parity odd term given in (6.7) is statistically isotropic.

The symmetric tensor $\omega_{ij}$ can be diagonalised or, equivalently, decomposed into a sum of the tensor products of its orthonormal eigenvectors $\hat{\omega}^I_i$,

$$\omega_{ij} = \sum_{I=1}^{3} \lambda_I \hat{\omega}^I_i \hat{\omega}^I_j \,, \tag{6.10}$$

where the eigenvalues satisfy $\sum_I \lambda^I = 0$.

2. The cross-correlation with dark matter can be non-zero only if statistical isotropy is violated. Assuming that the vector field is fluctuating in some fixed direction $\hat{\boldsymbol{\omega}}$, the cross-correlation takes the form

$$\left\langle \delta(\mathbf{k}) \Sigma_i(\mathbf{k}') \right\rangle = (2\pi)^3 W_i P_{\delta\Sigma}(k) \delta^{(3)}(\mathbf{k} + \mathbf{k}') \,, \tag{6.11}$$

where $W_i$ is transverse since $\Sigma_i$ is a pure vector field i.e. divergence free. A non-vanishing $\langle \delta \Sigma_i \rangle$ always defines a preferred spatial direction $\hat{\omega}_i$ and therefore violates statistical isotropy.

## 6.3 Correlation function

Galaxy number counts are observed in redshift-space, rather than in real-space. The leading correction arising from the fact that we observe on the light-cone is the Kaiser term, or redshift-space distortion [200], which is included in the number counts $\Delta_g$ as

$$\Delta_g(\mathbf{x}) = \delta_{\rm g}(\mathbf{x}) - \frac{1}{\mathcal{H}} n^i \partial_i (n^j v_j(\mathbf{x}))\,.$$

Here $\delta_g$ is the tracer's density perturbation, related to the dark matter density perturbation via the bias expansion $\delta_g \simeq b\cdot\delta_c + ...$, and $v_i$ is the peculiar velocity field. We have also defined the line-of-sight direction $\mathbf{n}$ as

$$\mathbf{n} \equiv \frac{\mathbf{x}}{\chi}\,,$$

i.e. the unit vector in the direction of the galaxy lying at $\mathbf{x} = \chi(z)\mathbf{n}$, with the observer located at $\mathbf{x} = 0$. Splitting the velocity into the scalar and vector parts, as in eq. (6.2), we have

$$\Delta_g(\mathbf{x}) = \delta_{\rm g}(\mathbf{x}) - \frac{1}{\mathcal{H}} n^i n^j \big(\partial_i\partial_j v(\mathbf{x}) + \partial_i \Sigma_j(\mathbf{x})\big)\,. \tag{6.12}$$

The effects of vector perturbations in the general relativistic number counts were derived in [192] and studied in detail in chapter 2, where we found that – akin to scalar perturbations – redshift-space distortion and (at high redshift) lensing are the dominant effects. Since in the relativistic angular power spectra, $C_\ell(z_1, z_2)$, the light-cone effects cannot easily be extracted, we study here the impact of the vector modes on the two-point correlation function of galaxies.

The two-point correlation function is defined as

$$\xi(\mathbf{x}_1, \mathbf{x}_2, z_1, z_2) = \langle \Delta_g(\mathbf{x}_1, z_1)\Delta_g(\mathbf{x}_2, z_2)\rangle\,.$$

Without redshift-space distortion, and neglecting subdominant evolution effects, the correlation function depends only on the galaxies' separation

$$r \equiv |\mathbf{x}_1 - \mathbf{x}_2|\,,$$

and on the mean distance of the pair from the observer $\bar\chi = \frac{1}{2}(\chi_1 + \chi_2)$ or, equivalently, its mean redshift $\bar z = \frac{1}{2}(z_1 + z_2)$. Redshift-space distortion introduces an additional dependence on the orientation of the pair with respect to the line-of-sight $\mathbf{n}$ (we work in the small angle or flat-sky limit where we neglect the difference between the line-of-sight to $\mathbf{x}_1$ and $\mathbf{x}_2$). It is customary to expand $\xi$ in a basis of Legendre polynomials so that, in the flat-sky approximation, $\mathbf{n}_1 = \mathbf{n}_2 = \mathbf{n}$ we can write

$$\xi(\bar z, \mathbf{r}, \mathbf{n}) = \sum_\ell \xi_\ell(\bar z, r)\mathcal{P}_\ell(\mu)\,, \tag{6.13}$$

where $\mathcal{P}_\ell$ is the Legendre polynomial of degree $\ell$ and $\mu = \mathbf{n}\cdot\hat{\mathbf{r}}$, with $\hat{\mathbf{r}}$ being the direction of the vector connecting the two galaxies.

Let us now review the standard flat-sky expression for the correlation function in the presence of scalar perturbations (see e.g. [294] for details). We will use this result both

for comparison with the vector case and to compute our covariance matrix in section 6.4. Including the Kaiser term we write

$$\xi^{\rm iso}_{\rm (s)}(\bar{z}, r, \mu) = c_0(\bar{z}) I^0_0(\bar{z}, r) - c_2(\bar{z}) I^0_2(\bar{z}, r)\mathcal{P}_2(\mu) + c_4(\bar{z}) I^0_4(\bar{z}, r)\mathcal{P}_4(\mu)\,. \tag{6.14}$$

We can identify the multipole coefficients in eq. (6.13) as

$$\xi_\ell(r, \bar{z}) = i^\ell c_\ell(\bar{z}) I^0_\ell(\bar{z}, r)\,. \tag{6.15}$$

Following the notation of this thesis, we have also used the definition (4.27):

$$I^0_\ell(\bar{z}, r) = \int \frac{{\rm d}k}{2\pi^2}\, k^2 P(\bar{z}, k) j_\ell(kr)\,, \tag{6.16}$$

together with the coefficients given in eq. (4.33)-(4.35):

$$c_0 = b^2 + \frac{2}{3}bf + \frac{f^2}{5}\,, \tag{6.17}$$

$$c_2 = \frac{4}{3}bf + \frac{4}{7}f^2\,, \tag{6.18}$$

$$c_4 = \frac{8}{35}f^2\,. \tag{6.19}$$

Here $j_n$ is the $n$-order spherical Bessel function, $f$ is the growth rate, $f \equiv d\ln D_1/d\ln a$ (with $D_1$ being the linear growth function), and $P(\bar{z}, k)$ is the matter power spectrum at redshift $\bar{z}$. We have made the standard assumption that the galaxy bias $b$ is deterministic and, like the growth rate $f$ in ΛCDM, it is scale independent.

We now turn to the study of the vector component. We split the vector contribution to the correlation function into a statistically isotropic and anisotropic part

$$\xi_{\rm (v)} = \xi^{\rm iso}_{\rm (v)} + \xi^{\rm ani}_{\rm (v)}\,, \tag{6.20}$$

where we have emphasised that the source of violation of statical isotropy comes from the vector sector. First, we summarise the structure of the isotropic contributions to the correlation function coming from vector perturbations and we then propose a general framework to compute the anisotropic part.

The new vector contribution to the correlation function in eq. (6.20) comprises three terms:

1. Cross-correlation with the density
2. Cross-correlation with the scalar velocity
3. Auto-correlation.

The first two vanish in flat sky since they are odd under $\mathbf{n} \to -\mathbf{n}$ and $\xi$ is evidently even, see chapter 4. Hence combining eqs. (6.12) and (6.3) we write

$$\xi_{\rm (v)} = \frac{1}{\mathcal{H}(z_1)\mathcal{H}(z_2)} \int \frac{{\rm d}^3k}{(2\pi)^3} k^2 (\mathbf{n}_1\cdot\hat{\mathbf{k}})(\mathbf{n}_2\cdot\hat{\mathbf{k}}) W_{ij}(\hat{\mathbf{k}}) n_1^i n_2^j P_\Sigma(k) e^{i\mathbf{k}\cdot\mathbf{r}}\,.$$

This object has a complicated tensor structure, which characterises the anisotropy of the vector field. However, when isotropy is assumed we simply write $W_{ij} = \delta_{ij} - \hat{k}_i\hat{k}_j$, so that, see [74],

$$\xi^{\rm iso}_{\rm (v)} = \frac{1}{\mathcal{H}^2}\int \frac{{\rm d}^3k}{(2\pi)^3}k^2(\mathbf{n}\cdot\hat{\mathbf{k}})^2\big(1+(\mathbf{n}\cdot\hat{\mathbf{k}})^2\big)P_\Sigma(k)e^{i\boldsymbol{k}\cdot\boldsymbol{x}}\,.$$

Rewriting the $\mathbf{n}\cdot\hat{\mathbf{k}}$ contributions in terms of Legendre polynomials and integrating over the direction of $\mathbf{k}$, we obtain for the isotropic contribution [74]

$$\xi^{\rm iso}_{\rm (v)}(\bar{z},r,\mu) = \frac{2}{15}\mathcal{P}_0(\mu)C_0^\Sigma(r) - \frac{2}{21}\mathcal{P}_2(\mu)C_2^\Sigma(r) - \frac{8}{35}\mathcal{P}_4(\mu)C_4^\Sigma(r)\,, \tag{6.21}$$

with

$$C_\ell^\Sigma(r) = \frac{1}{2\pi^2}\frac{1}{\mathcal{H}^2}\int {\rm d}k\, k^4 P_\Sigma(k) j_\ell(kr)\,. \tag{6.22}$$

The $C_\ell^\Sigma$ are the vector equivalent of the $I_\ell^n$: to avoid heavy notation we set $\mathcal{H}^{-2}I_\ell^{0,\Sigma} = C_\ell^\Sigma$. Notice here the extra $k^2$ factor multiplying $P_\Sigma$, which is absorbed in the scalar case when the velocity power spectrum is re-expressed in terms of the density power spectrum.

Statistically isotropic vector perturbations modify the shape of the multipoles coefficients in the Legendre expansion of $\xi$. One can estimate this effect and study its detectability. This was the strategy followed in [74]. In the anisotropic case however, the standard multipole expansion fails to capture the additional angular dependence encoded in $W_{ij}$. In the next section we therefore consider the decomposition of this dependence into bipolar spherical harmonics (BipoSH).

### 6.3.1 Statistically anisotropic contribution

When statistical isotropy is violated, the correlation function is no longer only a function of $\mu = \mathbf{n}\cdot\hat{\mathbf{r}}$. Therefore, the standard expansion in Legendre polynomials does not properly describe the angular dependence of $\xi$. The correlation function can however be expanded in terms of the orthonormal set of bipolar spherical harmonics (see appendix B.4). Since this approach captures an arbitrary angular dependence of the observable under consideration, it has been used in cosmology to analyse CMB [167, 168, 37, 249, 112, 78] and LSS [175, 172, 290, 291, 240, 52, 278, 36, 285] data.

In the small angle approximation the correlation function depends on two directions $\xi(\mathbf{n},\mathbf{r})$, we hence expand

$$\xi(\mathbf{r},\mathbf{n},\bar{z}) = \sum_{\ell\ell' JM}\xi^{JM}_{\ell\ell'}(x,\bar{z})X^{JM}_{\ell\ell'}(\hat{\mathbf{r}},\mathbf{n})\,, \tag{6.23}$$

with

$$\begin{aligned} X^{JM}_{\ell\ell'}(\hat{\mathbf{r}},\mathbf{n}) &= \{Y_\ell(\hat{\mathbf{r}})\otimes Y_{\ell'}(\mathbf{n})\}_{JM} \\ &= \sum_{mm'}\mathbf{C}^{JM}_{\ell m\ell' m'}Y_{\ell m}(\hat{\mathbf{r}})Y_{\ell' m'}(\mathbf{n})\,, \end{aligned} \tag{6.24}$$

where $\mathbf{C}^{JM}_{\ell m\ell' m'}$ are the Clebsch Gordan coefficients which are related to the Wigner 3j symbols by,

$$\mathbf{C}^{JM}_{\ell m\ell' m'} = (-)^{\ell-\ell'+M}\sqrt{2J+1}\begin{pmatrix}\ell & \ell' & J\\ m & m' & -M\end{pmatrix}. \tag{6.25}$$

In other words, $X^{JM}_{\ell\ell'}(\hat{\mathbf{r}},\mathbf{n})$ isolates the total angular momentum $J$ and helicity $M$ contribution. The useful property of the BipoSH $X^{JM}_{\ell\ell'}$ is that they filter the isotropic signal into the $J=0$ mode and any non-zero coefficient with $J>0$ indicates anisotropy. In fact, if there is no anisotropic signal in the power spectrum, i.e. if $\xi$ depends on $\mathbf{n}$ only via $\mu=\hat{\mathbf{r}}\cdot\mathbf{n}$, we can compute the coefficients via

$$\xi^{JM}_{\ell\ell'} = \int d\Omega_{\mathbf{n}}\int d\Omega_{\mathbf{r}}\,\xi(\mathbf{r},\mathbf{n},\bar{z})X^{JM*}_{\ell\ell'}\,, \tag{6.26}$$

and we simply obtain

$$\xi^{JM}_{\ell\ell'}(r,\bar{z}) = \frac{4\pi}{\sqrt{2\ell+1}}\xi_\ell(r,\bar{z})\delta_{J,0}\delta_{M,0}\delta_{\ell,\ell'}\,, \tag{6.27}$$

recovering the expansion of eq. (6.13). In particular, we see that no off-diagonal component is generated (we have $\ell=\ell'$) and that all the isotropic signal is contained in the $J=0$ coefficient. On the other hand if anisotropy is included we will generate $J\geq 1$ and $\ell\neq\ell'$ modes. Therefore, to search for anisotropy we only look at the $J\geq 1$ modes, and we set $\xi=\xi^{\rm ani}_{\rm (v)}$ in the expansion of eq. (6.23).

We focus on the computation of the statistically anisotropic contribution to the galaxy correlation function (6.3). To this end, it is useful to compute the anisotropic contribution to the power spectrum of (6.3) and then Fourier transform it. Explicitly, the Fourier transformation of galaxy number counts in the Kaiser approximation, eq. (6.3), is given by

$$\langle\tilde{\Delta}_g(\mathbf{k},\mathbf{n},\bar{z})\tilde{\Delta}_g(\mathbf{k}',\mathbf{n},\bar{z})\rangle = (2\pi)^3 P_g(\mathbf{k},\mathbf{n},\bar{z})\,\delta(\mathbf{k}+\mathbf{k}')\,, \tag{6.28}$$

where the power spectrum is given by (omitting the dependence on $\mathbf{n},\bar{z}$)

$$\begin{aligned}P_g(\mathbf{k}) &= P^{\rm iso}_{\rm (s)} + P^{\rm iso}_{\rm (v)} + P^{\rm ani}_{\rm (v)}\\ &= \left(b+f(\mathbf{n}\cdot\hat{\mathbf{k}})^2\right)^2 P_{\delta\delta}(k) - \frac{k^2}{\mathcal{H}^2}\omega(\mathbf{n}\cdot\hat{\mathbf{k}})^2(1-(\mathbf{n}\cdot\hat{\mathbf{k}})^2)P_\Sigma(k)\\ &\quad - \frac{k^2}{\mathcal{H}^2}(\mathbf{n}\cdot\hat{\mathbf{k}})^2\hat{n}^i\hat{n}^j\omega^A_{ij}P_\Sigma(k)\,,\end{aligned} \tag{6.29}$$

where all the isotropic contribution is in the first line and the anisotropic one, $P^{\rm ani}_{\rm (v)}$, is in the second line. The tensor $\omega^A_{ij}$ is defined in eq. (6.9). The isotropic contribution depends on directions only through the angle between the mode $\mathbf{k}$ and the line-of-sight, i.e. it can be expanded in a basis of Legendre polynomials as

$$P^{\rm iso}(\mathbf{k},\mathbf{n},\bar{z}) = \sum_\ell p_\ell(k,\bar{z})\mathcal{P}_\ell(\mathbf{n}\cdot\hat{\mathbf{k}})\,. \tag{6.30}$$

We observe that this is not a specific property of redshift-space distortions but simply a consequence of statistical isotropy. Hence eq. (6.30) holds for all the relativistic contributions to the galaxy number counts.

When statistical isotropy is violated, we expand the power spectrum in terms of the orthonormal set of bipolar spherical harmonics, as

$$P^{\rm ani}_{\rm (v)}(\mathbf{k},\mathbf{n},\bar{z}) = \sum_{\ell\ell' JM} \pi^{JM}_{\ell\ell'}(\bar{z},k) X^{JM}_{\ell\ell'}(\hat{\mathbf{k}},\mathbf{n})\,, \tag{6.31}$$

where

$$X^{JM}_{\ell\ell'}(\hat{\mathbf{k}},\mathbf{n}) = \sum_{mm'} \mathbf{C}^{JM}_{\ell m\ell' m'} Y_{\ell m}(\hat{\mathbf{k}}) Y_{\ell' m'}(\mathbf{n})\,. \tag{6.32}$$

In the case where there is not anisotropic signal in the power spectrum, the coefficients $\pi^{JM}_{\ell\ell'}$ simply reduce to

$$\pi^{JM}_{\ell\ell'} = \frac{4\pi}{\sqrt{2\ell+1}} p_\ell(k)\delta_{J,0}\delta_{M,0}\delta_{\ell,\ell'}\,, \tag{6.33}$$

and we recover the expansion of eq. (6.30). For convenience, we can split the anisotropic contribution to the power spectrum (6.29) in three contributions

$$P^{\rm ani}_{\rm (v)}(\mathbf{k}) = -\frac{k^2}{\mathcal{H}^2}(\mathbf{n}\cdot\hat{\mathbf{k}})^2 \hat{n}^i\hat{n}^j\omega^A_{ij} P_\Sigma(k) = P^{\rm (a)}(\mathbf{k}) + P^{\rm (b)}(\mathbf{k}) + P^{\rm (c)}(\mathbf{k}) \tag{6.34}$$

where we have separated the three cases:

(a) $\omega^A_{ij} = \omega_{ij}$ ,

(b) $\omega^A_{ij} = -\omega_{il}\hat{k}^l\hat{k}_j - \omega_{lj}\hat{k}^l\hat{k}_i$ ,

(c) $\omega^A_{ij} = \omega_{lm}\hat{k}^l\hat{k}^m\hat{k}_i\hat{k}_j$ ,

so that

$$P^{\rm ani}_{\rm (v)}(\mathbf{k},\mathbf{n},\bar{z}) = \sum_{\ell\ell' JM} \left(\pi^{JM({\rm a})}_{\ell\ell'} + \pi^{JM({\rm b})}_{\ell\ell'} + \pi^{JM({\rm c})}_{\ell\ell'}\right) X^{JM}_{\ell\ell'}(\hat{\mathbf{k}},\mathbf{n})\,. \tag{6.35}$$

Note that this splitting has no direct physical interpretation: each contribution has a scalar component which however disappears in the sum of eq. (6.35). These contributions can be written in terms of the eigenvectors and eigenvalues $\hat{\omega}^I$ and $\lambda_I$. After a long but straightforward computation we find

$$\pi^{JM({\rm a})}_{\ell\ell'} = -\frac{16\pi^{3/2}}{45}\frac{k^2}{\mathcal{H}^2}P_\Sigma(k)\sum_I \lambda_I Y^*_{2M}(\hat{\omega}_I)\left(\delta_{\ell,0}\delta_{\ell',2} + 2\sqrt{\frac{2\ell'+1}{5}}\begin{pmatrix}2 & 2 & \ell'\\ 0 & 0 & 0\end{pmatrix}\delta_{\ell,2}\right)\delta_{J,2}\,, \tag{6.36}$$

$$\begin{aligned}\pi^{JM({\rm b})}_{\ell\ell'} = &-\frac{16\pi^{3/2}}{5}\frac{k^2}{\mathcal{H}^2}P_\Sigma(k)\sqrt{(2\ell+1)(2\ell'+1)}\sqrt{\frac{2}{15}}\sum_I \lambda_I Y^*_{2M}(\hat{\omega}_I)\\ &\times\left[2\begin{pmatrix}3 & 1 & \ell\\ 0 & 0 & 0\end{pmatrix}\begin{pmatrix}3 & 1 & \ell'\\ 0 & 0 & 0\end{pmatrix}\begin{Bmatrix}1 & 2 & 1\\ \ell & 3 & \ell'\end{Bmatrix} + 3\begin{pmatrix}1 & 1 & \ell\\ 0 & 0 & 0\end{pmatrix}\begin{pmatrix}1 & 1 & \ell'\\ 0 & 0 & 0\end{pmatrix}\begin{Bmatrix}1 & 2 & 1\\ \ell & 1 & \ell'\end{Bmatrix}\right]\delta_{J,2}\,,\end{aligned} \tag{6.37}$$

$$\pi_{\ell\ell'}^{JM(\mathrm{c})} = -\frac{16\pi^{3/2}}{15}\frac{k^2}{\mathcal{H}^2}P_\Sigma(k)\sum_I \lambda_I Y^*_{2M}(\hat{\omega}_I)\Bigg[\frac{1}{5}\delta_{\ell,2}\delta_{\ell',0} + \frac{8}{105}\sqrt{2\ell+1}\begin{pmatrix}4 & 2 & \ell\\ 0 & 0 & 0\end{pmatrix}\delta_{\ell',4} + \frac{4}{7\sqrt{5}}\sqrt{2\ell+1}\begin{pmatrix}2 & 2 & \ell\\ 0 & 0 & 0\end{pmatrix}\delta_{\ell',2}\Bigg]\delta_{J,2}\,, \tag{6.38}$$

where curly brackets $\{\}$ denote the Wigner 6j-symbols. We first note that vector anisotropies can only generate $J = 2$ modes. This is not surprising as they are the product of two $j = 1$ states which can give either $J = 0$ which is isotropic or $J = 2$. The triangular relation imposed by the 3j and 6j symbols determines the limits of the sum in the expansion in eq. (6.35). It is easy to see that both $\ell$ and $\ell'$ have to be even and, more precisely, in $\{0, 2, 4, 6\}$. We can now reconstruct the correlation function (6.3) from the power spectrum. This is similar to the isotropic case in which the Fourier- and real-space coefficients in the Legendre expansion are related by

$$\xi_\ell(r) = i^\ell \int \frac{k^2 dk}{2\pi^2} j_\ell(kr) p_\ell(k)\,. \tag{6.39}$$

Explicitly, the coefficients of the BipoSH expansion of the correlation function, eq. (6.23), are related to the ones of the power spectrum, eq. (6.31) by

$$\xi_{\ell\ell'}^{JM}(r) = i^\ell \int \frac{k^2 dk}{2\pi^2} j_\ell(kr)\pi_{\ell\ell'}^{JM}(k)\,. \tag{6.40}$$

With this we can rewrite the real-space version of eqs. (6.36)-(6.38) in terms of the $C_\ell^\Sigma$, which we defer to an appendix: eqs. (6.71)-(6.73). The sum of the three contributions can be cast in matrix form as (remember all terms with $J \neq 2$ vanish)

$$\left(\xi_{\ell\ell'}^{2M}\right) = \frac{16\pi^{3/2}}{5}\sum_I \lambda_I Y^*_{2M}(\hat{\omega}_I)\begin{pmatrix} 0 & 0 & \frac{1}{35}C_0^\Sigma & 0 & 0 & 0 & 0\\ 0 & 0 & 0 & 0 & 0 & 0 & 0\\ \frac{1}{25}C_2^\Sigma & 0 & -\frac{1}{5}\sqrt{\frac{2}{35}}C_2^\Sigma & 0 & \frac{2}{225}\sqrt{\frac{2}{7}}C_2^\Sigma & 0 & 0\\ 0 & 0 & 0 & 0 & 0 & 0 & 0\\ 0 & 0 & 0 & 0 & -\frac{4}{9\sqrt{385}}C_4^\Sigma & 0 & 0\\ 0 & 0 & 0 & 0 & 0 & 0 & 0\\ 0 & 0 & 0 & 0 & -\frac{8}{63\sqrt{55}}C_6^\Sigma & 0 & 0\end{pmatrix}, \tag{6.41}$$

where $C_\ell^\Sigma = C_\ell^\Sigma(z, r)$. Equation (6.41) is one of the main results of this chapter. It shows in complete generality that *any* anisotropic signal induced by redshift-space distortion in the galaxy correlation function is encoded in the functions $\xi_{\ell\ell'}^{2M}$ (which depend in principle on redshift and on galaxy separation). The six non-zero coefficients $\boldsymbol{\xi} = \{\xi_{02}^{2M}, \xi_{20}^{2M}, \xi_{22}^{2M}, \xi_{24}^{2M}, \xi_{44}^{2M}, \xi_{64}^{2M}\}$ are therefore the equivalent of the monopole, quadrupole and hexadecapole that are measured in standard redshift surveys, when anisotropies are assumed to be absent. As we will show below, these six coefficients can be directly extracted from catalogs of galaxies, by averaging over pairs of galaxies with an appropriate weighting. A detection of a non-zero $\xi_{\ell\ell'}^{2M}$ would represent a smoking gun for the presence of anisotropies in the galaxies peculiar velocities.

Note that the dependence of the $\xi_{\ell\ell'}^{2M}$ on the model responsible for the anisotropies is encoded in the $C_\ell^\Sigma(z,r)$ and in the eigenvectors $\hat{\omega}_I$ and eigenvalues $\lambda_I$. In the following, we construct estimators for the six non-zero coefficients $\boldsymbol{\xi}$ and we forecast the detectability of these coefficients with future surveys.

## 6.4 Forecast for LSS surveys

We now forecast the constraints on the anisotropy parameters – which we define later – as expected from future redshift surveys. In the next section we define our estimators for the BipoSH coefficients and compute their covariance matrix.

### 6.4.1 Estimator & covariance

To estimate the expansion coefficients the obvious choice is to weight the correlation function by $X_{\ell\ell'}^{2M}$, in the same way that we weight the two-point function by the Legendre polynomials $\mathcal{P}_\ell$ to estimate the multipoles. In a binned survey the estimator is

$$\hat{\xi}_{\ell\ell'}^{2M}(r) = a_N \sum_{i,j} \Delta_i \Delta_j X_{\ell\ell'}^{2M*}(\hat{r}_{ij}, \hat{n}_{ij}) \delta_K(r_{ij} - r)\,, \tag{6.42}$$

where $\delta_K$ is the Kronecker delta, $\Delta_i$ the galaxy over-density in the bin labelled by the index $i$ (as in eq. (4.42)) and we have defined $\mathbf{r}_{ij} = \mathbf{x}_i - \mathbf{x}_j$, $\mathbf{n}_{ij} = 1/2(\mathbf{x}_i + \mathbf{x}_j)$. The normalisation factor $a_N$ is found by imposing that the estimator is unbiased,

$$\left\langle \hat{\xi}_{\ell\ell'}^{2M} \right\rangle = \xi_{\ell\ell'}^{2M}\,, \tag{6.43}$$

in the continuous limit

$$\sum_i \to \frac{1}{L_p^3} \int_V d^3x_i\,, \quad \delta_K(r_{ij} - r) \to L_p \delta_D(r_{ij} - r)\,, \tag{6.44}$$

where $L_p$ denotes the pixel size and $V$ is the total volume of the survey. We obtain

$$a_N = \frac{3L_p^5}{Vr^2}\,. \tag{6.45}$$

We also have $a_N = 1/N(r)$, where $N(r)$ is the number of pixels which contribute to the estimator. The variance of the estimator is defined as

$$\mathrm{var}\left(\hat{\xi}_{\ell\ell'}^{2M}\right) \equiv \mathrm{var}_{\ell\ell'}^M = \left\langle \left(\hat{\xi}_{\ell\ell'}^{2M}\right)^2 \right\rangle - \left\langle \hat{\xi}_{\ell\ell'}^{2M} \right\rangle^2\,, \tag{6.46}$$

and we recall that $\langle \Delta_i \Delta_j \rangle$ contains a Poisson noise contribution and a cosmic variance (CV) contribution,

$$\langle \Delta_i \Delta_j \rangle = \frac{1}{d\bar{N}} \delta_{ij} + C_{ij}^\Delta\,, \tag{6.47}$$

where $d\bar{N}$ is the mean number of galaxies per pixel. The correlation $C_{ij}^\Delta$ is due both to the scalar and vector parts of $\Delta_g$. However, the scalar component strongly dominates over the

vector one, so that we can neglect the latter. Physically, this reflects the fact that even though the coefficients $\xi^{2M}_{\ell\ell'}$ are constructed to remove the scalar isotropic signal and to isolate the vector anisotropic signal, the covariance of these coefficients is still affected (and dominated) by the scalar contribution. We then obtain three different contributions to the variance which are understood respectively as the Poisson term (P), the mixed term (M) and the CV term (C). Explicitly, we find

$$\mathrm{var}_P(r,r') = \frac{6V}{r^2 N_{\rm tot}^2}\delta_D(r-r')\,, \tag{6.48}$$

$$\mathrm{var}_M(r,r') = \frac{24}{\pi N_{\rm tot}}\int dk\, k^2 P(k,\bar{z}) j_\ell(kr) j_\ell(kr') \sum_w c_w \beta^w_{\ell\ell'}\,, \tag{6.49}$$

$$\mathrm{var}_C(r,r') = \frac{12}{\pi V}\int dk\, k^2 P^2(k,\bar{z}) j_\ell(kr) j_\ell(kr') \sum_\sigma \tilde{c}_\sigma \beta^\sigma_{\ell\ell'}\,, \tag{6.50}$$

where $N_{\rm tot}$ is the total number of tracers in the catalog and the indices $w,\sigma$ take values $w = 0,2,4$ and $\sigma = 0,2,4,6,8$. The explicit form of the coefficients $\beta^\sigma_{\ell\ell'}$ and details on the derivation of the various contributions of the variance can be found in appendix 6.A, where we also compute the covariance matrix of the estimator, defined as

$$\mathrm{cov}\left(\hat{\xi}^{2M_1}_{\ell_1\ell_1'}, \hat{\xi}^{2M_2}_{\ell_2\ell_2'}\right) \equiv \mathrm{cov}^{M_1M_2}_{\ell_1\ell_1'\ell_2\ell_2'} = \left\langle \hat{\xi}^{2M_1}_{\ell_1\ell_1'}\hat{\xi}^{2M_2}_{\ell_2\ell_2'}\right\rangle - \left\langle \hat{\xi}^{2M_1}_{\ell_1\ell_1'}\right\rangle\left\langle \hat{\xi}^{2M_2}_{\ell_2\ell_2'}\right\rangle\,. \tag{6.51}$$

### 6.4.2 Fisher forecasts

We now want to forecast the constraints on the anisotropic parameters from a survey. Given a model for the anisotropy power spectrum, i.e. a parametrization for $P_\Sigma$, we are left with the 5 degrees of freedom (d.o.f.) of the symmetric traceless tensor $\omega_{ij}$ and an overall amplitude $A_V$ for the vector power spectrum, which can be reabsorbed in a redefinition of $\omega_{ij}$. Following our decomposition in eq. (6.10) we identify the d.o.f. as the eigenvalues and eigenvectors of $\omega_{ij}$. On the one hand the eigenvalues are of zero-sum so that we can pick the first two $\lambda_1,\lambda_2$ as independent and the third one is fixed to $-(\lambda_1+\lambda_2)$. On the other hand we find it convenient to parametrize the three orthonormal eigenvectors $\hat{\omega}_I$ in terms of the three angles of an Euler-rotation which rotates the canonical basis of $\mathbb{R}^3$ into the $\hat{\omega}_I$,

$$\hat{\omega}_I \equiv R(\alpha,\beta,\gamma)\cdot\hat{e}_I\,, \tag{6.52}$$

where $\hat{e}_I$ are the three orthonormal vectors of $\mathbb{R}^3$ and $R(\alpha,\beta,\gamma)$ is the rotation matrix with Euler angles $\alpha,\beta,\gamma$. Furthermore we can absorb the amplitude $A_V$ in the eigenvalues by defining $\tilde{\lambda}_I = A_V\lambda_I$. In summary the 5 d.o.f. of the tensor $\bar{\omega}_{ij}$ and the overall amplitude $A_V$ are encoded in our parameter space

$$\theta = \{\tilde{\lambda}_1,\tilde{\lambda}_2,\alpha,\beta,\gamma\}\,. \tag{6.53}$$

The Fisher matrix is defined as

$$F_{\theta\theta'} \equiv \frac{1}{2}\frac{\partial^2\chi^2}{\partial\theta\partial\theta'} = \sum_{\mathcal{A},\mathcal{A}'}\frac{\partial\langle\hat{\xi}_{\mathcal{A}}\rangle}{\partial\theta}\bigg|_{\rm f}\mathrm{cov}^{-1}_{\mathcal{A}\mathcal{A}'}\frac{\partial\langle\hat{\xi}^*_{\mathcal{A}'}\rangle}{\partial\theta'}\bigg|_{\rm f} \tag{6.54}$$

where, schematically, $\mathcal{A} = \{\ell_1, \ell_1', M_1, x_i, z_1\}$, $\mathcal{A}' = \{\ell_2, \ell_2', M_2, x_j, z_2\}$, and the derivatives are evaluated at the fiducial model. The Fisher matrix contains therefore a sum over the six non-zero coefficients which constitute our data, over all pixels separations $x_i, x_j$ and over all bins of redshifts $z_i, z_j$. The covariance matrix properly accounts for all correlations between these quantities, except for the correlations between different redshift bins $z_i \neq z_j$, which we assume to be uncorrelated, since the bin size that we consider is sufficiently large. We then have

$$\mathrm{cov}_{\mathcal{A}\mathcal{A}'} = \mathrm{cov}_{\ell_1\ell_1'\ell_2\ell_2'}(r_i, r_j)\delta_{M_1M_2}\delta_{z_1z_2}\,. \tag{6.55}$$

We recall that, according to the Cramer-Rao inequality, the Fisher matrix provides a lower bound on the marginal parameter uncertainty $\sigma_\theta$ as

$$\sigma_\theta \geqslant \sqrt{(F^{-1})_{\theta\theta}}\,. \tag{6.56}$$

We start by constraining the parameters $\lambda_1, \lambda_2$. The sub-matrix is then written

$$\begin{aligned} F_{\tilde{\lambda}_A\tilde{\lambda}_B} &= \sum_{\{z_{\rm bin}\}}\sum_{i,j}\sum_{\ell_1\ell_1'\ell_2\ell_2'}\sum_{M}\frac{\partial\xi^{M}_{\ell_1\ell_1'}(r_i,z)}{\partial\tilde{\lambda}_A}\mathrm{cov}^{-1}_{\ell_1\ell_1'\ell_2\ell_2'}(r_i,r_j)\frac{\partial\xi^{M*}_{\ell_2\ell_2'}(r_j,z)}{\partial\tilde{\lambda}_B} \\ &= \sum_{\{z_{\rm bin}\}}\sum_{i,j}\sum_{\ell_1\ell_1'\ell_2\ell_2'}\frac{5}{4\pi}\left(2+\mathcal{P}_2(\delta_{AB})\right)\tilde{\xi}_{\ell_1\ell_1'}(r_i,z)\mathrm{cov}^{-1}_{\ell_1\ell_1'\ell_2\ell_2'}(r_i,r_j)\tilde{\xi}^{*}_{\ell_1\ell_1'}(r_j,z)\,, \end{aligned} \tag{6.57}$$

where we have defined

$$\xi^{2M}_{\ell_1\ell_1'} \equiv A_V\sum_I \lambda_I Y^*_{2M}(\hat{\omega}_I)\tilde{\xi}_{\ell_1\ell_1'}\,, \tag{6.58}$$

by explicitly writing the amplitude $A_V$ of $P_\Sigma$ out of the $C_\ell^\Sigma$. We normalize this amplitude such that $\lambda_{\rm max} \equiv 1$. The variables which determine the anisotropy are then the amplitude $A_V$, the ratio $\lambda_2/\lambda_1 = \lambda_2$ and the three angles $(\alpha, \beta, \gamma)$ which determine the orientation. For the second equal sign of eq. (6.57) we have performed the sum over $M$ using that

$$\frac{\partial\xi^{2M}_{\ell_1\ell_1'}}{\partial\tilde{\lambda}_A} = Y^*_{2M}(\hat{\omega}_A)\tilde{\xi}_{\ell_1\ell_1'} - Y^*_{2M}(\hat{\omega}_3)\tilde{\xi}_{\ell_1\ell_1'}\,, \tag{6.59}$$

together with the orthogonality properties of products of spherical harmonics. We observe that the final result does not depend on the fiducial values of the parameters $\tilde{\lambda}_I$ since they enter linearly in the estimator $\hat{\xi}^{2M}_{\ell_1\ell_2}$. We also note that we did not need to fix any fiducial direction $\hat{\omega}_I$ since the dependence on $\hat{\omega}_I$ cancels out in the final result.

In appendix 6.B we show that the off-diagonal blocks of the full Fisher matrix (6.54) are vanishing, hence $F_{\theta\theta'}$ has a block diagonal structure

$$[F_{\theta\theta'}] = \left[\begin{array}{c|c} F_{\lambda_A\lambda_B} & \mathbf{0} \\ \hline \mathbf{0} & F_{\alpha\beta\gamma} \end{array}\right]. \tag{6.60}$$

As a consequence of the block structure of the Fisher matrix, it follows that the constraints on the amplitudes $\lambda_I$ can be derived directly with eq. (6.57). In particular, they do not depend

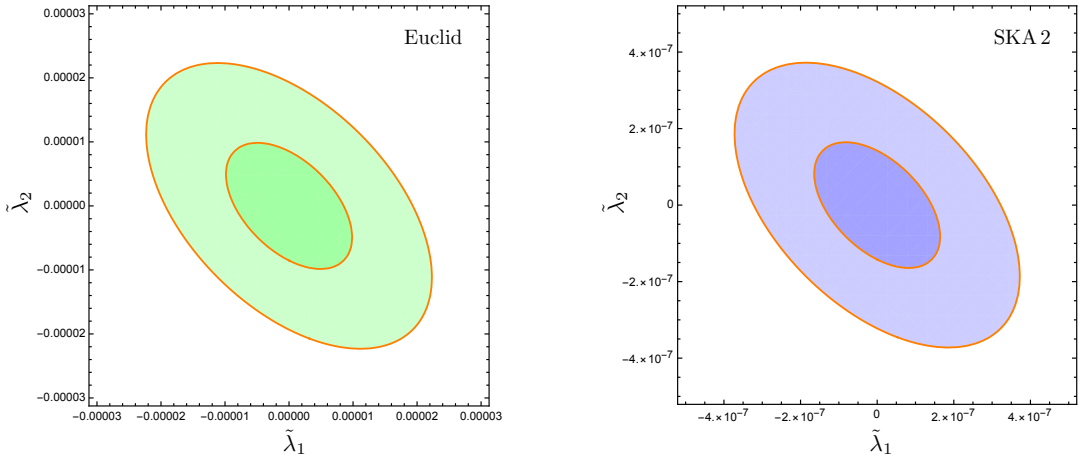


Figure 6.1: Constraints on amplitudes of anisotropies for the model (A). We have rescaled the parameters $\lambda_I$ as $\tilde{\lambda}_I \equiv A_V \lambda_I$. Compare this with the amplitude of the isotropic vorticity power spectrum generated by shell crossing in the standard cold dark matter scenario, where $A_{V,\mathrm{iso}} \sim 10^{-5}$, see e.g. Ref. [247].

on the fiducial values of the eigenvectors $\hat{\omega}_I$. This reflects the fact that the precision with which we can measure the eigenvalues does not depend on the direction of the anisotropy. The constraints on directions, i.e. $(\sigma_\alpha, \sigma_\beta, \sigma_\gamma)$, can be obtained by inverting the lower block of the Fisher matrix. It turns out that the constraints on each of the directions depend on the fiducial values of both the eigenvalues and the eigenvectors of $\bar{\omega}_{ij}$. However, this direction dependence is somewhat artificial, as we could have chosen our basis directions differently. Instead of considering each direction independently, it makes more sense to compute the volume of the ellipsoid described by the constrains on ($\alpha$, $\beta$, $\gamma$), using the Haar measure $d\mu = \sin\beta d\alpha d\beta d\gamma$. Note that with this non-normalized Haar measure, the volume of the rotation group $SO(3)$ is $2(2\pi)^2 \simeq 79$. We can think of this uncertainty volume as the inverse of a 'figure of merit' for the average accuracy with which we can recover the directional information. This combined direction constraint has the great advantage that it does not depend on the fiducial model for the directions, but only on the choice of the eigenvalues' ratio $\lambda_A/\lambda_B$ and the vector amplitude $A_V$. This remaining dependence is physical and simply reflects the fact that the precision with which we can measure the direction of the anisotropy does obviously depend on how large it is.

### 6.4.3 A model for vector perturbations

To illustrate how our general formalism can be used, we consider an explicit model in which a non-isotropic vector contribution to the galaxy peculiar velocities gives new contributions to the correlation function. We derive constraints on the directions and amplitudes of anisotropies for both a Euclid-like and SKA2-like survey. The specifications for these surveys are taken from [203] and [307] respectively: the two redshift ranges are $z \in [0.7, 2.0]$ for Euclid and $z \in [0.1, 2.0]$ for SKA2 and we split them into 14 and 19 bins of thickness $\Delta z = 0.1$

respectively, with $L_p = 2\,\mathrm{Mpc}/h$. This choice of $L_p$ is motivated by the fact that this pixel size gives the best constraints in [74]. Note that in the isotropic case, exploiting separations as small as $2\,\mathrm{Mpc}/h$ does require a good understanding of the scalar non-linear signal at those scales, which is highly non-trivial. In the anisotropic case however, since the scalar part does not contribute to the estimators $\hat{\xi}^{2M}_{\ell\ell'}$, but only to the covariance, we can exploit very small separations even without a very precise modelling of the scalar behaviour at those scales. As maximum separation we choose 40 Mpc/h.

Until this point our formalism has been model independent but, clearly, to forecast the detectability of the anisotropy parameters we have to assume a shape for $P_\Sigma(k)$. As an example we choose the isotropic vorticity power spectrum from N-body simulations while we note that, as we have stated before, the isotropic and anisotropic $P_\Sigma$ can in principle be different.

According to the numerical simulations of Ref. [247, 189], the vorticity power spectrum appears to evolve as $\mathcal{H}(z)^2 f(z)^2 D_1(z)^7$ at large scales. At small scales, the evolution has an additional scale-dependence, leading to a suppression of power at small scales at late times, see fig. 4 of [247]. In the following we will ignore this small-scale dependence and assume that the power spectrum at redshift $z$ is given by[3]

$$P_\Sigma(k,z) = P_\Sigma(k,z=0)\left(\frac{\mathcal{H}(z)f(z)}{\mathcal{H}_0 f(z=0)}\right)^2\left(\frac{D_1(z)}{D_1(z=0)}\right)^7 .$$

We use the vorticity power spectrum plotted in fig. 4 of [247] to construct the following fit for $P_\Sigma$,

$$P_\Sigma(k,z=0) = A_V\frac{(k/k_*)^{n_\ell}}{[1+(k/k_*)]^{n_\ell+n_s}} \quad \left(\mathrm{Mpc}/h\right)^3 ,$$

where the power at large scales is given by $n_\ell = 1.3$, the power at small scales by $n_s = 4.3$ and the transition scale by $k_* = 0.7\,h/\mathrm{Mpc}$. From fig. 4 of [247] we find that the predicted amplitude for $P_\Sigma$ is $A_V = 10^{-5}$.

In fig. 6.1 we use this spectrum to estimate the constraints on the eigenvalues $\tilde{\lambda}_{1,2}$. Note that there is no dependence on the fiducial values of the parameters $\tilde{\lambda}_I$ since they enter linearly in the estimator $\hat{\xi}^{2M}_{\ell_1\ell_2}$. Furthermore the constraints do not depend on the orientation of the eigenvectors due to the block diagonal structure of the Fisher matrix. The $1\sigma$-constraints on the amplitude of the eigenvalues are $\sigma_\lambda \simeq 6\times10^{-6}$ with Euclid and even $\sigma_\lambda \simeq 1\times10^{-7}$ with SKA2. It is also interesting to note that the constraints are better if both eigenvalues have the same sign. This is of course owing to the fact that then the norm of the third eigenvalue is larger. With the SKA and optimistic assumptions we should therefore be able to constrain an anisotropic vector signal with amplitude of 1% of the amplitude of the vorticity generated by shell-crossing in cold dark matter $A_{V,\mathrm{iso}} \sim 10^{-5}$ [247].

In fig. 6.2 we show the volume of the ellipsoid described by the constraints on $(\alpha,\beta,\gamma)$. As

[3]Note that the constraints obtained in this way are conservative, because we underestimate the vorticity power spectrum at small scales for large redshift.

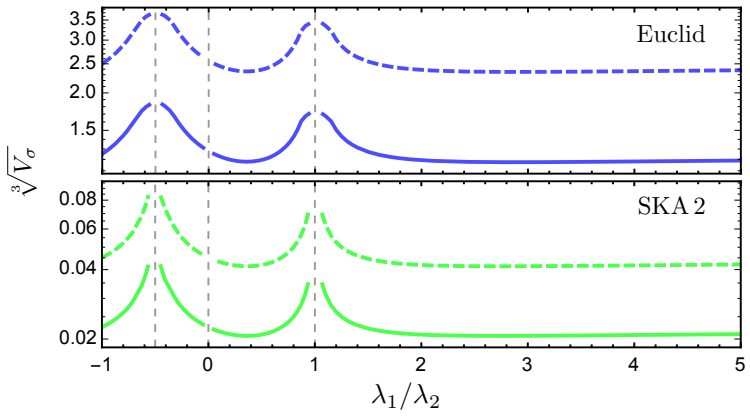


Figure 6.2: Volume of the $1\sigma$ (solid) and $3\sigma$ (dashed) ellipsoids in the $\alpha-\beta-\gamma$ space as a function of the ratio between the $\lambda_A$ and $\lambda_B$. The anisotropic amplitude is set to $A_V = 10^{-5}$. The constraint should be compared to the the cube root of the Haar volume $\sqrt[3]{79} \sim 4$.

we discussed above the constraint does not depend on the fiducial directions but it depends on the fiducial values of $\tilde{\lambda}_{1,2}$ or, equivalently, on the choice of $A_V$ and the ratio $\lambda_1/\lambda_2$. In the plot we fix the *biggest* eigenvalue to $\lambda_{\rm max} = A_V = 10^{-5}$. The features in the plot can be explained intuitively as follows. We first note that the constraint asymptotes to a constant for $\lambda_1/\lambda_2 > 1$: this is a result of two concurrent effects. On one hand, as we keep the largest eigenvalue, $\lambda_1$, fixed, the other, $\lambda_2$, becomes smaller, reducing the overall signature of the anisotropy. On the other hand, as the ratio increases, the departure from isotropy is more pronounced yielding better constraints. Note that we could have fixed the *smallest* eigenvalue equal to $A_V$: in this case as the ratio becomes bigger the overall signature of anisotropy increases and the two effects add up to give better constraints. Secondly the constraints are worst for $\lambda_1/\lambda_2 = 1$ or $-1/2$. In both cases this is because we approach a degeneracy: $\lambda_1 = \lambda_2$ or $\lambda_1 = \lambda_3$ respectively. Note that the constraints are slightly better in $\lambda_1 = \lambda_2$ w.r.t. the second case as the overall amplitude is bigger in this case. The absolute values of the volume show that Euclid constrains the direction of the anisotropy only loosely, while the constraints from SKA2 are excellent, for our choice of amplitude $A_V = 10^{-5}$. Note that the constraint on the volume scales as $A_V^3$, so that decreasing $A_V$ by an order of magnitude would degrade the bounds in fig. 6.2 by a factor 10.

## 6.5 Conclusions

In this chapter we have discussed the effects of an anisotropic vector component in the peculiar velocity field, focusing on the redshift-space distortions induced in the galaxy correlation function. We have presented a general method to isolate the anisotropic signal through a decomposition in bipolar spherical harmonics. We provide an analytical expression for the coefficients of this expansion which does not require the adoption of a specific model. We then show how one can practically use this approach to forecast constraints on the anisotropic

sector for two upcoming redshift surveys.

We derive two types of constraints, both on the total amplitude of the anisotropy and on the preferred direction (in terms of the $SO(3)$ volume of its Euler angles). We can compare our results with the constraints found in [74] for the isotropic case which of course has no preferred direction. Given the block-diagonal form of the Fisher matrix, we find that we are able to achieve similar constraints on the amplitude of the vector modes (since we also assume the same shape for the spectrum). Let us however note that even though the constraints are similar, the interpretation of the result in the anisotropic case is cleaner, since in this case the scalar degrees of freedom do not contribute to the estimators and therefore they do not need to be accurately modelled.

This work is meant as a study of the feasibility of detecting an anisotropic vector signal in the galaxy two-point function and together with the analysis carried out in [74], it represents a comprehensive study of the detectability of vector modes in the correlation function.

Given a model for the anisotropy, one needs to determine not only the eigenvalues and the directions of its eigenvectors, but also the corresponding vector power spectrum. Here, to provide a concrete example of our formalism, we just assumed this to be given by the vorticity spectrum generated by non-linear structure formation. In full generality the power spectrum could be reconstructed from the data as a function of multipole and redshift, at the price of much larger error bars.

# Appendices

## 6.A Covariance matrix

The variance of the estimator $\xi^{2M}_{\ell\ell'}$ is given by

$$\begin{aligned}\mathrm{var}\left(\hat{\xi}^{2M}_{\ell\ell'}\right) &= a_N^2 \sum_{ij}\sum_{km} \langle \Delta_i \Delta_j \Delta_k \Delta_m \rangle X^{2M}_{\ell\ell'}(\hat{r}_{ij}, \hat{n}_{ij}) X^{2M*}_{\ell\ell'}(\hat{r}_{km}, \hat{n}_{km}) \delta_K(r_{ij} - r) \delta_K(r_{km} - r') \\ &= \mathrm{var}_P + \mathrm{var}_M + \mathrm{var}_C \,.\end{aligned}$$

Since $\langle \Delta_i \Delta_j \rangle$ contains a Poisson noise contributions and a cosmic variance (CV) contribution

$$\langle \Delta_i \Delta_j \rangle = \frac{1}{d\bar{N}} \delta_{ij} + C^{\Delta}_{ij} \,, \tag{6.61}$$

where $d\bar{N}$ is the mean number of galaxies per pixel, the three different contributions to the variance are understood respectively as the Poisson term, the mixed term and the CV term. The first terms is easily found

$$\begin{aligned}\mathrm{var}_P(r, r') &= \frac{18 L_p^{10}}{V^2 (r r')^2} \frac{1}{d\bar{N}^2} \sum_{ij}\sum_{km} \delta_{ik}\delta_{jm} X^{2M}_{\ell\ell'}(\hat{r}_{ij}, \hat{n}_{ij}) X^{2M*}_{\ell\ell'}(\hat{r}_{km}, \hat{n}_{km}) \delta_K(r_{ij} - r) \delta_K(r_{km} - r') \\ &= \frac{6V}{r^2 N^2_{\mathrm{tot}}} \delta_D(r - r') \,,\end{aligned}$$

where we have set the factor $(1+(-1)^\ell)=2$ as only even $\ell$ appear in the expansion. The mixed term is

$$\begin{aligned}\mathrm{var}_M(r,r') &= \frac{18L_p^{10}}{V^2(rr')^2}\frac{1}{d\bar{N}}\sum_{ij}\sum_{km}\left(\delta_{ik}C^\Delta_{jm}+\delta_{jm}C^\Delta_{ik}\right)X^{2M}_{\ell\ell'}(\hat{r}_{ij},\hat{n}_{ij})X^{2M*}_{\ell\ell'}(\hat{r}_{km},\hat{n}_{km})\\ &\quad\times\delta_K(r_{ij}-r)\delta_K(r_{km}-r')\\ &= \frac{18L_p^{10}}{V^2(rr')^2}\frac{2}{d\bar{N}}\sum_{ij}\sum_{m}C^\Delta_{jm}X^{2M}_{\ell\ell'}(\hat{r}_{ij},\hat{n}_{ij})X^{2M*}_{\ell\ell'}(\hat{r}_{im},\hat{n}_{im})\delta_K(r_{ij}-r)\delta_K(r_{im}-r')\,.\end{aligned}$$

We use the flat-sky expression for $C^\Delta_{ij}$

$$C^\Delta_{ij}(\bar{z}) = \frac{1}{(2\pi)^3}\int d^3k\; e^{i\mathbf{k}\cdot(\mathbf{x}_j-\mathbf{x}_i)}P(k,\bar{z})\Big(c_0\mathcal{P}_0(\hat{n}\cdot\hat{k})+c_2\mathcal{P}_2(\hat{n}\cdot\hat{k})+c_4\mathcal{P}_4(\hat{n}\cdot\hat{k})\Big)\,, \tag{6.62}$$

and we perform (in the continuous limit) the following change of variables $\mathbf{y}_j=\mathbf{x}_j-\mathbf{x}_i$, $\mathbf{y}_m=\mathbf{x}_m-\mathbf{x}_i$ together with $\mathbf{x}_i=\mathbf{n}$. We obtain

$$\mathrm{var}_M(r,r') = \frac{24}{\pi N_{\rm tot}}\int dk\,k^2P(k,\bar{z})j_\ell(kr)j_\ell(kr')\Big(c_0\beta^0_{\ell\ell'}+c_2\beta^2_{\ell\ell'}+c_4\beta^4_{\ell\ell'}\Big)\,, \tag{6.63}$$

where we have defined the coefficients

$$\beta^\sigma_{\ell\ell'} = (2\ell+1)(2\ell'+1)\begin{pmatrix}\sigma & \ell & \ell\\ 0&0&0\end{pmatrix}\begin{pmatrix}\sigma & \ell' & \ell'\\ 0&0&0\end{pmatrix}\begin{Bmatrix}\ell' & \ell & 2\\ \ell & \ell' & \sigma\end{Bmatrix}\,. \tag{6.64}$$

Finally the CV term is given by

$$\mathrm{var}_C(r,r') = \frac{18L_p^{10}}{V^2(rr')^2}\sum_{ij}\sum_{km}C^\Delta_{jm}C^\Delta_{ik}X^{2M}_{\ell\ell'}(\hat{r}_{ij},\hat{n}_{ij})X^{2M*}_{\ell\ell'}(\hat{r}_{km},\hat{n}_{km})\delta_K(r_{ij}-r)\delta_K(r_{km}-r')\,,$$

we can perform a similar change of variable as above $\mathbf{y}_j=\mathbf{x}_j-\mathbf{x}_i$, $\mathbf{y}_m=\mathbf{x}_m-\mathbf{x}_k$ so that, after substituting eq. (6.62) twice, the two exponentials are written

$$e^{i\mathbf{k}\cdot(\mathbf{x}_m-\mathbf{x}_j)}e^{i\mathbf{k}'\cdot(\mathbf{x}_k-\mathbf{x}_i)}\to e^{i\mathbf{k}\cdot(\mathbf{y}_m-\mathbf{y}_j)}e^{i(\mathbf{k}+\mathbf{k}')\cdot(\mathbf{x}_k-\mathbf{x}_i)}\,, \tag{6.65}$$

and the integral over $\mathbf{x}_k$ enforces $\mathbf{k}=-\mathbf{k}'$. The angular integrals are performed with the properties of BiPoSH as before and we obtain

$$\mathrm{var}_C(r,r') = \frac{12}{\pi V}\int dk\,k^2P^2(k,\bar{z})j_\ell(kr)j_\ell(kr')\sum_\sigma\tilde{c}_\sigma\beta^\sigma_{\ell\ell'}\,, \tag{6.66}$$

where the $\tilde{c}_\ell$ are given in eqs. (4.60)-(4.64).

The computation for the off-diagonal covariance matrix, defined in eq. (6.51), follows the same steps with the exception that Poisson noise does not contribute for off-diagonal components as it is proportional to $\delta_{\ell_1\ell_2}\delta_{\ell'_1\ell'_2}\delta_{M_1M_2}$. Furthermore the mixed and Cosmic

contributions are proportional to $\delta_{M_1M_2}$ and the general case is obtained from eqs. (6.63) and (6.66) by substituting the product of spherical Bessel functions inside the integral with $j_{\ell_1}(r)j_{\ell_2}(r')$ and redefining the $\beta$ coefficients as

$$\beta^{\sigma}_{\ell_1\ell_1'\ell_2\ell_2'} = i^{\ell_2-\ell_1}\sqrt{(2\ell_1+1)(2\ell_1'+1)(2\ell_2+1)(2\ell_2'+1)}\begin{pmatrix}\sigma & \ell_1 & \ell_2\\ 0 & 0 & 0\end{pmatrix}\begin{pmatrix}\sigma & \ell_1' & \ell_2'\\ 0 & 0 & 0\end{pmatrix}\begin{Bmatrix}\ell_1' & \ell_1 & 2\\ \ell_2 & \ell_2' & \sigma\end{Bmatrix}.$$

## 6.B Fisher matrix

In this appendix we sketch a proof of why the off-diagonal blocks of the Fisher matrix (6.60) vanish, i.e. $F_{\lambda_A,\alpha_i} = 0$. We have

$$\begin{aligned}F_{\lambda_A,\alpha_i} &= \sum_{\{z_{\rm bin}\}}\sum_{i,j}\sum_{\ell_1\ell_1'\ell_2\ell_2'}\sum_{M}\frac{\partial\xi^{M}_{\ell_1\ell_1'}(r_i,z)}{\partial\lambda_A}{\rm cov}^{-1}_{\ell_1\ell_1'\ell_2\ell_2'}(r_i,r_j)\frac{\partial\xi^{M*}_{\ell_2\ell_2'}(r_j,z)}{\partial\alpha_i}\\ &= \sum_M\left(Y^*_{2M}(\hat\omega_A)-Y^*_{2M}(\hat\omega_3)\right)\frac{\partial}{\partial\alpha_i}\left(\sum_I\lambda_I Y_{2M}(\hat\omega_I)\right)\\ &\quad\times\sum_{\{z_{\rm bin}\}}\sum_{i,j}\sum_{\ell_1\ell_1'\ell_2\ell_2'}\tilde\xi^{M}_{\ell_1\ell_1'}(r_i,z){\rm cov}^{-1}_{\ell_1\ell_1'\ell_2\ell_2'}(r_i,r_j)\tilde\xi^{M*}_{\ell_1\ell_1'}(r_j,z)\,,\end{aligned}\tag{6.67}$$

with

$$\frac{\partial}{\partial\alpha_i}\left(\sum_I\lambda_I Y_{2M}(\hat\omega_I)\right) = \sum_I\lambda_I\left(\frac{\partial\theta_I}{\partial\alpha_i}\frac{\partial}{\partial\theta_I}+\frac{\partial\phi_I}{\partial\alpha_i}\frac{\partial}{\partial\phi_I}\right)Y_{2M}(\theta_I,\phi_I)\,,\tag{6.68}$$

and $(\theta_I,\phi_I)$ are the polar angles defining the directions of $\hat\omega_I$. We recall that

$$\begin{aligned}\partial_\theta Y_{2M}(\theta,\phi) &= -\frac{(\eth+\eth^*)}{2}Y_{2M}(\theta,\phi) = -\frac{\sqrt{6}}{2}\left({}_1Y_{2M}(\theta,\phi)-{}_{-1}Y_{2M}(\theta,\phi)\right),\\ \partial_\phi Y_{2M}(\theta,\phi) &= i\sin\theta\frac{(\eth-\eth^*)}{2}Y_{2M}(\theta,\phi) = i\sin\theta\frac{\sqrt{6}}{2}\left({}_1Y_{2M}(\theta,\phi)+{}_{-1}Y_{2M}(\theta,\phi)\right),\end{aligned}$$

where $\eth$ and $\eth^*$ are the spin-raising and -lowering operators respectively (see appendix B.3). For definiteness, let us consider the case $\lambda_A = \lambda_1$ and $\alpha_i = \alpha$ in eq. (6.67). One has

$$F_{\lambda_1,\alpha} = i\frac{\sqrt{6}}{2}\sum_M\left(Y^*_{2M}(\hat\omega_1)-Y^*_{2M}(\hat\omega_3)\right)\sum_I\lambda_I\sin\theta_I\left({}_1Y_{2M}(\hat\omega_I)+{}_{-1}Y_{2M}(\hat\omega_I)\right)[\dots]\,,\tag{6.69}$$

where the $[\dots]$ represents the part of the Fisher matrix (6.67) which does not depend on $\hat\omega_I$. We recall

$$\sqrt{\frac{4\pi}{2\ell+1}}\sum_{m'}{}_mY_{\ell m'}(\theta_1,\phi_1)\,{}_sY^*_{\ell m'}(\theta_2,\phi_2) = {}_sY^*_{\ell -m}(\beta,\alpha)e^{is\gamma}\,,\tag{6.70}$$

where here $(\alpha,\beta,\gamma)$ are the Euler angles of the rotation rotating the direction $(\theta_2,\phi_2)$ in $(\theta_1,\phi_1)$ and not the angles defined in eq. (6.52). In eq. (6.69) the products is between two harmonics evaluated either at the same directions or at orthogonal directions. In our case we

have $\ell = 2$, $s = 0$ and $m = 1$. Furthermore $(\beta, \alpha, \gamma)$ denotes a rotation by either 0 or $\pi/2$ since either $\hat{\omega}_1 = \hat{\omega}_2$ or they enclose and angle of $\pi/2$. In other words, $R(\beta, \alpha, \gamma)\boldsymbol{e}_3 = \pm\boldsymbol{e}_I$ where $I \in \{1, 2, 3\}$ and $Y_{\ell m}(\beta, \alpha) = Y_{\ell m}(R^{-1}(\beta, \alpha, \gamma)\boldsymbol{e}_3) = Y_{\ell m}(\pm\boldsymbol{e}_I)$, see [131]. The Euler angle $\gamma$ is irrelevant here since a rotation around $\boldsymbol{e}_z$ leaves $\boldsymbol{e}_z$ invariant. But for the cartesian axes $\boldsymbol{e}_I$, $\vartheta$ is either 0 or $\pi/2$ and $Y_{21}(\vartheta, \varphi) \propto \sin\vartheta\cos\vartheta$ vanishes. This completes the proof that the off-diagonal boxes in the Fisher matrix vanish.

## 6.C $\xi^{2M}_{\ell\ell'}$

The explicit expressions for the real-space version of eqs. (6.36)-(6.38) are given by

$$\xi^{2M(\mathrm{a})}_{\ell\ell'} = -\frac{16\pi^{3/2}}{45} C^{\Sigma}_{\ell}(z, r) \sum_I \lambda_I Y^*_{2M}(\hat{\omega}_I) \left( \delta_{\ell,0}\delta_{\ell',2} + 2\sqrt{\frac{2\ell'+1}{5}} \begin{pmatrix} 2 & 2 & \ell' \\ 0 & 0 & 0 \end{pmatrix} \delta_{\ell,2} \right), \tag{6.71}$$

$$\begin{aligned} \xi^{2M(\mathrm{b})}_{\ell\ell'} = &-\frac{16\pi^{3/2}}{5} C^{\Sigma}_{\ell}(z, r) \sqrt{(2\ell+1)(2\ell'+1)} \sqrt{\frac{2}{15}} \sum_I \lambda_I Y^*_{2M}(\hat{\omega}_I) \\ &\times \left[ 2 \begin{pmatrix} 3 & 1 & \ell \\ 0 & 0 & 0 \end{pmatrix} \begin{pmatrix} 3 & 1 & \ell' \\ 0 & 0 & 0 \end{pmatrix} \begin{Bmatrix} 1 & 2 & 1 \\ \ell & 3 & \ell' \end{Bmatrix} + 3 \begin{pmatrix} 1 & 1 & \ell \\ 0 & 0 & 0 \end{pmatrix} \begin{pmatrix} 1 & 1 & \ell' \\ 0 & 0 & 0 \end{pmatrix} \begin{Bmatrix} 1 & 2 & 1 \\ \ell & 1 & \ell' \end{Bmatrix} \right], \end{aligned} \tag{6.72}$$

$$\begin{aligned} \xi^{2M(\mathrm{c})}_{\ell\ell'} = &-\frac{16\pi^{3/2}}{15} C^{\Sigma}_{\ell}(z, r) \sum_I \lambda_I Y^*_{2M}(\hat{\omega}_I) \left[ \frac{1}{5}\delta_{\ell,2}\delta_{\ell',0} + \frac{8}{105}\sqrt{2\ell+1} \begin{pmatrix} 4 & 2 & \ell \\ 0 & 0 & 0 \end{pmatrix} \delta_{\ell',4} \right. \\ &\left. + \frac{4}{7\sqrt{5}}\sqrt{2\ell+1} \begin{pmatrix} 2 & 2 & \ell \\ 0 & 0 & 0 \end{pmatrix} \delta_{\ell',2} \right]. \end{aligned} \tag{6.73}$$

# CHAPTER 7

## Ensemble average on the light-cone

**Based on:**

[230] E. Mitsou, R. Durrer, F. Scaccabarozzi, V. Tansella and J. Yoo "*Observer terms and ensemble averages*"
**in preparation**

**Abstract.** We analyse here the averaging procedure of cosmological observable from a theoretical and observational point of view. In this technical chapter we first carefully define and discuss the differences between theory and observers N-point functions. We then show how, under the ergodic hypothesis, on the one hand averaging over fields at the observer position poses no difficulty but on the other hand their contribution is relegated to the unobservable monopole. This justifies the approach we detailed in section 4.2.2.

## 7.1 Introduction

A crucial tool for relating theory and observations in cosmology is the assumption of statistical homogeneity and isotropy. Theoretically we can only provide statistical predictions, i.e. ensemble averages over several universe realisations, but observationally we only have access to a single realisation of the universe and a single light-cone within that realisation (and of course the light-cone interior but in cosmology we essentially measure light coming from different sources). The assumption of statistical homogeneity and isotropy along with the application of the ergodic theorem allows one to effectively treat different parts of the universe as different realisations and thus to connect the theoretical predictions to observations. Truthfully, a formal proof of ergodicity for a random process is not usually easy [15] and in cosmology it is perhaps best regarded as a common-sense hypothesis.

The requirement for the ergodic hypothesis to be applicable, i.e. for spatial averages to be approximated by statistical ones, is the observational availability of a large enough number of source points. Indeed, the common motto is that the theorist is allowed to ensemble average a given product of fields evaluated at source positions, because the observer probes several of these positions. This viewpoint is perfectly sufficient as long as one is only interested in the lowest-order approximation where a cosmological observable is entirely determined by the value of fields at the source position.

In the era of precision cosmology, however, the above approximation is no longer valid, because observations are able to capture several sub-leading effects which depend on fields evaluated on the whole line of sight from the source to the observer (as we have discussed in previous chapters). As one approaches the observer on its past light-cone, the number of observable points decreases and therefore so does the validity of the ergodic hypothesis. The extreme case is the observer point itself, for which we can only have a single measurement.

In recent years, studies concerning non-trivial effects of averaging in cosmology have appeared in the literature [71, 320], but the question we want to answer in this chapter is the following. Theoretically we can certainly perform ensemble averages of fields at, and in the vicinity of, the observer position, but are we then allowed to use the ergodic hypothesis to compare the results with observations?

To understand the relevance of this issue, note first that the usual approach in the literature, and the one we have adopted in this thesis until this point, is to avoid at least part of the issue by simply neglecting the fields at the observer position (see e.g. [73, 72, 122, 294, 295]). We will see that this is a fair procedure in the following. As for the line-of-sight integrated terms, they are ensemble averaged just like the source terms, which implicitly assumes that ergodicity applies on all points, independently of how close they are to the observer position. However another school of thought in the community considers observer terms fundamental as they must be taken into account in order to obtain gauge-invariant predictions [59, 147, 273]. Moreover, if fields at the observer are retained when computing correlation functions, i.e. ensemble averages of products of observables, one must perform that average on all points of the line of sight, *including* the observer point, in order to obtain expressions that are free of spurious infrared divergences [60]. In fact, from the mathematical viewpoint, this is the only consistent way to proceed, because if we impose statistical homogeneity (which is an essential assumptions for ergodicity to hold [311]) then no point can be privileged in space. Thus, if one wants to consider non-random field values at the observer, then one must abandon statistical homogeneity. The issue we have presented in this introduction can therefore be restated as the fact that the only well-defined theoretical computation involves ensemble averaging *all* the terms involved in the observable, while ergodicity is difficult to apply in the vicinity of the observer.

## 7.2 Definitions and conventions

A cosmological observable is a function of two space-time points $f(x_o; x_s)$, the "observer" point $x_o^\mu$ and the "source" point $x_s^\mu$, that are constrained to lie on a light-like geodesic. For simplicity we will exclusively work within linear perturbation theory around FLRW space-

time with $t$ an arbitrary time-parametrisation and we will also fix the time of the observer to zero $t_o = 0$. We can then trade, as we have done throughout this work, the constrained $x_s^\mu$ information for the corresponding fundamental observables that are the observed redshift $z$ and the observed position in the sky $\mathbf{n}$, the latter being a unit-normed vector in the rest-frame of the observer. We can thus parametrise the observables as $f(\vec{x}_o; z, \mathbf{n})$, so that all involved variables are unconstrained, i.e. $z$ and $\mathbf{n}$ parametrise the past light-cone of the observer at $\vec{x}_o$. On the other hand, $\vec{x}_o$ parametrises the past light-cones whose tips lie in the $t = 0$ hypersurface.

We will work with perturbation fields $\Phi_a$ which, for the purpose of this chapter, can be thought of as "Bardeen variables", which is effectively the same as working in the longitudinal gauge. With this specification, the FLRW space-time on which these fields live is uniquely defined. When promoting the $\Phi_a$ to stochastic fields, linearity and statistical invariance under the Euclidean group implies that the Fourier modes $\Phi_a(t, \vec{k})$ are independent random variables and that the probability distribution function (PDF) is of the form

$$P_t[\Phi] = \prod_{\vec{k}\in\mathbb{R}^3} P_{t,\vec{k}}(\Phi(\vec{k}))\,, \qquad P_{t,\vec{k}}(\Phi(\vec{k})) = P_{t,k}(\Phi(\vec{k}))\,. \tag{7.1}$$

Moreover, in the absence of primordial non-Gaussianity, linearity implies a Gaussian PDF:

$$P_{t,k}(\Phi(\vec{k})) \sim \exp\left[-\frac{1}{2}\, K_{ab}(t,k)\, \Phi_a(\vec{k})\, \Phi_b^*(\vec{k})\right], \tag{7.2}$$

which we do not need to specify here. The ensemble average of a product of fields at different times is defined as usual, i.e. we first note that $\Phi_a(t, \vec{k})$ can be expressed in terms of the fields at some reference time, say $t = 0$, through a linear relation[1]

$$\Phi_a(t, \vec{k}) = D_{ab}(t,k)\, \Phi_b(\vec{k})\,, \qquad \Phi_a(\vec{k}) = \Phi_a(0, \vec{k})\,, \tag{7.3}$$

so we can define (see appendix B.1)

$$\begin{aligned} \langle \Phi_{a_1}(t_1, \vec{k}_1) ... \Phi_{a_n}(t_n, \vec{k}_n)\rangle_P &= D_{a_1 b_1}(t_1, k_1) ... D_{a_n b_n}(t_n, k_n)\, \langle \Phi_{b_1}(\vec{k}_1) ... \Phi_{b_n}(\vec{k}_n)\rangle_P \\ &= D_{a_1 b_1}(t_1, k_1) ... D_{a_n b_n}(t_n, k_n) \\ &\quad \times \int \mathcal{D}\Phi\, P_0[\Phi]\, \Phi_{b_1}(\vec{k}_1) ... \Phi_{b_n}(\vec{k}_n)\,, \end{aligned} \tag{7.4}$$

and then Fourier-transform to real space if desired. The relative perturbation of $f$ is

$$\delta f(\vec{x}_o; z, \mathbf{n}) \equiv \frac{f(\vec{x}_o; z, \mathbf{n}) - \bar{f}(z)}{\bar{f}(z)}\,, \tag{7.5}$$

where $\bar{f}(z)$ is the background value and thus coincides with the ensemble average

$$\bar{f}(z) = \langle f(\vec{x}_o; z, \mathbf{n})\rangle_P\,. \tag{7.6}$$

[1] In the case of non-propagating fields, such as scalar perturbations, we have that $D(t,k) = D(t)$ is a growth function, whereas in the case of propagating fields, such as tensor modes, one must consider the field velocities as part of the independent set $\{\Phi_a\}$ to obtain the above relation.

Note that $\delta f$ is gauge-invariant (up to terms at the observer), thanks to the fact that we are using the observed (non-perturbative) redshift $z$. This is also dictated by Stewart lemma: if $\bar{f}$ has a known redshift dependence, say $\bar{f}(z) = D_f(z)\bar{f}_0$, then we can construct a quantity that vanishes at the background level $\langle f(z,\mathbf{x}) - f_0(\mathbf{x})D_f(z)\rangle_P = 0$ and eq. (7.5) is its perturbation. This quantity can then be split into three terms

$$\delta f = \delta f_o + \delta f_l + \delta f_s \,, \tag{7.7}$$

where $\delta f_o$ is made of fields evaluated at the observer position, $\delta f_s$ is made of fields evaluated at the source position and $\delta f_l$ is an integral of fields over the background line of sight. We will refer to these as the "observer", "source" and "line-of-sight" terms, respectively. Note that this separation is not unique because one can perform integrations by parts in $\delta f_l$ producing boundary terms which alter $\delta f_o$ and $\delta f_s$. In particular, depending on the way the expression $\delta f$ is derived, one can use this freedom to make all three terms individually gauge-invariant [273].

### 7.2.1 Observational and theoretical correlation functions

In what follows we will need to consider generic products of $f(\vec{x}_o; z_k, \mathbf{n}_k)$, so it will be important to work with a convenient angular parametrisation. A product of $N$ observables depends on $2N$ angles, out of which one can form $2N-3$ rotationally-invariant angles, i.e. "relative" angles. This is because the rotation group is 3-dimensional so three of the $2N$ angles simply amount to the freedom of choosing a reference frame. Concretely, we can choose the relative angular parametrisation where $\mathbf{n}_1$ is the azimuthal direction and $\mathbf{n}_\perp$ is a unit-vector normal to $\mathbf{n}_1$ such that

$$\begin{aligned} \mathbf{n}_2 &= \mathbf{n}_1 \cos\theta_2 + \mathbf{n}_\perp \sin\theta_2 \,, \\ \mathbf{n}_{k>2} &= \left[\mathbf{n}_\perp \cos\phi_k + (\mathbf{n}_1 \times \mathbf{n}_\perp)\sin\phi_k\right]\sin\theta_k + \mathbf{n}_1 \cos\theta_k \,, \end{aligned} \tag{7.8}$$

which involves indeed $2N-3$ independent SO(3)-invariant angles

$$\begin{aligned} \theta_k &= \cos^{-1}\left(\mathbf{n}_1 \cdot \mathbf{n}_k\right) \,, && k = 2, ..., N \,, \\ \phi_k &= \cos^{-1}\left(\frac{\mathbf{n}_2 \cdot \mathbf{n}_k - (\mathbf{n}_1 \cdot \mathbf{n}_2)(\mathbf{n}_1 \cdot \mathbf{n}_k)}{\sqrt{(1-(\mathbf{n}_1 \cdot \mathbf{n}_2)^2)\,(1-(\mathbf{n}_1 \cdot \mathbf{n}_k)^2)}}\right) \,, && k = 3, ..., N \,. \end{aligned} \tag{7.9}$$

The remaining three angles $\theta_1$, $\phi_1$ and $\phi_2$ must then be given with respect to some external set of orthonormal vectors $\hat{x}, \hat{y}, \hat{z}$ in the observer's rest-frame and correspond to a choice of reference frame $(\mathbf{n}_1, \mathbf{n}_\perp)$.

We can now define the "observational" correlation functions. The observer has access to $f(\vec{x}_o; z, \mathbf{n})$ on a single past light-cone $\vec{x}_o$ and for a single realisation of the universe. With this data, the observer can compute correlation functions by performing averages of $f$ products over all possible reference frames,

$$G^{\rm ob}(\vec{x}_o; \{z_k\}_{k=1}^N, \{\theta_k\}_{k=2}^N, \{\phi_k\}_{k=3}^N) \equiv \frac{1}{8\pi^2}\int \sin\theta_1 \,\mathrm{d}\theta_1 \,\mathrm{d}\phi_1 \,\mathrm{d}\phi_2 \prod_{k=1}^N f(\vec{x}_o; z_k, \mathbf{n}_k) \,, \tag{7.10}$$

which therefore depend only on the invariant/relative angles. On the other hand, the one-point function is simply the average over the observer sky

$$\bar{f}^{\rm ob}(\vec{x}_o;z) \equiv \frac{1}{4\pi}\int \sin\theta_1\,\mathrm{d}\theta_1\,\mathrm{d}\phi_1\, f(\vec{x}_o;z,\mathbf{n}_1)\,. \tag{7.11}$$

It is very important to note that these $N$-point functions depend on $\vec{x}_o$, not only because of the observer terms $\delta f_o$, but simply because a given universe realisation is not exactly homogeneous and isotropic. For instance, a fictitious observer located in the Holmberg galaxy[2], measuring the CMB temperature anisotropies would obtain a different map than ours, since it would correspond to another past light-cone. The two maps would be indistinguishable only statistically. Of course, we do not have access to the data for $\vec{x} \neq \vec{x}_o$, apart from the points that lie at the intersections of the $\vec{x}$ and $\vec{x}_o$ past light-cone. Nevertheless, it is important to keep in mind this implicit $\vec{x}_o$ dependence which comes from the fact that observation in a inhomogeneous universe is light-cone-dependent.

The integral in (7.10) admits a nice group-theoretical interpretation. Indeed, the set of frames is isomorphic to the SO(3) manifold, because $\mathbf{n}_1(\theta_1,\phi_1)$ and $\phi_2$ can be thought of as the direction and magnitude of a rotation, i.e. they form the vector $\vec{\theta} \equiv \phi_2\mathbf{n}_1$ that parametrises the group algebra $\vec{\theta}\cdot\vec{J} \in \mathfrak{so}(3)$, where $\vec{J}$ are the generators. By choosing the latter appropriately, one can interpret $\theta_1$, $\phi_1$ and $\phi_2$ as Euler angles $\beta$, $\gamma$ and $\alpha$, respectively. The integral in eq. (7.10) is therefore an integral over the SO(3) manifold and $\sin\theta_1\,\mathrm{d}\theta_1\,\mathrm{d}\phi_1\,\mathrm{d}\phi_2$ is the corresponding Haar measure (which we first introduced in chapter 6), so that we can use the notation

$$G^{\rm ob}(\vec{x}_o;\{z_k\}_{k=1}^N,\{\theta_k\}_{k=2}^N,\{\phi_k\}_{k=3}^N) = \langle\prod_{k=1}^N f(\vec{x}_o;z_k,\mathbf{n}_k)\rangle_{\rm SO(3)}\,. \tag{7.12}$$

On the theoretical side, the quantities for which we can make predictions are ensemble averages, to which we will refer here as "theoretical" $N$-point functions

$$G(\{z_k\}_{k=1}^N,\{\theta_k\}_{k=2}^N,\{\phi_k\}_{k=3}^N) \equiv \langle\prod_{k=1}^N f(\vec{x}_o;z_k,\mathbf{n}_k)\rangle_P\,. \tag{7.13}$$

As in the observational case, these functions solely depend on the relative angles and not on the choice of reference frame, because the PDF $P_t[\Phi]$ is invariant under rotations, so one can rotate $\theta_1$, $\phi_1$ and $\phi_2$ away. Contrary to the observational ones, however, these functions are also independent of $\vec{x}_o$, because the PDF is invariant under translations, so one can translate the arguments to $\vec{x}_o \to 0$ (without affecting the relative quantities $z_k$, $\theta_k$ and $\phi_k$).

## 7.3 The ergodic hypothesis and its practical approximation

We now wish to relate the theoretical and observational $N$-point functions. To that end, we start by considering the set of 3-dimensional field configurations over which we sum when performing an ensemble average, i.e. in eq. (7.4). This ensemble can be partitioned into

[2] A dwarf galaxy in the constellation Ursa Major, roughly 3 Mpc from the Milky Way.

equivalence classes, where two field configurations are deemed equivalent if they can be related by a Euclidean transformation. Denoting by $[\Phi]$ the equivalence classes, we can then describe any element in $[\Phi]$ as

$$\Phi_{R,\vec{a}}(\vec{x}) = \Phi_{1,0}(R\vec{x} + \vec{a})\,, \tag{7.14}$$

where $R$ is a rotation matrix, $\vec{a}$ a translation vector and $\Phi_{1,0}$ is some representative of the class. In Fourier space, this translates into

$$\Phi_{R,\vec{a}}(\vec{k}) = e^{i\vec{a}\cdot\vec{k}}\Phi_{1,0}(R\vec{k})\,, \tag{7.15}$$

and it will be convenient to parametrise $R$ by the three Euler angles $\theta_1$, $\phi_1$ and $\phi_2$. The reason for partitioning the set of configurations thusly is that the PDF gives the same weight to all the elements of a given class, thanks to its invariance under the Euclidean group $\mathbb{E} \equiv \mathrm{SO}(3) \times \mathbb{R}^3$. We can therefore split the functional integration in eq. (7.4) into an integral over the elements of a given class $[\Phi]$ followed by an integral over all possible classes. By the latter we mean an integral over suitably chosen representatives $\Phi_{1,0}$ such that the corresponding functional integral is well-defined.[3] The PDF will then factorise outside of the first integral to yield

$$\int \mathcal{D}\Phi\, P_0[\Phi]\, X[\Phi] = \int \mathcal{D}\Phi_{1,0}\, P_0[\Phi_{1,0}]\, \langle X[\Phi_{1,0}]\rangle_{\mathbb{E}}\,, \tag{7.16}$$

where $X[\Phi]$ represents the quantity we are averaging (essentially products of fields). The average over the Euclidean group is defined

$$\langle X[\Phi(\vec{x})]\rangle_{\mathbb{E}} \equiv \frac{1}{V}\int \mathrm{d}^3a\, \frac{1}{8\pi^2}\int \sin\theta_1\, \mathrm{d}\theta_1\, \mathrm{d}\phi_1\, \mathrm{d}\phi_2\, X[\Phi(R\vec{x} + \vec{a})]\,. \tag{7.17}$$

As one could expect, the ensemble average therefore contains a purely geometric average over the symmetry group of the PDF. The integral over the SO(3) subgroup of $\mathbb{E}$ was already encountered in the observational $N$-point functions, where it appeared as an average over reference frames. The average over the translation subgroup, however, would correspond to an average over all possible observer positions $\vec{x}_o$. More precisely, the "active" transformation of the field $\Phi(\vec{x}) \to \Phi(\vec{x} + \vec{a})$ can be interpreted "passively" as the change of observer position $\vec{x}_o \to \vec{x}_o - \vec{a}$.

The advantage of the factorisation in eq. (7.16) is that it disentangles the statistical and geometrical parts of the average. In particular, it implies that the ergodic hypothesis can be formulated as

$$\langle \prod_{k=1}^{N} f(\vec{x}_o; z_k, \mathbf{n}_k)\rangle_P \overset{\text{erg.}}{=} \langle \prod_{k=1}^{N} f(\vec{x}_o; z_k, \mathbf{n}_k)\rangle_{\mathbb{E}}\,, \tag{7.18}$$

since the ensemble average is already a Euclidean group average before even considering the choice of statistics. In terms of the theoretical and observational $N$-points functions this reads

$$\begin{aligned} G(\{z_k\}_{k=1}^N, \{\theta_k\}_{k=2}^N, \{\phi_k\}_{k=3}^N) &\overset{\text{erg.}}{=} \frac{1}{V}\int \mathrm{d}^3x_o\, G^{\text{ob}}(\vec{x}_o; \{z_k\}_{k=1}^N, \{\theta_k\}_{k=2}^N, \{\phi_k\}_{k=3}^N)\,, \\ \bar{f}(z) &\overset{\text{erg.}}{=} \frac{1}{V}\int \mathrm{d}^3x_o\, \bar{f}^{\text{ob}}(\vec{x}_o; z)\,, \end{aligned} \tag{7.19}$$

[3] The existence of such a splitting of the integration is a non-trivial mathematical assertion, whose proof, if possible, would go beyond the scope of this paper.

i.e. the ensemble average is equated to an average over all reference frames *and* light-cones (at least for infinite volume and Gaussian statistics). Note how both sides of the equation consistently have the same dependencies. Also, it is understood here that the left-hand side contains stochastic fields, whereas the right-hand side contains the actually observed realisation.

In practice, however, the information from several $\vec{x}_o$ is of course not available, so the best thing one can do is to use the standard approximation

$$\begin{aligned} G(\{z_k\}_{k=1}^N, \{\theta_k\}_{k=2}^N, \{\phi_k\}_{k=3}^N) &\simeq G^{\mathrm{ob}}(\vec{x}_o; \{z_k\}_{k=1}^N, \{\theta_k\}_{k=2}^N, \{\phi_k\}_{k=3}^N)\,, \\ \bar{f}(z) &\simeq \bar{f}^{\mathrm{ob}}(\vec{x}_o; z)\,. \end{aligned} \tag{7.20}$$

To estimate the error associated to this approximation, one usually considers the (statistical) covariance matrix

$$\begin{aligned} \sigma^2_{\mathrm{stat}}(\alpha_N, \alpha'_N) &= \langle \big[G^{\mathrm{ob}}(\vec{x}_o; \alpha_N) - G(\alpha_N)\big]\big[G^{\mathrm{ob}}(\vec{x}_o; \alpha'_N) - G(\alpha'_N)\big]\rangle_P \\ &= \langle G^{\mathrm{ob}}(\vec{x}_o; \alpha_N)\, G^{\mathrm{ob}}(\vec{x}_o; \alpha'_N)\rangle_P - G(\alpha_N)\, G(\alpha'_N)\,, \end{aligned} \tag{7.21}$$

where we have used the condensed entry notation

$$\alpha_N \equiv (\{z_k\}_{k=1}^N, \{\theta_k\}_{k=2}^N, \{\phi_k\}_{k=3}^N)\,, \tag{7.22}$$

and it is understood that the fields inside $G^{\mathrm{ob}}$ have been promoted to stochastic ones. More precisely, the "1-sigma" error in (7.20) is the square root of the diagonal $\sigma_{\mathrm{stat}}(\alpha_N, \alpha_N)$. On the other hand, one could also define a geometric covariance matrix

$$\begin{aligned} \sigma^2_{\mathrm{geo}}(\alpha_N, \alpha'_N) &= \frac{1}{V}\int \mathrm{d}^3x_o \big[G^{\mathrm{ob}}(\vec{x}_o; \alpha_N) - G(\alpha_N)\big]\big[G^{\mathrm{ob}}(\vec{x}_o; \alpha'_N) - G(\alpha'_N)\big] \\ &\overset{\text{erg.}}{=} \frac{1}{V}\int \mathrm{d}^3x_o\, G^{\mathrm{ob}}(\vec{x}_o; \alpha_N)\, G^{\mathrm{ob}}(\vec{x}_o; \alpha'_N) - G(\alpha_N)\, G(\alpha'_N) \\ &\overset{\text{erg.}}{=} (7.21)\,, \end{aligned} \tag{7.23}$$

since $G(\alpha_N)$ appears as the average of $G^{\mathrm{ob}}(\vec{x}_o; \alpha_N)$ over $\vec{x}_o$ in eq. (7.19). Not surprisingly, because of statistical homogeneity and ergodicity, we have

$$\sigma_{\mathrm{stat}} = \sigma_{\mathrm{geo}} \equiv \sigma\,, \tag{7.24}$$

as we show the appendix 7.A. This equality implies that the fundamental statistical uncertainty $\sigma_{\mathrm{stat}}$, usually known as "cosmic variance", can be interpreted as the error due to the fact that we observe a single universe realisation *and* from a single viewpoint $\vec{x}_o$. Indeed, if either one of these two conditions were dropped, under the ergodic hypothesis we could beat cosmic variance[4]. On the one hand, if we could observe a single realisation from all possible $\vec{x}_o$, then eq. (7.19) would allow us to match the theoretical predictions exactly. On the other hand, if we could observe all possible universe realisations, but from a single viewpoint $\vec{x}_o$, then we would be able to compute directly the theoretical $N$-point functions, which are independent

[4]This statement is only true for an infinite universe, as a compact universe would still have cosmic variance.

of $\vec{x}_o$. In both cases we would essentially be able to observe the expectation value of $G$, which of course has no variance. Note how crucial the assumption of statistical homogeneity and isotropy is in this argumentation.

Let us also make contact with the more common definition of cosmic variance in the context of the CMB power spectrum. In that case, cosmic variance is usually explained as the lack of enough $m$ values for low $\ell$, i.e. the small number of large sky patches over which to average. In the perspective considered here, we understand that this is due to the lack of alternative viewpoints $\vec{x}_o$. Indeed, if we had access to these, then we would have access to any region from multiple viewpoints at the intersections of different light-cones, which would then eliminate cosmic variance.

## 7.4 The subtlety of connected correlations functions

Until now we have only considered generic correlation functions, but for each $N$ the non-trivial information lies in the connected part. Given the fact that the complexity in the definition of spherical connected functions increases rapidly with $N$, here we will solely focus on the most relevant case for this thesis: the connected two-point functions. On the theoretical side we have

$$\begin{aligned}\tilde{G}(z_1,z_2,\theta_2) &\equiv G(z_1,z_2,\theta_2) - \bar{f}(z_1)\,\bar{f}(z_2) \\ &= \bar{f}(z_1)\,\bar{f}(z_2)\,\langle \delta f(\vec{x}_o;z_1,\mathbf{n}_1)\,\delta f(\vec{x}_o;z_2,\mathbf{n}_2)\rangle_P\,,\end{aligned} \tag{7.25}$$

where $\delta f$ was defined in eq. (7.5). On the observational side we have

$$\begin{aligned}\tilde{G}^{\rm ob}(\vec{x}_o;z_1,z_2,\theta_2) &\equiv G^{\rm ob}(\vec{x}_o;z_1,z_2,\theta_2) - \bar{f}^{\rm ob}(\vec{x}_o;z_1)\,\bar{f}^{\rm ob}(\vec{x}_o;z_2) \\ &= \langle \Delta f^{\rm ob}(\vec{x}_o;z_1,\mathbf{n}_1)\,\Delta f^{\rm ob}(\vec{x}_o;z_2,\mathbf{n}_2)\rangle_{\rm SO(3)}\,, \\ &= \bar{f}^{\rm ob}(\vec{x}_o;z_1)\,\bar{f}^{\rm ob}(\vec{x}_o;z_2)\,\langle \delta f^{\rm ob}(\vec{x}_o;z_1,\mathbf{n}_1)\,\delta f^{\rm ob}(\vec{x}_o;z_2,\mathbf{n}_2)\rangle_{\rm SO(3)}\,,\end{aligned}$$

where

$$\Delta f^{\rm ob}(\vec{x}_o;z,\mathbf{n}) = f(\vec{x}_o;z,\mathbf{n}) - \bar{f}^{\rm ob}(\vec{x}_o;z)\,,\quad \delta f^{\rm ob}(\vec{x}_o;z,\mathbf{n}) = \frac{\Delta f^{\rm ob}(\vec{x}_o;z,\mathbf{n})}{\bar{f}^{\rm ob}(\vec{x}_o;z)}\,. \tag{7.26}$$

Here we stress with the "ob" subscript that the fluctuations are computed with respect to the observational average $\bar{f}^{\rm ob}(\vec{x}_o;z)$ which is not the ensemble average $\bar{f}(z)$. Let us now see how the ergodic hypothesis (7.19) relates the theoretical and observational connected two-point functions. To that end, it will be convenient to decompose these in Legendre polynomials, as we have done in chapter 3,

$$\begin{aligned}\tilde{G}(z_1,z_2,\theta) &= \sum_{\ell=0}^{\infty}(2\ell+1)\,\mathcal{P}_\ell(\cos\theta)\,\tilde{G}_\ell(z_1,z_2)\,, \\ \tilde{G}^{\rm ob}(\vec{x}_o;z_1,z_2,\theta) &= \sum_{\ell=0}^{\infty}(2\ell+1)\,\mathcal{P}_\ell(\cos\theta)\,\tilde{G}^{\rm ob}_\ell(\vec{x}_o;z_1,z_2)\,,\end{aligned} \tag{7.27}$$

so that

$$\begin{aligned}\tilde{G}_\ell(z_1,z_2) &= G_\ell(z_1,z_2) - \bar{f}(z_1)\,\bar{f}(z_2)\,\delta_{\ell 0}\,,\\ \tilde{G}^{\rm ob}_\ell(\vec{x}_o;z_1,z_2) &= G^{\rm ob}_\ell(\vec{x}_o;z_1,z_2) - \bar{f}^{\rm ob}(\vec{x}_o;z_1)\,\bar{f}^{\rm ob}(\vec{x}_o;z_2)\,\delta_{\ell 0}\,,\end{aligned} \tag{7.28}$$

where $G_\ell$ and $G^{\rm ob}_\ell$ are the multipoles of the non-connected ones. Using eq. (7.19) in the Legendre basis we then find

$$\begin{aligned}\tilde{G}_\ell(z_1,z_2) &= G_\ell(z_1,z_2) - \bar{f}(z_1)\,\bar{f}(z_2)\,\delta_{\ell 0} \overset{\rm erg.}{=} \frac{1}{V}\int {\rm d}^3x_o\, G^{\rm ob}_\ell(\vec{x}_o;z_1,z_2) - \bar{f}(z_1)\bar{f}(z_2)\,\delta_{\ell 0}\\ &= \frac{1}{V}\int {\rm d}^3x_o\,\tilde{G}^{\rm ob}_\ell(\vec{x}_o;z_1,z_2) + \left[\frac{1}{V}\int {\rm d}^3x_o\,\bar{f}^{\rm ob}(\vec{x}_o;z_1)\,\bar{f}^{\rm ob}(\vec{x}_o;z_2) - \bar{f}(z_1)\,\bar{f}(z_2)\right]\delta_{\ell 0}\\ &= \frac{1}{V}\int {\rm d}^3x_o\,\tilde{G}^{\rm ob}_\ell(\vec{x}_o;z_1,z_2) + \sigma^2(z_1,z_2)\,\delta_{\ell 0}\,,\end{aligned} \tag{7.29}$$

i.e. the ergodic relation holds only up to a monopole term and the latter is nothing but the covariance matrix of the one-point function. We can understand this difference simply by the fact that, in order to obtain connected functions, one must subtract products of averages with different definitions in the theoretical and observational cases. To understand the monopole discrepancy in particular, note that $\tilde{G}^{\rm ob}_0(\vec{x}_o;z_1,z_2)\equiv 0$ by construction

$$\begin{aligned}\tilde{G}^{\rm ob}_0 &= \frac{1}{2}\int \sin\theta_2\,{\rm d}\theta_2\,\tilde{G}^{\rm ob}(\vec{x}_o;z_1,z_2,\theta_2)\\ &= \frac{1}{16\pi^2}\int \sin\theta_1\,{\rm d}\theta_1\,{\rm d}\phi_1\,\sin\theta_2\,{\rm d}\theta_2\,{\rm d}\phi_2 \Delta f^{\rm ob}(\vec{x}_o;z_1,\mathbf{n}_1)\,\Delta f^{\rm ob}(\vec{x}_o;z_2,\mathbf{n}_2)\\ &= \left[\frac{1}{4\pi}\int {\rm d}\Omega_1\,\Delta f^{\rm ob}(\vec{x}_o;z_1,\mathbf{n}_1)\right]\left[\frac{1}{4\pi}\int {\rm d}\Omega_2\,\Delta f^{\rm ob}(\vec{x}_o;z_2,\mathbf{n}_2)\right] = 0\,,\end{aligned} \tag{7.30}$$

since each factor in the end is identically zero. On the other hand, the theoretical monopole of $\tilde{G}_0(z_1,z_2)$ is not zero generically. To see this, remember first that the ensemble average can be partitioned as in eq. (7.16), thus leading to a statistical average of directional averages as above. The difference, however, is that the directional average of $\delta f^{\rm ob}$ is zero by definition, while the one of $\delta f$ is not zero because $\delta f$ is the fluctuation around the ensemble average $\bar{f}(z)$, not the sphere average $\bar{f}^{\rm ob}(\vec{x}_o;z)$. As a result of eq. (7.29) the ergodic relation for connected two-point functions holds for $\ell > 0$

$$\tilde{G}_{\ell>0}(z_1,z_2) \overset{\rm erg.}{=} \frac{1}{V}\int {\rm d}^3x_o\,\tilde{G}^{\rm ob}_{\ell>0}(\vec{x}_o;z_1,z_2)\,, \tag{7.31}$$

and the ergodic approximation (eq. (7.20) for the generic N-point functions) holds, for the connected two-point function, in the form

$$\tilde{G}_{\ell>0}(z_1,z_2) \simeq \tilde{G}^{\rm ob}_{\ell>0}(\vec{x}_o;z_1,z_2)\,. \tag{7.32}$$

On the other hand the $\ell = 0$ case, along with $\tilde{G}^{\rm ob}_0 \equiv 0$, simply states that the monopole of the theoretical connected two-point function is the (cosmic) variance of the one-point function

$$\sigma^2(z_1,z_2) = \tilde{G}_0(z_1,z_2)\,. \tag{7.33}$$

Another relation we must check in the connected case is eq. (7.24), i.e. that both deviations of variance coincide. Expressing the covariance matrix of the connected two-point function in terms of the connected one and using (7.24) one can prove that the statistical and geometric uncertainties on $\tilde{G}_\ell(\vec{x}_o; z_1, z_2)$ are equal for $\ell > 0$

$$\tilde{\sigma}_{\mathrm{geo},\ell\ell}(z_1, z_2, z_1, z_2) = \tilde{\sigma}_{\mathrm{stat},\ell\ell}(z_1, z_2, z_1, z_2)\,, \qquad \ell > 0\,, \tag{7.34}$$

but not for $\ell = 0$.

## 7.5 Discussion

We now have the required argument to tackle the question that was raised in the introduction, i.e. of whether we can ensemble average the terms that are close and/or at the observer point. The ergodic hypothesis (7.19) relates, in an infinite universe, the quantity that is predicted by the theorist $G(...)$ *not* to the one that observer actually measures $G^{\mathrm{ob}}(\vec{x}_o; ...)$, but rather to an average over all the possible light-cones $\vec{x}_o$ of $G^{\mathrm{ob}}(\vec{x}_o; ...)$. By considering all possible $\vec{x}_o$, we also have a "large enough" number of observer points, just as for the source points, so it is completely legitimate to ensemble average the observer terms as well.

The discomfort arises only because of the ergodic *approximation* (7.20), which is the only relation one can use in practice and contains indeed a single $\vec{x}_o$ on the observer side. However, we showed that the error related to privileging $\vec{x}_o$, i.e. $\sigma_{\mathrm{geo}}$, is nothing but the usual statistical error $\sigma_{\mathrm{stat}}$ associated with this approximation, i.e. cosmic variance. This means that, by ensemble averaging *all* terms in the theoretical N-point functions $G$, we are not getting any further from the observed quantities than the usual statistical uncertainty.

The situation is slightly more involved in the case of connected correlation functions, which are ultimately where the interesting information lies. In particular, in the two-point function case, all of the above conclusions hold for all multipoles except for the monopole. As we have anticipated in chapter 4, we have formally proven here that the monopole is exactly zero on the observational side, while it can be in general non-zero in the theoretical computation. Let us also go back to an argument that we have raised in chapter 4: the subtraction of the monopole for the regularisation of the IR divergence of the correlation function. The reason for subtracting $\tilde{G}_0$ was, as we said, two-fold: (i) $\tilde{G}_0^{\mathrm{obs}} = 0$ by construction and (ii) the correlation function converges only after this operation. We have however neglected in our discussion the terms at the observer $\delta f_o$. It has been shown in the literature [59, 147, 273] that including the contributions from these terms regularise the theoretical monopole $G_0$. Furthermore we have argued here that the ensemble average of fields at the observer position poses no difficulty but, on the contrary, it is the sensible procedure to ensure that statistical homogeneity is enforced. Terms at the observer, together with super-horizon long wavelength modes, only contribute the the monopole of the two-point function and we have proven in this chapter that the ergodic hypothesis cannot be applied on the monopole. In other words, although keeping track of observer terms and ensemble averaging over them is possible, they

contribute to a quantity that cannot be matched with observations. This justifies the approach we have used in chapter 4 of simply removing the monopole from the theoretical computation.

Finally, as a interesting side-note, let us highlight the fact that eq. (7.33) provides the cosmic variance uncertainty for the average observable. Usually one thinks of cosmic variance as a scale-dependent uncertainty, thus affecting only scale-dependent quantities such as correlation functions. Here, however, we nicely recover the fact that even average measurements of observables are of course affected by the fact that we can only observe them at $\vec{x}_o$. More precisely, the theoretical prediction for the observed quantity $\bar{f}^{\rm ob}(\vec{x}_o; z)$ is $\bar{f}(z) \pm \sigma(z)$, where $\sigma(z)$ is consistently parametrically smaller than $\bar{f}(z)$. For instance, in the case of the CMB temperature $f \equiv T_{\rm CMB}$ we have

$$\frac{\tilde{G}_0}{\bar{T}^2_{\rm CMB}} \sim \left(\frac{\Delta T_{\rm CMB}}{\bar{T}_{\rm CMB}}\right)^2 \sim 10^{-8}\,, \qquad \Rightarrow \qquad \frac{\sigma}{\bar{T}_{\rm CMB}} \sim 10^{-4}\,. \tag{7.35}$$

We then recover the well-know fact that one can of course measure the average CMB temperature at $\vec{x}_o$ with arbitrary precision. However, only the first four non-trivial digits of this number will be representative of this quantity in the universe and therefore cosmologically relevant. The rest of the digits will be strongly dependent on $\vec{x}_o$.

# Appendices

## 7.A Proof of $\sigma_{\mathbf{stat}} = \sigma_{\mathbf{geom}}$

We will show that the two non-trivial terms in the second lines of Eqs. (7.21) and (7.23) are equal. First note that

$$\frac{1}{V}\int \mathrm{d}^3x_o\, G^{\mathrm{ob}}(\vec{x}_o;\alpha_N)\, G^{\mathrm{ob}}(\vec{x}_o;\alpha'_N) = \frac{1}{8\pi^2}\int \sin\theta'_1\,\mathrm{d}\theta'_1\,\mathrm{d}\phi'_1\,\mathrm{d}\phi'_2 \\ \times \frac{1}{V}\int \mathrm{d}^3x_o\,\frac{1}{8\pi^2}\int \sin\theta_1\,\mathrm{d}\theta_1\,\mathrm{d}\phi_1\,\mathrm{d}\phi_2 \prod_{k=1}^{N} f(\vec{x}_o;z_k,\mathbf{n}_k)\, f(\vec{x}_o;z_k,\mathbf{n}'_k)\,,$$

where the second line looks like the $\vec{x}_o$ average of the observer $2N$-point function. The only subtlety is that the angles in $\mathbf{n}'_k$ are relative to the $(\mathbf{n}'_1,\mathbf{n}'_\perp)$ frame, not the $(\mathbf{n}_1,\mathbf{n}_\perp)$ one. Nevertheless, since we are integrating over all $(\mathbf{n}'_1,\mathbf{n}'_\perp)$ frames (see first line), we can rotate the latter such that $\theta'_1$, $\phi'_1$ and $\phi'_2$ are redefined to be the relative angles $\theta_{N+1}$, $\phi_{N+1}$ and $\phi_{N+2}$ with respect to $(\mathbf{n}_1,\mathbf{n}_\perp)$ in the product of $2N$ observables. Thus, using the ergodic theorem

$$\frac{1}{V}\int \mathrm{d}^3x_o\, G^{\mathrm{ob}}(\vec{x}_o;\alpha_N)\, G^{\mathrm{ob}}(\vec{x}_o;\alpha'_N) \overset{\text{erg.}}{=} \frac{1}{8\pi^2}\int \sin\theta'_1\,\mathrm{d}\theta'_1\,\mathrm{d}\phi'_1\,\mathrm{d}\phi'_2 \\ \times G(\{z_k\}_{k=1}^N,\{z'_k\}_{k=1}^N,\{\theta_k\}_{k=2}^N,\{\theta'_k\}_{k=1}^N,\{\phi_k\}_{k=3}^N,\{\phi'_k\}_{k=1}^N)\,. \tag{7.36}$$

On the other hand, proceeding similarly for the non-trivial term of the statistical covariance matrix, we find[5]

$$\begin{aligned}\langle G^{\rm ob}(\vec{x}_o;\alpha_N)\, G^{\rm ob}(\vec{x}_o;\alpha'_N)\rangle_P &= \frac{1}{64\pi^4}\int \sin\theta_1\,\mathrm{d}\theta_1\,\mathrm{d}\phi_1\,\mathrm{d}\phi_2\,\sin\theta'_1\,\mathrm{d}\theta'_1\,\mathrm{d}\phi'_1\,\mathrm{d}\phi'_2 \\ &\qquad\times \langle\prod_{k=1}^{N} f(\vec{x}_o;z_k,\mathbf{n}_k)\, f(\vec{x}_o;z'_k,\mathbf{n}'_k)\rangle_P \\ &= \frac{1}{64\pi^4}\int \sin\theta_1\,\mathrm{d}\theta_1\,\mathrm{d}\phi_1\,\mathrm{d}\phi_2\,\sin\theta'_1\,\mathrm{d}\theta'_1\,\mathrm{d}\phi'_1\,\mathrm{d}\phi'_2 \\ &\qquad\times G(\{z_k\}_{k=1}^N,\{z'_k\}_{k=1}^N,\{\theta_k\}_{k=2}^N,\{\theta'_k\}_{k=1}^N,\{\phi_k\}_{k=3}^N,\{\phi'_k\}_{k=1}^N) \\ &= \frac{1}{8\pi^2}\int \sin\theta'_1\,\mathrm{d}\theta'_1\,\mathrm{d}\phi'_1\,\mathrm{d}\phi'_2 \\ &\qquad\times G(\{z_k\}_{k=1}^N,\{z'_k\}_{k=1}^N,\{\theta_k\}_{k=2}^N,\{\theta'_k\}_{k=1}^N,\{\phi_k\}_{k=3}^N,\{\phi'_k\}_{k=1}^N)\,,\end{aligned}$$

which is indeed the same as (7.36).

[5]The last equality holds because the $2N$-point function is independent of the reference frame angles $\theta_1$, $\phi_1$ and $\phi_2$.

# CHAPTER 8

## Summary and conclusions

In this thesis we analysed different probes of the large scales structures of the universe in terms of the truly observable coordinates, namely the redshift $z$ and the angular position $\mathbf{n}$ of the sources. In recent years a lot of effort has been put into the fully relativistic characterisation of LSS observables, considering the full set of light-cone effects. The latter arise as our observations are limited to our past light-cone. On the one hand, as light-like geodesics are conformally invariant, the background universe has the light-cone geometry of Minkowski space. On the other hand, in a universe with structures, introducing fluctuations of the metric induces perturbations to the light-cone which must be taken into account if we want to correctly relate theory and observations. The most relevant example of this mapping from real-space coordinates to light-cone coordinates (redshift-space) is Redshift Space Distortion, which is responsible for the famous *fingers of God* and *pancakes of God*. While RSD has been routinely included in the analysis of redshift surveys, other projection effects have been generally neglected. The reason for this is that they are suppressed by powers of $\mathcal{H}/k$, hence they can become relevant only at very large scales[1]. However, planned and future galaxies surveys promise to deliver very precise and deep large scale observations of the galaxy distribution where relativistic effects (especially weak lensing) contribute to the signal. We can make a wishful comparison with the history of CMB observations, where very accurate measurements of the temperature fluctuations and the polarisation have allowed us to determine cosmological parameters with a precision of 1% and better. Now we plan to continue this success story with LSS surveys.

From a theoretical point of view the observable of choice, the one more suited for a full-sky, relativistic description of galaxy clustering is the angular power spectrum of number counts $C_\ell$ (introduced in chapter 2). On the other hand experimental effort has been generally directed to the two-point correlation function $\xi(z_1, z_2, \theta)$ (introduced in chapter 3). This thesis

[1] RSD and also lensing are not suppressed by powers of $\mathcal{H}/k$, hence they are the most important effects.

is mainly focussed on the latter. Even from the theory side, the two-point function has some nice properties that qualify it as an observable which is complementary to the $C_\ell$. The most important feature of $\xi(z_1, z_2, \theta)$ is the possibility of performing an analysis in terms of its multipoles $\xi_\ell(r)$ which allows to isolate certain contributions in a subset of the allowed values of $\ell$. With the $C_\ell$ on the other hand there is no simple way to isolate – for example – RSD, since each multipole $\ell$ is a non-trivial combination of density and velocity. The bulk of this thesis is devoted to the study of the full-sky, fully relativistic two-point correlation function.

In chapter 2 we have introduced the galaxy number counts and computed how projection effects due to scalar, vector and tensor perturbations affect this observable. We have obtained a general expression which can be applied for all situations where linear cosmological perturbation theory is valid. We have employed it to compute the contribution to the galaxy number counts from vector perturbations which are induced from the usual scalar perturbations at second order in perturbation theory. While these terms are certainly present in the standard ΛCDM cosmology, they are very small. It is however interesting to note that, for high redshift surveys, the total ratio of the vector-induced and scalar-induced effects is increasing, even though the second order vectors are smaller at higher redshift. This is due to the fact that at high redshift the lensing term increases while the density and redshift space distortions are less relevant. Therefore the lensing term becomes more relevant and for this contribution vector perturbations are least suppressed.

In chapter 3 we began our investigation of the galaxy two-point function, presenting the theoretical framework for the study of the full-sky, fully relativistic multipoles of the correlation function. We pointed out that even though these functions are *not* model independent – as a cosmological model must be used to convert angles and redshifts into distances – they are useful for several reasons. First they are well adapted to describe the 3-dimensional information present in large-scale structures. This is not the case for the observable $C_\ell$ angular-redshift power spectrum for which we cannot employ very fine redshift binning due to under-sampling. Second, the multipoles of the correlation function and of the power spectrum contain important information about the growth of perturbations which is difficult to isolate in the angular-redshift power spectrum. We have computed these quantities within linear perturbation theory and with the halofit approximation, showing how they are affected by large-scale relativistic effects and by lensing, the importance of which is bigger at high redshift. Furthermore we discovered that the presence of higher multipoles in both, the correlation function and the power spectrum, might represent an ideal observational target to identify the lensing term.

In chapter 4 we detail how the results of chapter 3 have been employed to write the code COFFE. The code allows for a fast and accurate computation of the relativistic two-point correlation function and its multipoles. We have also introduced two estimators of the $\xi_\ell$ and computed their covariance. We discussed some subtleties regarding the two-point function and presented forecast on the detectability of the lensing signal in the galaxy correlation function, finding that upcoming galaxy survey will be able to detect it in the multipoles. This

opens the possibility of testing gravity from the clustering signal alone as it allows to put constraints in the $(\Sigma, \mu)$ plane of GR modifications.

In chapter 5 we pointed out the existence of a second feature in the matter two-point function, besides the acoustic peak. This feature, positioned at twice the distance of the BAO peak, is understood – in the early universe – as a trough in the baryon-baryon correlation for separations bigger than twice the sound horizon at $z_{\rm drag}$. The feature is clearly visible in models with an high baryon fraction while in a realistic cosmological model it is a very small effect. We proved this with a $\chi^2$ analysis that showed that – even in an SKA-like survey – it is not possible to distinguish between the models with and without the second feature. Note that in a Fourier space analysis the effect we have described is correctly modelled if the template $P(k)$ is generated from a Boltzmann code such as CLASS or CAMB.

In chapter 6, we presented a suitable decomposition to discuss the signal induced by anisotropic vector perturbation in the galaxy two-point function and perform a Fisher forecast to determine the detectability of the parameters which characterise the anisotropy with planned or futuristic galaxy catalogs. A general method to isolate the anisotropic signal is obtained through a decomposition in bipolar spherical harmonics. We provided an analytical expression for the coefficients of this expansion which does not require the adoption of a specific model and we have derived two types of constraints, both on the total amplitude of the anisotropy and on the preferred direction (in terms of the SO(3) volume of its Euler angles).

In chapter 7 we analysed the averaging procedure of cosmological observable from a theoretical and observational point of view. We then showed how, under the ergodic hypothesis, on the one hand averaging over fields at the observer position poses no difficulty but on the other hand their contribution is relegated to the unobservable monopole, for which the ergodic approximation cannot be employed.

As a final remark we argue that future directions of this line of work should be aimed at bridging the gap between theoretical understanding of galaxy clustering and the complications entailed in observations. One important aspect that we over-simplified in this work is *biasing*: the relationship between the spatial distribution of galaxies (which is what we measure) and the underlying dark matter density field (which is what we characterise theoretically). Throughout this thesis we have employed the common approximation of a scale-independent and linear galaxy bias, justified by the fact that at large scales (where relativistic effects are most important) this is a fair assumption. Furthermore galaxy survey analyses that are only aimed at measuring the BAO scale, can usually overlook this problem and include the effect of bias into the nuisance parameters of their two-point function fit. In the future however, if we are interested into the determination of cosmological parameters at the 1% precision level, the bias problem has to be studied in conjunction with the projection effects. A similar argument holds for non-linear effects as most of the scales interesting for the study of LSS are affected by non-linear gravitational evolution. On the one hand the computation presented in chapter 2 has been pushed to higher order in perturbation theory by several authors, while

on the other hand (usually Newtonian) N-body simulations are the best bet to push into the mildly non-linear regime. Finally let us also point out that the magnification bias $s$ and the evolution bias $f_{\rm evo}$ are usually considered contamination of the signal in cosmology due to the big uncertainty on them. They are however important probes of galaxy evolution, as they are linked to the luminosity function of galaxies.

# APPENDIX A

## Background & Cosmological perturbation theory

This appendix is mainly based on [131].

## A.1 The background cosmology

In this section we review the basic equations and concepts of the background evolution of the universe. We present the relevant aspects of this subject for self-completeness of this thesis, while we refer to many great cosmology books for an in-depth treatment.

As we discussed in the Introduction the guide for a mathematical description of the cosmos' evolution is the *cosmological principle*, which states that at large scales (let's say $\gg 10\,\mathrm{Mpc}$) the universe is approximately homogenous and isotropic. In technical terms this means that it exists a preferred time coordinate, 'cosmic time' $t$, such that the 4-dimensional manifold $\mathcal{M}$ is foliated into 3-spaces $\Sigma_t = \{x^i | x^\mu = (t, x^i) \in \mathcal{M}\}$ of constant curvature. Cosmic time is the proper time of an observer which sees a spatially homogeneous and isotropic universe. The metric is hence given by

$$ds^2 = \bar{g}_{\mu\nu} dx^\mu dx^\nu = -dt^2 + a^2(t)\gamma_{ij} dx^i dx^j = a^2(\eta)(-d\eta^2 + \gamma_{ij} dx^i dx^j)\,, \tag{A.1}$$

where we have introduced the scale factor $a(t)$ which is linked to cosmological redshift via

$$1 + z = \frac{a_0}{a}\,, \qquad a_0 \equiv a(\eta_0)\,. \tag{A.2}$$

For the second equal sign of eq. (A.1) we have also defined the conformal time $\eta$, related to $t$ via $d\eta = dt/a$. We write the spatial metric $\gamma_{ij}$, in spherical coordinates, as

$$\gamma_{ij} dx^i dx^j = d\chi^2 + S_K^2(\chi) d\Omega^2 = d\chi^2 + S_K^2(\chi)(d\theta^2 + \sin^2\theta d\phi^2)\,, \tag{A.3}$$

where $K$ is the curvature parameter and we have defined

$$\begin{cases} S_K(\chi) = \frac{1}{\sqrt{K}}\sin(\sqrt{K}\chi) & K > 0\,, \\ S_K(\chi) = \chi & K = 0\,, \\ S_K(\chi) = \frac{1}{\sqrt{K}}\sinh(\sqrt{K}\chi) & K < 0\,. \end{cases} \tag{A.4}$$

The coordinates $(\chi, \theta, \phi)$ are referred as comoving coordinates: a particle moving on a background geodesic remains at $(\chi, \theta, \phi) = \text{const}$ as the universe expands. We denote with a prime derivatives w.r.t. cosmic time $\partial_t a = a'$ and with a dot derivatives w.r.t. conformal time $\partial_\eta a = \dot{a}$. The Hubble parameter is then defined as

$$H = \frac{a'}{a}\,, \tag{A.5}$$

and for a generic function of time we have

$$f' = \frac{\dot{f}}{a} \qquad f'' = \frac{\ddot{f}}{a^2} - \mathcal{H}\frac{\dot{f}}{a^2}\,, \tag{A.6}$$

where we have introduced the comoving Hubble parameter

$$\mathcal{H} = \frac{\dot{a}}{a} = aH\,. \tag{A.7}$$

As in this thesis we always set $a_0 = 1$, we have

$$\mathcal{H}(\eta_0) \equiv \mathcal{H}_0 = H(t_0) \equiv H_0 \equiv h \cdot 100\,\text{km/s/Mpc}\,,$$

with $h \simeq 0.7$.

The evolution of the scale factor $a(\eta)$ is governed by Einstein equations

$$R_{\mu\nu} - \frac{1}{2}Rg_{\mu\nu} \equiv G_{\mu\nu} = 8\pi G T_{\mu\nu} - \Lambda g_{\mu\nu}\,, \tag{A.8}$$

where $R_{\mu\nu}$, $G_{\mu\nu}$ are respectively the Riemann and Einstein tensors and $R$ is the Ricci scalar. For their definitions see section B.2. $\Lambda$ is the cosmological constant and $T_{\mu\nu}$ is the energy momentum tensor which - because of homogeneity and isotropy - can be written in terms of the (background) energy-density $\bar{\rho}$ and the pressure $\bar{p}$ as

$$\bar{T}_{\mu\nu} = \begin{pmatrix} -\bar{\rho}\bar{g}_{00} & \mathbf{0} \\ \mathbf{0} & \bar{p}\bar{g}_{ij} \end{pmatrix}. \tag{A.9}$$

In a FLRW universe the Einstein equation are

$$\begin{aligned} H^2 + \frac{K}{a^2} &= \frac{8\pi G}{3}\bar{\rho} + \frac{\Lambda}{3}\,, \\ 2\frac{a''}{a} + H^2 + \frac{K}{a^2} &= -8\pi G\bar{p} + \Lambda\,, \end{aligned} \tag{A.10}$$

or

$$\begin{aligned} \mathcal{H}^2 + K &= \frac{8\pi G}{3} a^2 \bar{\rho} + \frac{\Lambda a^2}{3}\,, \\ 2\dot{\mathcal{H}} + \mathcal{H}^2 + K &= -8\pi G a^2 \bar{p} + a^2 \Lambda\,. \end{aligned} \tag{A.11}$$

It is also sometimes useful to write them as

$$\begin{aligned} 4\pi G a^2 \bar{\rho}(1+w) &= \mathcal{H}^2 - \dot{\mathcal{H}} + K\,, \\ 2\dot{\mathcal{H}} &= -\frac{1+3w}{2}(\mathcal{H}^2 + K)\,. \end{aligned} \tag{A.12}$$

Furthermore energy conservation imposes $\nabla_\mu T^{\mu\nu} = 0$, from which

$$\dot{\bar{\rho}} = -3\mathcal{H}(\bar{\rho} + \bar{p})\,. \tag{A.13}$$

We can specify an equation of state for the fluid under consideration $\bar{p} = w\bar{\rho}$ such that in the case $w = \text{const}$, eq. (A.13) yields

$$\bar{\rho} = \bar{\rho}_0 a^{-3(1+w)}\,, \tag{A.14}$$

and we can infer the evolution of the energy-density for the different components: for pressureless matter (or *dust*) we have $w = 0$, hence $\bar{\rho}_m \sim a^{-3}$. For relativistic particles or radiation $w = 1/3$, hence $\bar{\rho}_\gamma \sim a^{-4}$. For the cosmological constant $w = -1$ and $\bar{\rho}_\Lambda = \text{const}$.

We introduce the adiabatic sound speed $c_s$ determined by

$$c_s = \sqrt{\dot{\bar{p}}/\dot{\bar{\rho}}}\,. \tag{A.15}$$

From this definition and eq. (A.13) we can write

$$\dot{w} = 3\mathcal{H}(1+w)(w - c_s^2)\,. \tag{A.16}$$

Hence $w = \text{const}$ only if $w = -1$ or $w = c_s^2$.

Note that in the absence of dark energy, $\Lambda = 0$, eq. (A.10) implies that for a specific value of the energy-density

$$\bar{\rho}_c \equiv \frac{3H^2}{8\pi G}\,, \tag{A.17}$$

we obtain $K = 0$. The value $\bar{\rho}_c$ is called the *critical* density and corresponds to the value of the energy-density for which the spatial geometry is flat. It is customary to define, for every species $X$, the density parameter $\Omega_X(\eta) = \bar{\rho}_X(\eta)/\bar{\rho}_c(\eta)$. In particular in this work we define

$$\begin{aligned} \Omega_m &= \Omega_m(\eta_0) = \frac{\bar{\rho}_m(\eta_0)}{\bar{\rho}_c(\eta_0)}\,, & \Omega_\gamma &= \Omega_\gamma(\eta_0) = \frac{\bar{\rho}_\gamma(\eta_0)}{\bar{\rho}_c(\eta_0)}\,, \\ \Omega_\Lambda &= \Omega_\Lambda(\eta_0) = \frac{\Lambda}{3H_0^2}\,, & \Omega_K &= \Omega_K(\eta_0) = -\frac{K}{a_0^2 H_0^2}\,, \\ \Omega_b &= \Omega_b(\eta_0) = \frac{\bar{\rho}_b(\eta_0)}{\bar{\rho}_c(\eta_0)}\,, & \Omega_\nu &= \Omega_\nu(\eta_0) = \frac{\bar{\rho}_\nu(\eta_0)}{\bar{\rho}_c(\eta_0)}\,, \end{aligned} \tag{A.18}$$

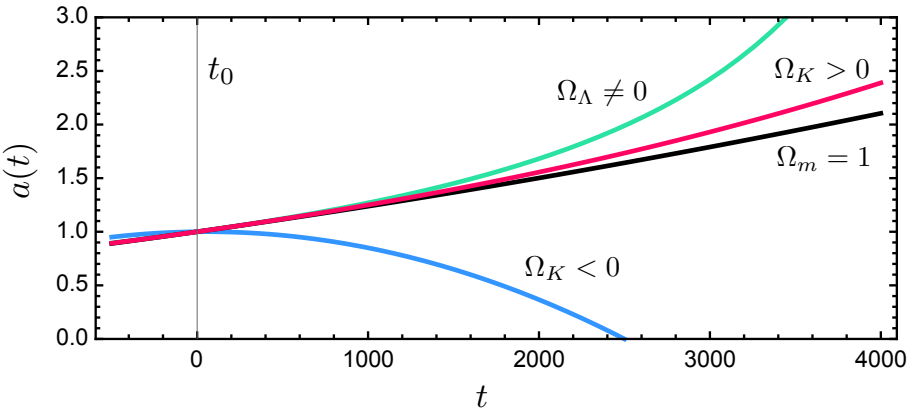


Figure A.1: The 'fate of the universe' plot which shows how different combinations of the density parameters determine the evolution of the scale factor $a(t)$.

for total matter, radiation, dark energy, curvature, baryons and neutrinos respectively. With these definitions we can divide eq. (A.10) by $H^2$ and obtain

$$1 = \sum_X \Omega_X(\eta)\,. \tag{A.19}$$

This relation is usually employed to fix the dark energy content of a flat universe ($\Omega_K = 0$) via

$$\Omega_\Lambda = 1 - \sum_{X\neq\Lambda} \Omega_X\,. \tag{A.20}$$

The $\Omega_X$ parameters fix the background evolution of the universe (i.e. $a(t)$) and the usual examples are given in figure A.1. In general the differential equation for the scale factor has no analytic solution while some notable exceptions are usually discussed in any cosmology book.

If all the $w_X$ are constants, eq. (A.10) can be written in terms of the evolution of the Hubble parameter as

$$H(a) = H_0\sqrt{\sum_X \Omega_X a^{-3(1+w_X)}}\,, \tag{A.21}$$

or, in a more familiar way,

$$H(z) = H_0\sqrt{\Omega_\gamma(1+z)^4 + \Omega_m(1+z)^3 + \Omega_\Lambda + \dots}\,. \tag{A.22}$$

Let us now briefly discuss the last subject of this section: cosmological distances and horizons. A question we could ask is how far light could have travelled since $t = 0$ in the absence of interactions? From the metric (A.1) and $ds^2 = 0$ we obtain

$$\eta = \int_0^t \frac{dt'}{a(t')}\,. \tag{A.23}$$

Since no information can propagate further on the comoving frame, conformal time $\eta$ provides a comoving horizon. The proper distance to the horizon gives the *particle* horizon

$$R_H(t) = a(t) \int_0^t \frac{dt'}{a(t')} \,. \tag{A.24}$$

This leads to the definition of the comoving distance

$$\chi = \eta_0 - \eta = \int_t^{t_0} \frac{dt'}{a(t')} = \int_0^z \frac{dz'}{H(z)} \,, \tag{A.25}$$

that can be thought of as the distance with the expansion 'factored out', so that the comoving distance between two object remains constant in time if they move only with the Hubble flow. The particle horizon should not be confused with the notion of Hubble radius defined as $H^{-1}$: events separated by a distance greater that $R_H$ were never in causal contact while events separated by a distance greater than $H(t)^{-1}$ are not in causal contact at time $t$. In comoving coordinates the Hubble radius is given by $\mathcal{H}^{-1}$.

Common ways to measure the distance in astronomy and cosmology are the angular diameter distance and the luminosity distance. The latter is defined as

$$\mathcal{D}_L(z) = \sqrt{\frac{L}{4\pi F}} \,, \tag{A.26}$$

where $L$ is the luminosity of a source at redshift $z$ - namely the energy emitted in all directions per second - and $F$ is its flux - namely the energy received per second per unit area. The angular diameter distance is defined as

$$\mathcal{D}_A(z) = \frac{a}{\sqrt{|\Omega_K|}H_0} S_K\left(\sqrt{|\Omega_K|}H_0 \int_0^z \frac{dz'}{H(z')}\right) , \tag{A.27}$$

which, for $K = 0$, reduces to $\mathcal{D}_A(z) = \chi(z)/(1+z)$. The Etherington relation links $\mathcal{D}_A$ to $\mathcal{D}_L$

$$\mathcal{D}_L(z) = (1+z)^2 \mathcal{D}_A(z) \,, \tag{A.28}$$

where one factor $(1+z)$ comes from the change in proper time and the other is due to the redshift of the photon energy. As a last remark let us expand the comoving distance around $t = t_*$. The scale factor can be written

$$a(t) \simeq a(t_*)\left[1 + H_*(t-t_*) - \frac{1}{2} q_* H_*^2 (t-t_*)^2 + ...\right] , \tag{A.29}$$

where we have introduced the deceleration parameter

$$q(t) = -\frac{a(t)a''(t)}{a'^2(t)} \,. \tag{A.30}$$

In the same way, using eq. (A.2), we obtain

$$t_* - t \simeq \frac{1}{H_*}\left[z - \left(1 + \frac{1}{2}q_*\right)z^2 + ...\right]. \tag{A.31}$$

With this and eq. (A.25) we obtain

$$\chi(z) \simeq \frac{1}{H_0}\left[z - \frac{1}{2}\left(1 + q_0\right)z^2 + ...\right], \tag{A.32}$$

and we sometimes use in this work the approximation $\chi(z) \simeq z/H_0$, for $z \ll 1$.

## A.2 Perturbation theory

For the moment we have only described the properties of the idealised background universe, isotropic and homogeneous. Clearly, the true metric of the universe is not the FLRW metric of eq. (A.1) as we can observe structures which are not isotropic nor homogeneous. Nevertheless observations show that, at least on large scale, the 'true' metric is 'close' to the background one. Essentially these inhomogeneities grew out of small variations of the geometry and of the energy-momentum tensor, which we treat in linear perturbation theory. In other words we can write the metric $g_{\mu\nu}$ as

$$g_{\mu\nu} \simeq \bar{g}_{\mu\nu} + a^2 h_{\mu\nu}\,, \tag{A.33}$$

where $\bar{g}_{\mu\nu}$ is the background metric and $h_{\mu\nu}$ a small perturbation around it, parametrised as

$$h_{\mu\nu}dx^\mu dx^\nu = -2Ad\eta^2 - 2B_i d\eta dx^i + 2Q_{ij}dx^i dx^j\,. \tag{A.34}$$

Note that we only deal with a flat background here as we generally set $\Omega_K = 0$ throughout this thesis.

### A.2.1 SVT decomposition

It is customary to perform the scalar-vector-tensor (SVT) decomposition of the perturbations. The reason is twofold: firstly, as we will see in a moment, this allows to explicitly count the number of degrees of freedom. Secondly, and more importantly, the scalar, vector and tensor d.o.f. evolve independently at first order, i.e. the corresponding Einstein equations are decoupled. We then decompose $B_i$ and $Q_{ij}$ as

$$\begin{aligned} B_i &= \underbrace{\partial_i B}_{(S)} + \underbrace{\hat{B}_i}_{(V)}\,, \\ Q_{ij} &= \underbrace{-C\delta_{ij} + \left(\partial_i\partial_j - \frac{1}{3}\nabla^2\right)E}_{(S)} + \underbrace{\frac{1}{2}\left(\partial_i\hat{E}_j + \partial_j\hat{E}_i\right)}_{(V)} + \underbrace{\hat{E}_{ij}}_{(T)}\,. \end{aligned} \tag{A.35}$$

Here $\hat{B}_i$ and $\hat{E}_i$ are true vectors degrees of freedom, $\partial_i\hat{E}^i = \partial_i\hat{B}^i = 0$, and $\hat{E}_{ij}$ is a true tensor, $\partial_i\hat{E}^{ij} = E^i_i = 0$. The 10 degrees of freedom of the metric have been decomposed in 4+4+2

SVT d.o.f.: the scalars $A, B, C, E$, the transverse vectors $\hat{E}_i$, $\hat{B}_i$ and the transverse-traceless tensor $\hat{E}_{ij}$. A similar decomposition holds for the energy momentum tensor $T_{\mu\nu}$. In general any rank-2 tensor can be decomposed by means of the projector

$$P_{\mu\nu} = g_{\mu\nu} + u_\mu u_\nu \,, \tag{A.36}$$

onto the subspace normal to $u^\mu = dx^\mu/dt$, where $t$ is the proper time along the word-line. We can then write [145]

$$T_{\mu\nu} = \rho u_\mu u_\nu + q_\mu u_\nu + q_\nu u_\mu + p P_{\mu\nu} + \Sigma_{\mu\nu} \,. \tag{A.37}$$

The energy density $\rho$ is defined as the time-like eigenvalue given as

$$T^\mu_\nu u^\nu = -\rho u^\mu \,, \qquad u^\mu u_\mu = -1, \,, \tag{A.38}$$

so that $\rho = T^{\mu\nu} u_\mu u_\nu$ is the relativistic energy density. Furthermore $\frac{1}{3} P^{\mu\nu} T_{\mu\nu}$ is the relativistic pressure, $-P^\nu_\mu T_{\nu\sigma} u^\sigma$ is the relativistic momentum density and

$$\Sigma_{\mu\nu} = -\left( P^\alpha_{(\mu} P^\beta_{\nu)} - \frac{1}{3} P_{\mu\nu} P^{\alpha\beta} \right) T_{\alpha\beta} \,,$$

where $()$ denotes symmetrisation, is the anisotropic (trace-free) stress tensor. Note that the component $u^0$ is fixed by the normalisation

$$u^0 = \frac{1}{a}(1 - A) \,, \tag{A.39}$$

and we further set

$$u^i = \frac{1}{a} v^i = \frac{1}{a} \left( -\partial^i v + \hat{v}^i \right) \,, \tag{A.40}$$

where we have decomposed $v$ into its scalar and vector component $\hat{v}_i = v_i^{(V)}$, $\partial^i \hat{v}_i = 0$. The spatial part of the momentum density is given by $q_i = (\bar{\rho} + \bar{p}) v_i$. At first order we write the perturbation in the energy density and in the pressure as $\rho = \bar{\rho}(1 + \delta)$ and $p = \bar{p} + \delta p$ so that the perturbed part of $T_{\mu\nu}$ is given by

$$\delta T^0_0 = -\bar{\rho}\, \delta \,, \tag{A.41}$$

$$\delta T^0_j = (\bar{\rho} + \bar{p})(v_j - B_j) \,, \tag{A.42}$$

$$\delta T^j_0 = -(\bar{\rho} + \bar{p}) v^j \,, \tag{A.43}$$

$$\delta T^i_j = \delta p\, \delta^i_j + \Sigma^i_j \,. \tag{A.44}$$

We already performed the SVT decomposition on $v_i$, while for the metric fields it was given in eq. (A.35). For the anisotropic stress we define

$$\Sigma_{ij} = \underbrace{\left( \partial_i \partial_j - \frac{1}{3} \nabla^2 \right) \Sigma}_{(S)} + \underbrace{\frac{1}{2} \left( \partial_i \hat{\Sigma}_j + \partial_j \hat{\Sigma}_i \right)}_{(V)} + \underbrace{\hat{\Sigma}_{ij}}_{(T)} \,. \tag{A.45}$$

### A.2.2 Gauge problem

We now go back to the issue we have already briefly discussed in the Introduction: the *gauge problem*. We have considered the first order perturbations $(h_{\mu\nu}, \delta T_{\mu\nu})$ on top of a FLRW background $\bar{g}_{\mu\nu}, \bar{T}_{\mu\nu}$; however, since the theory is invariant under diffeomorphism (coordinate transformation), the perturbations are not uniquely defined, but depend on our gauge choice. In other words when we wrote down the metric in eqs. (A.33)-(A.34) we implicitly chose a space-time slicing and defined spatial coordinates on the constant time hyper-surfaces. A different slicing choice will change the value of the perturbation fields. To show this let us consider a generic coordinates transformation given by

$$x^\mu \longrightarrow \tilde{x}^\mu = x^\mu + \zeta^\mu(x^\nu)\,, \tag{A.46}$$

where we split the vector $\zeta^\mu$ in $\zeta^0 = \alpha$, $\zeta^i = \partial^i\beta + \hat{\beta}^i$. The gauge transformation (A.46) for a tensor $F$ is given in terms of the Lie derivative along the vector $\zeta^\nu$

$$\tilde{F}(\tilde{x}^\nu) = F(x^\nu) + L_\zeta F(x^\nu)\,, \tag{A.47}$$

so that

$$\tilde{F}_{\mu\nu} = F_{\mu\nu} + F_{\mu\nu,\sigma}\zeta^\sigma + \zeta^\sigma_{,\mu}F_{\sigma\nu} + \zeta^\sigma_{,\nu}F_{\sigma\mu}\,. \tag{A.48}$$

In particular for the metric tensor $h_{\mu\nu}$ this implies

$$\begin{aligned}
A &\to A - \dot{\alpha} - \mathcal{H}\alpha\,, && \text{(A.49)}\\
B &\to B + \alpha - \dot{\beta}\,, && \text{(A.50)}\\
\hat{B}_i &\to \hat{B}_i - \dot{\hat{\beta}}_i\,, && \text{(A.51)}\\
C &\to C - \mathcal{H}\alpha - \frac{1}{3}\nabla^2\beta\,, && \text{(A.52)}\\
E &\to E - \beta && \text{(A.53)}\\
\hat{E}_i &\to \hat{E}_i - \hat{\beta}_i\,, && \text{(A.54)}\\
\hat{E}_{ij} &\to \hat{E}_{ij}\,. && \text{(A.55)}
\end{aligned}$$

On other hand for the energy momentum tensor $T_{\mu\nu}$ we obtain

$$\begin{aligned}
\delta &\to \delta + 3(1+w)\mathcal{H}\alpha\,, && \text{(A.56)}\\
\delta p &\to \delta p + 3\frac{c_s^2}{w}(1+w)\mathcal{H}\alpha\,, && \text{(A.57)}\\
v &\to v - \dot{\beta}\,, && \text{(A.58)}\\
\hat{v}_i &\to \hat{v}_i + \dot{\hat{\beta}}_i\,, && \text{(A.59)}\\
\Sigma_{ij} &\to \Sigma_{ij}\,. && \text{(A.60)}
\end{aligned}$$

It is then clear that if we start in a gauge where - for example - $g_{00}$ is unperturbed ($A = 0$), a coordinate transformation can generate an unphysical perturbation $\tilde{A} = -\dot{\alpha} - \mathcal{H}\alpha$. Similarly we can remove a perturbation from the metric with an appropriate gauge choice. We are

left with the problem of identifying which fields are a physical perturbation and which are just spurious *gauge modes*. The solution is to introduce gauge invariant variables, i.e. special combination of metric perturbation which do not transform under a gauge transformation, and which therefore represents physical perturbations. For the metric the most important gauge invariant variables are given by the *Bardeen* potentials defined as

$$\Psi \equiv A + \mathcal{H}(B - \dot{E}) + (\dot{B} - \ddot{E}), \tag{A.61}$$

$$\Phi \equiv C - \mathcal{H}(B - \dot{E}) + \frac{1}{3}\nabla^2 E, \tag{A.62}$$

while for the energy-momentum tensor the *comoving gauge* density perturbation is gauge invariant:

$$\delta_c = \delta + 3\mathcal{H}(1+w)(v - B). \tag{A.63}$$

Another approach to the gauge problem is to fix the gauge. Out of the ten degrees of freedom (one in $A$, three in $B_i$ and six in $Q_{ij}$) of (A.34) we can use the freedom in the gauge transformation to fix four of them. Different choices of gauge are used in cosmology. Our pick for this thesis is *Poisson gauge*, given by the choice

$$B = E = \hat{E}_i = 0, \tag{A.64}$$

so that we 'gauge away' two scalar d.o.f. and two vector d.o.f.. The metric is then given, as in eq. (2.1), by

$$\mathrm{d}s^2 = a^2\left[-(1+2\Psi)\mathrm{d}\eta^2 - 2S_i\,\mathrm{d}\eta\mathrm{d}x^i + \left[(1-2\Phi)\delta_{ij} + 2H_{ij}\right]\mathrm{d}x^i\mathrm{d}x^j\right], \tag{A.65}$$

where our gauge condition dictates $A = \Psi$, $C = \Phi$ and we have defined $S_i = \hat{B}_i$, $H_{ij} = \hat{E}_{ij}$, so that $\partial^i S_i = \partial^i H_{ij} = H^i_{\ i} = 0$. Other gauges widely used in cosmology are: *comoving* gauge ($B = v$ and $C = 0$), *synchronous* gauge ($A = B = 0$) and *spatially flat* gauge ($C = E = 0$). In the last sentence we have neglected vector perturbations ($B_i = 0$) so that a gauge choice is made by fixing only two scalar degrees of freedom.

### A.2.3 Einstein, Euler & continuity equations

We can now write down the Einstein equation for our metric (A.65), switching to Fourier space as it is most relevant for this thesis (note that we denote with the same letter $\Psi(\mathbf{x})$ and $\Psi(\mathbf{k})$). The first-order part of the '00' equation gives

$$k^2\Phi + 3\mathcal{H}(\dot{\Phi} + \mathcal{H}\Psi) = -4\pi G a^2 \bar{\rho}\delta. \tag{A.66}$$

The '$0i$' equations are

$$k_i(\dot{\Phi} + \mathcal{H}\Psi) = -(\dot{\mathcal{H}} - \mathcal{H}^2)k_i v, \tag{A.67}$$

$$k^2 S_i = -4(\dot{\mathcal{H}} - \mathcal{H}^2)(\hat{v}_i - S_i), \tag{A.68}$$

while the '$ij$' equations give

$$(\partial_\eta + 2\mathcal{H})k^2 S_i = 8\pi G a^2 k^2 \hat{\Sigma}_j \,, \tag{A.69}$$

$$\tilde{D}_{ij}(\Phi - \Psi) = 8\pi G a^2 \tilde{D}_{ij}\Sigma \,, \tag{A.70}$$

$$\ddot{\Phi} + 3\mathcal{H}\dot{\Phi} + (2\dot{\mathcal{H}} + \mathcal{H}^2)\Phi = 4\pi G a^2 \delta p \,, \tag{A.71}$$

$$(\partial_\eta^2 + 2\mathcal{H}\partial_\eta + k^2)H_{ij} = 8\pi G a^2 \hat{\Sigma}_{ij} \,, \tag{A.72}$$

with $\tilde{D}_{ij} = \frac{1}{3}\delta_{ij}k^2 - k_i k_j$. Combining eqs. (A.66) with (A.67),(A.63) and (A.12) we obtain *Poisson* equation

$$4\pi G a^2 \bar{\rho}\, \delta_c = -k^2 \Phi \,, \tag{A.73}$$

or, using $\bar{\rho}_m = \Omega_m \bar{\rho}_c a^{-3}$ and $4\pi G\bar{\rho}_c = \frac{3}{2}\mathcal{H}_0^2$,

$$\frac{3\mathcal{H}_0^2 \Omega_m}{2a}\, \delta_c = -k^2 \Phi \,. \tag{A.74}$$

Note that this is a Newtonian equation which holds at the fully relativistic level when the density variable is the comoving gauge one and the potential is the one defined in Poisson gauge.

The second set of perturbation equations can be derived from the energy-momentum conservation

$$\nabla_\mu T^{\mu\nu} = 0 \,. \tag{A.75}$$

In particular for $\nu = 0$ we find the relativistic version of the *continuity* equation

$$\dot{\delta} + (1+w)(-k^2 v - 3\dot{\Phi}) + 3\mathcal{H}\left(\frac{\delta p}{\delta \bar{\rho}} - w\right)\delta = 0 \,, \tag{A.76}$$

and for $\nu = i$ we obtain the relativistic version of *Euler* equation

$$\dot{V} + \mathcal{H}V - 3\mathcal{H}wV - k\Psi = \frac{\delta p}{(1+w)\bar{\rho}} \,, \tag{A.77}$$

where we have introduced the variable $V$, defined as $v = k^{-1}V$, such that $V(\mathbf{x})$ is dimensionless.

Note that the Einstein equations and the energy-momentum conservation form a redundant, but consistent, set of equations because of the Bianchi identities.

Let us also stress that in the case we consider a mixture of several fluids in the universe, eqs. (A.76),(A.77) hold if the energy-momentum of the different components is separately conserved. In this case we can specify those equation for a particular component. For example - in the case of (pressure-less) matter - Euler equation is written

$$\dot{V} + \mathcal{H}V - k\Psi = 0 \,. \tag{A.78}$$

On the other hand the Einstein equations determine the metric induced by the full perturbations

$$\delta\rho = \sum_X \delta\rho_X \,, \qquad \delta p = \sum_X \delta p_X \,, \qquad V = \sum_X V_X \,, \qquad \Sigma^{ij} = \sum_X \Sigma_X^{ij} \,. \tag{A.79}$$

### A.2.4 Linear growth

If we want to understand how fluctuation in the universe grow to form the structure we see today, we must start with the initial condition. Any mode of interest today was outside the Hubble radius if we go back far into the past. Inflation sets the initial condition for these super-horizon modes. Inflationary models usually predict the power spectrum of the comoving curvature perturbation $\zeta$ which, in a generic gauge, is defined as

$$\zeta \equiv -C - \frac{1}{3}\nabla^2 E + \mathcal{H}(B - v) = -\Phi - \frac{2}{3(1+w)}\left(\frac{\dot{\Phi}}{\mathcal{H}} + \Phi\right), \tag{A.80}$$

and we switched to Poisson gauge for the second equal sign. It can be shown that Einstein equations imply that

$$\frac{d\ln\zeta}{d\ln a} \sim \left(\frac{k}{\mathcal{H}}\right)^2, \tag{A.81}$$

so that on super-horizon scales ($k \ll \mathcal{H}$), $\zeta$ is constant. This means that the value of $\zeta_{\mathbf{k}}$ at horizon exit during inflation is conserved until horizon entry at later time, for each mode $\mathbf{k}$. The task is then to relate the constant super-horizon value $\zeta_{\mathbf{k}}$ to the super-horizon gravitational potential $\Phi_{\mathbf{k}}$ through radiation domination and matter/radiation equality[1] and then study the evolution of $\Phi_{\mathbf{k}}$ (and the relevant energy-density perturbations) after it enters the horizon. Clearly the evolution of the fluctuations depends on whether they enter the horizon during radiation or matter domination. In matter domination, as a result of the fact that cold dark matter is pressure-less, all modes experience uniform growth, independent of the wavenumber $\mathbf{k}$.

In short we write schematically, for each species and metric perturbation $X$,

$$X_{\mathbf{k}}(\eta) = \zeta_{\mathbf{k}} \times \left\{\text{Transfer Function}(k)\right\}_X \times \left\{\text{Growth Function}(\eta)\right\}_X. \tag{A.82}$$

The transfer function describes the evolution of perturbations through the epochs of horizon-crossing and radiation/matter transition, while the growth function describes the wavelength-independent growth at late times. It's convenient to group together eq. (A.82) and simply write

$$X_{\mathbf{k}}(\eta) \equiv \zeta_{\mathbf{k}}\, S_X(k,\eta). \tag{A.83}$$

To solve for the transfer function $S_X(k,\eta)$ one needs in principle the full hierarchy of Boltzmann equations (see e.g. [131], Chapter 4) and Einstein equations. In fairness a great deal of insights can be found analytically with just some approximations (see e.g. [128], Chapter 7) but for the precision required by modern observations one needs to rely on Boltzmann codes such as CMB-FAST, CLASS or CAMB. We will not enter in the details here but we

[1] This is how the famous factor 9/10 comes: $\Phi_{\mathbf{k}}$ is also conserved on super-horizon scale if the equation of state $w$ is constant, the change in $w$ from radiation domination (RD) to matter domination (MD) implies $\Phi_{\rm MD} = 9/10\,\Phi_{\rm RD}$.

stress that, at late times, Einstein equations provide a link between the transfer function of different species. For example Poisson equation neglecting radiation and, for non-clustering dark energy $\delta_c^{(\rm DE)} = 0$, is given by

$$\frac{3\mathcal{H}_0^2\Omega_m}{2a}\,\delta_c^{(m)} = -k^2\Phi\,. \tag{A.84}$$

so that the transfer functions of the gravitational potential $S_\Phi$ and the one of the matter perturbation $S_D$ are related by

$$S_\Phi = -\frac{3\Omega_m}{2a}\left(\frac{\mathcal{H}_0}{k}\right)^2 S_D\,. \tag{A.85}$$

As we said, at later time than equality, the evolution is wavelength-independent and to find the growth of matter perturbation we can use eq. (A.71) for pressure-less dust which gives

$$\ddot{\Phi} + 3\mathcal{H}\dot{\Phi} + (2\dot{\mathcal{H}} + \mathcal{H}^2)\Phi = 0\,, \tag{A.86}$$

and, given $\bar{\rho}_m \sim a^{-3}$, eq. (A.84) implies $\Phi \sim \delta_c^{(m)}/a$, so that

$$\ddot{\delta}_c^{(m)} + \mathcal{H}\dot{\delta}_c^{(m)} + (\dot{\mathcal{H}} - \mathcal{H}^2)\delta_c^{(m)} = 0\,, \tag{A.87}$$

or

$$\frac{d^2}{da^2}\delta_c^{(m)} + \left(\frac{\dot{\mathcal{H}}}{a\mathcal{H}^2} + \frac{3}{a}\right)\frac{d}{da}\delta_c^{(m)} - \frac{3}{2}\Omega_m\frac{\mathcal{H}_0^2}{a^3\mathcal{H}^2}\delta_c^{(m)} = 0\,. \tag{A.88}$$

Integrating this equation twice we find

$$D_1(a) = \frac{5\Omega_m}{2}\frac{H(a)}{H_0}\int_0^a \frac{da'}{(a'H(a')/H_0)^3}\,, \tag{A.89}$$

where we define

$$\delta_c^{(m)}(\eta) = \delta_c^{(m)}(\eta_*)\frac{D_1(\eta)}{D_1(\eta_*)}\,. \tag{A.90}$$

At late time we have then factored out the time-dependence of $S_D$ as

$$S_D(\eta, k) = S_D(\eta_*, k)\frac{D_1(\eta)}{D_1(\eta_*)}\,. \tag{A.91}$$

The continuity equation gives

$$kV = -\dot{\delta}_c^{(m)} = -\delta_c^{(m)}\frac{\dot{D}}{D} = -\mathcal{H}f\delta_c^{(m)}\,, \tag{A.92}$$

with the velocity growth rate defined as

$$f = \frac{d\ln D}{d\ln a}\,, \tag{A.93}$$

so that

$$S_V = -\frac{\mathcal{H}f}{k} S_D \,. \tag{A.94}$$

Neglecting anisotropic stress we trivially obtain, from eq. (A.70),

$$S_\Phi = S_\Psi \,, \tag{A.95}$$

while we can also write

$$S_{\dot{\Phi}} = -\frac{3\Omega_m}{2a} \left(\frac{\mathcal{H}_0}{k}\right)^2 \mathcal{H}(f-1) S_D \,. \tag{A.96}$$

# APPENDIX B

## Useful Math

## B.1 Statistics of random fields

Let us start by defining a *random field*: an application $F : \mathcal{S} \to \{\text{random variable}\}$ which assign to every point $\mathbf{x} \in \mathcal{S}$ a random variable. We can think of $\mathcal{S}$ being some constant-time hyper-surface and the matter fluctuation $\delta(\mathbf{x})$ as the random variable or $\mathcal{S}$ being the CMB sky and the CMB temperature $T(\mathbf{n})$ as the random variable. In the first case the field has zero mean, i.e. $\langle\delta\rangle = 0$ while in the second case $\langle T\rangle = \bar{T} \neq 0$. The brackets $\langle[...]\rangle$ represent the ensemble average or the expectation value of the field $F$:

$$\langle F\rangle(\mathbf{x}) = \int \mathcal{D}F\, P[F]\, F(\mathbf{x})\,, \tag{B.1}$$

where the integral is a functional integral over the fields configurations weighted by the probability distribution function, which is a functional $P[F]$ corresponding to the probability of realising some field configuration. *Correlators* of fields are expectation values of products of fields at different points on $\mathcal{S}$. For example the two-point function is defined

$$\xi(\mathbf{x},\mathbf{y}) = \langle F(\mathbf{x})F(\mathbf{y})\rangle = \int \mathcal{D}F\, P[F]\, F(\mathbf{x})F(\mathbf{y})\,, \tag{B.2}$$

while in general an $N-$point function is written

$$\langle F(\mathbf{x}_1)F(\mathbf{x}_2)...F(\mathbf{x}_N)\rangle = \int \mathcal{D}F\, P[F]\, F(\mathbf{x}_1)F(\mathbf{x}_2)...F(\mathbf{x}_N)\,. \tag{B.3}$$

Fields in cosmology are usually treated as statistically *homogeneous* and *isotropic*. Statistical homogeneity for fields in **real space** means that the statistical properties of the translated field are the same as the original field:

$$P[F(\mathbf{x})] = P[F(\mathbf{x}+\mathbf{w})] \text{ with } \mathbf{w} \in \mathcal{S}\,. \tag{B.4}$$

Statistical isotropy means that the statistical properties of the rotated field are the same:

$$P[F(\mathbf{x})] = P[F(R\mathbf{x})]\,. \tag{B.5}$$

These two properties translate into the facts that the expectation value is independent of the position and the two-point function only depends on the distance between the two points, i.e.

$$\langle F\rangle(\mathbf{x}) = \langle F\rangle = \bar{F}\,, \tag{B.6}$$

$$\xi(\mathbf{x},\mathbf{y}) = \xi(|\mathbf{x}-\mathbf{y}|)\,. \tag{B.7}$$

In **Fourier space** these conditions translate into

$$\langle F(\mathbf{k})F^*(\mathbf{k}')\rangle = (2\pi)^3\delta(\mathbf{k}-\mathbf{k}')P_F(k)\,. \tag{B.8}$$

To see this we can simply insert eq. (B.7) into the Fourier transform

$$\begin{aligned}\langle F(\mathbf{k})F^*(\mathbf{k}')\rangle &= \int d^3\mathbf{x}d^3\mathbf{x}'\,\langle F(\mathbf{x})F(\mathbf{x}')\rangle e^{i(\mathbf{k}\cdot\mathbf{x}-\mathbf{k}'\cdot\mathbf{x}')}\\ &= \int d^3\mathbf{x}d^3\mathbf{x}'\,\xi_F(\mathbf{x},\mathbf{x}')e^{i(\mathbf{k}\cdot\mathbf{x}-\mathbf{k}'\cdot\mathbf{x}')}\\ &= \int d^3\mathbf{x}d^3\mathbf{x}'\,\xi_F(|\mathbf{x}-\mathbf{x}'|)e^{i(\mathbf{k}\cdot(\mathbf{x}-\mathbf{x}')-(\mathbf{k}'-\mathbf{k})\cdot\mathbf{x}')}\\ &= \int d^3\mathbf{r}d^3\mathbf{x}'\,\xi_F(r)e^{i(\mathbf{k}\cdot\mathbf{r}-(\mathbf{k}'-\mathbf{k})\cdot\mathbf{x}')}\\ &= (2\pi)^3\delta(\mathbf{k}-\mathbf{k}')\tilde{\xi}_F(k) = (2\pi)^3\delta(\mathbf{k}-\mathbf{k}')P_F(k)\,.\end{aligned} \tag{B.9}$$

For the fourth equals sign we made the variable transform $\mathbf{r} = \mathbf{x}-\mathbf{x}'$ and for the last equals sign we used the fact that the integral of $e^{i\mathbf{k}\cdot\mathbf{x}}$ is a delta function. Finally in **angular space**: we know that $\xi(\mathbf{x},\mathbf{y})$ is only a function of the distance between the two points hence, on the sphere, the angular correlation function is only a function of the scalar product $\cos\theta = \hat{\mathbf{x}}\cdot\hat{\mathbf{y}}$. We can then expand it in terms of Legendre polynomials as

$$\xi(\theta) = \frac{1}{4\pi}\sum_\ell (2\ell+1)C_\ell\mathcal{P}_\ell(\cos\theta)\,. \tag{B.10}$$

A generic field on the sphere can be expanded in spherical harmonics

$$F(\mathbf{n}) = \sum_{\ell m} f_{\ell m}Y_{\ell m}(\hat{\mathbf{n}})\,, \tag{B.11}$$

and in this case, statistical homogeneity and isotropy ensure

$$\langle f_{\ell m}f^*_{\ell' m'}\rangle = \delta_{\ell\ell'}\delta_{mm'}C_\ell\,. \tag{B.12}$$

This can be easily proved with the aid of eq. (B.10), that can be written (see section B.3)

$$\begin{aligned}\xi(\theta) &= \frac{1}{4\pi}\sum_\ell (2\ell+1)C_\ell\mathcal{P}_\ell(\cos\theta) = \sum_{\ell m} C_\ell Y_{\ell m}(\hat{\mathbf{x}})Y^*_{\ell m}(\hat{\mathbf{y}})\\ &= \sum_{\ell m\ell' m'}\langle f_{\ell m}f^*_{\ell' m'}\rangle Y_{\ell m}(\hat{\mathbf{x}})Y^*_{\ell' m'}(\hat{\mathbf{y}})\,.\end{aligned} \tag{B.13}$$

Integration over the sphere gives eq. (B.12)

$$\sum_{\ell m} C_\ell \underbrace{\int d\Omega\, Y_{\ell m}(\hat{\mathbf{x}})Y^*_{\ell m}(\hat{\mathbf{y}})}_{1} = \sum_{\ell m\ell' m'}\langle f_{\ell m}f^*_{\ell' m'}\rangle \underbrace{\int d\Omega\, Y_{\ell m}(\hat{\mathbf{x}})Y^*_{\ell m}(\hat{\mathbf{y}})}_{\delta_{\ell\ell'}\delta_{mm'}}\,. \tag{B.14}$$

## B.2 Differential Geometry definitions

We present in this appendix some differential geometry definitions commonly used in general relativity, to fix the notation of this thesis. Einstein's summation convention is assumed throughout this work on space-time and space indices.

We consider a four-dimensional pseudo-Riemannian spacetime given by a manifold $\mathcal{M}$ and a metric $g$ with signature $(-,+,+,+)$. For a given choice of coordinates $x_\mu$ with $\mu = 0,..,3$ the metric is given by the 10 components of a $4\times 4$ symmetric tensor $ds^2 = g_{\mu\nu}dx^\mu dx^\nu$ . The indices of contra- and covariant tensor fields are raised and lowered with the metric

$$g_{\beta\nu}T^{\alpha\nu} = T^\alpha_\beta = g^{\alpha\nu}T_{\mu\beta}\,, \tag{B.15}$$

where $g^{\mu\nu}$ is the inverse of the metric which satisfies

$$g_{\mu\alpha}g^{\alpha\nu} = \delta^\nu_\mu\,. \tag{B.16}$$

The Christoffel symbols are defined by

$$\Gamma^\mu_{\alpha\beta} = \frac{1}{2}g^{\mu\nu}\left[\partial_\alpha g_{\nu\beta} + \partial_\beta g_{\nu\alpha} - \partial_\nu g_{\alpha\beta}\right], \tag{B.17}$$

where $\partial_\alpha$ is the partial derivative w.r.t. $x^\alpha$. The covariant derivative in coordinate representation for contra- and covariant vectors is then written as

$$\nabla_\mu\xi^\nu = \partial_\mu\xi^\nu + \Gamma^\nu_{\mu\sigma}\xi^\sigma\,, \tag{B.18}$$

$$\nabla_\mu\eta_\nu = \partial_\mu\eta_\nu - \Gamma^\sigma_{\mu\nu}\eta_\sigma\,, \tag{B.19}$$

while for a generic tensor:

$$\nabla_\mu T^{\alpha_1\ldots\alpha_r}_{\beta_1\ldots\beta_s} = \partial_\mu T^{\alpha_1\ldots\alpha_r}_{\beta_1\ldots\beta_s} + \sum_{m=1}^{r}\Gamma^{\alpha_m}_{\mu\sigma}T^{\alpha_1\ldots\sigma\ldots\alpha_r}_{\beta_1\ldots\beta_s} - \sum_{m=1}^{s}\Gamma^\sigma_{\mu\beta_m}T^{\alpha_1\ldots\alpha_r}_{\beta_1\ldots\sigma\ldots\beta_s}\,, \tag{B.20}$$

where the index $\sigma$ is taken at the $m^{\text{th}}$ position. The Riemann curvature tensor is defined by

$$R^\alpha_{\beta\mu\nu} = \partial_\mu\Gamma^\alpha_{\nu\beta} - \partial_\nu\Gamma^\alpha_{\mu\beta} + \Gamma^\rho_{\beta\nu}\Gamma^\alpha_{\mu\rho} - \Gamma^\rho_{\beta\mu}\Gamma^\alpha_{\nu\rho}\,, \tag{B.21}$$

such that if we lower one index, the tensor $R_{\alpha\beta\mu\nu} = g_{\alpha\sigma}R^\sigma_{\beta\mu\nu}$ is anti-symmetric in the first $(\alpha\beta)$ and second $(\mu\nu)$ pair of indices and symmetric in the pair exchange $(\alpha\beta)\leftrightarrow(\mu\nu)$. The first and second Bianchi identities read

$$R_{\alpha\beta\mu\nu} + R_{\alpha\mu\nu\beta} + R_{\alpha\nu\beta\mu} = 0\,, \tag{B.22}$$

$$\nabla_\gamma R_{\alpha\beta\mu\nu} + \nabla_\mu R_{\alpha\beta\nu\gamma} + \nabla_\nu R_{\alpha\beta\gamma\mu} = 0\,. \tag{B.23}$$

The Ricci tensor and the Riemann scalar are given by

$$R_{\mu\nu} = R^\alpha_{\mu\alpha\nu}\,, \qquad R = R^\mu_\mu\,. \tag{B.24}$$

The Einstein tensor is build from these quantities

$$G_{\mu\nu} = R_{\mu\nu} - \frac{1}{2} R g_{\mu\nu} \,, \tag{B.25}$$

and is related to the energy-momentum tensor via Einstein's field equations

$$G_{\mu\nu} = 8\pi G \, T_{\mu\nu} \,. \tag{B.26}$$

The second Bianchi identity and the symmetries of the Riemann tensor imply $\nabla_\mu G^\mu_\nu = 0$ so that the energy-momentum tensor is covariantly conserved $\nabla_\mu T^\mu_\nu = 0$.

## B.3 Spherical Harmonics

Spherical harmonics $Y_{\ell m}$ form a basis for (square-integrable) functions on the sphere. They are extremely useful in cosmology as, since we observe fields as functions of $\mathbf{n}$ and $z$, we can decompose them in terms of $Y_{\ell m}$. We first discuss the *Legendre Polynomials* as we will give the Spherical harmonics' definition in terms of them.

### Legendre polynomials

The Legendre polynomials $\mathcal{P}_\ell$ form an orthonormal set of polynomials on the interval $[-1, 1]$ and they are solutions of the Legendre's differential equation

$$(1 - x^2)\mathcal{P}''_\ell(x) - 2x P'_\ell(x) + \ell(\ell + 1)\mathcal{P}_\ell(x) = 0 \,. \tag{B.27}$$

The explicit expression for the $\mathcal{P}_\ell$ can be obtain either from Rodrigues' formula

$$\mathcal{P}_\ell(x) = \frac{1}{2^\ell \ell!} \frac{d^\ell}{dx^\ell} (x^2 - 1)^\ell \,, \tag{B.28}$$

or, given $\mathcal{P}_0 = 1$ and $\mathcal{P}_1 = x$, from the recursion relation

$$(\ell + 1)\mathcal{P}_{\ell+1} = (2\ell + 1) x \mathcal{P}_\ell - \ell \mathcal{P}_{\ell-1} \,. \tag{B.29}$$

Integrals of one polynomial can be performed using

$$\mathcal{P}_\ell = \frac{1}{2\ell + 1} \frac{d}{dx} \left( \mathcal{P}_{\ell+1} - \mathcal{P}_{\ell-1} \right) \,. \tag{B.30}$$

Integrals of two polynomial satisfy the orthogonality condition

$$\int_{-1}^{1} dx \, \mathcal{P}_{\ell_1}(x) \mathcal{P}_{\ell_2}(x) = \frac{2}{2\ell_1 + 1} \delta_{\ell_1 \ell_2} \,, \tag{B.31}$$

while integrals of three polynomials are given in terms of Wigner 3j symbols as

$$\int_{-1}^{1} dx \, \mathcal{P}_{\ell_1}(x) \mathcal{P}_{\ell_2}(x) \mathcal{P}_{\ell_3}(x) = 2 \begin{pmatrix} \ell_1 & \ell_2 & \ell_3 \\ 0 & 0 & 0 \end{pmatrix}^2 \,. \tag{B.32}$$

Additional properties of the polynomials are given by their symmetry or antisymmetry:

$$\mathcal{P}_\ell(-x) = (-)^\ell \mathcal{P}_\ell(x)\,, \tag{B.33}$$

and (by convention) we also have

$$\mathcal{P}_\ell(1) = 1\,, \qquad \mathcal{P}'_\ell(1) = \frac{\ell(\ell+1)}{2}\,. \tag{B.34}$$

**Associated Legendre functions**

From the Legendre polynomials we can define the *Associated Legendre functions* as

$$\mathcal{P}_{\ell m}(x) = (1-x^2)^{m/2}\frac{d^m}{dx^m}\mathcal{P}_\ell(x) = (1-x^2)^{m/2}\frac{1}{2^\ell \ell!}\frac{d^{\ell+m}}{dx^{\ell+m}}(x^2-1)^\ell\,. \tag{B.35}$$

The parity and the orthogonality relations are consequences of their definitions in terms of $\mathcal{P}_\ell$ and are given by

$$\mathcal{P}_{\ell m}(-x) = (-)^{\ell+m}\mathcal{P}_{\ell m}(x)\,, \tag{B.36}$$

$$\int_{-1}^{1} dx\, \mathcal{P}_{\ell_1 m}(x)\mathcal{P}_{\ell_2 m}(x) = \frac{2}{2\ell_1+1}\frac{(\ell_1-m)!}{(\ell_1+m)!}\delta_{\ell_1\ell_2}\,. \tag{B.37}$$

**Spherical harmonics**

We can now finally define the Spherical harmonics

$$Y_{\ell m}(\mathbf{n}) = (-)^m\sqrt{\frac{2\ell+1}{4\pi}\frac{(\ell-m)!}{(\ell+m)!}}\,e^{im\phi}\,\mathcal{P}_{\ell m}(\cos\theta)\,, \tag{B.38}$$

where we recall that the $Y_{\ell m}$ are function on the sphere and we define $\mathbf{n} = (\theta,\phi)$. The spherical harmonics are eigenfunctions of the Laplacian on the sphere:

$$\Delta_\Omega Y_{\ell m} = -\ell(\ell+1)Y_{\ell m}\,. \tag{B.39}$$

The Laplace spherical harmonics form a complete set of orthonormal functions (see eq. (B.43)) and thus form an orthonormal basis: any function on the sphere $f(\mathbf{n})$ can be expanded as

$$f(\mathbf{n}) = \sum_{\ell=0}^{\infty}\sum_{m=-\ell}^{\ell} f_{\ell m}Y_{\ell m}(\mathbf{n}) \tag{B.40}$$

with

$$f_{\ell m} = \int d\Omega_{\mathbf{n}}\, f(\mathbf{n})Y^*_{\ell m}(\mathbf{n})\,. \tag{B.41}$$

From the parity transformation properties and the orthogonality of the associated Legendre functions, eqs. (B.36),(B.37), we conclude

$$Y_{\ell m}(-\mathbf{n}) = (-)^\ell Y^*_{\ell m}(-\mathbf{n}) \qquad \text{and} \qquad Y_{\ell -m}(\mathbf{n}) = (-)^m Y^*_{\ell m}(\mathbf{n})\,. \tag{B.42}$$

Orthogonality implies

$$\int d\Omega_{\mathbf{n}}\, Y_{\ell_1 m_1}(\mathbf{n}) Y^*_{\ell_2 m_2}(\mathbf{n}) = \delta_{\ell_1 \ell_2}\delta_{m_1 m_2}\,. \tag{B.43}$$

Integrals of the product of three spherical harmonics are computed as

$$\int d\Omega_{\mathbf{n}}\, Y_{\ell_1 m_1}(\mathbf{n}) Y_{\ell_2 m_2}(\mathbf{n}) Y_{\ell_3 m_3}(\mathbf{n}) = \sqrt{\frac{(2\ell_1+1)(2\ell_2+1)(2\ell_3+1)}{4\pi}} \begin{pmatrix} \ell_1 & \ell_2 & \ell_3 \\ 0 & 0 & 0 \end{pmatrix} \begin{pmatrix} \ell_1 & \ell_2 & \ell_3 \\ m_1 & m_2 & m_3 \end{pmatrix},$$

while the product of any number of spherical harmonics can be integrated using eq. (B.43) and the addition rule

$$Y_{\ell_1 m_1}(\mathbf{n}) Y_{\ell_2 m_2}(\mathbf{n}) = \sqrt{\frac{(2\ell_1+1)(2\ell_2+1)}{4\pi}} \sum_{\ell_3 m_3} (2\ell_3{+}1) \begin{pmatrix} \ell_1 & \ell_2 & \ell_3 \\ 0 & 0 & 0 \end{pmatrix} \begin{pmatrix} \ell_1 & \ell_2 & \ell_3 \\ m_1 & m_2 & m_3 \end{pmatrix} Y^*_{\ell_3 m_3}(\mathbf{n})\,.$$

The last equation deals with $Y_{\ell m}$s of different orders but with the same argument $\mathbf{n}$. For the opposite situation, i.e. spherical harmonics of the same order but different arguments, one relies on the addition theorem

$$\mathcal{P}_\ell(\mathbf{n}_1 \cdot \mathbf{n}_2) = \frac{4\pi}{2\ell+1} \sum_{m=-\ell}^{\ell} Y_{\ell m}(\mathbf{n}_1) Y^*_{\ell m}(\mathbf{n}_2)\,. \tag{B.44}$$

The addition theorem can be derived by considering the behavior of the spherical harmonics under a rotation $\mathbf{R}$ (see [131], Appendix A4.2.3). Here we only report the result as it is often useful: it can be shown that

$$Y_{\ell m}(\mathbf{R}^{-1}\mathbf{n}) = \sum_{m_1} \mathcal{D}^{(\ell)}_{m_1 m}(\mathbf{R}) Y_{\ell m_1}(\mathbf{n})\,, \tag{B.45}$$

where $\mathcal{D}^{(\ell)}_{m_1 m}$ are elements of the Wigner D-matrix. This confirms the intuition that a rotation cannot change the order of the harmonics, but linearly mix spherical harmonics of the same degree. This is also linked to the fact that the $Y_{\ell m}$s of degree $\ell$ are the basis for the irreducible representation of the $SO(3)$ group of dimension $(2\ell+1)$. See [300], Chapter 7.4 for more details.

### Spin-weighted Spherical harmonics

Spin-weighted spherical harmonics are generalisations of the standard spherical harmonics and –like the usual spherical harmonics– are functions on the sphere ${}_sY_{\ell m}(\mathbf{n})$. The difference is that the spin-weighted harmonics have an additional U(1) symmetry characterised by a spin weight $s$. In other words a function $f$ with spin weight $s = 0$ does not transform under a rotation of our basis: ${}_0f'(\mathbf{n}') = {}_0f(\mathbf{n})$. On the other hand a spin-weighted function satisfy ${}_sf'(\mathbf{n}') = {}_sf(\mathbf{n})e^{-is\gamma}$ for some angle $\gamma$. For $s = 0$ we then recover the standard spherical harmonics ${}_0Y_{\ell m} = Y_{\ell m}$.

Spin-weighted harmonics are useful to expand a spin$-s$ component of a tensor field on the sphere. They are defined via

$$\begin{aligned} {}_sY_{\ell m}(\mathbf{n}) = {}_sY_{\ell m}(\theta,\phi) = (-)^m \sqrt{\frac{2\ell+1}{4\pi}\frac{(\ell+m)!(\ell-m)!}{(\ell+s)!(\ell-s)!}}(\sin\theta/2)^{2\ell} e^{im\phi} \\ \times \sum_\sigma \binom{\ell-s}{\sigma}\binom{\ell+s}{\sigma+s-m}(-)^{\ell-\sigma-s}(\cot\theta/2)^{2\sigma+s-m}, \end{aligned} \tag{B.46}$$

where the sum over $\sigma$ runs over all the values for which the binomial coefficients are non-zero. For each spin $s$ they form a complete set of orthonormal function on the sphere

$$\int d\Omega\, {}_sY_{\ell m}(\mathbf{n})\, {}_sY^*_{\ell m}(\mathbf{n}) = \delta_{\ell\ell'}\delta_{mm'}\,, \tag{B.47}$$

and

$$\sum_{\ell m} {}_sY_{\ell m}(\mathbf{n})\, {}_sY^*_{\ell m}(\mathbf{n}') = \delta(\phi-\phi')\delta(\cos\theta-\cos\theta')\,. \tag{B.48}$$

They can also be derived starting from the standard harmonics and using the spin-raising and -lowering operators

$$\eth\, {}_sY_{\ell m} = \left(s\cot\theta - \partial_\theta - \frac{i}{\sin\theta}\partial_\phi\right) {}_sY_{\ell m}\,, \tag{B.49}$$

$$\eth^*\, {}_sY_{\ell m} = \left(-s\cot\theta - \partial_\theta + \frac{i}{\sin\theta}\partial_\phi\right) {}_sY_{\ell m}\,, \tag{B.50}$$

which give

$$\eth\, {}_sY_{\ell m} = \sqrt{(\ell-s)(\ell+s+1)}\, {}_{s+1}Y_{\ell m}\,, \tag{B.51}$$

$$\eth^*\, {}_sY_{\ell m} = -\sqrt{(\ell+s)(\ell-s+1)}\, {}_{s-1}Y_{\ell m}\,. \tag{B.52}$$

A useful properties which we have employed in this thesis is the generalised addition theorem: let $(\alpha,\beta,\gamma)$ be the Euler angles which rotates $\mathbf{n}_2$ into $\mathbf{n}_1$, we then have

$$\sqrt{\frac{4\pi}{2\ell+1}}\sum_{m'} {}_sY_{\ell m'}(\theta_2,\phi_2)\, {}_{-m}Y^*_{\ell m'}(\theta_1,\phi_1) = {}_sY_{\ell m}(\beta,\alpha)e^{-is\gamma}\,. \tag{B.53}$$

We are now interested in finding an operator which acts in the same way that $\mathbf{L}^2 \equiv -\Delta_\Omega$ acts on the spin-0 harmonics, i.e.

$$\mathbf{L}^2 Y_{\ell m} = \ell(\ell+1)Y_{\ell m}\,. \tag{B.54}$$

We call this operator $\mathbf{L}^2_{(s)}$ and we want the spin-weighted spherical harmonics to be eigenfunctions of this operator

$$\mathbf{L}^2_{(s)}\ {}_sY_{lm} = \ell(\ell+1)\ {}_sY_{\ell m}\,.$$

To construct this operator we follow Tansella (2015): we see that, by definition, the commutators satisfy

$$[\mathbf{L}^2_{(s)}, \eth] = [\mathbf{L}^2_{(s)}, \eth^*] = 0\,,$$

and we make the ansatz $\mathbf{L}^2_{(s)} = -\Delta^2_\Omega + \mathbf{K}_{(s)}$. The commutation relation $[\mathbf{L}^2_{(s)}, \eth] = 0$ implies that

$$\mathbf{L}^2_{(s+1)}\,\eth_{(s)} = \eth_{(s)}\mathbf{L}^2_{(s)}\,,$$

which gives

$$[-\Delta^2_\Omega, \eth_{(s)}] = \eth_{(s)}\mathbf{K}_{(s)} - \mathbf{K}_{(s+1)}\eth_{(s)}\,.$$

For $s = 0$ (given that $\mathbf{K}_{(0)} = 0$ since $\mathbf{L}^2_{(s)}$ must reduce to $\mathbf{L}^2$ for $s = 0$)

$$\mathbf{K}_{(1)}\eth = [\eth, \Delta^2_\Omega]\,,$$

explicitly,

$$\mathbf{K}_{(1)}\left(-\partial_\theta - \frac{i}{\sin\theta}\partial_\phi\right) = \frac{1}{\sin^2\theta}\left(\frac{-i}{\sin\theta}\partial_\phi + 2\frac{\cos\theta}{\sin\theta}\partial^2_\phi - \partial_\theta + 2i\,\cos\theta\,\partial_\phi\partial_\theta\right),$$

and we find

$$\mathbf{K}_{(1)} = \frac{1}{\sin^2\theta}\left(1 - 2i\,\cos\theta\,\partial_\phi\right).$$

We can do the same procedure with $[\mathbf{L}^2_{(s)}, \eth^*] = 0$ to find an expression for $\mathbf{K}_{(-1)}$. With this procedure every $\mathbf{K}_{(s)}$ can be found by recursion: the expression we are looking for is then

$$\mathbf{K}_{(s)} = -i\,\frac{2s\,\cos\theta}{\sin^2\theta}\partial_\phi + \frac{s^2}{\sin^2\theta}\,,$$

to give

$$\mathbf{L}^2_{(s)} = -\left(\partial^2_\theta + \frac{\cos\theta}{\sin\theta}\partial_\theta + \frac{1}{\sin^2\theta}\partial^2_\phi\right) - i\,\frac{2s\,\cos\theta}{\sin^2\theta}\partial_\phi + \frac{s^2}{\sin^2\theta}\,. \tag{B.55}$$

## B.4 BiPoSH

We have seen in section B.1 how the correlation function of a statical isotropic random field on the sphere can be expanded in terms of Legendre polynomials (eq. (B.10)). If the field is not assumed to be isotropic then the two-point correlation function will depend in general on the two different directions $\mathbf{n}_1$ and $\mathbf{n}_2$. We then need a basis in which the two-point correlation function can be expanded: this can be obtained by means of the Bipolar Spherical Harmonics (BiPoSH). We write

$$\xi_F(\mathbf{n}_1, \mathbf{n}_2) = \sum_{JM\ell_1\ell_2} f^{JM}_{\ell_1\ell_2}\{Y_{\ell_1} \otimes Y_{\ell_2}\}_{JM}\,. \tag{B.56}$$

We call the $f^{JM}_{\ell_1\ell_2}$ the BiPoSH coefficients and the $\{Y_{\ell_1} \otimes Y_{\ell_2}\}_{JM}$ are the bipolar spherical harmonics. BiPoSH functions are irreducible tensor product of two spherical harmonics with different arguments and, most importantly, they form an orthonormal basis on $\mathbb{S}^2 \otimes \mathbb{S}^2$. We can express them in terms of standard spherical harmonics as

$$X^{JM}_{\ell\ell'}(\hat{\mathbf{n}}_1, \mathbf{n}_2) = \{Y_\ell(\mathbf{n}_1) \otimes Y_{\ell'}(\mathbf{n}_2)\}_{JM} = \sum_{mm'} \mathbf{C}^{JM}_{\ell m\ell' m'} Y_{\ell m}(\hat{\mathbf{n}}_1) Y_{\ell' m'}(\mathbf{n}_2)\,, \tag{B.57}$$

where $\mathbf{C}^{JM}_{\ell m \ell' m'}$ are the Clebsch-Gordan coefficients which are related to the Wigner 3j symbols by,

$$\mathbf{C}^{JM}_{\ell m \ell' m'} = (-)^{\ell - \ell' + M} \sqrt{2J+1} \begin{pmatrix} \ell & \ell' & J \\ m & m' & -M \end{pmatrix} . \tag{B.58}$$

In other words, $X^{JM}_{\ell\ell'}(\hat{\mathbf{n}}_1, \mathbf{n}_2)$ isolates the total angular momentum $J$ and helicity $M$ contribution. The BiPoSH coefficients are computed via

$$f^{JM}_{\ell\ell'} = \int d\Omega_1 \int d\Omega_2 \; \xi_F(\mathbf{n}_1, \mathbf{n}_2) X^{JM*}_{\ell\ell'} . \tag{B.59}$$

The useful property of the BiPoSH $X^{JM}_{\ell\ell'}$ that we exploit in chapter 6, is that they filter the isotropic signal into the $J = 0$ mode and any non-zero coefficient with $J > 0$ indicates anisotropy. In fact, if the random field $F$ is statistically isotropic then the expansion in eq. (B.56) has only the non-zero coefficients

$$f^{00}_{\ell\ell} = (-)^{\ell} \sqrt{2\ell+1} C_\ell \, , \tag{B.60}$$

i.e. we recover the standard expansion of eq. (B.10).

# Bibliography


[1] K. N. Abazajian et al. CMB-S4 Science Book, First Edition. 2016. arXiv:1610.02743.

[2] T. Abbott et al. The dark energy survey. 2005. arXiv:astro-ph/0510346.

[3] M. Abramowitz and I. Stegun. *Handbook of Mathematical Functions*. Dover Publications, New York, 9th printing edition, 1970.

[4] I. Achitouv, C. Blake, P. Carter, J. Koda, and F. Beutler. Consistency of the growth rate in different environments with the 6-degree Field Galaxy Survey: Measurement of the void-galaxy and galaxy-galaxy correlation functions. *Phys. Rev.*, D95(8):083502, 2017. arXiv:1606.03092, doi:10.1103/PhysRevD.95.083502.

[5] L. Ackerman, S. M. Carroll, and M. B. Wise. Imprints of a Primordial Preferred Direction on the Microwave Background. *Phys. Rev.*, D75:083502, 2007. [Erratum: Phys. Rev.D80,069901(2009)]. arXiv:astro-ph/0701357, doi:10.1103/PhysRevD.75.083502,10.1103/PhysRevD.80.069901.

[6] R. Adam et al. Planck 2015 results. I. Overview of products and scientific results. *Astron. Astrophys.*, 594:A1, 2016. arXiv:1502.01582, doi:10.1051/0004-6361/201527101.

[7] J. Adamek, D. Daverio, R. Durrer, and M. Kunz. General relativity and cosmic structure formation. *Nature Physics*, 12,:346–349, 2016. arXiv:1509.01699, doi:10.1038/nphys3673.

[8] J. Adamek, D. Daverio, R. Durrer, and M. Kunz. gevolution: a cosmological N-body code based on General Relativity. *JCAP*, 1607(07):053, 2016. arXiv:1604.06065, doi:10.1088/1475-7516/2016/07/053.

[9] J. Adamek, R. Durrer, and V. Tansella. Lensing signals from Spin-2 perturbations. *JCAP*, 1601(01):024, 2016. arXiv:1510.01566, doi:10.1088/1475-7516/2016/01/024.

[10] C. Adams and C. Blake. Improving constraints on the growth rate of structure by modelling the density-velocity cross-correlation in the 6dF Galaxy Survey. 2017. arXiv:1706.05205.

[11] P. A. R. Ade et al. Planck 2015 results. XIII. Cosmological parameters. *Astron. Astrophys.*, 594:A13, 2016. arXiv:1502.01589, doi:10.1051/0004-6361/201525830.

[12] P. A. R. Ade et al. Planck 2015 results. XV. Gravitational lensing. *Astron. Astrophys.*, 594:A15, 2016. arXiv:1502.01591, doi:10.1051/0004-6361/201525941.

[13] P. A. R. Ade et al. Planck 2015 results. XVI. Isotropy and statistics of the CMB. *Astron. Astrophys.*, 594:A16, 2016. arXiv:1506.07135, doi:10.1051/0004-6361/201526681.

[14] P. A. R. Ade et al. Planck 2015 results. XX. Constraints on inflation. *Astron. Astrophys.*, 594:A20, 2016. arXiv:1502.02114, doi:10.1051/0004-6361/201525898.

[15] R. J. Adler. *The Geometry of Random Fields*. 1981.

[16] A. Aghamousa et al. The DESI Experiment Part I: Science,Targeting, and Survey Design. 2016. arXiv:1611.00036.

[17] S. Alam, F. D. Albareti, C. Allende Prieto, F. Anders, S. F. Anderson, T. Anderton, B. H. Andrews, E. Armengaud, É. Aubourg, S. Bailey, and et al. The Eleventh and Twelfth Data Releases of the Sloan Digital Sky Survey: Final Data from SDSS-III. *ApJS* , 219:12, July 2015. arXiv:1501.00963, doi:10.1088/0067-0049/219/1/12.

[18] S. Alam et al. The Eleventh and Twelfth Data Releases of the Sloan Digital Sky Survey: Final Data from SDSS-III. *Astrophys. J. Suppl.*, 219(1):12, 2015. arXiv:1501.00963, doi:10.1088/0067-0049/219/1/12.

[19] S. Alam et al. The clustering of galaxies in the completed SDSS-III Baryon Oscillation Spectroscopic Survey: cosmological analysis of the DR12 galaxy sample. *Mon. Not. Roy. Astron. Soc.*, 470(3):2617–2652, 2017. arXiv:1607.03155, doi:10.1093/mnras/stx721.

[20] F. D. Albareti, C. Allende Prieto, A. Almeida, F. Anders, S. Anderson, B. H. Andrews, A. Aragón-Salamanca, M. Argudo-Fernández, E. Armengaud, E. Aubourg, and et al. The 13th Data Release of the Sloan Digital Sky Survey: First Spectroscopic Data from the SDSS-IV Survey Mapping Nearby Galaxies at Apache Point Observatory. *ApJS* , 233:25, Dec. 2017. arXiv:1608.02013, doi:10.3847/1538-4365/aa8992.

[21] R. A. Alpher, H. Bethe, and G. Gamow. The origin of chemical elements. *Phys. Rev.*, 73:803–804, Apr 1948. URL: https://link.aps.org/doi/10.1103/PhysRev.73.803, doi:10.1103/PhysRev.73.803.

[22] R. A. Alpher and R. Herman. Evolution of the Universe. *Nature* , 162:774–775, Nov. 1948. doi:10.1038/162774b0.

[23] C. Amsler et al. Review of Particle Physics. *Phys. Lett.*, B667:1–1340, 2008. doi:10.1016/j.physletb.2008.07.018.

[24] K. N. Ananda, C. Clarkson, and D. Wands. The Cosmological gravitational wave background from primordial density perturbations. *Phys.Rev.*, D75:123518, 2007. arXiv:gr-qc/0612013, doi:10.1103/PhysRevD.75.123518.

[25] L. Anderson, E. Aubourg, S. Bailey, D. Bizyaev, M. Blanton, A. S. Bolton, J. Brinkmann, J. R. Brownstein, A. Burden, A. J. Cuesta, L. A. N. da Costa, K. S. Dawson, R. de Putter, D. J. Eisenstein, J. E. Gunn, H. Guo, J.-C. Hamilton, P. Harding, S. Ho, K. Honscheid, E. Kazin, D. Kirkby, J.-P. Kneib, A. Labatie, C. Loomis, R. H. Lupton, E. Malanushenko, V. Malanushenko, R. Mandelbaum, M. Manera, C. Maraston, C. K. McBride, K. T. Mehta, O. Mena, F. Montesano, D. Muna, R. C. Nichol, S. E. Nuza, M. D. Olmstead, D. Oravetz, N. Padmanabhan, N. Palanque-Delabrouille, K. Pan, J. Parejko, I. Pâris, W. J. Percival, P. Petitjean, F. Prada, B. Reid, N. A. Roe, A. J. Ross, N. P. Ross, L. Samushia, A. G. Sánchez, D. J. Schlegel, D. P. Schneider, C. G. Scóccola, H.-J. Seo, E. S. Sheldon, A. Simmons, R. A. Skibba, M. A. Strauss, M. E. C. Swanson, D. Thomas, J. L. Tinker, R. Tojeiro, M. V. Magaña, L. Verde, C. Wagner, D. A. Wake, B. A. Weaver, D. H. Weinberg, M. White, X. Xu, C. Yèche, I. Zehavi, and G.-B. Zhao. The clustering of galaxies in the SDSS-III Baryon Oscillation Spectroscopic Survey: baryon acoustic oscillations in the Data Release 9 spectroscopic galaxy sample. *M.N.R.A.S.* , 427:3435–3467, Dec. 2012. arXiv:1203.6594, doi:10.1111/j.1365-2966.2012.22066.x.

[26] L. Anderson et al. The clustering of galaxies in the SDSS-III Baryon Oscillation Spectroscopic Survey: baryon acoustic oscillations in the Data Releases 10 and 11 Galaxy samples. *Mon. Not. Roy. Astron. Soc.*, 441(1):24–62, 2014. arXiv:1312.4877, doi:10.1093/mnras/stu523.

[27] S. Andrianomena, C. Clarkson, P. Patel, O. Umeh, and J.-P. Uzan. Non-linear relativistic contributions to the cosmological weak-lensing convergence. *JCAP*, 1406:023, 2014. arXiv:1402.4350, doi:10.1088/1475-7516/2014/06/023.

[28] S. Anselmi and M. Pietroni. Nonlinear Power Spectrum from Resummed Perturbation Theory: a Leap Beyond the BAO Scale. *JCAP*, 1212:013, 2012. arXiv:1205.2235, doi:10.1088/1475-7516/2012/12/013.

[29] S. Anselmi, G. D. Starkman, and R. K. Sheth. Beating non-linearities: improving the Baryon Acoustic Oscillations with the linear point. *Mon. Not. Roy. Astron. Soc.*, 455(3):2474–2483, 2016. arXiv:1508.01170, doi:10.1093/mnras/stv2436.

[30] G. B. Arfken and H. J. Weber. *Mathematical Methods for Physicists*. Academic Press, New York, sixth edition edition, 2001.

[31] M. Ata et al. The clustering of the SDSS-IV extended Baryon Oscillation Spectroscopic Survey DR14 quasar sample: first measurement of baryon acoustic oscillations between

redshift 0.8 and 2.2. *Mon. Not. Roy. Astron. Soc.*, 473(4):4773–4794, 2018. arXiv:1705.06373, doi:10.1093/mnras/stx2630.

[32] T. Baldauf, M. Mirbabayi, M. Simonovic, and M. Zaldarriaga. Equivalence Principle and the Baryon Acoustic Peak. *Phys. Rev.*, D92(4):043514, 2015. arXiv:1504.04366, doi:10.1103/PhysRevD.92.043514.

[33] T. Baldauf, E. Schaan, and M. Zaldarriaga. On the reach of perturbative descriptions for dark matter displacement fields. *JCAP*, 1603(03):017, 2016. arXiv:1505.07098, doi:10.1088/1475-7516/2016/03/017.

[34] E. Barausse, S. Matarrese, and A. Riotto. The Effect of inhomogeneities on the luminosity distance-redshift relation: Is dark energy necessary in a perturbed Universe? *Phys. Rev.*, D71:063537, 2005. arXiv:astro-ph/0501152, doi:10.1103/PhysRevD.71.063537.

[35] J. M. Bardeen. Gauge-invariant cosmological perturbations. *Phys. Rev. D*, 22:1882–1905, Oct 1980. URL: https://link.aps.org/doi/10.1103/PhysRevD.22.1882, doi:10.1103/PhysRevD.22.1882.

[36] N. Bartolo, A. Kehagias, M. Liguori, A. Riotto, M. Shiraishi, and V. Tansella. Detecting higher spin fields through statistical anisotropy in the CMB and galaxy power spectra. *Phys. Rev.*, D97(2):023503, 2018. arXiv:1709.05695, doi:10.1103/PhysRevD.97.023503.

[37] S. Basak, A. Hajian, and T. Souradeep. Statistical isotropy of cmb polarization maps. *Phys. Rev.*, D74:021301, 2006. arXiv:astro-ph/0603406, doi:10.1103/PhysRevD.74.021301.

[38] S. Bashinsky and E. Bertschinger. Position-space description of the cosmic microwave background and its temperature correlation function. *Phys. Rev. Lett.*, 87:081301, 2001. arXiv:astro-ph/0012153, doi:10.1103/PhysRevLett.87.081301.

[39] S. Bashinsky and E. Bertschinger. Dynamics of cosmological perturbations in position space. *Phys. Rev.*, D65:123008, 2002. arXiv:astro-ph/0202215, doi:10.1103/PhysRevD.65.123008.

[40] B. A. Bassett and R. Hlozek. Baryon Acoustic Oscillations. 2009. arXiv:0910.5224.

[41] D. Baumann. Inflation. In *Physics of the large and the small, TASI 09, proceedings of the Theoretical Advanced Study Institute in Elementary Particle Physics, Boulder, Colorado, USA, 1-26 June 2009*, pages 523–686, 2011. URL: https://inspirehep.net/record/827549/files/arXiv:0907.5424.pdf, arXiv:0907.5424, doi:10.1142/9789814327183_0010.

[42] D. Baumann, F. Beutler, R. Flauger, D. Green, M. Vargas-Magana, A. Slosar, B. Wallisch, and C. Yeche. First Measurement of Neutrinos in the BAO Spectrum. 2018. arXiv:1803.10741.

[43] D. Baumann, D. Green, and B. Wallisch. Searching for Light Relics with Large-Scale Structure. 2017. arXiv:1712.08067.

[44] D. Baumann, D. Green, and M. Zaldarriaga. Phases of New Physics in the BAO Spectrum. *JCAP*, 1711(11):007, 2017. arXiv:1703.00894, doi:10.1088/1475-7516/2017/11/007.

[45] D. Baumann, A. Nicolis, L. Senatore, and M. Zaldarriaga. Cosmological Non-Linearities as an Effective Fluid. *JCAP*, 1207:051, 2012. arXiv:1004.2488, doi:10.1088/1475-7516/2012/07/051.

[46] D. Baumann, P. J. Steinhardt, K. Takahashi, and K. Ichiki. Gravitational Wave Spectrum Induced by Primordial Scalar Perturbations. *Phys. Rev.*, D76:084019, 2007. arXiv:hep-th/0703290, doi:10.1103/PhysRevD.76.084019.

[47] J. E. Bautista, M. Vargas-Magaña, K. S. Dawson, W. J. Percival, J. Brinkmann, J. Brownstein, B. Camacho, J. Comparat, H. Gil-Marín, E.-M. Mueller, J. A. Newman, A. Prakash, A. J. Ross, D. P. Schneider, H.-J. Seo, J. Tinker, R. Tojeiro, Z. Zhai, and G.-B. Zhao. The SDSS-IV extended Baryon Oscillation Spectroscopic Survey: Baryon Acoustic Oscillations at redshift of 0.72 with the DR14 Luminous Red Galaxy Sample. *ArXiv e-prints*, Dec. 2017. arXiv:1712.08064.

[48] J. D. Bekenstein. Relativistic gravitation theory for the MOND paradigm. *Phys. Rev.*, D70:083509, 2004. [Erratum: Phys. Rev.D71,069901(2005)]. arXiv:astro-ph/0403694, doi:10.1103/PhysRevD.70.083509,10.1103/PhysRevD.71.069901.

[49] E. Belgacem, Y. Dirian, S. Foffa, and M. Maggiore. Nonlocal gravity. Conceptual aspects and cosmological predictions. 2017. arXiv:1712.07066.

[50] F. Bernardeau, S. Colombi, E. Gaztanaga, and R. Scoccimarro. Large scale structure of the universe and cosmological perturbation theory. *Phys. Rept.*, 367:1–248, 2002. arXiv:astro-ph/0112551, doi:10.1016/S0370-1573(02)00135-7.

[51] D. Bertacca, R. Maartens, and C. Clarkson. Observed galaxy number counts on the lightcone up to second order: II. Derivation. *JCAP*, 1411(11):013, 2014. arXiv:1406.0319, doi:10.1088/1475-7516/2014/11/013.

[52] D. Bertacca, R. Maartens, A. Raccanelli, and C. Clarkson. Beyond the plane-parallel and Newtonian approach: Wide-angle redshift distortions and convergence in general relativity. *JCAP*, 1210:025, 2012. arXiv:1205.5221, doi:10.1088/1475-7516/2012/10/025.

[53] G. Bertone, D. Hooper, and J. Silk. Particle dark matter: Evidence, candidates and constraints. *Phys. Rept.*, 405:279–390, 2005. arXiv:hep-ph/0404175, doi:10.1016/j.physrep.2004.08.031.

[54] E. Bertschinger. Self - similar secondary infall and accretion in an Einstein-de Sitter universe. *Astrophys. J. Suppl.*, 58:39, 1985. doi:10.1086/191028.

[55] E. Bertschinger. Cosmological dynamics: Course 1. In *Proceedings, Les Houches Summer School on Cosmology and Large Scale Structure (Session 60): Les Houches, France, August 1-28, 1993*, pages 273–348, 1993. arXiv:astro-ph/9503125.

[56] F. Beutler, C. Blake, M. Colless, D. H. Jones, L. Staveley-Smith, L. Campbell, Q. Parker, W. Saunders, and F. Watson. The 6dF Galaxy Survey: baryon acoustic oscillations and the local Hubble constant. *M.N.R.A.S.* , 416:3017–3032, Oct. 2011. arXiv:1106.3366, doi:10.1111/j.1365-2966.2011.19250.x.

[57] F. Beutler, C. Blake, M. Colless, D. H. Jones, L. Staveley-Smith, L. Campbell, Q. Parker, W. Saunders, and F. Watson. The 6dF Galaxy Survey: Baryon Acoustic Oscillations and the Local Hubble Constant. *Mon. Not. Roy. Astron. Soc.*, 416:3017–3032, 2011. arXiv:1106.3366, doi:10.1111/j.1365-2966.2011.19250.x.

[58] D. Bianchi, M. Chiesa, and L. Guzzo. Improving the modelling of redshift-space distortions - I. A bivariate Gaussian description for the galaxy pairwise velocity. *Mon. Not. Roy. Astron. Soc.*, 446:75–84, 2015. arXiv:1407.4753, doi:10.1093/mnras/stu2080.

[59] S. G. Biern and J. Yoo. Correlation function of the luminosity distances. *JCAP*, 1709(09):026, 2017. arXiv:1704.07380, doi:10.1088/1475-7516/2017/09/026.

[60] S. G. Biern and J. Yoo. Gauge-Invariance and Infrared Divergences in the Luminosity Distance. *JCAP*, 1704(04):045, 2017. arXiv:1606.01910, doi:10.1088/1475-7516/2017/04/045.

[61] C. Blake, E. A. Kazin, F. Beutler, T. M. Davis, D. Parkinson, S. Brough, M. Colless, C. Contreras, W. Couch, S. Croom, D. Croton, M. J. Drinkwater, K. Forster, D. Gilbank, M. Gladders, K. Glazebrook, B. Jelliffe, R. J. Jurek, I.-H. Li, B. Madore, D. C. Martin, K. Pimbblet, G. B. Poole, M. Pracy, R. Sharp, E. Wisnioski, D. Woods, T. K. Wyder, and H. K. C. Yee. The WiggleZ Dark Energy Survey: mapping the distance-redshift relation with baryon acoustic oscillations. *M.N.R.A.S.* , 418:1707–1724, Dec. 2011. arXiv:1108.2635, doi:10.1111/j.1365-2966.2011.19592.x.

[62] D. Blas, M. Garny, M. M. Ivanov, and S. Sibiryakov. Time-Sliced Perturbation Theory for Large Scale Structure I: General Formalism. *JCAP*, 1607(07):052, 2016. arXiv:1512.05807, doi:10.1088/1475-7516/2016/07/052.

[63] D. Blas, M. Garny, M. M. Ivanov, and S. Sibiryakov. Time-Sliced Perturbation Theory II: Baryon Acoustic Oscillations and Infrared Resummation. *JCAP*, 1607(07):028, 2016. arXiv:1605.02149, doi:10.1088/1475-7516/2016/07/028.

[64] D. Blas, M. Garny, and T. Konstandin. On the non-linear scale of cosmological perturbation theory. *JCAP*, 1309:024, 2013. arXiv:1304.1546, doi:10.1088/1475-7516/2013/09/024.

[65] D. Blas, M. Garny, and T. Konstandin. Cosmological perturbation theory at three-loop order. *JCAP*, 1401(01):010, 2014. arXiv:1309.3308, doi:10.1088/1475-7516/2014/01/010.

[66] D. Blas, J. Lesgourgues, and T. Tram. The Cosmic Linear Anisotropy Solving System (CLASS) II: Approximation schemes. *JCAP*, 1107:034, 2011. arXiv:1104.2933, doi:10.1088/1475-7516/2011/07/034.

[67] D. Blas, J. Lesgourgues, and T. Tram. The Cosmic Linear Anisotropy Solving System (CLASS). Part II: Approximation schemes. *JCAP* , 7:034, July 2011. arXiv:1104.2933, doi:10.1088/1475-7516/2011/07/034.

[68] J. K. Bloomfield, E. E. Flanagan, M. Park, and S. Watson. Dark energy or modified gravity? An effective field theory approach. *JCAP*, 1308:010, 2013. arXiv:1211.7054, doi:10.1088/1475-7516/2013/08/010.

[69] J. R. Bond, S. Cole, G. Efstathiou, and N. Kaiser. Excursion set mass functions for hierarchical Gaussian fluctuations. *Astrophys. J.*, 379:440, 1991. doi:10.1086/170520.

[70] C. Bonvin. Isolating relativistic effects in large-scale structure. *Class. Quant. Grav.*, 31(23):234002, 2014. arXiv:1409.2224, doi:10.1088/0264-9381/31/23/234002.

[71] C. Bonvin, C. Clarkson, R. Durrer, R. Maartens, and O. Umeh. Cosmological ensemble and directional averages of observables. *JCAP*, 1507(07):040, 2015. arXiv:1504.01676, doi:10.1088/1475-7516/2015/07/040.

[72] C. Bonvin and R. Durrer. What galaxy surveys really measure. *Phys. Rev.*, D84:063505, 2011. arXiv:1105.5280, doi:10.1103/PhysRevD.84.063505.

[73] C. Bonvin, R. Durrer, and M. A. Gasparini. Fluctuations of the luminosity distance. *Phys. Rev.*, D73:023523, 2006. [Erratum: Phys. Rev.D85,029901(2012)]. arXiv:astro-ph/0511183, doi:10.1103/PhysRevD.85.029901,10.1103/PhysRevD.73.023523.

[74] C. Bonvin, R. Durrer, N. Khosravi, M. Kunz, and I. Sawicki. Redshift-space distortions from vector perturbations. *JCAP*, 1802(02):028, 2018. arXiv:1712.00052, doi:10.1088/1475-7516/2018/02/028.

[75] C. Bonvin and P. Fleury. Testing the equivalence principle on cosmological scales. *JCAP*, 1805(05):061, 2018. arXiv:1803.02771, doi:10.1088/1475-7516/2018/05/061.

[76] C. Bonvin, L. Hui, and E. Gaztanaga. Asymmetric galaxy correlation functions. *Phys. Rev.*, D89(8):083535, 2014. arXiv:1309.1321, doi:10.1103/PhysRevD.89.083535.

[77] C. Bonvin, L. Hui, and E. Gaztanaga. Optimising the measurement of relativistic distortions in large-scale structure. *JCAP*, 1608(08):021, 2016. arXiv:1512.03566, doi:10.1088/1475-7516/2016/08/021.

[78] L. G. Book, M. Kamionkowski, and T. Souradeep. Odd-parity bipolar spherical harmonics. *Phys. Rev. D* , 85(2):023010, Jan. 2012. arXiv:1109.2910, doi:10.1103/PhysRevD.85.023010.

[79] B. Bose, K. Koyama, M. Lewandowski, F. Vernizzi, and H. A. Winther. Towards Precision Constraints on Gravity with the Effective Field Theory of Large-Scale Structure. 2018. arXiv:1802.01566.

[80] F. R. Bouchet. Introductory overview of Eulerian and Lagrangian perturbation theories. In *Dark matter in the universe. Proceedings, 132nd course of the International School of Physics *Enrico Fermi*, Varenna, Italy, July 25-August 4, 1995*, pages 565–599, 1995. arXiv:astro-ph/9603013.

[81] R. H. Brandenberger. Inflationary cosmology: Progress and problems. In *IPM School on Cosmology 1999: Large Scale Structure Formation Tehran, Iran, January 23-February 4, 1999*, 1999. arXiv:hep-ph/9910410.

[82] R. H. Brandenberger. Back reaction of cosmological perturbations and the cosmological constant problem. In *18th IAP Colloquium on the Nature of Dark Energy: Observational and Theoretical Results on the Accelerating Universe Paris, France, July 1-5, 2002*, 2002. arXiv:hep-th/0210165.

[83] M. Bruni, D. B. Thomas, and D. Wands. Computing General Relativistic effects from Newtonian N-body simulations: Frame dragging in the post-Friedmann approach. *Phys. Rev.*, D89(4):044010, 2014. arXiv:1306.1562, doi:10.1103/PhysRevD.89.044010.

[84] T. Buchert. Lagrangian theory of gravitational instability of Friedman-Lemaitre cosmologies: Generic third order model for nonlinear clustering. *Mon. Not. Roy. Astron. Soc.*, 267:811–820, 1994. arXiv:astro-ph/9309055, doi:10.1093/mnras/267.4.811.

[85] T. Buchert. Dark Energy from Structure: A Status Report. *Gen. Rel. Grav.*, 40:467–527, 2008. arXiv:0707.2153, doi:10.1007/s10714-007-0554-8.

[86] T. Buchert et al. Is there proof that backreaction of inhomogeneities is irrelevant in cosmology? *Class. Quant. Grav.*, 32:215021, 2015. arXiv:1505.07800, doi:10.1088/0264-9381/32/21/215021.

[87] T. Buchert and S. Rasanen. Backreaction in late-time cosmology. *Ann. Rev. Nucl. Part. Sci.*, 62:57–79, 2012. arXiv:1112.5335, doi:10.1146/annurev.nucl.012809.104435.

[88] P. Bull. Extending cosmological tests of General Relativity with the Square Kilometre Array. *Astrophys. J.*, 817(1):26, 2016. arXiv:1509.07562, doi:10.3847/0004-637X/817/1/26.

[89] J. E. Campagne, J. Neveu, and S. Plaszczynski. Angpow: a software for the fast computation of accurate tomographic power spectra. *Astron. Astrophys.*, 602:A72, 2017. arXiv:1701.03592, doi:10.1051/0004-6361/201730399.

[90] J. E. Campagne, S. Plaszczynski, and J. Neveu. The Galaxy Count Correlation Function in Redshift Space Revisited. *Astrophys. J.*, 845(1):28, 2017. arXiv:1703.02818, doi:10.3847/1538-4357/aa7cf8.

[91] J. Campbell. *The Masks of God: Primitive mythology*. Secker and Warburg, 1960.

[92] W. Cardona, R. Durrer, M. Kunz, and F. Montanari. Lensing convergence and the neutrino mass scale in galaxy redshift surveys. *Phys. Rev.*, D94(4):043007, 2016. arXiv:1603.06481, doi:10.1103/PhysRevD.94.043007.

[93] C. L. Carilli and S. Rawlings. Science with the Square Kilometer Array: Motivation, key science projects, standards and assumptions. *New Astron. Rev.*, 48:979, 2004. arXiv:astro-ph/0409274, doi:10.1016/j.newar.2004.09.001.

[94] J. Carlson, M. White, and N. Padmanabhan. Critical look at cosmological perturbation theory techniques. *Phys. Rev. D* , 80(4):043531, Aug. 2009. arXiv:0905.0479, doi:10.1103/PhysRevD.80.043531.

[95] J. J. M. Carrasco, M. P. Hertzberg, and L. Senatore. The Effective Field Theory of Cosmological Large Scale Structures. *JHEP*, 09:082, 2012. arXiv:1206.2926, doi:10.1007/JHEP09(2012)082.

[96] S. M. Carroll. The Cosmological constant. *Living Rev. Rel.*, 4:1, 2001. arXiv:astro-ph/0004075, doi:10.12942/lrr-2001-1.

[97] J. L. Cervantes-Cota and G. Smoot. Cosmology today-A brief review. *AIP Conf. Proc.*, 1396:28–52, 2011. arXiv:1107.1789, doi:10.1063/1.3647524.

[98] A. Challinor and A. Lewis. Linear power spectrum of observed source number counts. *Phys. Rev. D* , 84(4):043516, Aug. 2011. arXiv:1105.5292, doi:10.1103/PhysRevD.84.043516.

[99] A. Challinor and A. Lewis. The linear power spectrum of observed source number counts. *Phys.Rev.*, D84:043516, 2011. arXiv:1105.5292, doi:10.1103/PhysRevD.84.043516.

[100] S. Chen and D. J. Schwarz. Fluctuations of differential number counts of radio continuum sources. *Phys. Rev.*, D91(4):043507, 2015. arXiv:1407.4682, doi:10.1103/PhysRevD.91.043507.

[101] C.-H. Chuang et al. The clustering of galaxies in the completed SDSS-III Baryon Oscillation Spectroscopic Survey: single-probe measurements from DR12 galaxy clustering ? towards an accurate model. *Mon. Not. Roy. Astron. Soc.*, 471(2):2370–2390, 2017. arXiv:1607.03151, doi:10.1093/mnras/stx1641.

[102] C.-H. Chuang and Y. Wang. Modeling the Anisotropic Two-Point Galaxy Correlation Function on Small Scales and Improved Measurements of $H(z)$, $D_A(z)$, and $\beta(z)$ from the Sloan Digital Sky Survey DR7 Luminous Red Galaxies. *Mon. Not. Roy. Astron. Soc.*, 435:255–262, 2013. arXiv:1209.0210, doi:10.1093/mnras/stt1290.

[103] C.-H. Chuang and Y. Wang. Using Multipoles of the Correlation Function to Measure $H(z)$, $D_A(z)$, and $\beta(z)$ from Sloan Digital Sky Survey Luminous Red Galaxies. *Mon. Not. Roy. Astron. Soc.*, 431:2634, 2013. arXiv:1205.5573, doi:10.1093/mnras/stt357.

[104] C. Clarkson. Local gauge-invariance at any order in cosmological perturbation theory. 2011. arXiv:1108.4513.

[105] C. Clarkson, G. Ellis, J. Larena, and O. Umeh. Does the growth of structure affect our dynamical models of the universe? The averaging, backreaction and fitting problems in cosmology. *Rept. Prog. Phys.*, 74:112901, 2011. arXiv:1109.2314, doi:10.1088/0034-4885/74/11/112901.

[106] T. Clifton, P. G. Ferreira, A. Padilla, and C. Skordis. Modified Gravity and Cosmology. *Phys. Rept.*, 513:1–189, 2012. arXiv:1106.2476, doi:10.1016/j.physrep.2012.01.001.

[107] D. Clowe, A. Gonzalez, and M. Markevitch. Weak-Lensing Mass Reconstruction of the Interacting Cluster 1E 0657-558: Direct Evidence for the Existence of Dark Matter. *ApJ* , 604:596–603, Apr. 2004. arXiv:astro-ph/0312273, doi:10.1086/381970.

[108] C. Contreras et al. The WiggleZ Dark Energy Survey: measuring the cosmic growth rate with the two-point galaxy correlation function. 2013. [Mon. Not. Roy. Astron. Soc.430,924(2013)]. arXiv:1302.5178, doi:10.1093/mnras/sts608.

[109] P. Creminelli, G. D'Amico, J. Norena, and F. Vernizzi. The Effective Theory of Quintessence: the w<-1 Side Unveiled. *JCAP*, 0902:018, 2009. arXiv:0811.0827, doi:10.1088/1475-7516/2009/02/018.

[110] M. Crocce and R. Scoccimarro. Nonlinear Evolution of Baryon Acoustic Oscillations. *Phys. Rev.*, D77:023533, 2008. arXiv:0704.2783, doi:10.1103/PhysRevD.77.023533.

[111] A. J. Cuesta et al. The clustering of galaxies in the SDSS-III Baryon Oscillation Spectroscopic Survey: Baryon Acoustic Oscillations in the correlation function of LOWZ and CMASS galaxies in Data Release 12. *Mon. Not. Roy. Astron. Soc.*, 457(2):1770–1785, 2016. arXiv:1509.06371, doi:10.1093/mnras/stw066.

[112] G. Cusin, C. Pitrou, and J.-P. Uzan. Are we living near the center of a local void? *JCAP*, 1703(03):038, 2017. arXiv:1609.02061, doi:10.1088/1475-7516/2017/03/038.

[113] G. Cusin, V. Tansella, and R. Durrer. Vorticity generation in the Universe: A perturbative approach. *Phys. Rev.*, D95(6):063527, 2017. arXiv:1612.00783, doi:10.1103/PhysRevD.95.063527.

[114] D. Daverio, M. Hindmarsh, M. Kunz, J. Lizarraga, and J. Urrestilla. Energy-momentum correlations for Abelian Higgs cosmic strings. *Phys. Rev.*, D93(8):085014, 2016. [Erratum: Phys. Rev.D95,no.4,049903(2017)]. arXiv:1510.05006, doi:10.1103/PhysRevD.95.049903,10.1103/PhysRevD.93.085014.

[115] T. Davis, C. Blake, D. Parkinson, S. Riemer-Sørensen, G. B. Poole, M. Scrimgeour, E. Kazin, F. Beutler, K. Glazebrook, M. Drinkwater, W. Couch, and WiggleZ Dark Energy Survey Team. The WiggleZ Dark Energy Survey: Final Results. In *American Astronomical Society Meeting Abstracts #221*, volume 221 of *American Astronomical Society Meeting Abstracts*, page 106.02, Jan. 2013.

[116] K. S. Dawson et al. The SDSS-IV extended Baryon Oscillation Spectroscopic Survey: Overview and Early Data. *Astron. J.*, 151:44, 2016. arXiv:1508.04473, doi:10.3847/0004-6256/151/2/44.

[117] P. de Bernardis et al. Exploring Cosmic Origins with CORE: The Instrument. 2017. arXiv:1705.02170.

[118] DES Collaboration, T. M. C. Abbott, and et.al. Dark Energy Survey Year 1 Results: Cosmological Constraints from Galaxy Clustering and Weak Lensing. *ArXiv e-prints*, Aug. 2017. arXiv:1708.01530.

[119] V. Desjacques, M. Crocce, R. Scoccimarro, and R. K. Sheth. Modeling scale-dependent bias on the baryonic acoustic scale with the statistics of peaks of Gaussian random fields. *Phys. Rev. D* , 82(10):103529, Nov. 2010. arXiv:1009.3449, doi:10.1103/PhysRevD.82.103529.

[120] V. Desjacques, M. Crocce, R. Scoccimarro, and R. K. Sheth. Modeling scale-dependent bias on the baryonic acoustic scale with the statistics of peaks of Gaussian random fields. *Phys. Rev.*, D82:103529, 2010. arXiv:1009.3449, doi:10.1103/PhysRevD.82.103529.

[121] V. Desjacques, D. Jeong, and F. Schmidt. Large-Scale Galaxy Bias. 2016. arXiv:1611.09787.

[122] E. Di Dio, R. Durrer, G. Marozzi, and F. Montanari. Galaxy number counts to second order and their bispectrum. *JCAP*, 1412:017, 2014. [Erratum: JCAP1506,no.06,E01(2015)]. arXiv:1407.0376, doi:10.1088/1475-7516/2014/12/017,10.1088/1475-7516/2015/06/E01.

[123] E. Di Dio, R. Durrer, G. Marozzi, and F. Montanari. The bispectrum of relativistic galaxy number counts. *JCAP*, 1601:016, 2016. arXiv:1510.04202, doi:10.1088/1475-7516/2016/01/016.

[124] E. Di Dio, F. Montanari, R. Durrer, and J. Lesgourgues. Cosmological Parameter Estimation with Large Scale Structure Observations. *JCAP*, 1401:042, 2014. arXiv:1308.6186, doi:10.1088/1475-7516/2014/01/042.

[125] E. Di Dio, F. Montanari, J. Lesgourgues, and R. Durrer. The CLASSgal code for Relativistic Cosmological Large Scale Structure. *JCAP*, 1311:044, 2013. arXiv:1307.1459, doi:10.1088/1475-7516/2013/11/044.

[126] E. Di Dio, F. Montanari, A. Raccanelli, R. Durrer, M. Kamionkowski, and J. Lesgourgues. Curvature constraints from Large Scale Structure. *JCAP*, 1606(06):013, 2016. arXiv:1603.09073, doi:10.1088/1475-7516/2016/06/013.

[127] E. Di Dio, H. Perrier, R. Durrer, G. Marozzi, A. Moradinezhad Dizgah, J. Norena, and A. Riotto. Non-Gaussianities due to Relativistic Corrections to the Observed Galaxy Bispectrum. *JCAP*, 1703(03):006, 2017. arXiv:1611.03720, doi:10.1088/1475-7516/2017/03/006.

[128] S. Dodelson. *Modern cosmology*. Academic Press, San Diego, CA, 2003. URL: https://cds.cern.ch/record/1282338.

[129] M. J. Drinkwater et al. The WiggleZ Dark Energy Survey: Survey Design and First Data Release. *Mon. Not. Roy. Astron. Soc.*, 401:1429–1452, 2010. arXiv:0911.4246, doi:10.1111/j.1365-2966.2009.15754.x.

[130] R. Durrer. Gauge invariant cosmological perturbation theory: A General study and its application to the texture scenario of structure formation. *Fund. Cosmic Phys.*, 15:209–339, 1994. arXiv:astro-ph/9311041.

[131] R. Durrer. *The Cosmic Microwave Background*. Cambridge University Press, 2008.

[132] R. Durrer, T. Kahniashvili, and A. Yates. Microwave background anisotropies from Alfven waves. *Phys. Rev.*, D58:123004, 1998. arXiv:astro-ph/9807089, doi:10.1103/PhysRevD.58.123004.

[133] R. Durrer, M. Kunz, and A. Melchiorri. Cosmic structure formation with topological defects. *Phys. Rept.*, 364:1–81, 2002. arXiv:astro-ph/0110348, doi:10.1016/S0370-1573(02)00014-5.

[134] R. Durrer and V. Tansella. Vector perturbations of galaxy number counts. *JCAP*, 1607(07):037, 2016. arXiv:1605.05974, doi:10.1088/1475-7516/2016/07/037.

[135] J. Ehlers and T. Buchert. Newtonian cosmology in Lagrangian formulation: Foundations and perturbation theory. *Gen. Rel. Grav.*, 29:733–764, 1997. arXiv:astro-ph/9609036, doi:10.1023/A:1018885922682.

[136] A. Einstein. Kosmologische Betrachtungen zur allgemeinen Relativitätstheorie. *Sitzungsberichte der Königlich Preußischen Akademie der Wissenschaften (Berlin), Seite 142-152.*, 1917.

[137] D. J. Eisenstein et al. Detection of the Baryon Acoustic Peak in the Large-Scale Correlation Function of SDSS Luminous Red Galaxies. *Astrophys. J.*, 633:560–574, 2005. arXiv:astro-ph/0501171, doi:10.1086/466512.

[138] D. J. Eisenstein and W. Hu. Power spectra for cold dark matter and its variants. *Astrophys. J.*, 511:5, 1997. arXiv:astro-ph/9710252, doi:10.1086/306640.

[139] D. J. Eisenstein and W. Hu. Baryonic features in the matter transfer function. *Astrophys. J.*, 496:605, 1998. arXiv:astro-ph/9709112, doi:10.1086/305424.

[140] D. J. Eisenstein, W. Hu, and M. Tegmark. Cosmic complementarity: $H(0)$ and $\Omega_m$ from combining CMB experiments and redshift surveys. *Astrophys. J.*, 504:L57–L61, 1998. arXiv:astro-ph/9805239, doi:10.1086/311582.

[141] D. J. Eisenstein, H.-j. Seo, and M. J. White. On the Robustness of the Acoustic Scale in the Low-Redshift Clustering of Matter. *Astrophys. J.*, 664:660–674, 2007. arXiv:astro-ph/0604361, doi:10.1086/518755.

[142] G. F. R. Ellis. Inhomogeneity effects in Cosmology. *Class. Quant. Grav.*, 28:164001, 2011. arXiv:1103.2335, doi:10.1088/0264-9381/28/16/164001.

[143] G. F. R. Ellis and M. Bruni. Covariant and Gauge Invariant Approach to Cosmological Density Fluctuations. *Phys. Rev.*, D40:1804–1818, 1989. doi:10.1103/PhysRevD.40.1804.

[144] G. F. R. Ellis, J. Hwang, and M. Bruni. Covariant and gauge-independent perfect-fluid robertson-walker perturbations. *Phys. Rev. D*, 40:1819–1826, Sep 1989. URL: https://link.aps.org/doi/10.1103/PhysRevD.40.1819, doi:10.1103/PhysRevD.40.1819.

[145] G. F. R. Ellis, R. Maartens, and M. A. H. MacCallum. *Relativistic Cosmology*. Mar. 2012.

[146] G. F. R. Ellis and H. van Elst. Cosmological models: Cargese lectures 1998. *NATO Sci. Ser. C*, 541:1–116, 1999. arXiv:gr-qc/9812046, doi:10.1007/978-94-011-4455-1_1.

[147] G. Fanizza, J. Yoo, and S. G. Biern. Non-linear general relativistic effects in the observed redshift. 2018. arXiv:1805.05959.

[148] A. Ferte, D. Kirk, A. R. Liddle, and J. Zuntz. Testing gravity on cosmological scales with cosmic shear, cosmic microwave background anisotropies, and redshift-space distortions. 2017. arXiv:1712.01846.

[149] J. A. Fillmore and P. Goldreich. Self-similiar gravitational collapse in an expanding universe. *Astrophys. J.*, 281:1–8, 1984. doi:10.1086/162070.

[150] K. B. Fisher. On the validity of the streaming model for the redshift space correlation function in the linear regime. *Astrophys. J.*, 448:494–499, 1995. arXiv:astro-ph/9412081, doi:10.1086/175980.

[151] K. B. Fisher, M. Davis, M. A. Strauss, A. Yahil, and J. P. Huchra. Clustering in the 1.2-JY IRAS Galaxy Redshift Survey - Part Two - Redshift Distortions and Xi/r/p, PI. *"Mon. Not. Roy. Astron. Soc."*, 267:927, Apr. 1994. arXiv:astro-ph/9308013, doi:10.1093/mnras/267.4.927.

[152] P. Fleury, C. Clarkson, and R. Maartens. How does the cosmic large-scale structure bias the Hubble diagram? *JCAP*, 1703(03):062, 2017. arXiv:1612.03726, doi:10.1088/1475-7516/2017/03/062.

[153] L. H. Ford. INFLATION DRIVEN BY A VECTOR FIELD. *Phys. Rev.*, D40:967, 1989. doi:10.1103/PhysRevD.40.967.

[154] A. Friedmann. Über die Möglichkeit einer Welt mit konstanter negativer Krümmung des Raumes. *Zeitschrift fur Physik*, 21:326–332, Dec. 1924. doi:10.1007/BF01328280.

[155] E. Gaztanaga, C. Bonvin, and L. Hui. Measurement of the dipole in the cross-correlation function of galaxies. *JCAP*, 1701(01):032, 2017. arXiv:1512.03918, doi:10.1088/1475-7516/2017/01/032.

[156] E. Gaztanaga, P. Norberg, C. M. Baugh, and D. J. Croton. Statistical analysis of galaxy surveys. 2. The 3-point galaxy correlation function measured from the 2dFGRS. *Mon. Not. Roy. Astron. Soc.*, 364:620–634, 2005. arXiv:astro-ph/0506249, doi:10.1111/j.1365-2966.2005.09583.x.

[157] M. Gerstenlauer, A. Hebecker, and G. Tasinato. Inflationary Correlation Functions without Infrared Divergences. *JCAP*, 1106:021, 2011. arXiv:1102.0560, doi:10.1088/1475-7516/2011/06/021.

[158] B. Ghosh, R. Durrer, and E. Sellentin. General Relativistic corrections in density-shear correlations. 2018. arXiv:1801.02518.

[159] H. Gil-Marin, J. Norena, L. Verde, W. J. Percival, C. Wagner, M. Manera, and D. P. Schneider. The power spectrum and bispectrum of SDSS DR11 BOSS galaxies ? I. Bias and gravity. *Mon. Not. Roy. Astron. Soc.*, 451(1):539–580, 2015. arXiv:1407.5668, doi:10.1093/mnras/stv961.

[160] A. Golovnev, V. Mukhanov, and V. Vanchurin. Vector Inflation. *JCAP*, 0806:009, 2008. arXiv:0802.2068, doi:10.1088/1475-7516/2008/06/009.

[161] L. Gradshteyn and L. Ryzhik. *Table of Integrals, Series and Products*. Academic Press, New York, sixth edition edition, 2000.

[162] H. S. Grasshorn Gebhardt and D. Jeong. Fast and accurate computation of projected two-point functions. *Phys. Rev.*, D97(2):023504, 2018. arXiv:1709.02401, doi:10.1103/PhysRevD.97.023504.

[163] G. Gubitosi, F. Piazza, and F. Vernizzi. The Effective Field Theory of Dark Energy. *JCAP*, 1302:032, 2013. [JCAP1302,032(2013)]. arXiv:1210.0201, doi:10.1088/1475-7516/2013/02/032.

[164] J. E. Gunn and J. R. Gott, III. On the Infall of Matter into Clusters of Galaxies and Some Effects on Their Evolution. *Astrophys. J.*, 176:1–19, 1972. doi:10.1086/151605.

[165] A. H. Guth. Inflationary universe: A possible solution to the horizon and flatness problems. *Phys. Rev. D* , 23:347–356, Jan. 1981. doi:10.1103/PhysRevD.23.347.

[166] T. Hahn. CUBA: A Library for multidimensional numerical integration. *Comput. Phys. Commun.*, 168:78–95, 2005. arXiv:hep-ph/0404043, doi:10.1016/j.cpc.2005.01.010.

[167] A. Hajian and T. Souradeep. Measuring statistical isotropy of the CMB anisotropy. *Astrophys. J.*, 597:L5–L8, 2003. arXiv:astro-ph/0308001, doi:10.1086/379757.

[168] A. Hajian and T. Souradeep. The Cosmic microwave background bipolar power spectrum: Basic formalism and applications. 2005. arXiv:astro-ph/0501001.

[169] A. Hall and C. Bonvin. Measuring cosmic velocities with 21 cm intensity mapping and galaxy redshift survey cross-correlation dipoles. *Phys. Rev.*, D95(4):043530, 2017. arXiv:1609.09252, doi:10.1103/PhysRevD.95.043530.

[170] A. Hall, C. Bonvin, and A. Challinor. Testing General Relativity with 21-cm intensity mapping. *Phys. Rev.*, D87(6):064026, 2013. arXiv:1212.0728, doi:10.1103/PhysRevD.87.064026.

[171] A. J. S. Hamilton. Linear redshift distortions: A Review. In *Ringberg Workshop on Large Scale Structure Ringberg, Germany, September 23-28, 1996*, 1997. URL: http://alice.cern.ch/format/showfull?sysnb=0255366, arXiv:astro-ph/9708102, doi:10.1007/978-94-011-4960-0_17.

[172] A. J. S. Hamilton and M. Culhane. Spherical redshift distortions. *Mon. Not. Roy. Astron. Soc.*, 278:73, 1996. arXiv:astro-ph/9507021, doi:10.1093/mnras/278.1.73.

[173] S. Hassani. *From Atoms to Galaxies: A Conceptual Physics Approach to Scientific Awareness*. Taylor & Francis, 2010.

[174] S. W. Hawking. Perturbations of an expanding universe. *Astrophys. J.*, 145:544–554, 1966. doi:10.1086/148793.

[175] A. F. Heavens and A. N. Taylor. A Spherical Harmonic Analysis of Redshift Space. *Mon. Not. Roy. Astron. Soc.*, 275:483–497, 1995. arXiv:astro-ph/9409027, doi:10.1093/mnras/275.2.483.

[176] A. F. Heavens and A. N. Taylor. Design and analysis of redshift surveys. *Mon. Not. Roy. Astron. Soc.*, 290:456, 1997. arXiv:astro-ph/9705215, doi:10.1093/mnras/290.3.456.

[177] L. Heisenberg. Generalization of the Proca Action. *JCAP*, 1405:015, 2014. arXiv:1402.7026, doi:10.1088/1475-7516/2014/05/015.

[178] G. Hinshaw, D. Larson, E. Komatsu, D. N. Spergel, C. L. Bennett, J. Dunkley, M. R. Nolta, M. Halpern, R. S. Hill, N. Odegard, L. Page, K. M. Smith, J. L. Weiland, B. Gold, N. Jarosik, A. Kogut, M. Limon, S. S. Meyer, G. S. Tucker, E. Wollack, and E. L. Wright. Nine-year Wilkinson Microwave Anisotropy Probe (WMAP) Observations: Cosmological Parameter Results. *ApJS* , 208:19, Oct. 2013. arXiv:1212.5226, doi:10.1088/0067-0049/208/2/19.

[179] S. R. Hinton et al. Measuring the 2D Baryon Acoustic Oscillation signal of galaxies in WiggleZ: Cosmological constraints. *Mon. Not. Roy. Astron. Soc.*, 464(4):4807–4822, 2017. arXiv:1611.08040, doi:10.1093/mnras/stw2725.

[180] G. W. Horndeski. Second-Order Scalar-Tensor Field Equations in a Four-Dimensional Space. *International Journal of Theoretical Physics*, 10:363–384, Sept. 1974. doi:10.1007/BF01807638.

[181] E. Hubble. A relation between distance and radial velocity among extra-galactic nebulae. *Proceedings of the National Academy of Sciences*, 15(3):168–173, 1929. URL: http://www.pnas.org/content/15/3/168, arXiv:http://www.pnas.org/content/15/3/168.full.pdf, doi:10.1073/pnas.15.3.168.

[182] L. Hui, E. Gaztanaga, and M. LoVerde. Anisotropic Magnification Distortion of the 3D Galaxy Correlation. 1. Real Space. *Phys. Rev.*, D76:103502, 2007. arXiv:0706.1071, doi:10.1103/PhysRevD.76.103502.

[183] L. Hui, E. Gaztanaga, and M. LoVerde. Anisotropic Magnification Distortion of the 3D Galaxy Correlation: II. Fourier and Redshift Space. *Phys. Rev.*, D77:063526, 2008. arXiv:0710.4191, doi:10.1103/PhysRevD.77.063526.

[184] V. Irsic, E. Di Dio, and M. Viel. Relativistic effects in Lyman-? forest. *JCAP*, 1602(02):051, 2016. arXiv:1510.03436, doi:10.1088/1475-7516/2016/02/051.

[185] M. Ishak, A. Upadhye, and D. N. Spergel. Probing cosmic acceleration beyond the equation of state: Distinguishing between dark energy and modified gravity models. *Phys. Rev.*, D74:043513, 2006. arXiv:astro-ph/0507184, doi:10.1103/PhysRevD.74.043513.

[186] J. C. Jackson. Fingers of God: A critique of Rees' theory of primoridal gravitational radiation. *Mon. Not. Roy. Astron. Soc.*, 156:1P–5P, 1972. arXiv:0810.3908, doi:10.1093/mnras/156.1.1P.

[187] T. Jacobson and D. Mattingly. Gravity with a dynamical preferred frame. *Phys. Rev.*, D64:024028, 2001. arXiv:gr-qc/0007031, doi:10.1103/PhysRevD.64.024028.

[188] B. Jain and E. Bertschinger. Second order power spectrum and nonlinear evolution at high redshift. *Astrophys. J.*, 431:495, 1994. arXiv:astro-ph/9311070, doi:10.1086/174502.

[189] G. Jelic-Cizmek, F. Lepori, J. Adamek, and R. Durrer. The Generation of Vorticity in Cosmological Large Scale Structure. 2018. arXiv:1806.05146.

[190] D. Jeong and M. Kamionkowski. Clustering Fossils from the Early Universe. *Phys. Rev. Lett.*, 108:251301, 2012. arXiv:1203.0302, doi:10.1103/PhysRevLett.108.251301.

[191] D. Jeong and F. Schmidt. Large-Scale Structure with Gravitational Waves I: Galaxy Clustering. *Phys. Rev.*, D86:083512, 2012. arXiv:1205.1512, doi:10.1103/PhysRevD.86.083512.

[192] D. Jeong and F. Schmidt. Large-Scale Structure Observables in General Relativity. *Class. Quant. Grav.*, 32(4):044001, 2015. arXiv:1407.7979, doi:10.1088/0264-9381/32/4/044001.

[193] D. Jeong, F. Schmidt, and C. M. Hirata. Large-scale clustering of galaxies in general relativity. *Phys. Rev. D* , 85(2):023504, Jan. 2012. arXiv:1107.5427, doi:10.1103/PhysRevD.85.023504.

[194] D. Jeong, F. Schmidt, and C. M. Hirata. Large-scale clustering of galaxies in general relativity. *Phys. Rev.*, D85:023504, 2012. arXiv:1107.5427, doi:10.1103/PhysRevD.85.023504.

[195] S. Jolicoeur, O. Umeh, R. Maartens, and C. Clarkson. Imprints of local lightcone projection effects on the galaxy bispectrum. Part II. *JCAP*, 1709(09):040, 2017. arXiv:1703.09630, doi:10.1088/1475-7516/2017/09/040.

[196] S. Jolicoeur, O. Umeh, R. Maartens, and C. Clarkson. Imprints of local lightcone projection effects on the galaxy bispectrum. III Relativistic corrections from nonlinear dynamical evolution on large-scales. *JCAP*, 1803(03):036, 2018. arXiv:1711.01812, doi:10.1088/1475-7516/2018/03/036.

[197] D. H. Jones et al. The 6dF Galaxy Survey: Final Redshift Release (DR3) and Southern Large-Scale Structures. *Mon. Not. Roy. Astron. Soc.*, 399:683, 2009. arXiv:0903.5451, doi:10.1111/j.1365-2966.2009.15338.x.

[198] N. Kaiser. Clustering in real space and in redshift space. *M.N.R.A.S.* , 227:1–21, July 1987. doi:10.1093/mnras/227.1.1.

[199] N. Kaiser. Clustering in real space and in redshift space. *M.N.R.A.S.*, 227:1–21, July 1987.

[200] N. Kaiser. Clustering in real space and in redshift space. *Mon. Not. Roy. Astron. Soc.*, 227:1–27, 1987.

[201] H. Kodama and M. Sasaki. Cosmological perturbation theory. *Progress of Theoretical Physics Supplement*, 78:1–166, 1984. doi:10.1143/PTPS.78.1.

[202] S. D. Landy and A. S. Szalay. Bias and variance of angular correlation functions. *ApJ* , 412:64–71, July 1993. doi:10.1086/172900.

[203] R. Laureijs, J. Amiaux, S. Arduini, J. . Augueres, J. Brinchmann, R. Cole, M. Cropper, C. Dabin, L. Duvet, A. Ealet, and et al. Euclid Definition Study Report. *ArXiv e-prints*, Oct. 2011. arXiv:1110.3193.

[204] R. Laureijs et al. Euclid Definition Study Report. 2011. arXiv:1110.3193.

[205] G. Lemaître. Expansion of the universe, A homogeneous universe of constant mass and increasing radius accounting for the radial velocity of extra-galactic nebulae. *M.N.R.A.S.* , 91:483–490, Mar. 1931. doi:10.1093/mnras/91.5.483.

[206] A. Lewis and A. Challinor. Weak gravitational lensing of the cmb. *Phys. Rept.*, 429:1–65, 2006. arXiv:astro-ph/0601594, doi:10.1016/j.physrep.2006.03.002.

[207] A. Lewis, A. Challinor, and A. Lasenby. Efficient computation of CMB anisotropies in closed FRW models. *Astrophys. J.*, 538:473–476, 2000. arXiv:astro-ph/9911177, doi:10.1086/309179.

[208] A. R. Liddle. An Introduction to cosmological inflation. In *Proceedings, Summer School in High-energy physics and cosmology: Trieste, Italy, June 29-July 17, 1998*, pages 260–295, 1999. arXiv:astro-ph/9901124.

[209] E. Lifshitz. Republication of: On the gravitational stability of the expanding universe. *J. Phys.(USSR)*, 10:116, 1946. [Gen. Rel. Grav.49,no.2,18(2017)]. doi:10.1007/s10714-016-2165-8.

[210] E. A. Lim. Can we see Lorentz-violating vector fields in the CMB? *Phys. Rev.*, D71:063504, 2005. arXiv:astro-ph/0407437, doi:10.1103/PhysRevD.71.063504.

[211] J. Lizarraga, J. Urrestilla, D. Daverio, M. Hindmarsh, and M. Kunz. New CMB constraints for Abelian Higgs cosmic strings. *JCAP*, 1610(10):042, 2016. arXiv:1609.03386, doi:10.1088/1475-7516/2016/10/042.

[212] C. S. Lorenz, D. Alonso, and P. G. Ferreira. The impact of relativistic effects on cosmological parameter estimation. 2017. arXiv:1710.02477.

[213] M. LoVerde, L. Hui, and E. Gaztanaga. Lensing corrections to features in the angular two-point correlation function and power spectrum. *Phys. Rev.*, D77:023512, 2008. arXiv:0708.0031, doi:10.1103/PhysRevD.77.023512.

[214] T. H.-C. Lu, K. Ananda, and C. Clarkson. Vector modes generated by primordial density fluctuations. *Phys. Rev.*, D77:043523, 2008. arXiv:0709.1619, doi:10.1103/PhysRevD.77.043523.

[215] T. H.-C. Lu, K. Ananda, C. Clarkson, and R. Maartens. The cosmological background of vector modes. *JCAP*, 0902:023, 2009. arXiv:0812.1349, doi:10.1088/1475-7516/2009/02/023.

[216] R. Maartens, F. B. Abdalla, M. Jarvis, and M. G. Santos. Overview of Cosmology with the SKA. *PoS*, AASKA14:016, 2015. arXiv:1501.04076.

[217] M. V. Magana et al. SDSS-III Baryon Oscillation Spectroscopic Survey: Analysis of Potential Systematics in Fitting of Baryon Acoustic Feature. 2013. arXiv:1312.4996.

[218] N. Makino, M. Sasaki, and Y. Suto. Analytic approach to the perturbative expansion of nonlinear gravitational fluctuations in cosmological density and velocity fields. *Phys. Rev.*, D46:585–602, 1992. doi:10.1103/PhysRevD.46.585.

[219] T. Matsubara. Nonlinear perturbation theory with halo bias and redshift-space distortions via the Lagrangian picture. *Phys. Rev.*, D78:083519, 2008. [Erratum: Phys. Rev.D78,109901(2008)]. arXiv:0807.1733, doi:10.1103/PhysRevD.78.109901,10.1103/PhysRevD.78.083519.

[220] T. Matsubara. Resumming Cosmological Perturbations via the Lagrangian Picture: One-loop Results in Real Space and in Redshift Space. *Phys. Rev.*, D77:063530, 2008. arXiv:0711.2521, doi:10.1103/PhysRevD.77.063530.

[221] T. Matsubara. Recursive solutions of Lagrangian perturbation theory. *Phys. Rev. D* , 92(2):023534, July 2015. arXiv:1505.01481, doi:10.1103/PhysRevD.92.023534.

[222] T. Matsubara. Recursive Solutions of Lagrangian Perturbation Theory. *Phys. Rev.*, D92(2):023534, 2015. arXiv:1505.01481, doi:10.1103/PhysRevD.92.023534.

[223] N. McCullagh and A. S. Szalay. Nonlinear Behavior of Baryon Acoustic Oscillations in Redshift Space from the Zel'dovich Approximation. *Astrophys. J.*, 798(2):137, 2015. arXiv:1411.1249, doi:10.1088/0004-637X/798/2/137.

[224] P. McDonald. Dark matter clustering: a simple renormalization group approach. *Phys. Rev.*, D75:043514, 2007. arXiv:astro-ph/0606028, doi:10.1103/PhysRevD.75.043514.

[225] P. McDonald. Gravitational redshift and other redshift-space distortions of the imaginary part of the power spectrum. *JCAP*, 0911:026, 2009. arXiv:0907.5220, doi:10.1088/1475-7516/2009/11/026.

[226] P. McDonald and U. Seljak. How to measure redshift-space distortions without sample variance. *JCAP*, 0910:007, 2009. arXiv:0810.0323, doi:10.1088/1475-7516/2009/10/007.

[227] A. Meiksin, M. J. White, and J. A. Peacock. Baryonic signatures in large scale structure. *Mon. Not. Roy. Astron. Soc.*, 304:851–864, 1999. arXiv:astro-ph/9812214, doi:10.1046/j.1365-8711.1999.02369.x.

[228] B. Menard, R. Scranton, M. Fukugita, and G. Richards. Measuring the galaxy-mass and galaxy-dust correlations through magnification and reddening. *Mon. Not. Roy. Astron. Soc.*, 405:1025–1039, 2010. arXiv:0902.4240, doi:10.1111/j.1365-2966.2010.16486.x.

[229] M. Milgrom. A modification of the Newtonian dynamics as a possible alternative to the hidden mass hypothesis. *ApJ* , 270:365–370, July 1983. doi:10.1086/161130.

[230] E. Mitsou, R. Durrer, S. Fulvio, V. Tansella, and J. Yoo. Observer terms and ensemble averages.

[231] H. Mo, F. van den Bosch, and S. White. *Galaxy formation and evolution*. Cambridge University Press, Cambridge, 9th printing edition, 2010.

[232] S. Mollerach, D. Harari, and S. Matarrese. CMB polarization from secondary vector and tensor modes. *Phys. Rev.*, D69:063002, 2004. arXiv:astro-ph/0310711, doi:10.1103/PhysRevD.69.063002.

[233] F. Montanari. *Relativistic effects in galaxy clustering*. PhD thesis, Geneva U., 2015. URL: http://archive-ouverte.unige.ch/unige:75513.

[234] F. Montanari and R. Durrer. An analytic approach to baryon acoustic oscillations. *Phys. Rev.*, D84:023522, 2011. arXiv:1105.1514, doi:10.1103/PhysRevD.84.023522.

[235] F. Montanari and R. Durrer. Measuring the lensing potential with tomographic galaxy number counts. *JCAP*, 1510(10):070, 2015. arXiv:1506.01369, doi:10.1088/1475-7516/2015/10/070.

[236] V. F. Mukhanov, H. A. Feldman, and R. H. Brandenberger. Theory of cosmological perturbations. *Phys.Rep.*, 215:203–333, June 1992. doi:10.1016/0370-1573(92)90044-Z.

[237] M. Nakashima and T. Kobayashi. The Music of the Aetherwave - B-mode Polarization in Einstein-Aether Theory. *Phys. Rev.*, D84:084051, 2011. arXiv:1103.2197, doi:10.1103/PhysRevD.84.084051.

[238] A. Obuljen, F. Villaescusa-Navarro, E. Castorina, and M. Viel. Baryon Acoustic Oscillations reconstruction with pixels. *JCAP*, 1709(09):012, 2017. arXiv:1610.05768, doi:10.1088/1475-7516/2017/09/012.

[239] A. Oka, S. Saito, T. Nishimichi, A. Taruya, and K. Yamamoto. Simultaneous constraints on the growth of structure and cosmic expansion from the multipole power spectra of the SDSS DR7 LRG sample. *Mon. Not. Roy. Astron. Soc.*, 439:2515–2530, 2014. arXiv:1310.2820, doi:10.1093/mnras/stu111.

[240] P. Papai and I. Szapudi. Non-Perturbative Effects of Geometry in Wide-Angle Redshift Distortions. *Mon. Not. Roy. Astron. Soc.*, 389:292, 2008. arXiv:0802.2940, doi:10.1111/j.1365-2966.2008.13572.x.

[241] P. J. E. Peebles and J. T. Yu. Primeval Adiabatic Perturbation in an Expanding Universe. *ApJ* , 162:815, Dec. 1970. doi:10.1086/150713.

[242] P. J. E. Peebles and J. T. Yu. Primeval adiabatic perturbation in an expanding universe. *Astrophys. J.*, 162:815–836, 1970. doi:10.1086/150713.

[243] A. A. Penzias and R. W. Wilson. A Measurement of Excess Antenna Temperature at 4080 Mc/s. *ApJ* , 142:419–421, July 1965. doi:10.1086/148307.

[244] S. Perlmutter et al. Measurements of Omega and Lambda from 42 high redshift supernovae. *Astrophys. J.*, 517:565–586, 1999. arXiv:astro-ph/9812133, doi:10.1086/307221.

[245] M. Pietroni. Flowing with Time: a New Approach to Nonlinear Cosmological Perturbations. *JCAP*, 0810:036, 2008. arXiv:0806.0971, doi:10.1088/1475-7516/2008/10/036.

[246] W. H. Press and P. Schechter. Formation of Galaxies and Clusters of Galaxies by Self-Similar Gravitational Condensation. *ApJ* , 187:425–438, Feb. 1974. doi:10.1086/152650.

[247] S. Pueblas and R. Scoccimarro. Generation of Vorticity and Velocity Dispersion by Orbit Crossing. *Phys. Rev.*, D80:043504, 2009. arXiv:0809.4606, doi:10.1103/PhysRevD.80.043504.

[248] A. R. Pullen and C. M. Hirata. Non-detection of a statistically anisotropic power spectrum in large-scale structure. *JCAP* , 5:027, May 2010. arXiv:1003.0673, doi:10.1088/1475-7516/2010/05/027.

[249] A. R. Pullen and M. Kamionkowski. Cosmic Microwave Background Statistics for a Direction-Dependent Primordial Power Spectrum. *Phys. Rev.*, D76:103529, 2007. arXiv:0709.1144, doi:10.1103/PhysRevD.76.103529.

[250] A. Raccanelli, D. Bertacca, O. Doré, and R. Maartens. Large-scale 3D galaxy correlation function and non-Gaussianity. *JCAP*, 1408:022, 2014. arXiv:1306.6646, doi:10.1088/1475-7516/2014/08/022.

[251] A. Raccanelli, D. Bertacca, D. Jeong, M. C. Neyrinck, and A. S. Szalay. Doppler term in the galaxy two-point correlation function: wide-angle, velocity, Doppler lensing and cosmic acceleration effects. 2016. arXiv:1602.03186.

[252] A. Raccanelli, D. Bertacca, R. Maartens, C. Clarkson, and O. Doré. Lensing and time-delay contributions to galaxy correlations. *Gen. Rel. Grav.*, 48(7):84, 2016. arXiv:1311.6813, doi:10.1007/s10714-016-2076-8.

[253] A. Raccanelli, F. Montanari, D. Bertacca, O. Doré, and R. Durrer. Cosmological Measurements with General Relativistic Galaxy Correlations. *JCAP*, 1605(05):009, 2016. arXiv:1505.06179, doi:10.1088/1475-7516/2016/05/009.

[254] A. Raccanelli, L. Samushia, and W. J. Percival. Simulating Redshift-Space Distortions for Galaxy Pairs with Wide Angular Separation. *Mon. Not. Roy. Astron. Soc.*, 409:1525, 2010. arXiv:1006.1652, doi:10.1111/j.1365-2966.2010.17388.x.

[255] A. Rajantie. Magnetic Monopoles in Field Theory and Cosmology. *Phil. Trans. Roy. Soc. Lond.*, A370:5705–5717, 2012. arXiv:1204.3073, doi:10.1098/rsta.2011.0394.

[256] C. Rampf. The recursion relation in Lagrangian perturbation theory. *JCAP* , 12:004, Dec. 2012. arXiv:1205.5274, doi:10.1088/1475-7516/2012/12/004.

[257] B. A. Reid et al. The clustering of galaxies in the SDSS-III Baryon Oscillation Spectroscopic Survey: measurements of the growth of structure and expansion rate at z=0.57 from anisotropic clustering. *Mon. Not. Roy. Astron. Soc.*, 426:2719, 2012. arXiv:1203.6641, doi:10.1111/j.1365-2966.2012.21779.x.

[258] B. A. Reid and M. White. Towards an accurate model of the redshift-space clustering of haloes in the quasi-linear regime. *M.N.R.A.S.* , 417:1913–1927, Nov. 2011. arXiv:1105.4165, doi:10.1111/j.1365-2966.2011.19379.x.

[259] P. H. F. Reimberg, F. Bernardeau, and C. Pitrou. Redshift-space distortions with wide angular separations. *JCAP*, 1601(01):048, 2016. arXiv:1506.06596, doi:10.1088/1475-7516/2016/01/048.

[260] A. G. Riess et al. Observational evidence from supernovae for an accelerating universe and a cosmological constant. *Astron. J.*, 116:1009–1038, 1998. arXiv:astro-ph/9805201, doi:10.1086/300499.

[261] A. Riotto. Inflation and the theory of cosmological perturbations. *ICTP Lect. Notes Ser.*, 14:317–413, 2003. arXiv:hep-ph/0210162.

[262] H. P. Robertson. Kinematics and World-Structure. *ApJ* , 82:284, Nov. 1935. doi:10.1086/143681.

[263] H. P. Robertson. Kinematics and World-Structure II. *ApJ* , 83:187, Apr. 1936. doi:10.1086/143716.

[264] H. P. Robertson. Kinematics and World-Structure III. *ApJ* , 83:257, May 1936. doi:10.1086/143726.

[265] V. C. Rubin and W. K. Ford, Jr. Rotation of the Andromeda Nebula from a Spectroscopic Survey of Emission Regions. *ApJ* , 159:379, Feb. 1970. doi:10.1086/150317.

[266] D. Saadeh, S. M. Feeney, A. Pontzen, H. V. Peiris, and J. D. McEwen. A framework for testing isotropy with the cosmic microwave background. *Mon. Not. Roy. Astron. Soc.*, 462(2):1802–1811, 2016. arXiv:1604.01024, doi:10.1093/mnras/stw1731.

[267] R. K. Sachs and A. M. Wolfe. Perturbations of a Cosmological Model and Angular Variations of the Microwave Background. *ApJ* , 147:73, Jan. 1967. doi:10.1086/148982.

[268] V. Salvatelli, F. Piazza, and C. Marinoni. Constraints on modified gravity from Planck 2015: when the health of your theory makes the difference. *JCAP*, 1609(09):027, 2016. arXiv:1602.08283, doi:10.1088/1475-7516/2016/09/027.

[269] L. Samushia, W. J. Percival, and A. Raccanelli. Interpreting large-scale redshift-space distortion measurements. *Mon. Not. Roy. Astron. Soc.*, 420:2102–2119, 2012. arXiv:1102.1014, doi:10.1111/j.1365-2966.2011.20169.x.

[270] A. G. Sanchez, C. M. Baugh, and R. Angulo. What is the best way to measure baryonic acoustic oscillations? *Mon. Not. Roy. Astron. Soc.*, 390:1470–1490, 2008. arXiv:0804.0233, doi:10.1111/j.1365-2966.2008.13769.x.

[271] A. Sandage. The Change of Redshift and Apparent Luminosity of Galaxies due to the Deceleration of Selected Expanding Universes. *ApJ* , 136:319, Sept. 1962. doi:10.1086/147385.

[272] S. Satpathy et al. The clustering of galaxies in the completed SDSS-III Baryon Oscillation Spectroscopic Survey: On the measurement of growth rate using galaxy correlation functions. *Mon. Not. Roy. Astron. Soc.*, 2016. [Mon. Not. Roy. Astron. Soc.469,1369(2017)]. arXiv:1607.03148, doi:10.1093/mnras/stx883.

[273] F. Scaccabarozzi, J. Yoo, and S. G. Biern. Galaxy Two-Point Correlation Function in General Relativity. 2018. arXiv:1807.09796.

[274] B. P. Schmidt et al. The High Z supernova search: Measuring cosmic deceleration and global curvature of the universe using type Ia supernovae. *Astrophys. J.*, 507:46–63, 1998. arXiv:astro-ph/9805200, doi:10.1086/306308.

[275] F. Schmidt, E. Pajer, and M. Zaldarriaga. Large-Scale Structure and Gravitational Waves III: Tidal Effects. *Phys.Rev.*, D89(8):083507, 2014. arXiv:1312.5616, doi:10.1103/PhysRevD.89.083507.

[276] R. Scoccimarro and J. Frieman. Loop Corrections in Nonlinear Cosmological Perturbation Theory. *ApJS* , 105:37, July 1996. arXiv:astro-ph/9509047, doi:10.1086/192306.

[277] R. K. Sheth, H. J. Mo, and G. Tormen. Ellipsoidal collapse and an improved model for the number and spatial distribution of dark matter haloes. *Mon. Not. Roy. Astron. Soc.*, 323:1, 2001. arXiv:astro-ph/9907024, doi:10.1046/j.1365-8711.2001.04006.x.

[278] M. Shiraishi, N. S. Sugiyama, and T. Okumura. Polypolar spherical harmonic decomposition of galaxy correlators in redshift space: Toward testing cosmic rotational symmetry. *Phys. Rev.*, D95(6):063508, 2017. arXiv:1612.02645, doi:10.1103/PhysRevD.95.063508.

[279] F. Simpson et al. CFHTLenS: Testing the Laws of Gravity with Tomographic Weak Lensing and Redshift Space Distortions. *Mon. Not. Roy. Astron. Soc.*, 429:2249, 2013. arXiv:1212.3339, doi:10.1093/mnras/sts493.

[280] R. E. Smith, R. Scoccimarro, and R. K. Sheth. Eppur Si Muove: On The Motion of the Acoustic Peak in the Correlation Function. *Phys. Rev.*, D77:043525, 2008. arXiv:astro-ph/0703620, doi:10.1103/PhysRevD.77.043525.

[281] T. P. Sotiriou and V. Faraoni. f(R) Theories Of Gravity. *Rev. Mod. Phys.*, 82:451–497, 2010. arXiv:0805.1726, doi:10.1103/RevModPhys.82.451.

[282] V. Springel et al. Simulating the joint evolution of quasars, galaxies and their large-scale distribution. *Nature*, 435:629–636, 2005. arXiv:astro-ph/0504097, doi:10.1038/nature03597.

[283] V. Springel, N. Yoshida, and S. D. M. White. GADGET: A Code for collisionless and gasdynamical cosmological simulations. *New Astron.*, 6:79, 2001. arXiv:astro-ph/0003162, doi:10.1016/S1384-1076(01)00042-2.

[284] J. M. Stewart. Perturbations of Friedmann-Robertson-Walker cosmological models. *Class. Quant. Grav.*, 7:1169–1180, 1990. doi:10.1088/0264-9381/7/7/013.

[285] N. S. Sugiyama, M. Shiraishi, and T. Okumura. Limits on statistical anisotropy from BOSS DR12 galaxies using bipolar spherical harmonics. *Mon. Not. Roy. Astron. Soc.*, 473(2):2737–2752, 2018. arXiv:1704.02868, doi:10.1093/mnras/stx2333.

[286] R. A. Sunyaev and Y. B. Zeldovich. Small-Scale Fluctuations of Relic Radiation. *ApSS* , 7:3–19, Apr. 1970. doi:10.1007/BF00653471.

[287] R. A. Sunyaev and Ya. B. Zeldovich. Small scale fluctuations of relic radiation. *Astrophys. Space Sci.*, 7:3–19, 1970.

[288] R. A. Sunyaev and Ya. B. Zeldovich. The Interaction of matter and radiation in the hot model of the universe. *Astrophys. Space Sci.*, 7:20–30, 1970.

[289] Y. Suto and M. Sasaki. Quasi nonlinear theory of cosmological selfgravitating systems. *Phys. Rev. Lett.*, 66:264–267, 1991. doi:10.1103/PhysRevLett.66.264.

[290] A. S. Szalay, T. Matsubara, and S. D. Landy. Redshift space distortions of the correlation function in wide angle galaxy surveys. *Astrophys. J.*, 498:L1, 1998. arXiv:astro-ph/9712007, doi:10.1086/311293.

[291] I. Szapudi. Wide angle redshift distortions revisited. *Astrophys. J.*, 614:51–55, 2004. arXiv:astro-ph/0404477, doi:10.1086/423168.

[292] V. Tansella. On the $2^{\text{nd}}$ feature of the matter two-point function. *Phys. Rev.*, D97(10):103520, 2018. arXiv:1804.05826, doi:10.1103/PhysRevD.97.103520.

[293] V. Tansella, C. Bonvin, G. Cusin, R. Durrer, M. Kunz, and I. Sawicki. Redshift-space distortions from vector perturbations II: Anisotropic signal. 2018. arXiv:1807.00731.

[294] V. Tansella, C. Bonvin, R. Durrer, B. Ghosh, and E. Sellentin. The full-sky relativistic correlation function and power spectrum of galaxy number counts: I. Theoretical aspects. *JCAP*, 1803(03):019, 2018. arXiv:1708.00492, doi:10.1088/1475-7516/2018/03/019.

[295] V. Tansella, G. Jelic-Cizmek, C. Bonvin, and R. Durrer. COFFE: a code for the full-sky relativistic galaxy correlation function. 2018. arXiv:1806.11090.

[296] A. Taruya and T. Hiramatsu. A Closure Theory for Non-linear Evolution of Cosmological Power Spectra. *Astrophys. J.*, 674:617, 2008. arXiv:0708.1367, doi:10.1086/526515.

[297] G. Tasinato. Cosmic Acceleration from Abelian Symmetry Breaking. *JHEP*, 04:067, 2014. arXiv:1402.6450, doi:10.1007/JHEP04(2014)067.

[298] K. Thepsuriya and A. Lewis. Accuracy of cosmological parameters using the baryon acoustic scale. *JCAP*, 1501(01):034, 2015. arXiv:1409.5066, doi:10.1088/1475-7516/2015/01/034.

[299] V. Trimble. The 1920 shapley-curtis discussion: Background, issues, and aftermath. 107, 06 1995.

[300] W. Tung. *Group Theory in Physics*. World Scientific, 1985.

[301] J. A. Tyson, G. P. Kochanski, and I. P. Dell'Antonio. Detailed mass map of CL0024+1654 from strong lensing. *Astrophys. J.*, 498:L107, 1998. arXiv:astro-ph/9801193, doi:10.1086/311314.

[302] O. Umeh, S. Jolicoeur, R. Maartens, and C. Clarkson. A general relativistic signature in the galaxy bispectrum: the local effects of observing on the lightcone. *JCAP*, 1703(03):034, 2017. arXiv:1610.03351, doi:10.1088/1475-7516/2017/03/034.

[303] P. Valageas. Dynamics of gravitational clustering I. building perturbative expansions. *Astron. Astrophys.*, 379:8, 2001. arXiv:astro-ph/0107015, doi:10.1051/0004-6361:20011309.

[304] T. S. van Albada, J. N. Bahcall, K. Begeman, and R. Sancisi. Distribution of dark matter in the spiral galaxy NGC 3198. *ApJ* , 295:305–313, Aug. 1985. doi:10.1086/163375.

[305] M. P. van Daalen, B. M. B. Henriques, R. E. Angulo, and S. D. M. White. The galaxy correlation function as a constraint on galaxy formation physics. *Mon. Not. Roy. Astron. Soc.*, 458(1):934–949, 2016. arXiv:1512.00008, doi:10.1093/mnras/stw405.

[306] L. Verde et al. The 2dF Galaxy Redshift Survey: The Bias of galaxies and the density of the Universe. *Mon. Not. Roy. Astron. Soc.*, 335:432, 2002. arXiv:astro-ph/0112161, doi:10.1046/j.1365-8711.2002.05620.x.

[307] E. Villa, E. Di Dio, and F. Lepori. Lensing convergence in galaxy clustering in ΛCDM and beyond. *JCAP*, 1804(04):033, 2018. arXiv:1711.07466, doi:10.1088/1475-7516/2018/04/033.

[308] Z. Vlah, U. Seljak, M. Y. Chu, and Y. Feng. Perturbation theory, effective field theory, and oscillations in the power spectrum. *JCAP*, 1603(03):057, 2016. arXiv:1509.02120, doi:10.1088/1475-7516/2016/03/057.

[309] A. G. Walker. On milne's theory of world-structure*. *Proceedings of the London Mathematical Society*, s2-42(1):90–127, 1937. URL: http://dx.doi.org/10.1112/plms/s2-42.1.90, doi:10.1112/plms/s2-42.1.90.

[310] Y. Wang et al. The clustering of galaxies in the completed SDSS-III Baryon Oscillation Spectroscopic Survey: tomographic BAO analysis of DR12 combined sample in configuration space. *Mon. Not. Roy. Astron. Soc.*, 469(3):3762–3774, 2017. arXiv:1607.03154, doi:10.1093/mnras/stx1090.

[311] S. Weinberg. *Gravitation and Cosmology: Principles and Applications of the General Theory of Relativity*. Wiley, New York, NY, 1972. URL: https://cds.cern.ch/record/100595.

[312] X. Xu, A. J. Cuesta, N. Padmanabhan, D. J. Eisenstein, and C. K. McBride. Measuring DA and H at z=0.35 from the SDSS DR7 LRGs using baryon acoustic oscillations. *Mon. Not. Roy. Astron. Soc.*, 431:2834, 2013. arXiv:1206.6732, doi:10.1093/mnras/stt379.

[313] X. Xu, A. J. Cuesta, N. Padmanabhan, D. J. Eisenstein, and C. K. McBride. Measuring $D_A$ and H at z=0.35 from the SDSS DR7 LRGs using baryon acoustic oscillations. *M.N.R.A.S.* , 431:2834–2860, May 2013. arXiv:1206.6732, doi:10.1093/mnras/stt379.

[314] X. Xu, N. Padmanabhan, D. J. Eisenstein, K. T. Mehta, and A. J. Cuesta. A 2% Distance to z=0.35 by Reconstructing Baryon Acoustic Oscillations - II: Fitting Techniques. *Mon. Not. Roy. Astron. Soc.*, 427:2146, 2012. arXiv:1202.0091, doi:10.1111/j.1365-2966.2012.21573.x.

[315] K. Yamamoto, M. Nakamichi, A. Kamino, B. A. Bassett, and H. Nishioka. A Measurement of the quadrupole power spectrum in the clustering of the 2dF QSO Survey. *Publ. Astron. Soc. Jap.*, 58:93–102, 2006. arXiv:astro-ph/0505115, doi:10.1093/pasj/58.1.93.

[316] K. Yamamoto, H. Nishioka, and Y. Suto. The cosmological light cone effect on the power spectrum of galaxies and quasars in wide-field redshift surveys. *Astrophys. J.*, 527:488–497, 1999. arXiv:astro-ph/9908006, doi:10.1086/308126.

[317] J. Yoo. General Relativistic Description of the Observed Galaxy Power Spectrum: Do We Understand What We Measure? *Phys.Rev.*, D82:083508, 2010. arXiv:1009.3021, doi:10.1103/PhysRevD.82.083508.

[318] J. Yoo. Relativistic Effect in Galaxy Clustering. *Class. Quant. Grav.*, 31:234001, 2014. arXiv:1409.3223, doi:10.1088/0264-9381/31/23/234001.

[319] J. Yoo and V. Desjacques. All-Sky Analysis of the General Relativistic Galaxy Power Spectrum. *Phys. Rev.*, D88(2):023502, 2013. arXiv:1301.4501, doi:10.1103/PhysRevD.88.023502.

[320] J. Yoo and R. Durrer. Gauge-Transformation Properties of Cosmological Observables and its Application to the Light-Cone Average. *JCAP*, 1709(09):016, 2017. arXiv:1705.05839, doi:10.1088/1475-7516/2017/09/016.

[321] J. Yoo, A. L. Fitzpatrick, and M. Zaldarriaga. A New Perspective on Galaxy Clustering as a Cosmological Probe: General Relativistic Effects. *Phys.Rev.*, D80:083514, 2009. arXiv:0907.0707, doi:10.1103/PhysRevD.80.083514.

[322] J. Yoo, N. Hamaus, U. Seljak, and M. Zaldarriaga. Going beyond the Kaiser redshift-space distortion formula: a full general relativistic account of the effects and their detectability in galaxy clustering. *Phys. Rev.*, D86:063514, 2012. arXiv:1206.5809, doi:10.1103/PhysRevD.86.063514.

[323] J. Yoo and U. Seljak. Wide Angle Effects in Future Galaxy Surveys. *Mon. Not. Roy. Astron. Soc.*, 447(2):1789–1805, 2015. arXiv:1308.1093, doi:10.1093/mnras/stu2491.

[324] J. Yoo and M. Zaldarriaga. Beyond the Linear-Order Relativistic Effect in Galaxy Clustering: Second-Order Gauge-Invariant Formalism. *Phys.Rev.*, D90:023513, 2014. arXiv:1406.4140.

[325] Ya. B. Zeldovich. Gravitational instability: An Approximate theory for large density perturbations. *Astron. Astrophys.*, 5:84–89, 1970.

[326] G.-B. Zhao et al. The clustering of the SDSS-IV extended Baryon Oscillation Spectroscopic Survey DR14 quasar sample: a tomographic measurement of cosmic structure growth and expansion rate based on optimal redshift weights. 2018. arXiv:1801.03043.

[327] G.-B. Zhao, L. Pogosian, A. Silvestri, and J. Zylberberg. Searching for modified growth patterns with tomographic surveys. *Phys. Rev.*, D79:083513, 2009. arXiv:0809.3791, doi:10.1103/PhysRevD.79.083513.

[328] T. G. Zlosnik, P. G. Ferreira, and G. D. Starkman. Modifying gravity with the Aether: An alternative to Dark Matter. *Phys. Rev.*, D75:044017, 2007. arXiv:astro-ph/0607411, doi:10.1103/PhysRevD.75.044017.

[329] F. Zwicky. Republication of: The redshift of extragalactic nebulae. *General Relativity and Gravitation*, 41:207–224, Jan. 2009. doi:10.1007/s10714-008-0707-4.